DOT/FAA/TC-26/03

Federal Aviation Administration
William J. Hughes Technical Center
Aviation Research Division
Atlantic City International Airport
New Jersey 08405

Flight Loads and Airframe Usage Analysis of Next-Generation Airtankers – CL-415

April 2026

Final report

U.S. Department of Transportation
Federal Aviation Administration

NOTICE

This document is disseminated under the sponsorship of the U.S. Department of Transportation in the interest of information exchange. The U.S. Government assumes no liability for the contents or use thereof. The U.S. Government does not endorse products or manufacturers. Trade or manufacturers' names appear herein solely because they are considered essential to the objective of this report. The findings and conclusions in this report are those of the author(s) and do not necessarily represent the views of the funding agency. This document does not constitute FAA policy. Consult the FAA sponsoring organization listed on the Technical Documentation page as to its use.

This report is available at the Federal Aviation Administration William J. Hughes Technical Center's Full-Text Technical Reports page: actlibrary.tc.faa.gov in Adobe Acrobat portable document format (PDF).

Technical Report Documentation Page

Form DOT F 1700.7 (8-72) Reproduction of completed page authorized

1. Report No.	2. Government Accession No.	3. Recipient's Catalog No.
DOT/FAA/TC-26/03		

4. Title and Subtitle	5. Report Date
Flight Loads and Airframe Usage Analysis of Next-Generation Airtankers – CL-415	April 2026
	6. Performing Organization Code

7. Author(s)	8. Performing Organization Report No.
Linda K. Kliment and Kamran Rokhsaz	

9. Performing Organization Name and Address	10. Work Unit No. (TRAIS)
Wichita State University 1845 Fairmount Wichita, KS 67260-0044	11. Contract or Grant No. Cooperative Agreement 17-G-004

12. Sponsoring Agency Name and Address	13. Type of Report and Period Covered
U.S. Department of Transportation Federal Aviation Administration Air Traffic Organization NextGen & Operations Planning Office of Research and Technology Development Washington, DC 20591	Phase I Final Report
	14. Sponsoring Agency Code ANM-210L

15. Supplementary Notes

The Federal Aviation Administration William J. Hughes Technical Center Aviation Research Division COR was Dr. Sohrob Mottaghi.

16. Abstract

This report presents the results of an analysis of operational data from a fleet of four CL-415 Super Scooper aircraft flown in support of the United States Forest Service aerial firefighting operations. The aircraft were equipped with IONode100 digital flight data recorders supported by Latitude Technologies Corporation. Data used for this report was collected over the calendar years 2015-2019 and consisted of approximately 4,700 hours of flight time, almost equally divided among the four airframes. The analysis has been limited to ground-air-ground segments of the missions, excluding ground operations. Missions have been divided into three groups: firefighting, ferry, and maintenance/training. Firefighting missions have been further divided into ten flight phases. Airframe usage has been examined for each flight and each phase of the flight.

The results have been compared with aircraft limitations on airspeeds, altitudes, and load factors pertaining to individual flap deflections. Unreliable pitch and roll angles have prevented examination of flights in unusual attitudes.

All aircraft are shown to have been flown well within the operation altitude limits. Incidents of excessive vertical acceleration and indicated airspeeds, for the corresponding flap deflection, are shown to have been common. Lack of clear indicators, such as weight on wheels, for water landings have prevented clear identification of points of contact with, and departure from, water landings. For airborne phases, vertical load factors due to gust and maneuver have been separated using the two-second rule. Frequency of occurrence of each type has been determined using the method of peaks-between-means. The results have been presented in the form of exceedance spectra per 1000 hours and per nautical mile for various altitude bands.

The report is concluded with some recommendations for improved data acquisition for further efforts.

17. Key Words	18. Distribution Statement
Flight profiles, Flight loads spectrum, Statistical loads data	This document is available to the U.S. public through the National Technical Information Service (NTIS), Springfield, Virginia 22161. This document is also available from the Federal Aviation Administration William J. Hughes Technical Center at actlibrary.tc.faa.gov.

19. Security Classif. (of this report)	20. Security Classif. (of this page)	21. No. of Pages	22. Price
Unclassified	Unclassified	156	

Acknowledgements

The work reported in this document was performed by the Flight Loads Group within the Department of Aerospace Engineering of the College of Engineering at Wichita State University (WSU). This effort was conducted under a cooperative agreement with the Federal Aviation Administration (FAA) (cooperative agreement 17-G-004) with funding provided by the United States Forest Service (USFS). At WSU, the principal investigators were Dr. Kamran Rokhsaz and Dr. Linda K. Kliment of the Department of Aerospace Engineering. The format used for presentation of the statistical data was adopted from the work previously performed by the principal investigators and the University of Dayton Research Institute (UDRI). The Program Manager for the FAA was Dr. Sohrob Mottaghi of the FAA William J. Hughes Technical Center for Advanced Aerospace. Technical guidance was provided by Mr. David Rathfelder of the FAA Policy & Standards Division. Worthy of recognition is the administrative support provided by Ms. Heather Castillo from the United States Forest Service (USFS).

Contents

Figures

Tables

Acronyms

Acronym	Definition
AGL	Above Ground Level
ASM	Aerial Supervision Module
DFDR	Digital Flight Data Recorder
FAA	Federal Aviation Administration
GAG	Ground-Air-Ground
GPS	Global Positioning System
KIAS	Knots Indicated Airspeed
MSL	Mean Sea Level
NED	National Elevation Dataset
NTSB	National Transportation Safety Board
OEM	Original Equipment Manufacturer
OLM	Operational Loads Monitoring
SEAT	Single-Engine-Airtanker
SFC	Specific Fuel Consumption
USFS	United States Forest Service
V_{MO}	Maximum Operating Speed
WSU	Wichita State University

Executive summary

This report details the results of an investigation into airframe usage and flight loads experienced by a fleet of four CL-415 aircraft used for aerial firefighting.

All aircraft were equipped with IONode Digital Flight Data Recorders (DFDRs) and the data was gathered over the calendar years 2015 through 2019. The recorded data included air data, inertial data, navigation data, and some information concerning systems such as flaps and the amount of water onboard. The air data consisted of various airspeeds, local pressure and temperature, and pressure altitude. The inertial data was comprised of linear accelerations, angular orientations, and angular rates. Navigation data were made of Global Positioning System (GPS) coordinates, altitude, and ground speed. The 2018-2019 data also included terrain elevation. None of the data included instantaneous aircraft weigh or the amount of fuel onboard.

The airframe usage information was extracted and presented in statistical formats consistent with past practices. Results were developed for various missions and different flight phases of firefighting flights, as well as for Ground-Air-Ground (GAG) cycles where appropriate. Comparisons were made with the aircraft limitations. A low-pass 8th order Butterworth filer was used to remove the effects of local and structural vibrations from the recorded vertical load factors. Vertical load factors were placed into gust and maneuver categories using the two-second rule. Frequency of occurrence of the vertical load factors was then determined and expressed in the form of exceedance spectra for various altitude bands. Consistent with previous observations, due to the low-altitude nature of the missions, the frequency of occurrence of the load factors correlated better with altitude Above Ground Level (AGL) than it did when categorized by altitude relative to Mean Sea Level (MSL). The flight loads spectra were compared with those of four other operations: Single-Engine-Airtankers (SEATs), Aerial Supervision Module (ASM)/leads, BAe-146/RJ-85 large airtankers, and a limited amount of agricultural spraying. The magnitude and the frequency of the load factors were shown to be larger than all but those of ASM/lead flights. Derived gust velocities were determined based on estimated aircraft weights. They were presented as cumulative occurrences per nautical mile for various MSL and AGL altitude bands for flight phases covering a wide range of altitudes. Derived gust velocities showed clear correlation with the latter.

The formats used in this report for presentation of the statistical results were kept consistent with those of previous documents related to operational loads monitoring (OLM) projects. They allow

convenient means of comparing the results with aircraft limitations and the results from other operations. The intent was to provide a document that could be used by the operators and the Original Equipment Manufacturers (OEMs) to better understand factors that affect the structural integrity of the aircraft. This information could also be used to refine regulations concerning the design of such aircraft.

1 Introduction

In response to Recommendation A-04-29 (NTSB, 2004) from the National Transportation Safety Board (NTSB), the United States Forest Service (USFS) began requiring all aircraft operating under contract to be equipped with Digital Flight Data Recorders (DFDRs). The recorded data, that is proprietary to the operators, is stored in a central repository managed by HBM-nCode Federal LLC. By contract, the data is made available to the USFS in its quest for continuous health monitoring of the fleet.

Wichita State University (WSU) is given access to this data for determining the statistical usage of the airframes and comparison of the results with the aircraft limitations. This information is also used to develop operational flight loads spectra. The results can be used by the Original Equipment Manufacturers (OEMs) and the operators to refine the aircraft limitations or maintenance and inspections schedules. If needed, these results can also be used by the regulating agencies to refine the standards governing such operations. Some examples of previous analyses can be found in Rokhsaz et al. (2014), Rokhsaz, Kliment and Bramlette (2011), Kliment et al. (2015), and Kliment, Rokhsaz, and Menon (2017).

In the past, the large airtanker fleet consisted mostly of reconfigured military aircraft. Following a 2012 report by the USFS and the Department of Interior (2012), the operators gradually replaced the legacy airtanker fleet with newer, faster, and more cost-effective aircraft. The current fleet consists mostly of civil transport aircraft modified as airtankers. One of the newer additions to the fleet, although not in the “large” airtanker category, is the Bombardier CL-415 Super Scooper. Unlike other airtankers, this amphibious aircraft was designed specifically for aerial firefighting.

The focus of the present three-year project was the operational loads monitoring (OLM) of the new fleet. Initially, airframe usage and flight loads from BAe-146-200 and Avro RJ-85A were analyzed. These aircraft were variants of the same design and at the time a large volume of recorded data was available from both. The results of this effort can be found in Rokhsaz et al. (2026). Later, emphasis was placed on a group of MD-87 and a fleet of DC-10-30 aircraft. While these aircraft differed substantially in size and payload, they had some similarities in layout and some systems. Additionally, two different DFDRs were used on the MD-87 aircraft, which allowed investigating possible effect of the recorders on the results. A full analysis of the MD-87 and DC-10 aircraft is expected to be completed in the future.

The final phase of this project was focused on the CL-415. By the start of this phase, four airframes had been operating for several years, resulting in a large volume of data. The data used for this report was collected from early 2015 through the end of 2019 calendar years.

2 Aircraft description

2.1 Weights and geometry

Some aircraft characteristics, dimensions, and limitations are shown in Table 1. Most of these values come from the Type Certificate Datasheet (2016) and Aircraft Flight Manual (1999). The dimensions were obtained from Lambert and Munson (1994). Additional limitations are given in Appendix A that will be discussed later. A basic schematic of the aircraft is shown in Figure 1.

Table 1: Weights and dimensions

Parameter	**Land Operation**	**Water Operation**
Maximum Ramp Weight (lb)	44,000	38,000
Maximum Takeoff Weight (lb)	43,850	37,850
Maximum Landing Weight (lb)	37,000	37,000
Maximum Zero Fuel Weight (lb)	43,000	43,000
Maximum Touchdown Weight for Water Pickup (lb)	---	36,200
Maximum Liftoff Weight after Water Pickup (lb)	---	47,000
Wing Area (ft^2)	1,080	
Wingspan (ft)	93.9	
Wing Aspect Ratio	8.2	
Overall Length	65.0	

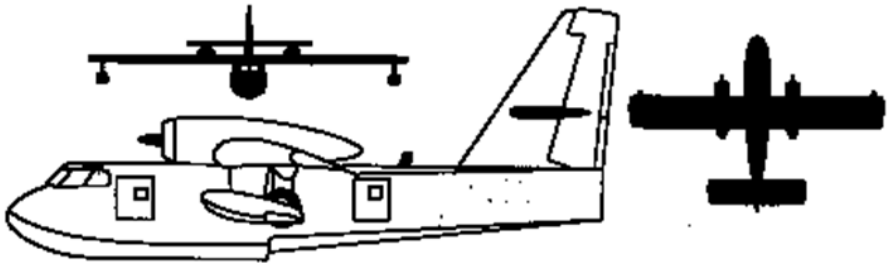

Figure 1: Schematic of CL-415

2.2 Water system

The CL-415 is equipped with four internal water tanks with total capacity of 1,621 gallons. Water can be dropped from four bay doors in salvo, trail, or be split into separate drops depending on targets and fire type. Drop heights range 100-150 feet (U.S. Forest Service Fire and Aviation Management, 2018). During the fill phase, the amount of water can exceed the above limit. However, the additional load is ejected through overflow vents on the side and the fill probes while they are retracted.

2.3 Anatomy of fills and drops

Figure 2 shows a typical sequence of a fill followed by a drop and the time history of various parameters. The filling operation starts with fill entry. In this phase, the aircraft is configured for water pick-up by lowering the flaps and the fill probe. Generally, the fill probes are lowered long before the start of the fill entry so their position cannot be used to mark the start of the fill phase. The flaps are usually placed in the second detent and the aircraft is slowed for contacting the water surface. The fill probes are located just aft of the step on the keel, so the aircraft contacts water shortly before the start of the fill.

The fill entry is followed by the fill phase. During this phase, the aircraft skims the water surface, usually without settling in, and the tanks are filled through the fill probes. While the maximum tank capacity is 1,621 gallons, at the end of the fill phase, the recorded water level can reach as high as 2,000 gallons, much of which is ejected through the overflow vents and the retracting fill probes during the exit from the fill. The aircraft weight can reach 47,000 pounds at the end of the fill. In this phase, the aircraft may be subjected to a large high-frequency vertical load factors stemming from water impact as shown in Figure 2(b). These are not “flight loads,” and therefore, cannot be categorized as gust or maneuver loads. It is not uncommon for the airspeed to drop slightly below the stall speed for the aircraft weight, as indicated in Figure 3(a). Also, due to the resolution of the terrain elevation data, sometimes the Above Ground Level (AGL) altitude becomes negative during this phase. This can be seen in Figure 3(b).

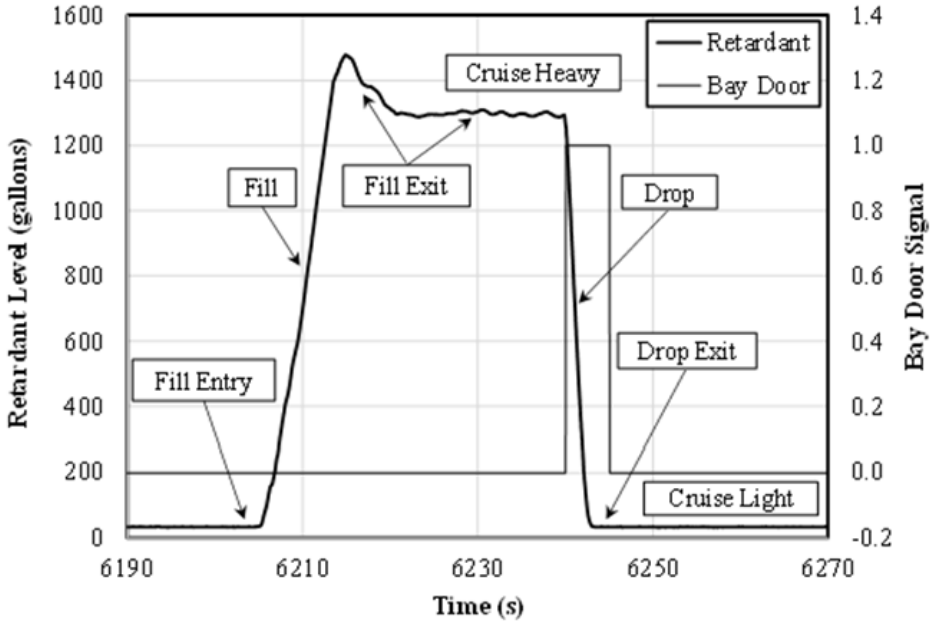

(a) Definition of Phases

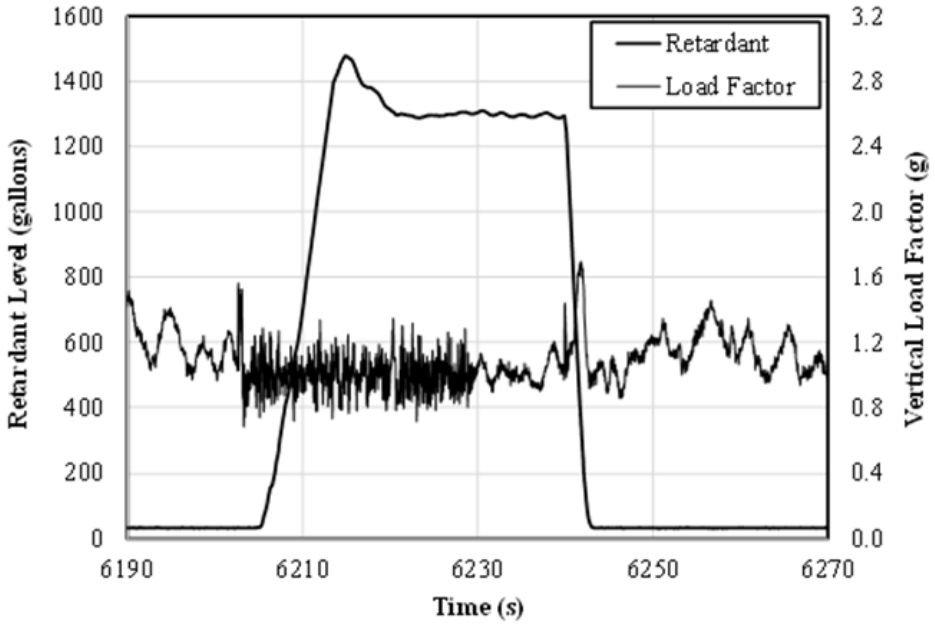

(b) Time History of Load Factor

Figure 2: Typical fill and drop sequence

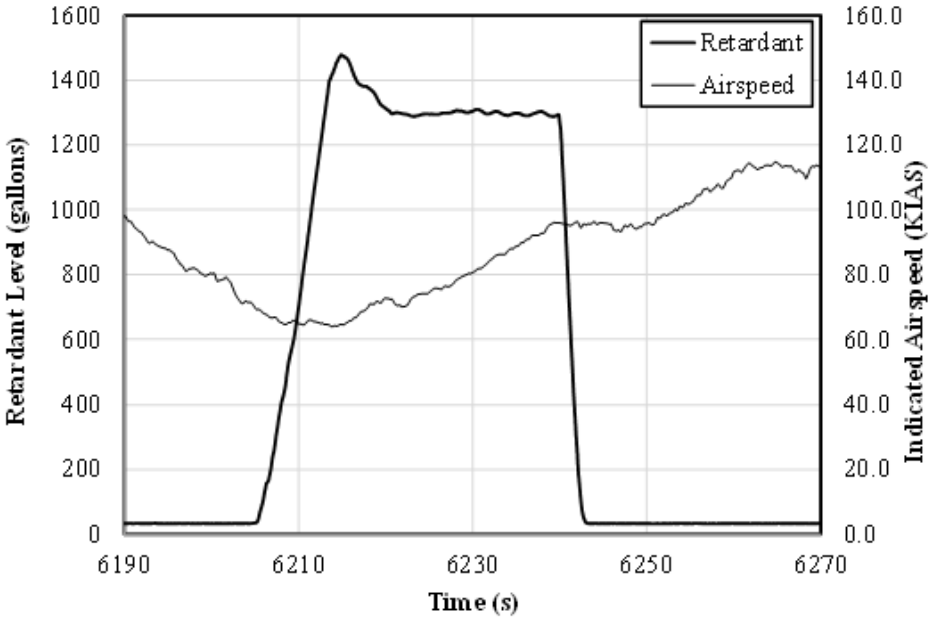

(a) Time History of Indicated Airspeed

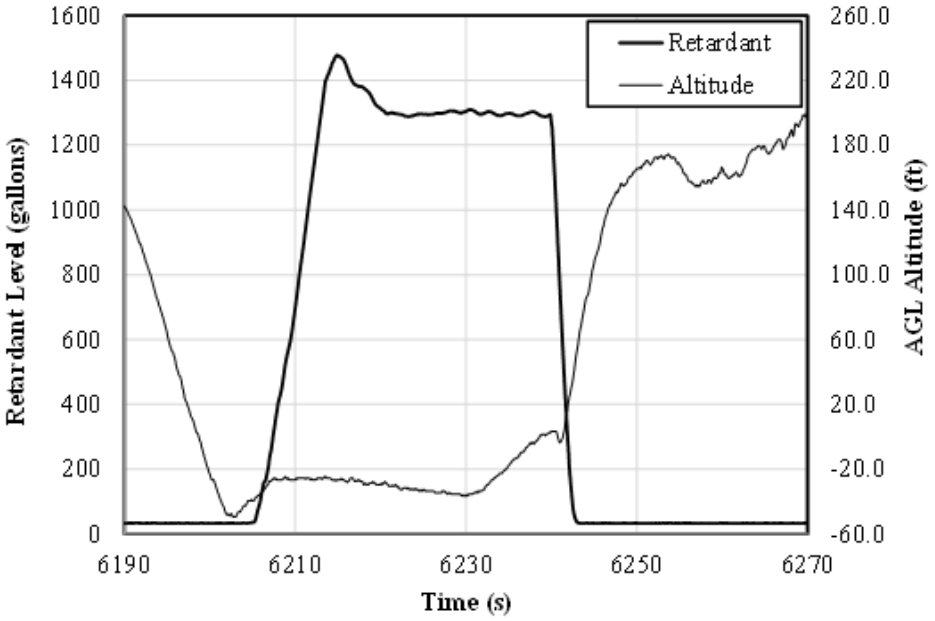

(b) Time History of AGL Altitude

Figure 3: Typical fill and drop sequence (continued)

The next phase is the fill exit. During this phase, the aircraft gains altitude while ejecting excess water. At the end of the fill exit phase, the water level does not exceed 1,600 gallons. Usually, the flaps are raised to the first detent or are retracted completely.

Just prior to entering the drop zone, the aircraft is configured for the drop phase. Again, flaps are lowered to the second detent and altitude is reduced for entry into the fire zone. This is followed by the drop phase when water is leaving the aircraft. The end of the drop phase cannot be determined solely based on the bay door positions. The bay doors remain open for some time after the water load has been depleted. Therefore, the end of the drop phase must be identified based on the water level in the tanks. Consistent with previous observations, the drop phase is accompanied with an increase in the vertical load factor.

The final phase in the process is drop exit, which is the egress from the fire zone. Flaps are raised from the second detent into the first or are retracted completely. It will be seen more clearly later that the variations in the vertical load factor during this phase are comparable with those of the drop phase, although with the aircraft being at a much lower weight.

Depending on the proximity of the water source to the fire zone, the fill and drop sequence can take a very short time. In the example shown here, the beginning of the fill entry and the end of the drop exit were only 45 seconds apart.

Drop phases could be identified easily from the combination of the water level and the bay door signal. However, fill phase required a more complex algorithm. At times, the crew would open the bay doors in flight without any water onboard. Invariably, this would result in a the flailing of the floats inside the tank, making it appear that the tanks were being filled in flight. Therefore, special algorithms were needed to bypass these false fills. Also, most of these occurred at indicated airspeeds above the bay door limit of 129 Knots Indicated Airspeed (KIAS).

3 Data collection

3.1 Flight data recorder

All aircraft were equipped with IONode DFDRs supported by Latitude Technologies Corporation. Their stored data was processed by Latitude software prior to storage in the HBM-nCode library in a uniform 32-Hz format. The recorders were mounted very close to the aircraft center of gravity, next to the water tanks.

3.2 Available data

The data used for this analysis consisted of files collected over the calendar years 2015 through 2019, summarized in Table 2. All data was available at a uniform 32-Hz rate. Not all the data could be used for analysis for several reasons including files that did not contain flights and

where the quality of the data was questionable. The yield rate of over 95% was higher than that seen from other aircraft.

Table 2: Number of files used for analysis

Aircraft	Date Range	Files with Flights	Useful Files	Flight Time (hr)
1	01-22-2015 to 12-13-2019	630	530	1,323.9
2	03-11-2016 to 11-20-2019	509	465	1,101.8
3	02-18-2016 to 11-20-2019	498	464	1,191.4
4	03-17-2016 to 12-17-2019	446	414	1,095.8
Total		2,083	1,873	4,713

4 Wichita State University data processing

4.1 Preprocessing

The data downloaded from the library was in different formats and contained different information depending on the date and the aircraft. Examples included re-ordering of the data columns, switching of some binary signals, and using different units. In addition, the files dated prior to 2018 did not contain ground elevation.

A uniform set of channels needed for usage and flight loads analysis was identified, which is shown in Table 3. Preprocessors tailored to individual data formats were developed and used to extract and output the pertinent information in this unified file format. The preprocessors also ensured uniformity of binary signals, such as those of squat switch and the bay doors. Finally, the flap deflections recorded in degrees were converted to discrete detents. When turning analog flap signals into detents, allowances were made in the limits to minimize interpretation of small noise in the data as rapid changes in the flap settings.

Table 3: Unified channel format for final analysis

Channel	Parameter	Channel	Parameter
1	Line Number	16	Roll Rate (degrees per second)
2	Elapsed Time (seconds)	17	Yaw Rate (degrees per second)
3	Latitude (degrees)	18	Dynamic Pressure (psf)
4	Longitude (degrees)	19	Static Pressure (psf)
5	Track (degrees)	20	Outside Air Temperature (F)

Channel	Parameter	Channel	Parameter
6	GPS Altitude (feet)	21	Indicated Airspeed (KIAS)
7	Pressure Altitude (feet)	22	Equivalent Airspeed (KEAS)
8	GPS Ground Speed (knots)	23	True Airspeed (KTAS)
9	Vertical Speed (feet per minute)	24	Weight on Wheels (binary)
10	Longitudinal Acceleration (g)	25	Flap Position (detent)
11	Lateral Acceleration (g)	26	Bay Door (binary)
12	Normal Acceleration (g)	27	Fill Probe (binary)
13	Pitch (degrees)	28	Water Quantity (gallons)
14	Pitch Rate (degrees per second)	29	Terrain Elevation* (feet)
15	Roll (degrees)		

* *Not available in all data files, obtained in post-processing*

4.2 Obtaining ground elevation

Earlier efforts showed strong correlation between flight loads spectra and AGL altitude for low-level operations. Data collected prior to 2018 did not contain terrain elevation needed for determining the AGL altitudes. The Global Positioning System (GPS) coordinates were used in the National Elevation Dataset (NED) (USGS, 2018) to obtain terrain elevation when it was not a recorded parameter. This dataset is maintained by the United States Geological Survey and contains terrain elevation with resolution of 1 arc-second, or approximately 30 meters for the contiguous United States. For some parts of the country, the resolution can be 1/3 to 1/9 arc-second, that is 10 to 3 meters.

Each set of coordinates had to be sent to the dataset via internet, which returned the corresponding ground elevation. Data transmissions rates made it impractical to perform this operation for every line of data. Therefore, ground elevation was found once per second (i.e., for every 32 lines) and was interpolated in between. Even at this reduced rate, processing each file would take approximately 15-30 minutes.

While GPS altitude was a recorded parameter, many files showed extremely large spikes in this parameter. Therefore, pressure altitude and terrain elevation were used to establish the local AGL altitude. Nonetheless, AGL altitude could not be determined with high accuracy due to the resolution of the ground elevation and uncertainties in pressure altitude. It was not uncommon to encounter negative AGL altitudes at very low-altitude phases of flight such as the fills.

In any event, the combined resolution of the elevation data and the pressure altitude prevented exact pinpointing of the AGL altitudes. Also, in those cases where the elevation data was recorded, the source and the resolution of the information was unknown. A sample comparison of the recorded elevations with those obtained from NED showed differences as large as 140 feet (43 m), as can be seen in Figure 4. Consequently, it was not unusual to encounter negative AGL altitudes in very low-level operations, such as fills. These uncertainties also prevented identification of the exact points of contact with, and departure from, water during fill entry and fill exit phases.

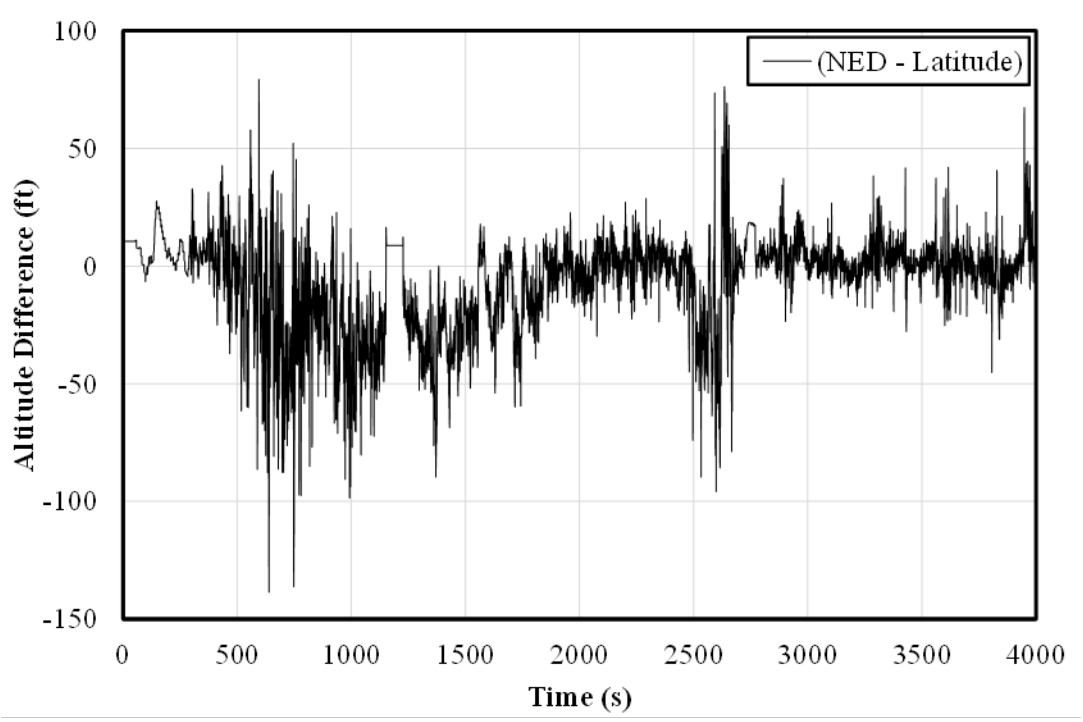

Figure 4: Sample difference in terrain elevation between NED and recorded data

4.3 Filtering vertical load factors

Earlier work proved that the 32-Hz collected vertical load factors could contain accelerations stemming from local or structural vibrations. This could lead to unrealistically high frequency of occurrence of the vertical gust load factors, as discussed in Rokhsaz et al. (2026) and Rokhsaz and Kliment (2019). Therefore, an eighth-order low-pass Butterworth filter with an 8-Hz cutoff frequency was used to remove the higher frequencies.

4.4 Flap settings

Flap deflections were recorded in degrees. Per Bombardier Aerospace (1999), flaps could be set at 0, 10, 15, or 25 degrees with corresponding airspeed and vertical load factor limitations. However, in practice, the recorded values did not match these settings exactly, as demonstrated in Figure 5. Therefore, the recorded signals were converted into discrete detents. The correspondence between the two is shown in Table 4. While this method worked well, it also introduced two additional issues.

First, the recorded signal occasionally hovered around one of the limits resulting in a large number of successive switches between two detents. This necessitated filtering of the discrete data to eliminate the spurious deflections.

The second problem was association of a detent with the flaps when they were in transit. An example is shown in the second part of Figure 5, which is a closeup view of the 7,400-7,550 seconds of the previous part. When the flaps were lowered to the second detent, the pre-processor assumed they were lowered to the first detent and then the second detent. This type of spurious detent identification was eliminated by the filtering logic. However, when the flaps were paused in retracting from the second detent, they were taken to be in the first detent for approximately 12.5 seconds. Because of the duration, the second "bump" could not be filtered out. This issue resulted in a number of apparent over-speeds and over-loads that will be seen in the *V-n* diagrams discussed later.

Table 4: Flap deflections in degrees and detents

Flaps per Handbook (deg)	**Recorded Values (deg)**	**Detents**
0	$0 < \text{Deflection} \leq 7$	Retracted
10	$7 < \text{Deflection} \leq 13$	1
15	$13 < \text{Deflection} \leq 19$	2
25	$19 < \text{Deflection}$	3

4.5 Derived and extracted parameters

4.5.1 Flight definition

As an amphibious aircraft, landings could be on land or on water. Ground landings and takeoffs could be determined with certainty from the status of the squat switch. However, water landings

and takeoffs had to be based on indicated airspeed and changes in altitude. It was important to distinguish a water landing from a fill in which the aircraft skimmed the surface without the hull settling in the water. A water landing marked the end of a flight, whereas skimming the surface for a fill was considered as part of a flight.

A water landing was assumed if the squat switch was in the “in-air” mode and the airspeed dropped below a predetermined level and was below that value ten seconds later. Water takeoff was assumed if the squat switch indicated “in-air” and the change in altitude was greater than 15 feet in 10 seconds. While this logic worked adequately, occasionally it led to false indications of water landing resulting in inclusion of landing impact loads in flight loads. This will be discussed later.

Flights were defined as takeoff to landing, be it on land or on water.

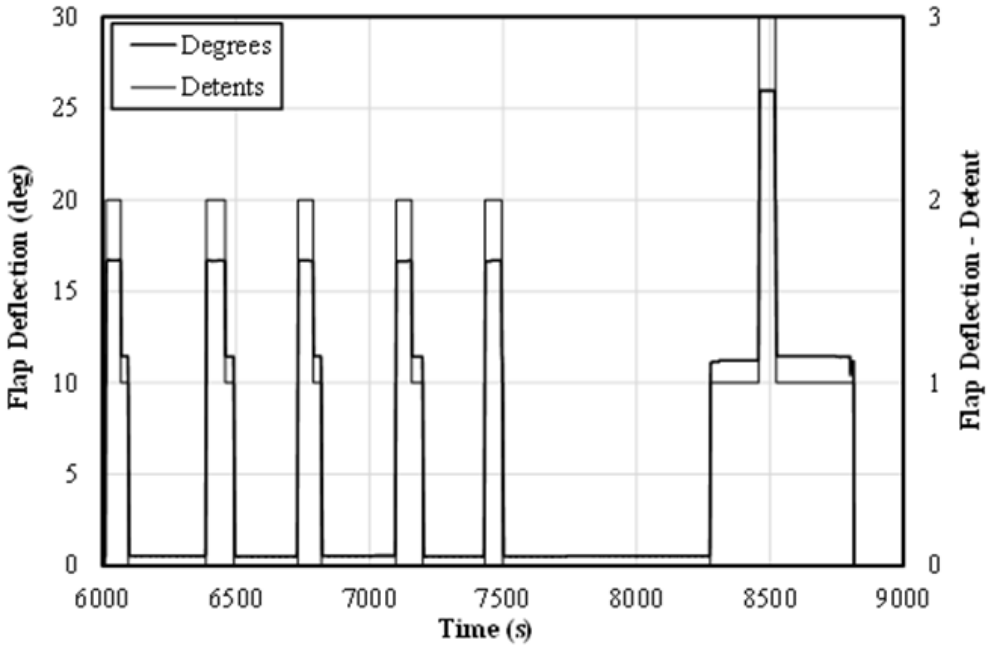

(a) Sample Recorded Flap versus Established Detents

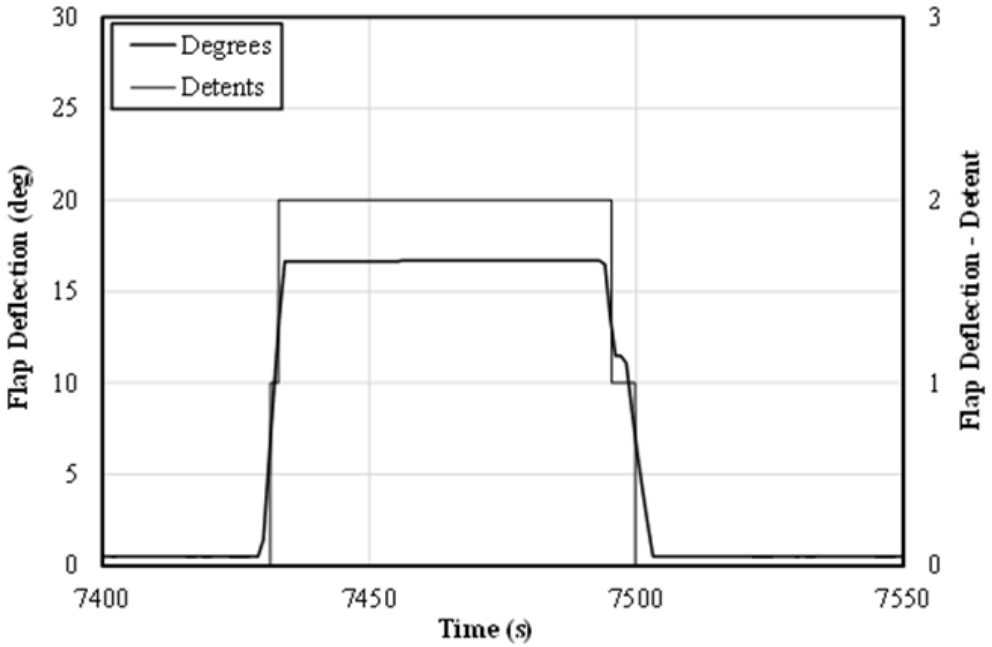

(b) Association of Flap Detent with Transition

Figure 5: Analog and discrete flap associations

4.5.2 Flight duration and distance

Total flight time was defined as the time between takeoff and landing based on the logic described above. Flight distances proved to be most reliable from time integration of the true airspeed.

4.5.3 Sign convention

Normal acceleration was defined positive as upward, along the positive *z*-axis, shown in Figure 6.

4.5.4 Peak and valley selection

Frequency of occurrence of flight loads were determined from the method of peak-between-means (ASTM International, 2005). In this method, only one extremum value is considered between every two crossings of the mean value. The "mean" value was defined as any load within the dead band of ±0.05 g. The same dead band values were used for gusts and maneuvers load factors. For derived gust velocities, the dead band was set at ±2.0 ft/s. This method was consistent with past practices and allowed direct comparison of the results with previous work.

4.5.5 Gust and maneuver load factor separation

The vertical load factors were normalized relative to their values during the ground phases. The values outside of the dead band that lasted two seconds or longer were attributed to maneuvers. Other occurrences were assumed to be due to atmospheric disturbances, or gusts. The rationale behind this two-second rule is described in detail in Rustenburg et al. (1999).

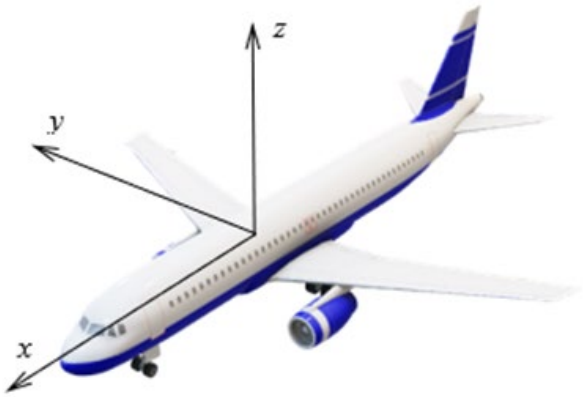

Figure 6: Sign convention for accelerations

4.5.6 Altitude bands

The spectra for gust and maneuver load factors and derived gust velocities, per 1000 hours and per nautical mile, were determined for discrete altitude bands shown in Table 5. The same values were used for AGL and Mean Sea Level (MSL) altitudes. In many cases, the volume of data for AGL altitudes above 4,500 feet was insufficient for developing meaningful spectra.

Table 5: MSL and AGL altitude bands

Bands	**Altitude (ft)**
1	< 500
2	500 – 1,500
3	1,500 – 4,500
4	4,500 – 9,500
5	9,500 – 14,500
6	> 14,500

4.5.7 Flight phase definition

The analysis was confined to airborne phases between takeoff and landing, be it on land or water. Ferry and maintenance/training missions consisted of only one phase, incorporated in cruise 2. However, firefighting missions were divided into ten distinct phases, shown schematically in Figure 7. Figure 8 shows the time history of an actual flight with two fills and two drops. The criteria for phase separation are given in more detail in Table 6. Due to some rapid turnaround cycles, it was essential to leave out some of the cruise light and cruise heavy parts of the flight to avoid overlapping of the phases.

In previous analyses, buffers were built between flight phases to avoid their overlapping in the transition process. This resulted in a small part of the data being omitted from the analysis. In the present case, this could not be done without leaving out a large fraction of the data due to the large number of phases. For example, a firefighting mission with 20 fills would result in the analysis of 162 individual phases. Using a one-minute buffer between the phases could result in omitting 2.7 hours of flight data in one mission. Therefore, no buffers were built in for transitioning from one flight phase into another. Consequently, in some cases, elements of one phase affected the results of the neighboring phases.

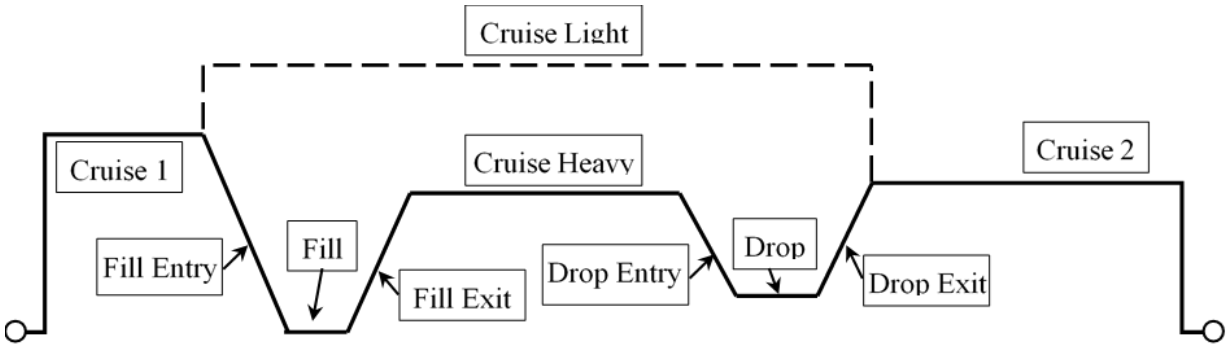

Figure 7: Flight phases for firefighting missions schematic

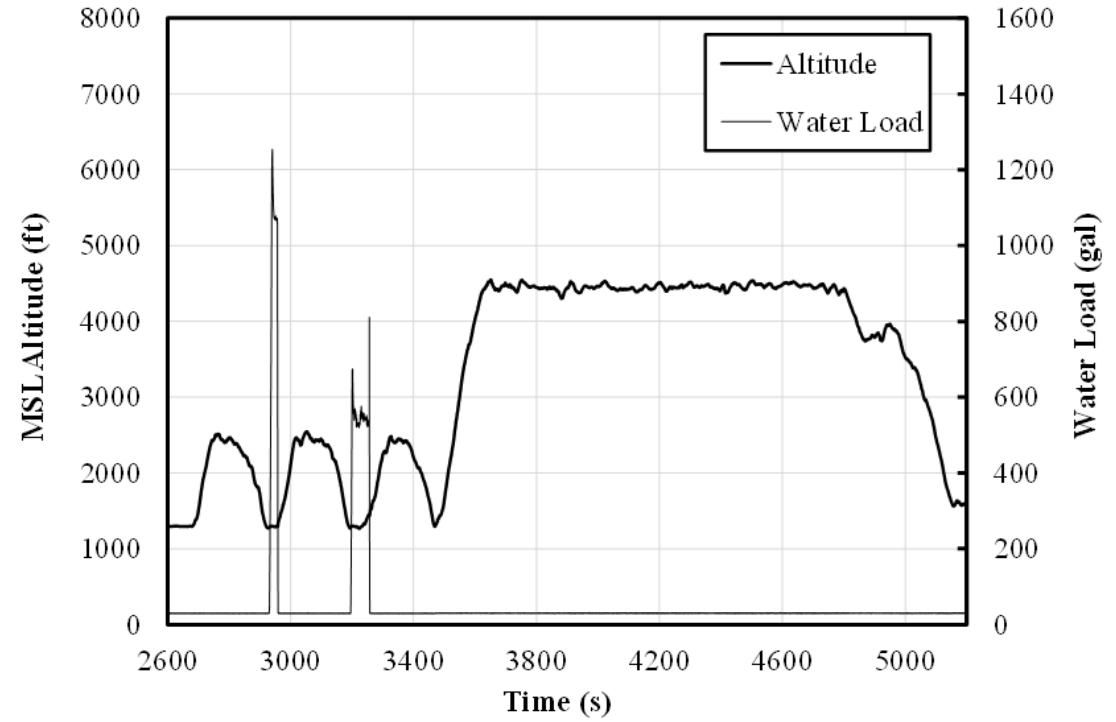

Figure 8: Flight time history for flight with two fills and two drops

4.5.8 Weight estimation

Determination of the derived gust velocities required knowing the instantaneous aircraft weight, which was not a recorded parameter. From Table 1, maximum takeoff weight after the first fill was assumed to be 47,000 pounds, including 15,000 pounds of water (i.e., 1,800 gallons @ 8.34 pounds/gallon). While this volume exceeded the total water capacity, it was not unusual to have this much onboard immediately at the end of the fill phase. The difference was assumed to be the aircraft weight, including fuel, at the start of the mission. Fuel burn rate was set at 0.56 pounds

per second. This corresponded to Specific Fuel Consumption (SFC) rate of 0.45 pounds per horsepower per hour for total power of 4,500 horsepower, slightly lower than 0.49 given in Majeed (2009). Fuel was assumed to be replenished at every landing. As the mission proceeded, the weight was adjusted based on the amount of water onboard and the fuel burn rate. This method resulted in "reasonable" time history of weight, although its accuracy is uncertain other than for firefighting missions.

Table 6: Flight phase separation criteria

Flight Phase	**Start**	**End**
Cruise 1	Start of flight plus 30 seconds	Start of first fill entry
Cruise 2	Start of flight plus 30 seconds for maintenance/training and ferry missions or end of last drop exit	End of flight minus 30 seconds
Fill Entry	One flap change before the start of the fill or 10 seconds	Start of fill
Fill	Initial water < 50 gal and change in water > 50 gal in one second and water level > 100 gal in three seconds and water level > 100 gal in five seconds and bay door is closed	Change in water < -10 gal over two consecutive half-seconds and water > 100 gal five seconds later and bay door is closed or fill probe retracting or 15 seconds after start
Fill Exit	End of fill	End of fill and one flap change or 10 seconds
Cruise Heavy (longer than 2 sec)	End of last fill exit	3 minutes or water drop more than 100 gallons 10 seconds ahead
Drop Entry	One flap change before the start of drop or 10 seconds	Start of drop
Drop	Opening of the bay door and water level changes more than 50 gals larger from 0.5 sec earlier to 1 sec later	Closing of the bay door and change in water level less than 5 gallons in two consecutive seconds
Drop Exit	End of drop	End of drop and one flap change or 10 seconds

Flight Phase	Start	End
Cruise Light (longer than 2 sec)	End of drop exit	3 minutes or water gain more than 100 gallons 10 seconds ahead

4.5.9 Derived gust velocities

Derived gust velocities were calculated from recorded normalized normal accelerations due to gusts.

$$U_{de} = \frac{\Delta n_z}{\bar{C}} \quad (1)$$

Where:

U_{de} = derived gust velocity (ft/s)

Δn_z = incremental vertical load factor (g)

The aircraft response factor, $\overline{C}$, was calculated from:

$$\bar{C} = \frac{\rho_0 V_e C_{L_\alpha} S}{2W} K_g \quad (2)$$

Where:

ρ_0 = 0.002377 slug/ft^3, standard sea level air density

V_e = equivalent airspeed (ft/s)

C_{L_α} = aircraft lift-curve slope (per radian)

S = wing reference area (ft^2)

W = instantaneous aircraft weight (lb)

K_g = $\frac{0.88\mu}{5.3+\mu}$, gust alleviation factor

μ = $\frac{2W}{\rho g \bar{c} C_{L_\alpha} S}$, reduced mass

ρ = air density at altitude from equation 3 (slug/ft^3)

g = 32.17 ft/s^2, acceleration of gravity

$\bar{c}$ = wing mean geometric chord (ft)

The outside air temperature and pressure were among the recorded parameters and were converted to the consistent units by the preprocessors. Therefore, the corresponding air density could be calculated from:

$$\rho = \frac{P}{\bar{R}T} \quad 3$$

Where:

P = static pressure (psf)

$\bar{R}$ = 1,716.3 ft-lb/slug-R, specific gas constant for air

T = absolute temperature (R)

From Etkin (1982), aircraft lift-curve slope, C_{L_α}, was determined as:

$$C_{L_\alpha} = C_{l_{\alpha,wb}}\left[1 + \frac{C_{l_{\alpha,t}}}{C_{l_{\alpha,wb}}}\frac{S_t}{S}\left(1 - \frac{\partial\varepsilon}{\partial\alpha}\right)\right] \quad 4$$

Where:

$C_{l_{\alpha,wb}}$ = wing lift-curve slope (per radian)

$C_{l_{\alpha,t}}$ = horizontal tail lift-curve slope (per radian)

S_t = horizontal tail area (ft^2)

S = wing area (ft^2)

$\frac{\partial\varepsilon}{\partial\alpha}$ = rate of change of downwash angle at the tail due to the wing (Dommasch, Sherby, & Connolly, 1967).

$$\frac{\partial\varepsilon}{\partial\alpha} \approx \frac{0.349 C_{l_{\alpha,wb}}}{\lambda^{0.3} A_r^{0.725}}\left(\frac{3\bar{c}}{l_t'}\right)^{0.25} \quad 5$$

Where:

λ = wing taper ratio

A_r = wing aspect ratio

$\bar{c}$ = wing mean geometric chord (ft)

l_t' = distance between the wing and the horizontal tail aerodynamic centers (ft)

From Roskam (2001), lift-curve slopes of individual lifting surfaces were found assuming thin airfoils with lift-curve slopes of 2π per radian according to:

$$\left(C_{l_\alpha}\right)_{\text{Wing or tail}} = \frac{2\pi A_r}{\sqrt{2+\left[4+A_r^2\beta^2\left(1+\frac{tan^2\Lambda}{\beta^2}\right)\right]}} \qquad 6$$

Where:

A_r = b^2/S, aspect ratio

b = span (ft)

β = $\sqrt{1-M^2}$, compressibility effect

M = V_t/a, flight Mach number

Λ = wing half-chord sweep angle (degrees or radian)

V_t = true airspeed (ft/s)

a = $\sqrt{\gamma \bar{R} T}$, local speed of sound (ft/s)

γ = 1.4, ratio of specific heat constants for air

5 Data presentation

5.1 Airframe usage

Statistical airframe usage information is given in appendix A. Table A-1 and Table A-2 show the list of tables and figures to follow. First, the results are presented for Ground-Air-Ground (GAG) cycles, followed by those for individual phases of firefighting flights. Results for ferry and maintenance/training flights are presented along with those of cruise 2 for firefighting missions.

5.1.1 Ground-air-ground usage

The number and some of the characteristics of the firefighting flight phases, as well as those of ferry and maintenance/training flights are shown in table A-3. The maximum altitudes for cruise 1 and cruise 2 of the firefighting flights were around 4,000 feet AGL. As discussed earlier, AGL altitudes were obtained from the difference between pressure altitude and ground elevation. Due to resolution of these parameters, the maximum AGL altitude for the fill phases was slightly negative, instead of zero. Most of the fill exit phases were cut off at 10 seconds, which explains the low maximum altitudes associated with these phases. The specifics of the individual phases of firefighting flights will be discussed in later sections. Finally, because of incomplete flights, flight phases that were shorter than two seconds, and/or cases that were dismissed for questionable data, the number phases do not match in this table.

Distribution of the number of flights by duration is shown in Figure A-1. Unlike the case of heavy airtankers, the longest flight durations were associated with firefighting operations (i.e., Fire Ops) with an average of 175.5 minutes. Understandably, the maintenance/training flights had the shortest duration.

Correlation of distance and duration for various missions are given in Figure A-2. It is clear from this figure that average flight speed was the highest for the ferry missions and the lowest for the firefighting missions. The longest firefighting mission lasted slightly less than six hours.

Maximum AGL and MSL altitudes can be compared in Figure A-3 and Figure A-4. In both cases, the highest altitudes were related to ferry flights. These results show that most of the flights remained below 12,000 feet AGL or 14,000 feet MSL altitudes. The latter was well below the aircraft's service ceiling of 20,000 feet.

Figure A-5 shows the number of flights by their number of fills and drops. Occasionally, multiple drops were performed per fill. Most flights had 1-20 fills and drops but it was not unusual to encounter missions with more than 20 fills and drops. This figure also includes the averages of fill time, drop time, water onboard, and water delivery per mission. It is obvious that the latter greatly exceeded the total delivered by a very large airtanker, although this was spread over a longer time. The amount of water delivered correlated with flight duration is given in Figure A-6. The data included in this figure indicates that approximately 5,800 gallons of water was delivered per flight hour. There was no direct correlation between the volume of water delivered and the flight duration.

Indicated airspeeds at takeoff and landing are shown in Figure A-7 and Figure A-8. The data used for these results included only those flights with reliable indicated airspeed. Corresponding

average indicated airspeeds were 84.4 KIAS and 61.5 KIAS. A minimum indicated airspeed of 58 KIAS was used to identify water landings. This corresponded to stall speed at 26,000 pounds with the flaps in the third detent. The vast majority of water landings were at or below this indicated airspeed. In a small number of cases the aircraft was slowed down below this airspeed during a fill which triggered a landing, missing the associate fill phase.

Figure A-9 shows the maximum vertical load factor at landing and coincident lateral load factor. Data from all flights was included in these results, regardless of the reliability of the indicated airspeed. Unavailability of the heading as a recorded parameter prevented understanding the source of the relatively large lateral load factor associated with a few ferry flights. However, the relatively large vertical load factor of 2.42 g for one of the firefighting flights was indeed due to a hard landing after a 4.2-hour mission. The remaining values did not reveal anything out of the ordinary.

The number of times the flaps were lowered into each detent are given in Table A-4 for each type of flight. This data pertains only to inflight flap deployments and does not include events before takeoff or after landing. This table also shows the average number of flap deployments per mission. It is obvious that the flaps were lowered and raised many more times per mission during firefighting flights due to multiple fills and drops. This data also shows that the first two flap detents were preferred for fills and drops, whereas the third detent was used mostly for landings.

5.1.2 Phase-specific usage

In presenting the usage results, cruise 1 and cruise 2 phases are shown next to each other for ease of comparison. The same logic is also used for cruise heavy and cruise light phases, as well as for fills and drops.

5.1.2.1 Cruise 1

Figure A-10 shows the correlation of distance and duration for cruise 1, which was specific only to firefighting missions. Based on these results, cruise 1 phases seldom lasted longer than two hours, with most being less than one hour. The corresponding distances were at most 200 nautical miles, with most being below 120 nautical miles. Maximum airspeeds averaged 175 KIAS and the average of the maximum altitudes was approximately 4,200 feet AGL. The latter can also be seen in Figure A-11 showing many of the phases clustered below 8,000 feet AGL.

To examine the phase-specific *V-n* diagrams, examination of the stall speeds and flap limitations is in order first. These limitations are shown in Table A-5 and Table A-6. Table A-5 is noteworthy that the vertical load factor limits for the flaps in the second detent cover a wider

range of values than those of any other flap setting. The stall speeds for two different weights are given in Table A-6. These values were extracted from various charts as seen in Bombardier Aerospace (1999). The upper weight limit is that of takeoff from water after a fill and is the absolute maximum weight in which the aircraft can be operated. The lower weight limit is the very lowest weight shown in the charts. Taking these limits into account, *V-n* diagrams were constructed for various flap settings at two different weights that were viewed as covering the majority of the flights. The subsequent *V-n* diagrams include only those cases with reliable indicated airspeed and also show a line at 10% above the V_{MO} for comparison.

The *V-n* diagram for cruise 1 with retracted flaps is presented in Figure A-12. The vertical load factors remained well below the limits. However, the indicated airspeed surpassed the maximum value of 187 KIAS in a noticeable number of cases, although never by more than 10%.

Figure A-13 shows the *V-n* diagram for cruise 1 with the flaps in the first detent. It is obvious that the vertical load factors remained more or less within the prescribed limits, but the maximum indicated airspeeds were again exceeded in many cases. Closer examination of these points revealed that they were mostly associated with flaps transitioning from the retracted position to the first detent and they did not last very long.

Cruise 1 cases with the flaps in the second detent generally indicated approaching water to fill. Again, the vertical load factors remained well below their limits. The indicated airspeeds remained close to V_{MO}, but slightly exceeded it in a few cases. There were too few cases of cruise 1 with the flaps in the third detents to result in a meaningful *V-n* diagram.

5.1.2.2 Cruise 2

The analysis code grouped cruise 2 phases with ferry and maintenance/training missions, although they were labeled separately. Examination of cruise 2 results starts with correlation of distance and duration, as presented in Figure A-15. Naturally, ferry missions lasted much longer than cruise 2 phases of firefighting flights, which seldom lasted longer than two hours. However, the airspeeds among the three different missions were comparable, with those of maintenance/training flights being slightly lower than the others. Also, average flight speed was slightly higher in cruise 2 than in cruise 1.

Maximum AGL altitude and corresponding distance are shown in Figure A-16. Much like in the case of cruise 1, cruise 2 phase of firefighting flights were never flown higher than 12,000 feet with most below 8,000 feet. Naturally, ferry missions covered longer distances, yet even their maximum altitudes never exceeded 16,000 feet AGL and mostly below 12,000 feet.

For clarity, the *V-n* diagrams of the firefighting flights were separated from those of other missions. These results are only for those cases with reliable indicated airspeed. The results with the flaps retracted are shown in Figure A-17. The maximum and minimum vertical load factors remained within the prescribed limits except for one firefighting case (-1.045 g at 143.5 KIAS) and one ferry case (+3.174 g at 150.6 KIAS) where the values were slightly out of bounds. However, the maximum airspeeds exceeded the limits for this flap setting in a noticeable number of cases. These exceedances were not limited to any specific mission. Nonetheless, the maximum indicated airspeeds remained less than 10% above V_{MO}.

The airspeed trends for cruise 2 with flaps in the first detent, shown in Figure A-18, were similar to those of cruise 1. However, in a handful of firefighting cases, the maximum vertical load factors were beyond the +2.0-g limit. Again, closer examination of these cases proved them to be associated with the flaps being in transit between the second detent and another setting. As a reminder, the allowable maximum load factors were larger for retracted flaps (+3.0 g) and the second detent (+3.25 g). The indicated airspeed exceeding V_{MO} and beyond appeared to be real and the examination of the original flight files did not reveal anomalies bringing into question the integrity of the recorded data.

Figure A- 19 shows the *V-n* diagrams for cruise 2 with the flaps in the second detent. Over-speeding was evident in a number of cases, although fewer than in the previous cases. There were a few cases of ferry and maintenance/training flights that showed relatively large load factors for the given airspeeds. Examination of the individual flight files proved these to be indeed the case. Based on the available information, the causes could only be speculated.

Finally, the results from the third flap detent are given in Figure A-20. This flap setting was used invariably for landings. The over-speeding associated with firefighting cases persisted.

5.1.2.3 Cruise heavy

Cruise heavy phases constituted flights between the fills and the drops and were limited to a maximum of 30 minutes by the analysis codes. The correlation of distance and duration for these phases is shown in Figure A-21, which shows the effect of the 30-minute limit. Average duration was 6.3 minutes at average airspeed of 151 KIAS. The vast majority of these phases lasted far less than the limit. The average airspeeds were slightly lower than those of cruise 1 and cruise 2 and the altitudes remained below 5,000 feet AGL for the most parts, as indicated in Figure A-22.

The probability of the amount of water onboard during cruise heavy phases is given in Figure A-23. Referring to the earlier anatomy of fills and drops, the volume of water at the start of the

phase could be higher than the load that was delivered. The numbers shown on these figures represent the averages of the maximum amount of water, the average amount of water during the phase, and the water load at the mid-point of the phase. Good correlation of the latter two values confirms the reliability of indicated volume.

The *V-n* diagrams for the cruise heavy phases for various flap settings are shown in Figure A-24, Figure A-25, and Figure A-26. In many instances, the flaps were not retracted in between the fills and the drops resulting in more cases with the flaps deployed. Some of the points shown in these figures might indicate the vertical load factor due to water impact, since the method of identifying the start and the end of the fill phases contains uncertainties. This is especially true for lower airspeeds with the flaps in the second detent. At higher speeds, when the aircraft were definitely inflight, there were very few cases in which the vertical load factors was in excess of the aircraft limits.

As indicated in these figures, incidents of over-speeding were not uncommon, especially when the flaps were lowered into the first detent. Most of these were related to the flaps transitioning from retracted to the second detent, passing through the first, prior to airspeed reduction for drop entry. It should be noted that the airspeed limit for the first and the second detents were the same.

5.1.2.4 Cruise light

Cruise light phases were the counterparts of cruise heavy and represented flights between the drops and the fills when the aircraft were roughly 12,000 pounds lighter. Only in a handful of cases did these phases last longer than 30 minutes, as shown in Figure A-27. The average airspeeds, at 165 KIAS, were slightly higher than those of cruise heavy phases. These phases lasted an average of 4.2 minutes and the maximum altitudes seldom reached above 5,000 feet AGL, as indicated in Figure A-28.

Figure A-29, Figure A-30, and Figure A-31show the *V-n* diagrams for cruise light phases. Frequent over-speeds can be seen in all three figures, as well as exceeding the maximum allowable vertical load factor in many cases with the flaps in the first detent. Cruise light and cruise heavy phases were the only ones in which the maximum indicated airspeeds exceeded V_{MO} by more than 10%, sometimes significantly more.

5.1.2.5 Fill entry

The probability of the maximum indicated airspeed for the fill entry phase is shown in Figure A-32. The small standard deviation of the airspeed indicates that these phases were flown with increased precision relative to cruise phases. This can also be seen in Figure A-33 that shows the *V-n* diagram for these phases, where no over-speeding was detected. However, many large

vertical load factors were recorded at low speeds, which with all certainty were due to water impact at the start of the fill phase. Fill entries were not performed with the flaps in other than the second detent.

5.1.2.6 Fill

Figure A-34 shows the probability of the maximum indicated airspeed during the fill phase. Average indicated airspeeds were 79.1 KIAS, well below the maximum allowable of 90 KIAS. Also, the probability of the duration of the fill phase is given in Figure A-35. Average duration was approximately 12 seconds, with many fills lasting much less. The analysis code allowed a maximum of 15 seconds for this phase.

During the fill phase, the aircraft were subject to relatively large vertical load factors from water impact. The fill probes are located just behind the step on the keel. In many cases the keel contacted the water prior to the probes. Therefore, most of the load factors shown in Figure A-36 were not "flight loads." It was impossible to separate the flight loads from water impact loads. In this figure, V_{MW} designates the maximum water speed of 90 KIAS. It is clear that there were very few cases where the aircraft were flown faster, and even then, by a very small margin. Fill phases were not flown in other flap settings.

5.1.2.7 Fill exit

The probability of the maximum indicated airspeed during the fill exit phases is shown in Figure A-37. While the average of the maximum airspeed in this phase was a relatively low 85 KIAS, it varied over a much broader range of values as indicated by its standard deviation. Generally, the aircraft were in their heaviest state at the start of the fill exit.

Figure A-38 shows the normal probability distribution and the cumulative probability for maximum, average, and mid-flight water load during fill exit phases. Generally, the maximum water onboard, which occurred at the very start of the fill exit, was higher than the rated water tank volume. However, the average water load and the water onboard at the middle of this phase were in agreement and were slightly lower than the maximum tank volume. Interestingly, these averages were almost 100-200 gallons higher than those detected during the cruise heavy phases that were discussed earlier. The difference indicated that excess water was still being shed from the aircraft during the fill exit phase.

Figure A-39 shows the *V-n* diagram for fill exit phases. Flaps were invariably in the second detent and the maximum airspeed was never exceeded. Again, the larger vertical load factors at lower speeds were likely due to overlapping of this phase and the end of the fill phase where the aircraft was still in contact with water.

5.1.2.8 Drop entry

The drop entry phases could be identified with more certainty than the flight phases associated with the fill phase from the combination of the bay door and flap signals. The start of this phase was marked by one flap change or 10 seconds before the start of the drop phase. The end was marked by the opening of the bay doors. Therefore, these phases were flown exclusively with the flaps in the second detent.

The probability of the maximum indicated airspeed during the drop entry phase is shown in Figure A-40. The average value of 120 KIAS was consistent with that used during the drop phase. However, in a noticeable number of cases, the maximum airspeed corresponding to the flap setting was exceeded, as indicated in Figure A-41. The maximum vertical load factors remained within the prescribed limits.

Average water onboard was 1,422 gallons that was only 20-30 gallons lower than the average during the cruise heavy phases. This seemed to support the earlier statement that water was still being shed from the aircraft during the fill exit phases.

5.1.2.9 Drop

The average of the maximum indicated airspeed during the drop phase was slightly lower than that of the drop entry, with comparable standard deviation, as evident from Figure A-42. This phase was the shortest of all at an average duration of 3.25 seconds, indicated in Figure A-43. The rate of water delivery in this phase was very comparable with that of a heavy airtanker which would release approximately 3,500 gallons of retardant in about 8 seconds.

During the drop phase, average AGL altitude was 175 feet, as shown in Figure A-44. However, the standard deviation was greater than the average. Both values must be viewed with some skepticism owing to the lack of fidelity in the terrain elevation and the pressure altitude, which were discussed earlier. It was not uncommon for the AGL altitude to be *negative* during the dop phase, some of which can be seen in this figure.

Usually, drops were initiated with the flaps in the second detent. However, at the end of the drop, the flaps were retracted quickly to the first detent, sometimes before the completion of the drop. One example is shown in Figure 9 where the flaps are moved from the second detent to the first in the middle of the drop. Consequently, in about 15% of the cases, data was available for flaps in the first detent as well, even though the flight profile was that for the second detent. This, along with the typical peak in the vertical load factor near the end of the drop resulted in exceeding the +2.0-g limit load factor when the flaps were in the first detent. The *V-n* diagrams

for the drop phase are shown in Figure A-45 and Figure A-46 for flaps in the first and the second detents, respectively.

Figure A-45 shows that in many events, the limits on indicated airspeed and vertical load factor were exceeded greatly. Most of the exceedances, especially in vertical load factor, were associated with the end of the drop phase after the release of the water load and with the flaps in transition between the two detents. In fact, Figure A-46, which represents about 85% of the cases, shows little exceedance in vertical load factor, but much more frequent surpassing of the associated maximum indicated airspeed. In a handful of cases, the indicated airspeed was in excess of 10% above the limit.

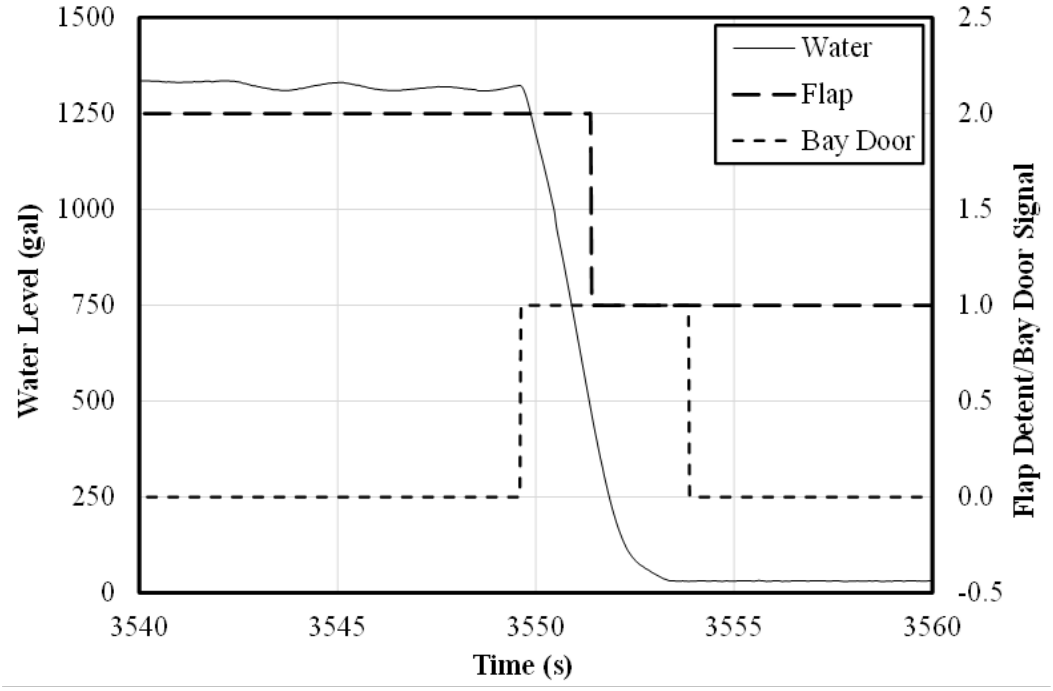

Figure 9: Example of early flap retraction during drop phase

Consistent with past observations, a relatively large increase in the vertical load factor accompanied most drops. An example is shown in Figure 10 where the vertical load factor increased by more than 1g during the drop. This behavior is not only due to the sudden loss of weight, which at best would result in a +0.30-g change in the vertical load factor.

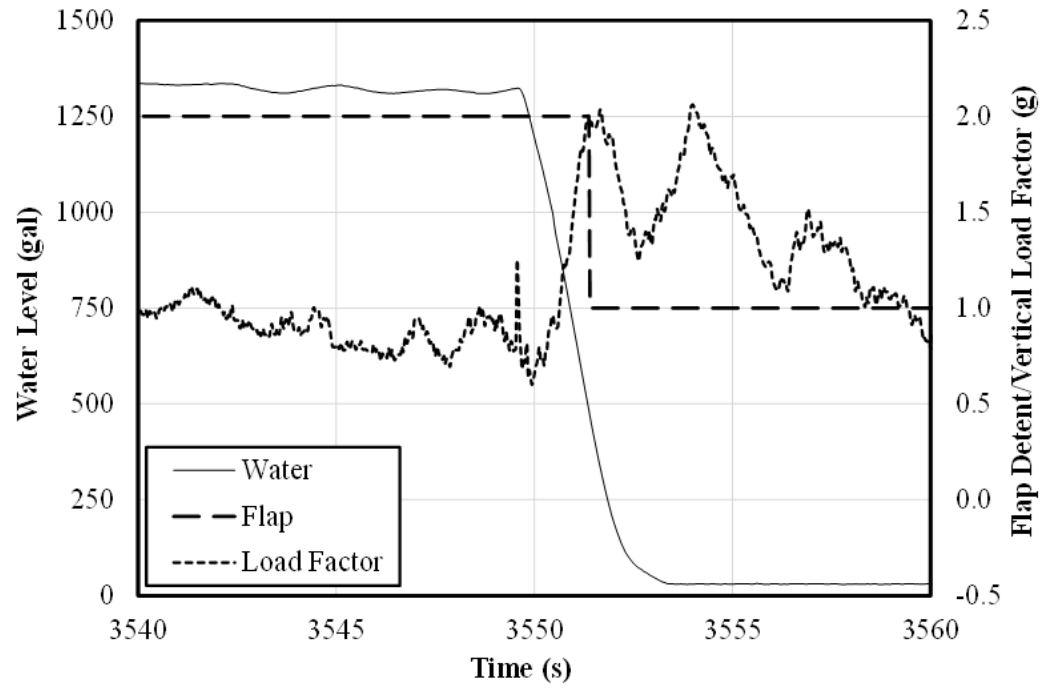

Figure 10: Impact of water release on vertical load factor

Additional contributing factors could be aerodynamic interference, sudden change in the center of gravity location, or crew action. In any event, the additional load factors almost invariably fall in the maneuver load category because they last longer than two seconds.

5.1.2.10 Drop exit

Drop exit phases lasted anywhere from one time step (1/32 second) to the maximum duration limit of 10 seconds. Maximum altitudes seldom exceeded 1,000 feet AGL. Probability of maximum indicated airspeed in drop exit phases is shown in Figure A-47. While the average was close to those of drop entry and drop phases, the standard deviation was quite larger. Therefore, it was not unusual to observe maximum indicated airspeeds more than 140 KIAS. This can also be seen in Figure A-47 and Figure A-49. For reasons explained in the previous section, drop exits entailed having the flaps in the first or the second detents. Vertical load factors did not reach the heights of the previous two flight phases, but over-speeding was common. Due to the short 10-second duration limit, it is unlikely that the over-speeding cases were related to overlaps with cruise light phases.

5.2 Fight loads

The results of the flight loads analyses and the related exceedance spectra are shown in Appendices B and C. Appendix B is devoted to the results presented by AGL altitude bands.

These include flight loads spectra from various firefighting phases and for ferry and maintenance/training missions. The results pertaining to MSL altitude bands are contained in Appendix C. In the latter case, the emphasis is placed on cruise phases that were carried out over a wider range of altitude bands.

5.2.1 Results by AGL altitude

Appendix B contains the figures and tables associated with flight loads arranged by AGL altitudes. The list of tables is given in Table B- 1, followed by the list of figures in Table B-2.

Table B-3 shows the total distance and duration associated with various phases of firefighting missions, as well as those of ferry and maintenance/training flights. According to these results, the longest flight durations were those of cruise heavy and cruise light phases, followed by ferry missions. However, the former two flight phases were punctuated by repeated fills and drops. It is noteworthy that the figures given in this table may not match exactly those in the subsequent sections for a number of reasons including removal of untrustworthy data and roundoff errors. However, the differences are extremely small.

The flight durations and distances associated with cruise phases, including ferry and maintenance/training mission are shown in Table B-4 through Table B-9. This information is presented side-by-side to facilitate the comparison of these phases. It is clear from Table B-4 and Table B-5 that cruise 1 and cruise 2 phases were flown mostly below 9,500 feet AGL (i.e., altitude bands 1-4). However, cruise heavy and cruise light phases, shown in Table B-6 and Table B-7, were flown mostly below 4,500 feet AGL, with the majority below 1,500 feet AGL (75% and 83% respectively). Also, it was noted that cruise light phases were flown at a slightly higher average speed than cruise heavy phases, while they covered a shorter total distance.

The results from ferry missions are presented in Table B-8. As expected, ferry missions were flown at much higher altitudes, reaching 14,500 feet AGL. Very little time was spent above this altitude in any of the flights. Consequently, the exceedance spectra that will follow was generally void of information in this region. Very little data was available for maintenance/training flights, as shown in Table B-9 and most flights were limited to lower altitude bands.

The cumulative occurrences of incremental gust and maneuver load factors for cruise 1, for various AGL altitude bands, are shown in Figure B- 1 and Figure B-2. Each figure shows the results per 1000 hours and per nautical mile. The amount of data from the highest two altitude bands was extremely limited, resulting in much scatter in the results. However, the results from the other altitude bands show the dependence of the frequency of occurrence on altitude. This

can be seen more clearly in the maneuver loads spectra of Figure B-2. The magnitudes and the frequencies of occurrence were consistent with past observations. Cruise 1 phases showed the largest difference in the frequency of occurrence of positive and negative incremental maneuver load factors at the lowest altitudes compared with other cruise phases.

Similar results for cruise 2 flight phases are shown in Figure B-3 and Figure B-4. However, in this case, the dependence of the gust loads on altitude is somewhat clearer than in the case of cruise 1 phases with a slightly higher frequency of occurrence. The maneuver loads spectra, given in Figure B-4, showed similar trends with slightly lower frequencies of occurrence but similar magnitudes.

Figure B-5 and Figure B-6 show the cumulative occurrences of incremental gust and maneuver load factors for cruise heavy phases. As discussed earlier, these phases were flown almost exclusively below 4,500 feet AGL with a few cases above this altitude. This is evident in Figure B-5 where the results are concentrated in these altitude bands. The frequency of occurrence of the gust loads was lower than those of the cruise 1 and cruise 2, perhaps owing to the higher weights and slower flight speeds. The maneuver load factors were also slightly smaller than those of other cruise phases. These were in contrast with cruise light phases where incremental gust and maneuver load factors were larger and more frequent, as shown in Figure B-7 and Figure B-8. For example, incremental gust load factor of +1.0 g and larger were more frequent by an order of magnitude for cruise light phases. The same was true to incremental maneuver load factors. In both cases, the effect of AGL altitude on maneuver load factors was more pronounced than on gust load factors.

The results for ferry flights are shown in Figure B-9 and Figure B-10. These missions were flown over a wide range of altitudes. Therefore, the correlation of the frequency of occurrence of the load factors with AGL altitudes is more prominent in their cumulative occurrence of the incremental gust load factors. Also, these missions did not entail as much maneuvering as firefighting flight phases did. Consequently, their incremental maneuver load factors spanned over a much narrower range than those of other cruise phases.

The cumulative occurrences of incremental gust and maneuver load factors for the maintenance/training flights are shown in Figure B-11 and Figure B-12. These results are based on a very limited amount of data and AGL altitude bands below 9,500 feet AGL. In lower three altitude bands, good correlation can be seen with the gust loads results from ferry flights. At higher altitude bands, scarcity of the recorded data rendered the results unreliable.

Durations and distances associated in various AGL altitude bands for fill entry, fill, and fill exit phases are summarized in Table B-10, Table B-11, and Table B-12. It is evident that all three phases were almost exclusively flown in the lowest altitude band. Fill entry and fill exit phases were limited to a maximum duration of 10 seconds, and therefore, their total times and distances are very similar. Also, as discussed earlier, touchdown and liftoff points of these phases could not be determined with certainty. Therefore, the load factors associated with these phases include some from water impact.

Cumulative occurrences of incremental gust and maneuver load factor for fill entry are shown in Figure B-13 and Figure B-14. The dominance of the positive gust load factors is an indication of the influence of water impact loads during this phase, much as it was shown in the usage results. Also, while the maneuver load factor spectra are given in Figure B-14, their reliability can be legitimately questioned due to the factors discussed earlier.

Figure B-15 shows the cumulative occurrence of incremental vertical load factor during fill phases. In this case, the load factors were almost entirely due to contact with water, as opposed to “flight” loads. Therefore, their separation into gust and maneuver loads would not be meaningful, so the results in this figure are based on all load factors encountered during the fill phase. The magnitudes and the frequencies compare well with those of the fill entry phase and both are much larger than those of the cruise phases. However, in this case, the load factors are more akin to landing impact loads.

The results from the fill exit are shown in Figure B-16 and Figure B-17. Cumulative occurrences of the incremental gust load factors bear some resemblance to those of fill entry, although with lower frequencies and magnitudes. It is likely that the lower magnitudes are due to the higher wing loading during this phase. Figure B-17is given here for the sake of completeness. Obviously, no conclusion can be drawn from this figure regarding cumulative occurrences of the incremental maneuver loads related to fill exit phases.

Total distances and durations for drop entry, drop, and drop exit phases are summarized in Table B-13, Table B-14, and Table B-15. Unlike the fill cases, these phases could be identified accurately from a combination of the bay door signal, water tank level, and flap states. It is clear from this data that the majority of these phases were flown below 500 feet AGL. The inclusion of the data from other than the lowest altitude band was only due to uncertainties in the terrain elevation. It should also be noted that the scarcity of recorded data in the third altitude band rendered the related results somewhat questionable.

The cumulative occurrences of the incremental gust load factor for drop entry are shown in Figure B-18. Consistent with the earlier discussion of the *V-n* diagram for this flight phase, the gust load factors were found to be much larger and more frequent for this phase than those presented earlier. At incremental value of +1.0 g, the cumulative occurrences were one order of magnitude more frequent than those of fill entry and two orders of magnitude larger than those of cruise phases. Also, cumulative occurrences of incremental maneuver load factors, given in Figure B-19, revealed higher frequencies of occurrence than those of cruise phases, especially associated with larger load factors.

Similar results were obtained from the drop phases, shown in Figure B-20 and Figure B-21, but with significant magnification in magnitudes and frequency of occurrence. The incremental gust load factors as large as +2.5 g were detected, as evident from Figure B-20. At incremental gust load factor of +1.0 g, the cumulative occurrence for the lowest altitude band was more than three times the order of magnitude of the same during cruise 1 phase. The same was true for incremental maneuver load factors presented in Figure B-21. Both sets of results were quite consistent with those from other airtankers during the drop phase. Also, as discussed earlier, the positive maneuver load factors shown in Figure B-21 were mostly driven by the spike in this parameter associated with the drop phases. While this is seen in data from all types of airtankers, it is unclear whether the increased load factors are due to crew action or some external cause such as aerodynamics or changes in the location of the aircraft center of gravity.

Finally, the results from the drop exit phases are shown in Figure B-22 and Figure B-23. The frequency of occurrence of the incremental gust load factors were similar to those of the drop entry phase, except for more frequent and larger negative values. Again, the frequency of occurrence was about two orders of magnitude larger than those of cruise phases. The same was true for the maneuver load factors shown in Figure B-23. The maneuver load factors during the drop exit phases were second in magnitude to those of the drop phases. This behavior was also in agreement with previous observations of other airtankers.

5.2.2 Results by MSL altitude

Flight loads spectra were also considered when grouped by MSL altitude bands. The results of this analysis are presented in Appendix C. The results discussed in this section are limited to those flight phases where wider ranges of altitude bands were represented. Therefore, this discussion does not include the results from phases directly connected to fills and drops that were flown very close to the terrain. Table C-1 and Table C-2contain the lists of tables and figures that are included in the appendix, respectively.

Table C-3, Table C-4, Table C-5, and Table C-6 show a summary of durations and distances flown in various cruise phases, while similar results for ferry and training/maintenance flights are given in Table C-7 and Table C-8. The totals shown in these tables differ slightly from those presented in Appendix B due to exclusion of data that was deemed unreliable from various analyses and some roundoff error. Nonetheless, the largest difference between the two sets is still less than 1.5%.

The results shown here indicate that these phases were flown over a wide range of MSL altitude bands reaching 14,500 feet. However, this was more a reflection of the wide range of terrain elevations over which these missions were conducted. Ferry flights were the only missions that were flown in altitude bands above 14,500 feet, as shown in Table C-7. Even then, the amount of time spent there was only 1.2% of total ferry flight time. Consequently, in the flight loads spectra that follow, results from above 14,500 feet are not statistically reliable.

Flight loads spectra from cruise 1 are shown in Figure C-1 and Figure C-2. Cumulative occurrences of incremental gust load factors in Figure C-1 show the same trends as those expressed by AGL altitude bands. However, whereas the altitude dependence on the frequency of the load factors was somewhat apparent in the latter case, dependence on MSL altitude was not clear in this case. Likewise, the dependence of the incremental maneuver load factor on AGL altitudes was more pronounced than on MSL altitude that is presented in Figure C-2. Nonetheless, in both cases, maneuver load factors proved more sensitive to altitude than did the gust loads.

Cumulative occurrences of incremental gust and maneuver load factors for cruise 2 are shown in Figure C-3 and Figure C-4. Unlike their AGL counterparts, presented in Figure B-3 and Figure B-4, these results are void of any dependence of the load factors on MSL altitude, especially in the case of the gust load factors. The maneuver load factors do show such a dependence weakly, but not in as pronounced a manner as was present in Figure B-4.

The same trends can also be observed for other cruise phases, shown in Figure C-5 through Figure C-8. In Figure C-5 and Figure C-7, the cumulative occurrences of incremental gust load factors from all altitude bands appear coincident, although considerably different between cruise heavy and cruise light phases. The same is true for maneuver loads spectra shown in Figure C-6 and Figure C-8.

Even in the case of ferry flights that covered a wider range of altitudes, the dependence of the frequency of occurrence of the load factors on MSL altitude was not very clear. This can be observed clearly in Figure C-9 and Figure C-10.

Finally, the flight loads spectra for maintenance/training flight are presented in Figure C-11 and Figure C-12. Again, these results were based on a very limited amount of data, preventing the drawing of any definitive conclusions.

5.2.3 Comparisons with other aircraft

In Appendix D, flight loads spectra are compared among flight phases and with other operations. In the interest of brevity, only cumulative occurrences per 1000 hours are shown and discussed. In addition, in the case of CL-415, only airborne phases are presented to eliminate any influence from water impact loads associated with fill entry, fill, and fill exit phases. The figures to be discussed are summarized in Table D-1.

Cumulative occurrences of incremental vertical gust load factors for various flight phases and missions are shown in Table D-1. This figure shows the results for all altitude bands combined. Also, for clarity, the results from the phases related to drops are shown separately. In the first part of this figure, results are compared from different cruise phases. Ferry and maintenance/training missions are included in this part due to their similarity with cruise phases. This figure shows clearly that the highest frequency of occurrence of the vertical gust load factors were in conjunction with cruise light phases, in all likelihood due to the lower wing loadings and slightly higher flight speeds. The lowest frequencies occurred during cruise heavy phases and ferry missions. This could be attributed to the higher wing loading of cruise heavy phases and the higher overall altitudes of the ferry missions.

In the second part of Table D-1, cumulative occurrences of incremental vertical gust load factors are compared among drop entry, drop, and drop exit phases. This figure also shows the results from ferry missions for reference. It is evident from this figure that the drop phases involved the largest load factors, with two to three orders of magnitude in frequency relative to ferry missions. This was consistent with previous observations (Rokhsaz et al. (2014); Rokhsaz et al. (2011); Rokhsaz et al. (2026); Rokhsaz & Kliment (2016)). It was also noted that the positive load factors were more frequent than the negative load factors, whereas they were equally represented in cruise phases.

Cumulative occurrences of incremental maneuver load factors are compared among flight phases in Figure D-2. Again, for clarity, flight phases surrounding the drop are shown separately in

comparison with ferry missions for reference. Much like in the previous case, cruise light phases showed the highest frequency of occurrence of the maneuver load factors, while ferry missions had the fewest. The other cruise phases and the maintenance/training missions occurred with almost equal magnitude and frequency. However, maneuver load factors, shown in the second part of this figure, occurred with significantly large magnitude and frequency during the drop, followed by the drop exit phases. At the incremental load factor of +1.0 g, maneuver load factors from the drop phases were more than four orders of magnitude more frequent than those of ferry flights. The higher frequencies and magnitudes were consistent with those of other airtankers, although they were both quite larger in this case. However, it should be noted that these phases constituted a very small fraction of the total flight time.

The CL-415 is a completely different design from other airtankers or civilian operations that were examined earlier. Therefore, it was difficult to find a single "similar" aircraft to which its flight loads spectra could be compared. The aircraft could be considered as a next-generation airtanker but was substantially lighter than BAe-146 and RJ-85 (2026) with flight profiles that were vastly different. Agricultural aircraft that were addressed in Rokhsaz and Kliment (2016) were flown with flight profiles somewhat similar to that of CL-415, with many turns and much low-level maneuvering, but were significantly lighter and were subject to much more gradual changes in aircraft weight. Single-Engine Airtankers (SEATs) (Rokhsaz & Kliment, 2016) were subject to large in-flight changes of weight but performed only one or two drops per mission. Finally, the Aerial Supervision Module (ASM)/lead aircraft (Kliment, Rokhsaz, & Menon, 2017) had flight profiles most similar to that of CL-415 without carrying a water load. Therefore, in the next two figures, flight loads spectra from CL-415 are compared with those of all of the above aircraft. It should be noted that on the agricultural, the SEATs, and the ASM/lead aircraft the data was collected at 8 Hz. Rokhsaz and Kliment (2019) showed that this could lead to slightly lower frequencies of occurrence of the gust load factor, but maneuver load frequencies remained unaffected.

Cumulative occurrences of incremental vertical gust load factors are compared in Figure D-3. Except for the agricultural operations, all data was obtained from aerial firefighting missions. Also, to prevent water impact loads from affecting the CL-415 spectra, the results from fill entry, fill, and fill exit phases were excluded for this comparison. It is obvious from this figure that the gust loads had the same frequency and magnitude as those of the ASM/lead aircraft that had very similar flight profiles and were flown in the same environment. The two aircraft also had similar wing loadings and were flown in the same range of altitude for long periods. On the other hand, the lowest frequencies were associated with the BAe-146/RJ-85 and PZL-M18 used for

agricultural operations. The former could be attributed to the much larger wing loading and the fact these aircraft were in cruise altitudes over most of their flights. The lower cumulative occurrences of the incremental gust load factors for the SEATs and the agricultural operations were puzzling.

Likewise, Figure D-4 shows the cumulative occurrences of incremental maneuver load factors for the five operations. The frequency of occurrence agreed well with those of ASM/lead aircraft, especially at higher values. Again, the lowest frequencies were from the BAe-146/RJ-85 that typically spent a small part of their flight profiles in the fire zone and were flown in cruise phases most of the time with little need for maneuvering.

5.3 Derived gust velocities

The results of the derived gust velocities are contained in Appendix E. Derived gust velocities were determined for all phases except those where the load factors contained water impact loads. They were also determined for ferry and maintenance/training missions. Results presented in this appendix were established per nautical mile and placed in AGL and MSL altitude bands where the aircraft were flown over a wide range of altitudes. Finally, these results are based on estimated aircraft instantaneous weights that may entail large uncertainties for ferry and maintenance/training missions.

Cumulative occurrences of derived gust velocities per nautical mile for cruise 1 phases are shown in Figure E-1 and Figure E-2. The first figure shows clearly how the frequency of occurrence of the derived gust velocities correlated well with AGL altitude bands. Comparing the two figures reveals that much of the results that appeared in the lowest AGL altitude band were distributed among the second and third lowest MSL altitude bands. This led to fewer occurrences per altitude band in the latter case.

Results for cruise 2 phases are given in Figure E-4 and Figure E-5. These results bear the same trends as those of cruise 1 phases, namely better correlation with AGL altitude bands. However, in this case, the gust velocities from the lowest MSL altitude band are more prominently present. In terms of frequency of occurrence, the results from cruise 1 and cruise 2 were very similar, although the magnitudes were slightly larger for the former, especially in the lower altitude bands.

Figure E-5, Figure E-6, Figure E-7, and Figure E-8 show the cumulative occurrences of the derived gust velocities for cruise heavy and cruise light phases, respectively. Among the cruise phases, cruise heavy and cruise light phases were flown at the lowest altitudes. Therefore, ample

data was available for both in the lowest altitude bands. The magnitude and the frequency were the largest for these phases. The magnitude of the derived gust velocity depended directly on the aircraft weight, which was estimated for these flights. Therefore, the agreement in magnitudes between cruise heavy and cruise light phases indirectly validates the weight estimation method for the firefighting missions.

The flight phases surrounding the drop were flown at very lowest AGL altitudes. Therefore, for these phases, the results are presented only based on their AGL altitudes. Figure E-9, Figure E-10, and Figure E-11show the cumulative derived gust velocities for drop entry, drop, and drop exit phases. Consistent with the gust loads spectra that were discussed earlier, these results show these phases were flown in the lowest altitude bands. The inclusion of data from other altitude bands was only due to uncertainties related to terrain elevation. Cumulative occurrences of the derived gust velocities for these three phases proved to be larger and more frequent than those of cruise phases by as much as three orders of magnitude. However, this was true only for the larger values of the derived gust velocity. At smaller values close to the dead band, the cumulative occurrences for these phases were similar to those of cruise phases.

By their nature, ferry flights covered the widest range of altitudes. The cumulative occurrences of their derived gust velocities are shown in Figure E-12 and Figure E-13. Surprisingly, despite good representation from all altitude bands, their correlation with MSL altitude bands is much less evident than with AGL altitude bands. Obviously, the results for the lowest AGL altitude band pertains to flight times immediately after takeoff or before landing. Again, the data from the lowest AGL altitude band was dispersed among the second and the third MSL altitude bands with little representation in the first. In general, the distribution of magnitude and frequency of the derived gust velocities from ferry flight compared well with those of cruise 1 and cruise 2.

Finally, the results from the maintenance/training missions are given in Figure E-14 and Figure E-15. It should be noted that these results are based on very few hours of flight time and did not span over a wide range of altitudes. Again, clear correlation of the results with AGL altitude bands is evident in Figure E-14, while Figure E-15 shows somewhat of the dependence on MSL altitudes. These figures also show that the occurrences of derived gust velocities were more frequent in these missions than in ferry flights although the magnitudes were a little smaller.

6 Conclusions and recommendations

6.1 Conclusions

In-flight recorded data from four CL-415 airframes were used for airframe usage and flight loads analysis. Missions were of three categories: aerial firefighting, ferry, and maintenance/training missions. Firefighting flights were further divided into ten individual phases. Results were extracted and reported for each flight phase and for ground-air-ground cycles where appropriate. The data amounted to just over 4,700 hours of flight operations.

6.1.1 Airframe usage

The longest flights were the firefighting missions in which the average duration was 175.5 minutes, almost four times as long as those of heavy airtankers. The longest firefighting mission lasted almost six hours. Firefighting missions with more than 20 fills and drops were not unusual. On average, 5,500 gallons of water was delivered per flight hour. Maximum altitudes seldom exceeded 14,500 feet with most of the flights below 12,000 feet AGL or 14,000 feet MSL. No flight near the service ceiling of 20,000 feet was detected.

In the absence of any other indicator, water landings could be estimated only based on the airspeed. This led to the overlapping of the some of the flight phases surrounding fills and inclusion of water impact loads during these phases. Such water impact loads were shown to be significant.

Most cruise 1 and cruise 2 phases were flown well below the aircraft service ceiling and lasted less than one hour. Vertical load factors remained within the prescribed limits, but the maximum operating airspeeds for the corresponding flap settings were surpassed although by no more than 10%. The over-speeding cases were observed in all three mission types.

Cruise heavy and cruise light phases lasted an average of 6.3 minutes and 4.3 minutes, with average airspeeds of 151 KIAS and 165 KIAS, respectively. In most cases, vertical load factors exceeding the corresponding flap settings were related to flaps transitioning between two detents. Maximum allowable load factor was exceeded repeatedly, especially during cruise light phases with the flaps in the first detent.

The fill phase was defined as the segment where the tanks were being filled. This phase could be isolated very clearly. However, fill entry and fill exit phases could not be separated with clarity leading to inclusion of some water impact loads among their flight loads. Combining these phases into one focused on identification of water impact loads may be advisable.

Drop entry, drop, and drop exit phases could be identified with certainty. These phases subjected the aircraft to the most severe in-flight load factors. Drops were performed with the flaps in the second detent. However, in many instances, the flaps were retracted from the second detent into the first before the conclusion of the drop. Since the maximum allowable load factor for the first detent was lower than that of the second, this action led to exceeding the limit load factors. The drop rates were consistent with those observed on heavy airtankers. The lack of precision in determining the terrain elevation led to inaccuracies in determining the AGL altitude during these phases. However, a 175-foot average AGL altitude was associated with drop phases.

6.1.2 Flight loads

Vertical accelerations were separated into those due to gusts and maneuvers. In each category, the cumulative occurrences of the incremental load factors were established for various AGL altitude bands. For the four cruise phases, the ferry, and the maintenance/training missions, which were flown over a wide range of altitudes, flight loads spectra were also developed for MSL altitude bands. The results were expressed per 1000 hours and per nautical mile.

The longest cumulative flight durations were those of cruise heavy and cruise light phases, punctuated by repeated fills and drops. The third longest cruise phase belonged to ferry missions, which also covered the widest range of altitudes. In general, firefighting cruise phases were flown at relatively low AGL altitudes. Most cruise 1 and cruise 2 phases remained under 9,500 feet AGL while the vast majority of cruise heavy and cruise light phases took place below 4,500 feet AGL.

The cumulative occurrences of the incremental gust and maneuver load factors from cruise 1 and cruise 2 showed a clear correlation with AGL altitude bands. The same trends could not be seen clearly when the results were placed in MSL altitude bands. This was consistent with previous observations.

Cruise heavy phases showed a slightly lower cumulative occurrences of incremental load factors than cruise 1 and cruise 2 phases. Cruise light phases were flown at somewhat lower altitudes than cruise heavy phases and contained larger and more frequent incremental load factors than the latter. These phases were also flown at slightly higher airspeeds.

Cumulative occurrences of incremental gust and maneuver load factors were presented for fill entry, fill, and fill exit phases. However, since the associated load factors included those due to contact with the water, they could not be strictly called flight loads. This was especially true for

the fill phase where almost all vertical accelerations were due to water impact. These accelerations were shown to be significant.

Cumulative occurrences of gust and maneuver load factors for drop entry, drop, and drop exit phases were developed. It was shown that the largest vertical maneuver load factors were in conjunction with the drop phases, followed by those of drop exit and drop entry. The frequency of occurrence of the vertical load factors in these phases was between one and three orders of magnitude larger than those of cruise phases. These results were consistent with previous observations of firefighting missions.

Cumulative occurrences of incremental gust and maneuver load factors were compared among different flight phases. For this purpose, the results from all altitude bands were combined. Among the cruise phases, the most frequent vertical gust load factors were observed to be associated with the cruise light phases that were flown at relatively low weights and somewhat higher airspeeds. Cumulative gust load factors from the drop phases were shown to be two to three orders of magnitude more frequent than those of cruise phases, followed by drop exit and drop entry phases. The same trends were also observed in the cumulative incremental vertical maneuver load factors.

Flight loads spectra for the airborne phases were also compared with those of firefighting missions from BAe-146/RJ-85, SEATS, and ASM/lead aircraft, and agricultural spraying. Each of these operations was deemed to have some similarities with CL-415 firefighting missions. All flight phases were combined for these comparisons, but the gust and the maneuver load factors were kept separate. In addition, fill entry, fill, and fill exit phases were left out to prevent inclusion of water impact loads.

Vertical gust load factors were shown to have magnitudes and frequencies very similar to those of ASM/lead aircraft. However, these loads were shown to be more frequent than those of heavy airtankers by two to three orders of magnitude. The same trends were observed regarding maneuver load factors although the results from CL-415 were slightly less frequent at lower load factors.

6.1.3 Derived gust velocities

Derived gust velocities were determined based on estimated aircraft weights and were shown as exceedance spectra per nautical mile. The results were established for flight phases that were free of water impact loads. For the cases that covered the largest range of AGL and MSL altitude bands, results were presented for both. Again, clear correlation of the frequency of the derived

gust velocities with AGL altitude bands was observed in every case. Ferry missions showed the largest magnitude and frequency of occurrence in the lowest AGL altitude band, followed by cruise 1. There was good agreement between the results from cruise heavy and cruise light phases.

6.2 Recommendations

1. Clear identification of the points of contact with, and departure from, the water source proved to be extremely challenging. If the aircraft are equipped with radio altimeter, direct recording of the AGL altitude would facilitate this process greatly.

2. Grouping of the flight phases that contain water impact loads is recommended, with focus on these load factors that can be significant.

3. Latitude Technologies technical specifications of the IONode recording system (n.d.) states clearly that correct recording of angular positions (i.e., pitch, roll, and yaw) "Requires initial setup to achieve indicated accuracies." The recorded data showed large and unreasonable variations in these parameters, bringing into question their initial setups. This has been a persistent problem with IONode data and has been observed on other aircraft.

4. Regarding angular rates and linear accelerations, Latitude Technologies technical specifications also states that for "Accuracies depend on installation environment and calibration." Therefore, periodic examination and calibration of the recorded indicated airspeed and vertical accelerations is highly recommended to safeguard against sensor drifts.

5. Some of the overload cases are exacerbated by the aircraft's unusual limit load factors for various flap settings. Appropriate inspection procedures have to be established if the observed exceedances of maximum airspeed and maximum vertical load factor are indeed real.

6. There were many instances in which the crew cycled the bay doors in flight. In most of these instances, the airspeed was above the limit of 129 KIAS.

7 References

ASTM International. (2005). *Standard Practices for Cycle Counting in Fatigue Analysis, ASTM E 1049-85 (Reapproved 2005).* doi:10.1520/E1049-85R17

Bombardier Aerospace. (1999). *Canadair 415 Model CL-215-6B11, Airplane Flight Manual, Product Support Publication No. 491.* Montreal, Quebec.

Dommasch, D., Sherby, S., & Connolly, T. (1967). *Airplane Aerodynamics – Fourth Edition.* New York, NY: Pitman Publishing Corporation.

Etkin, B. (1982). *Dynamics of Flight, Stability and Control – Second Edition.* New York, NY: John Wiley & Sons.

FAA. (2016). *Type Certificate Data Sheet A14EA, Revision 11.*

Kliment, L., Rokhsaz, K., & Menon, A. (2017). *Further Airframe Usage and Operational Loads Monitoring of ASM/Lead Aircraft.* Report DOT/FAA/TC-17/40. Federal Aviation Administration. doi:10.13140/RG.2.2.12345.42087

Kliment, L., Rokhsaz, K., Nelson, J., Terning, B., & Weinstein, E. (2015). Usage and Flight Loads Analysis of King Airs in Aerial Firefighting Missions. *AIAA Journal of Aircraft, 52*(3), 910-916. doi:10.2514/1.C032877

Lambert, M., & Munson, K. (Eds.). (1994). *Jane's All the World's Aircraft, 1994-1995 Issue.* Alexandria, VA: Jane's Information Group, Inc.

Latitude Technologies IONode Technical Specifications. (n.d.). Retrieved February 2021, from https://www.latitudetech.com/hardware/ionode-flight-data-monitoring

Majeed, O. (2009). *Parametric Specific Fuel Consumption Analysis of the PW120A Turboprop Engine.* Document Ref: SRS-TSD-002 Rev. 1. Specific Range Solutions Ltd.

NTSB. (2004). *Safety Recommendations A-04-29 through -33.* National Transportation Safety Board, National Transportation Safety Board. National Transportation Safety Board.

NWCG. (2020). *National Wildfire Coordinating Group, PMS 507*. Retrieved from NWCG Airtanker Base Directory: https://www.nwcg.gov/publications/pms507

Rokhsaz, K., & Kliment, L. (2016). *Preliminary Comparison of Agricultural and Single-Engine Air Tanker Operational Loads.* FAA Report DOT/FAA/TC-16/9, Final Report Contract Monitor: Dr. Edward Weinstein.

Rokhsaz, K., & Kliment, L. (2019). Effect of Data Filtering on Flight Loads Spectra. *AIAA Aviation and Aeronautics Forum and Exposition, AIAA-2019-3367.* Dallas, TX, June 17-21: American Institute of Aeronautics and Astronautics (AIAA). doi:10.2514/6.2019-3367

Rokhsaz, K., Kliment, L., & Bramlette, R. (2011). *Usage and Maneuver Loads Monitoring of Heavy Air Tankers.* DOT/FAA/AR-11/7. Federal Aviation Administration.

Rokhsaz, K., Kliment, L., & Rollins, E. (2026). *Flight Loads and Airframe Usage Analysis of Next-Generation Airtankers – BAe-146 and RJ-85.* FAA Technical Report DOT/FAA/TC-20/13. Federal Aviation Administration. doi:https://doi.org/10.21949/1f49-b349

Rokhsaz, K., Kliment, L., Nelson, J., & Newcomb, J. (2014). Operational Assessment of Heavy Air Tankers. *AIAA Journal of Aircraft, 51*(1), 62-77. doi:10.2514/1.C031922

Roskam, J. (2001). *Airplane Flight Dynamics and Automatic Flight Controls – Part I.* Lawrence, Kansas: DARcorporation, Third Printing.

Rustenburg, J., Skinn, D., & Tipps, D. (1999). *An Evaluation of Methods to Separate Maneuver and Gust Load Factors from Measured Acceleration Time Histories.* FAA Report DOT/FAA/AR-99/14.

U.S. Forest Service Fire and Aviation Management. (2018). CL-415 Amphibious Water Scooping Aircraft User Guide. *AWSA User Guide, 4*(29).

USDA. (2012). *Large Airtanker Modernization Strategy.* USDA Forest Service.

USGS. (2018). *National Elevation Dataset.* Retrieved July 2019, from https://gishubdata.nd.gov/dataset/usgs-national-elevation-dataset-ned

A Usage data presentation

Figures

Tables

Table A-1: Statistical formats – tables of usage data

Usage Data	**Table**
Number and Summary Characteristics of Phases	A-3
Frequency of Flap Usage	A-4
Flap Limitations	A-5
Stall Speeds	A-6

Table A-2: Statistical formats – figures of usage data

Figure Title	**Figure**
OVERALL FLIGHT	
Number of Flights by Duration	A-1
Correlation of Distance and Duration for Overall Flight	A-2
Maximum AGL Altitude and Coincident Distance	A-3
Maximum MSL Altitude and Coincident Distance	A-4
Number of Flights and Corresponding Fills and Drops	A-5
Total Water Delivered vs. Flight Duration	A-6
Takeoff Indicated Airspeed	A-7
Landing Indicated Airspeed	A-8
Landing Maximum Vertical Load Factor and Coincident Lateral Load Factor	A-9
CRUISE 1 PHASE	
Correlation of Distance and Duration – Cruise 1	A-10
Maximum AGL Altitude and Coincident Distance – Cruise 1	A-11
V-n Diagram with Flaps Retracted – Cruise 1	A-12
V-n Diagram with Flaps in Detent 1 – Cruise 1	A-13
V-n Diagram with Flaps in Detent 2 – Cruise 1	A-14
CRUISE 2 PHASE	
Correlation of Distance and Duration – Cruise 2	A-15
Maximum AGL Altitude and Coincident Distance – Cruise 2	A-16
V-n Diagram with Flaps Retracted – Cruise 2	A-17
V-n Diagram with Flaps in Detent 1 – Cruise 2	A-18
V-n Diagram with Flaps in Detent 2 – Cruise 2	A-19

Figure Title	Figure
DROP EXIT PHASE	
Probability of Maximum Airspeed – Drop Exit	A-47
V-n Diagram with Flaps in Detent 1 – Drop Exit	A-48
V-n Diagram with Flaps in Detent 2 – Drop Exit	A-49

Table A-3: Number and summary characteristics of phases

Flight Phase	Number of Cases	Average of		
		Max. AGL Altitude (ft)	Max. Indicated Airspeed (KIAS)	Water Load (gal)
Cruise 1	1,089	4,233.0	174.9	39.5
Fill Entry	12,467	67.0	97.0	32.2
Fill	12,396	-6.9	79.1	668.0
Fill Exit	12,467	4.1	85.0	1,561.1
Cruise Heavy	12,167	1,800.1	157.0	1,454.2
Drop Entry	12,469	367.8	119.9	1,422.6
Drop	12,467	172.5	118.0	612.8
Drop Exit	12,419	334.8	121.0	35.6
Cruise Light	11,357	1,437.7	171.1	32.5
Cruise 2 Fire Ops	1,115	3,747.0	174.3	34.2
Ferry	412	6,658.3	176.9	31.7
Maint./Training	292	2,414.5	157.2	32.0

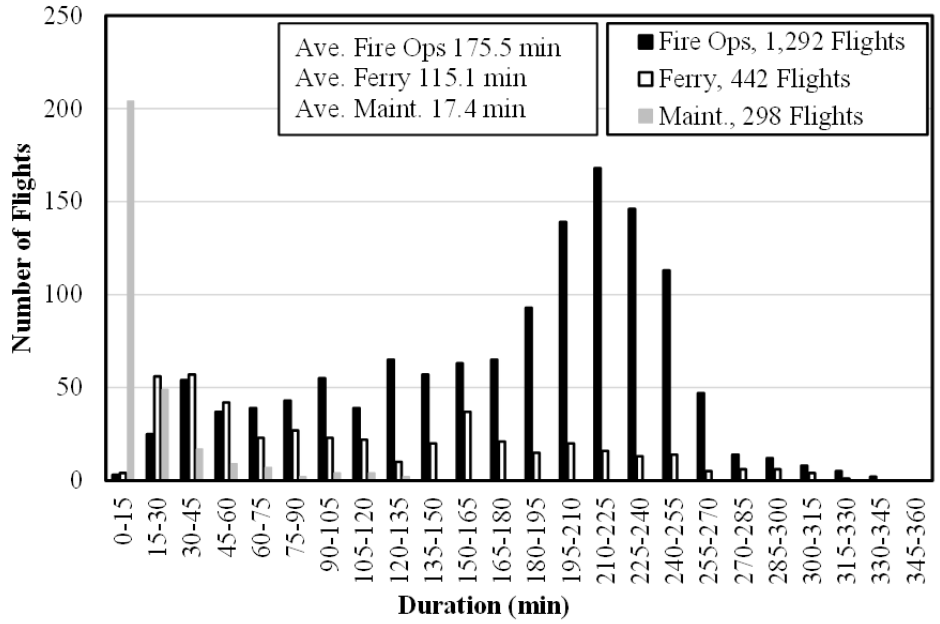

Figure A-1: Number of flights by duration

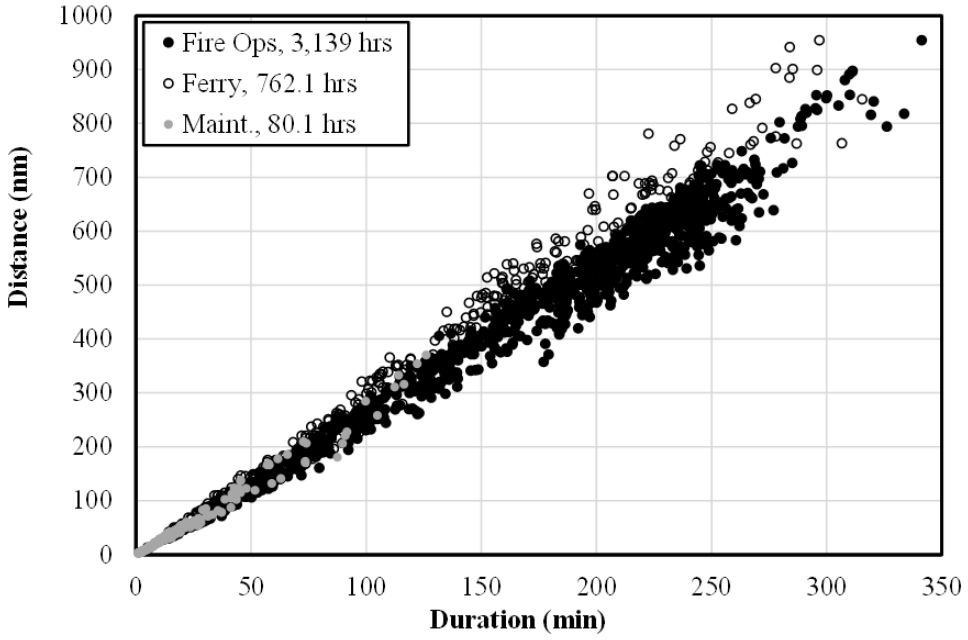

Figure A-2: Correlation of distance and duration for overall flight

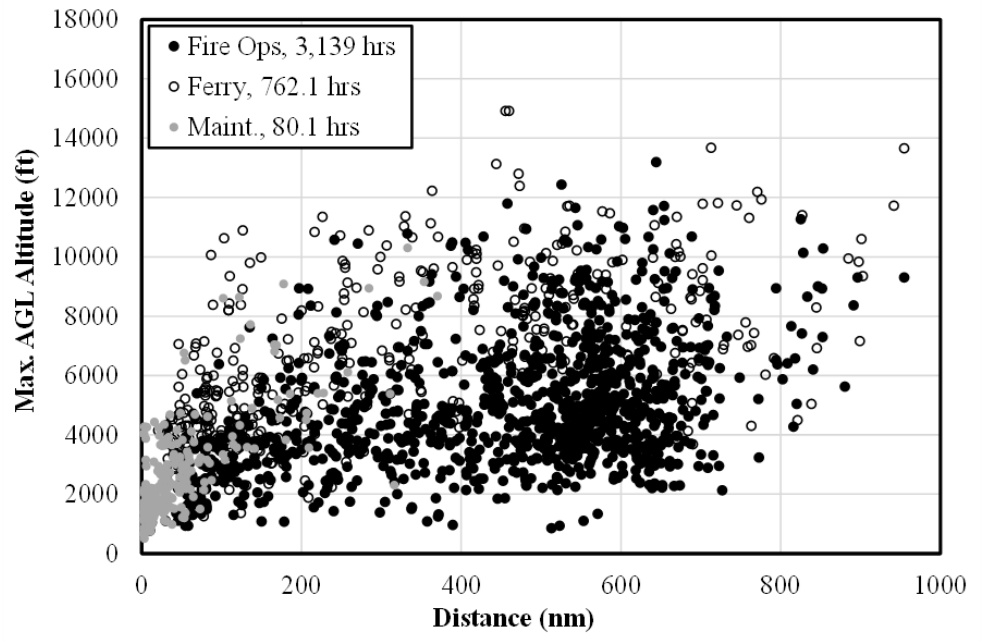

Figure A-3: Maximum AGL altitude and coincident distance

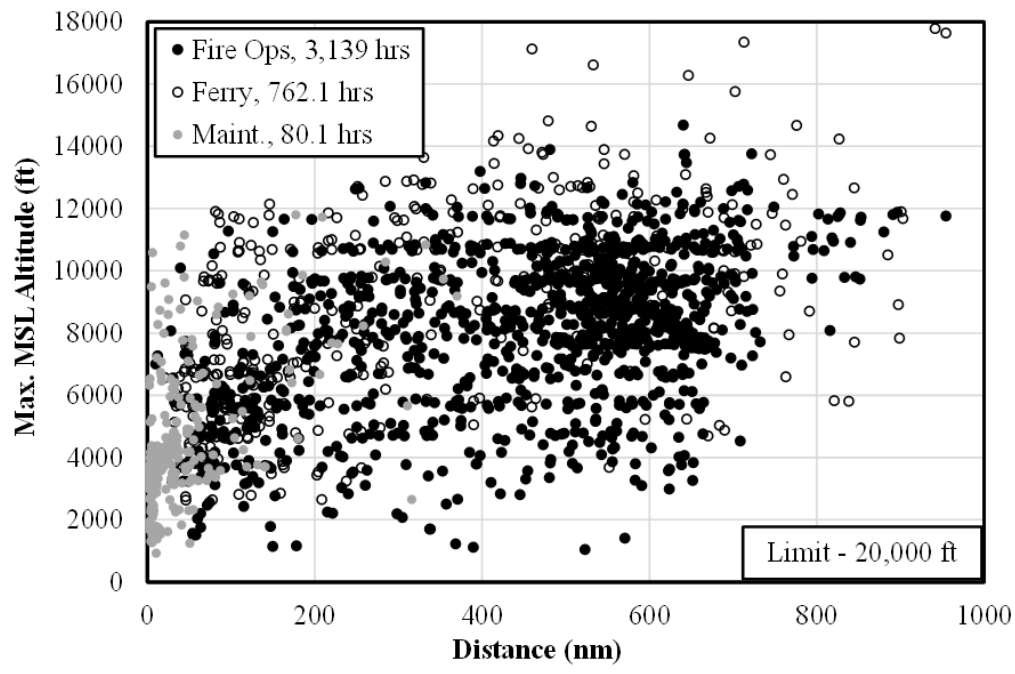

Figure A-4: Maximum MSL altitude and coincident distance

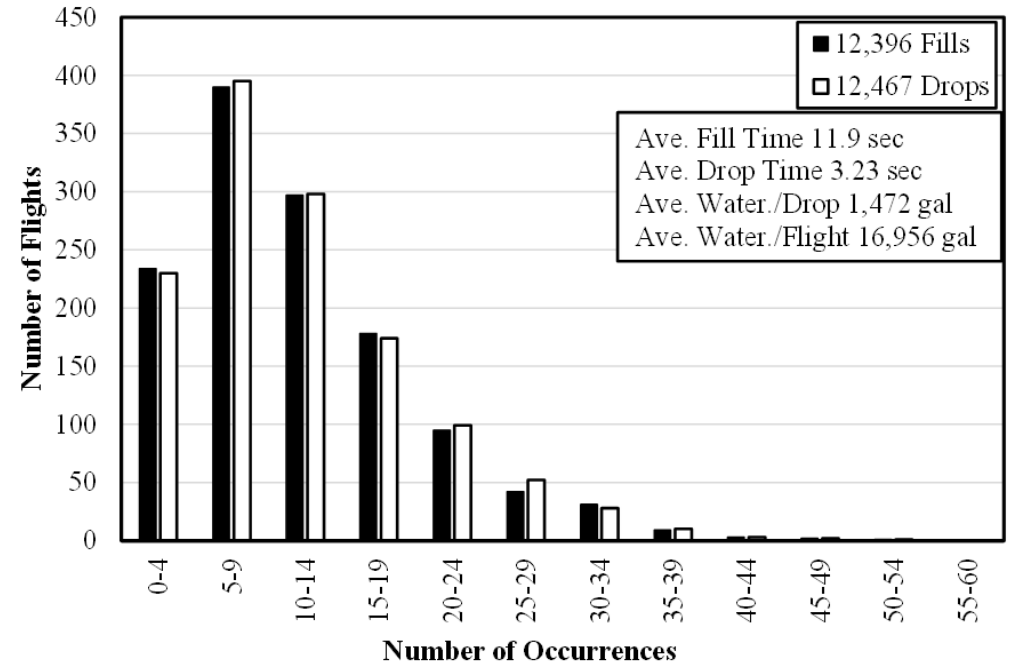

Figure A-5: Number of flights and corresponding fills and drops

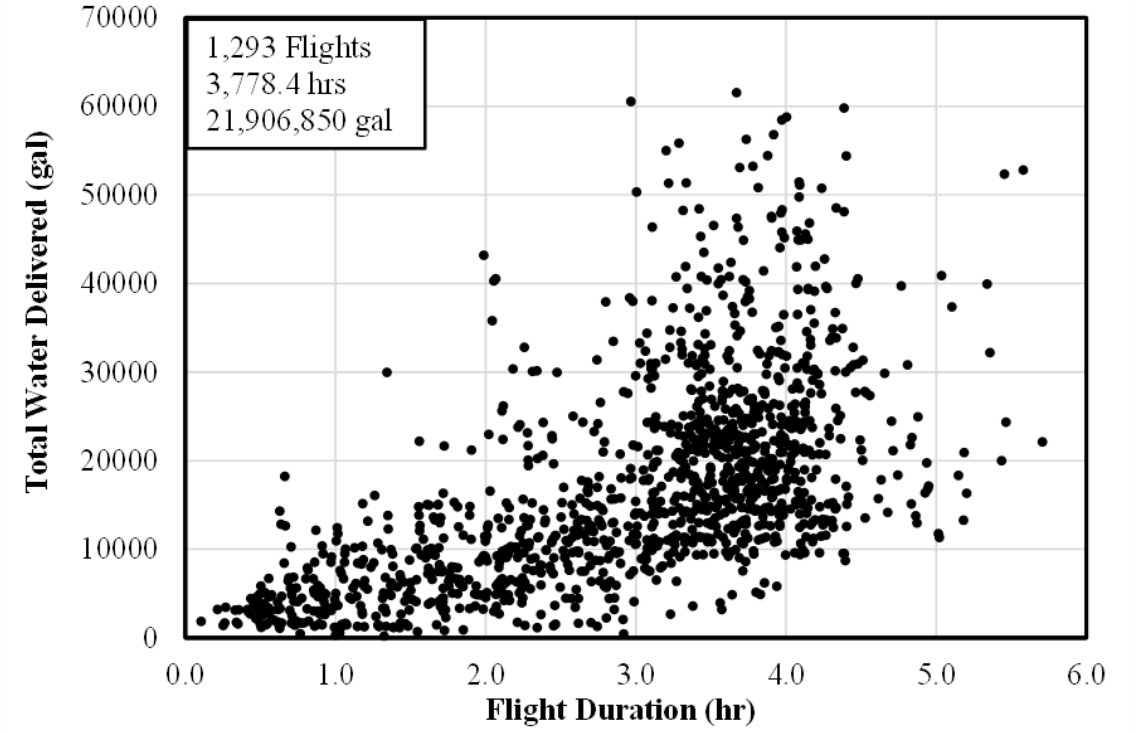

Figure A-6: Total water delivered vs. Flight duration

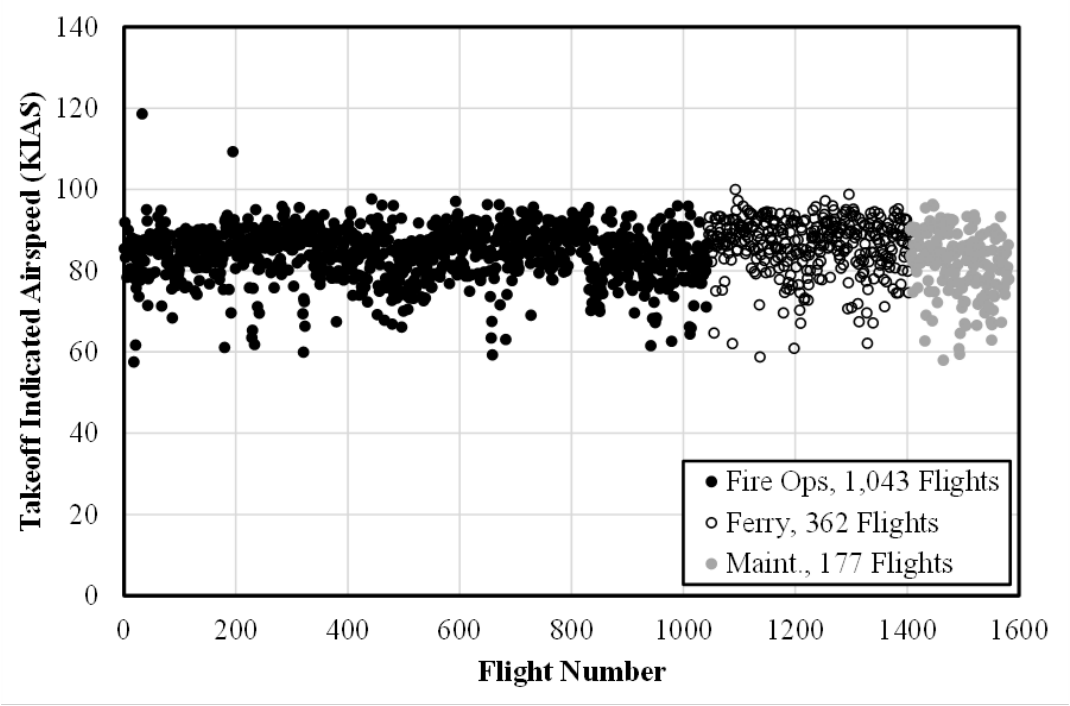

Figure A-7: Takeoff indicated airspeeds

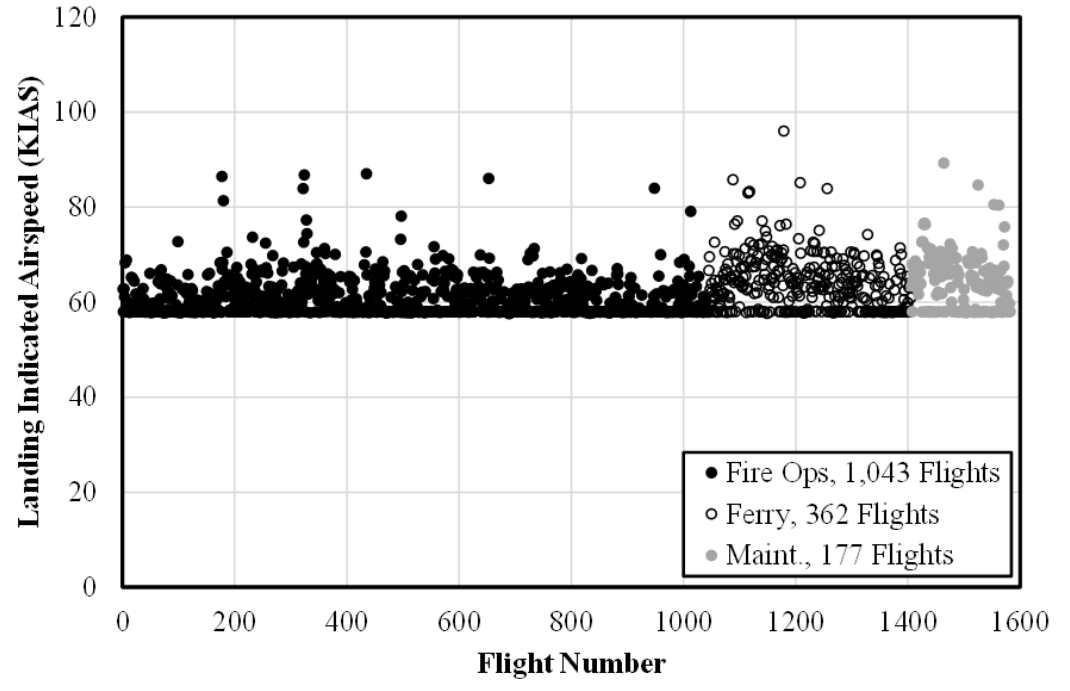

Figure A-8: Landing indicated airspeed

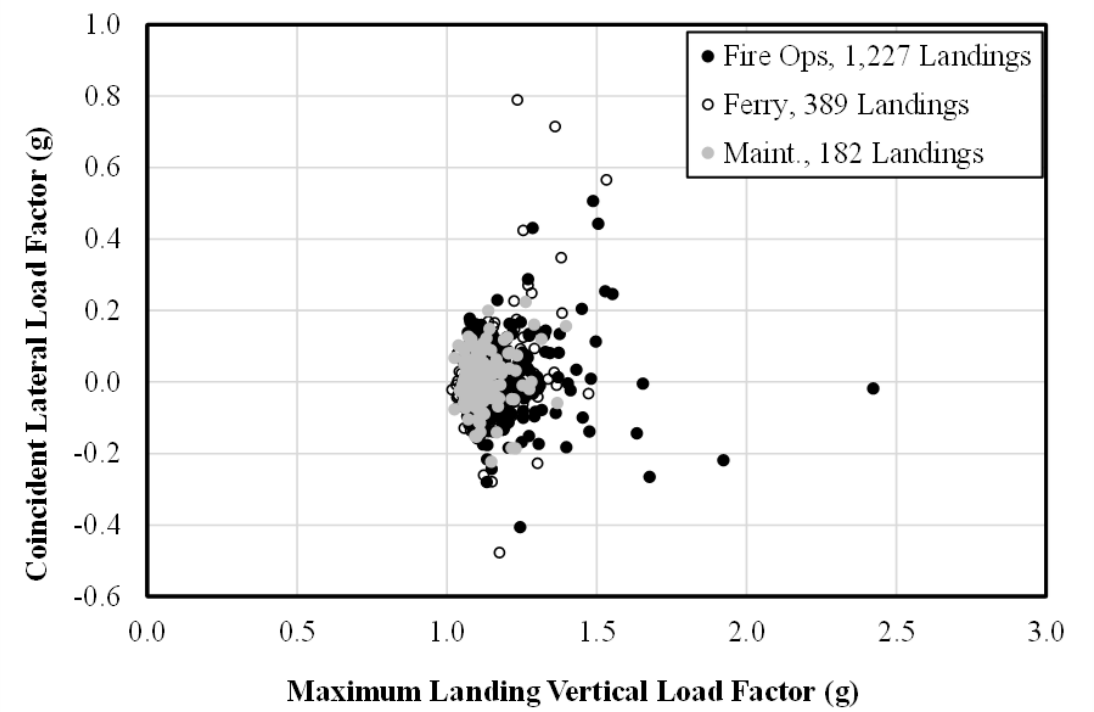

Figure A-9: Landing maximum vertical load factor and coincident lateral load factor

Table A-4: Frequency of flap usage

Missions	**Number**	**Detent 1**	**Detent 2**	**Detent 3**
Firefighting	1,292	25,499	31,267	2,124
Ferry	442	617	505	451
Maintenance/Training	298	366	310	257
Per Mission				
Firefighting	---	19.74	24.20	1.64
Ferry	---	1.40	1.14	1.02
Maintenance/Training	---	1.23	1.04	0.86

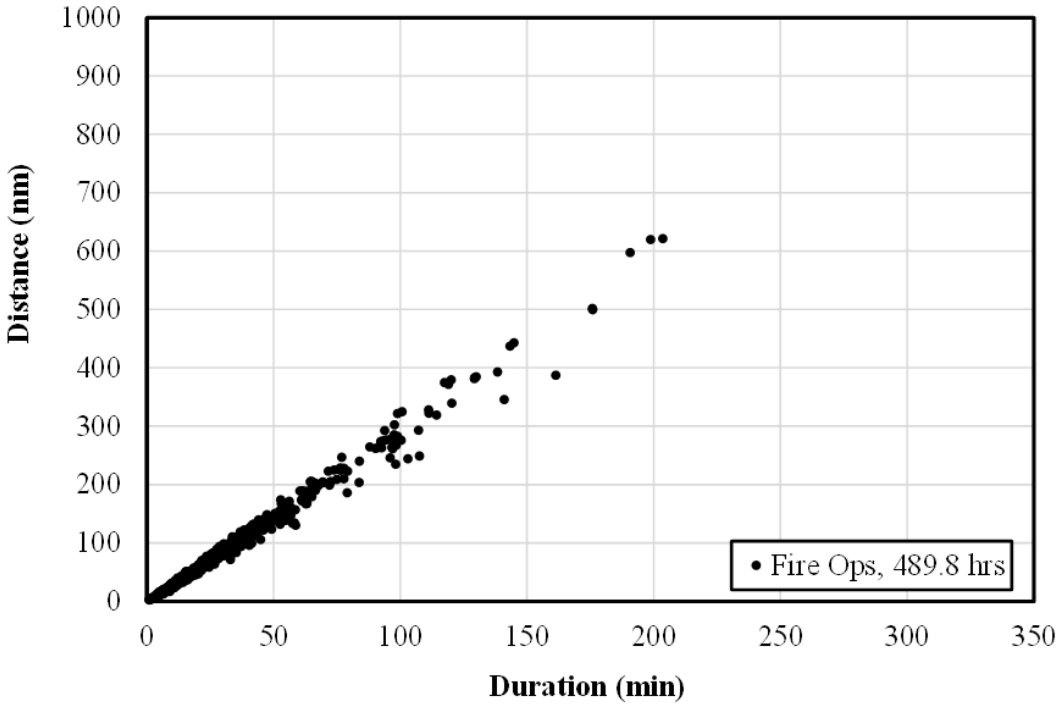

Figure A-10: Correlation of distance and duration – Cruise 1

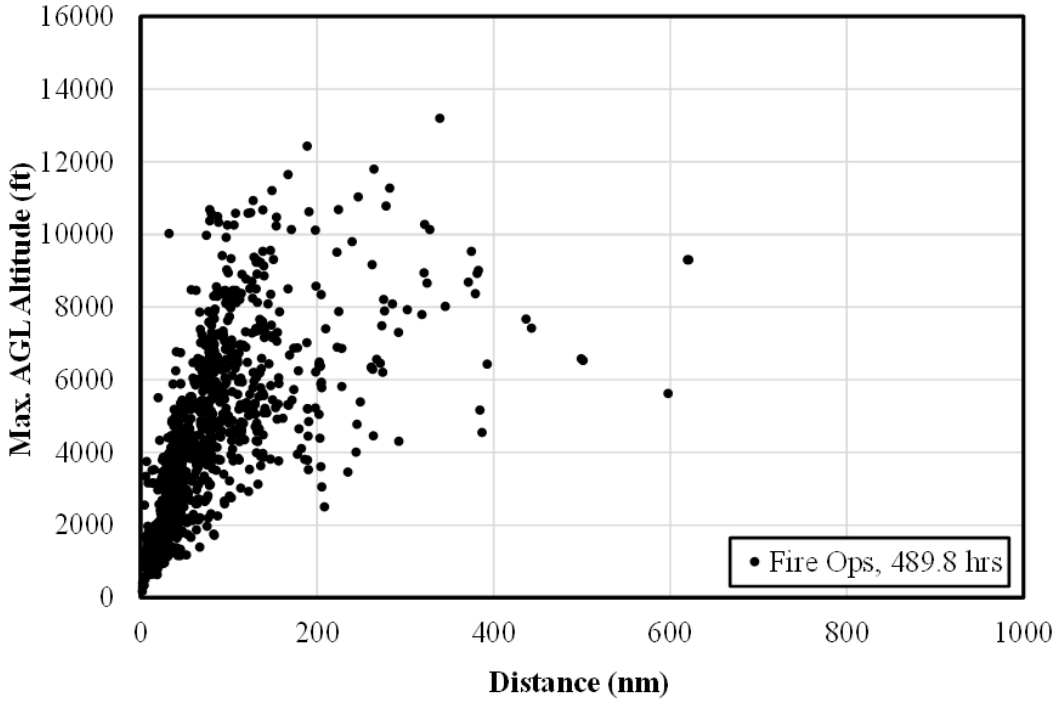

Figure A-11: Maximum AGL altitude and coincident distance – Cruise 1

Table A-5: Flap limitations

Flaps Settings	**Max. Airspeed (KIAS)**	**Min./Max. Vertical Load Factor (g)**
Retracted	187	-1.0/+3.0
Detent 1 – 10 deg	138	0.0/+2.0
Detent 2 – 15 deg	138	-1.0/+3.25
Detent 3 – 25 deg	119	0.0/+2.0

Table A-6: Stall speeds

Flaps Settings	**Stall Speed (KIAS) 26,000 lb**	**Stall Speed (KIAS) 47,000 lb**
Retracted	69.0	93.0
Detent 1 – 10 deg	63.8	85.7
Detent 2 – 15 deg	61.0	82.2
Detent 3 – 25 deg	58.2	69.0*

* *Limited to 37,000 pounds*

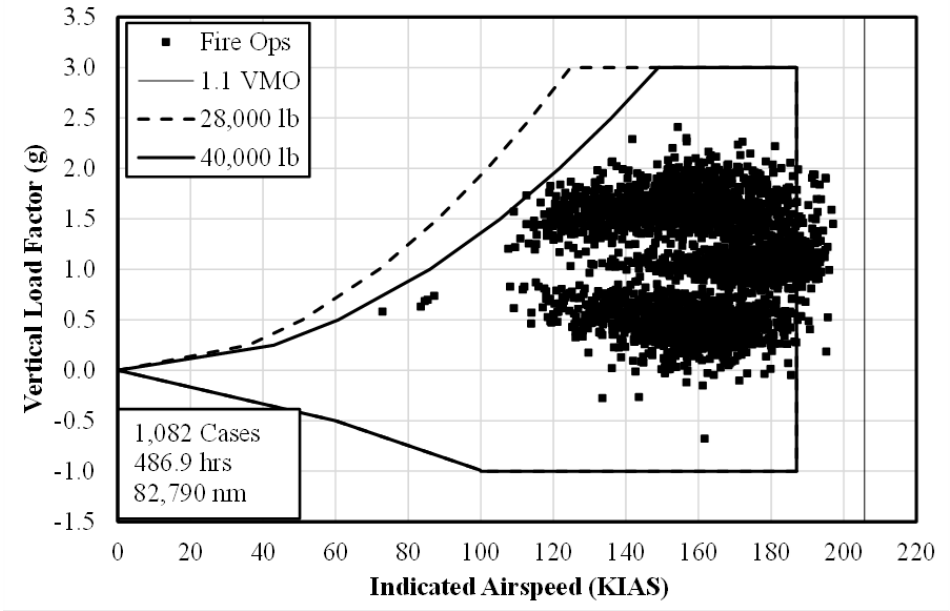

Figure A-12: V-n diagram with flaps retracted – Cruise 1

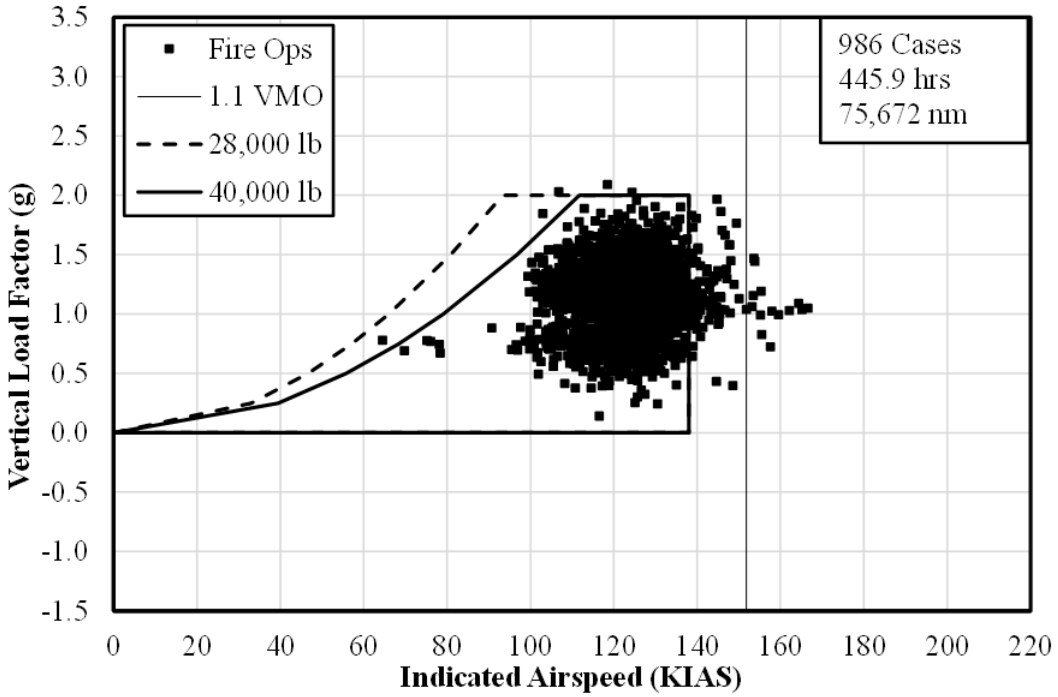

Figure A-13: *V-n* diagram with flaps in detent 1 – Cruise 1

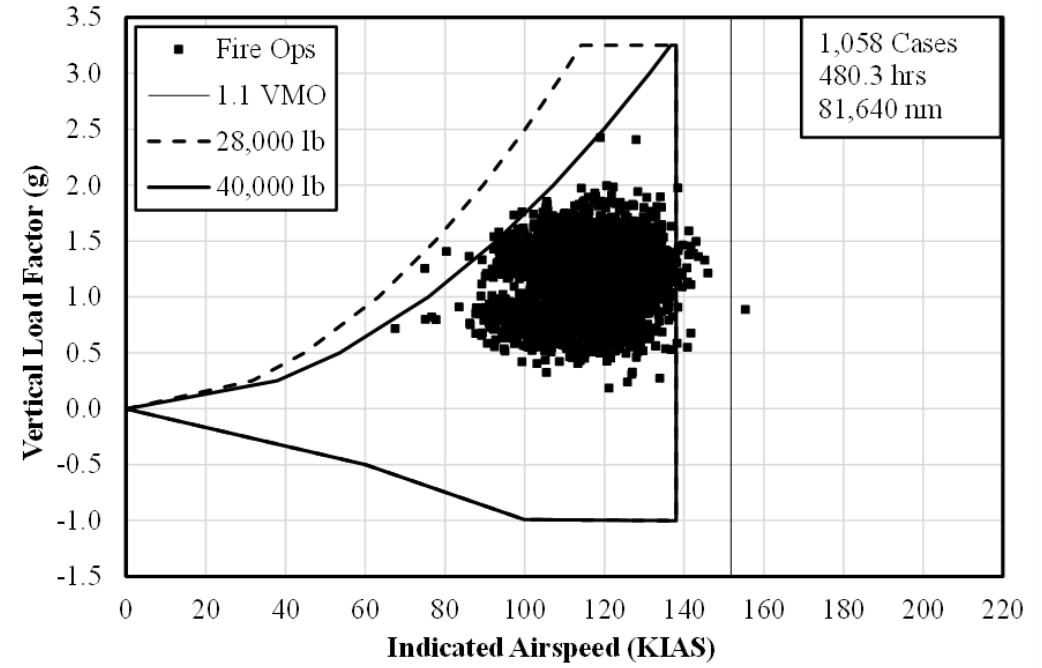

Figure A-14: *V-n* diagram with flaps in detent 2 – Cruise 1

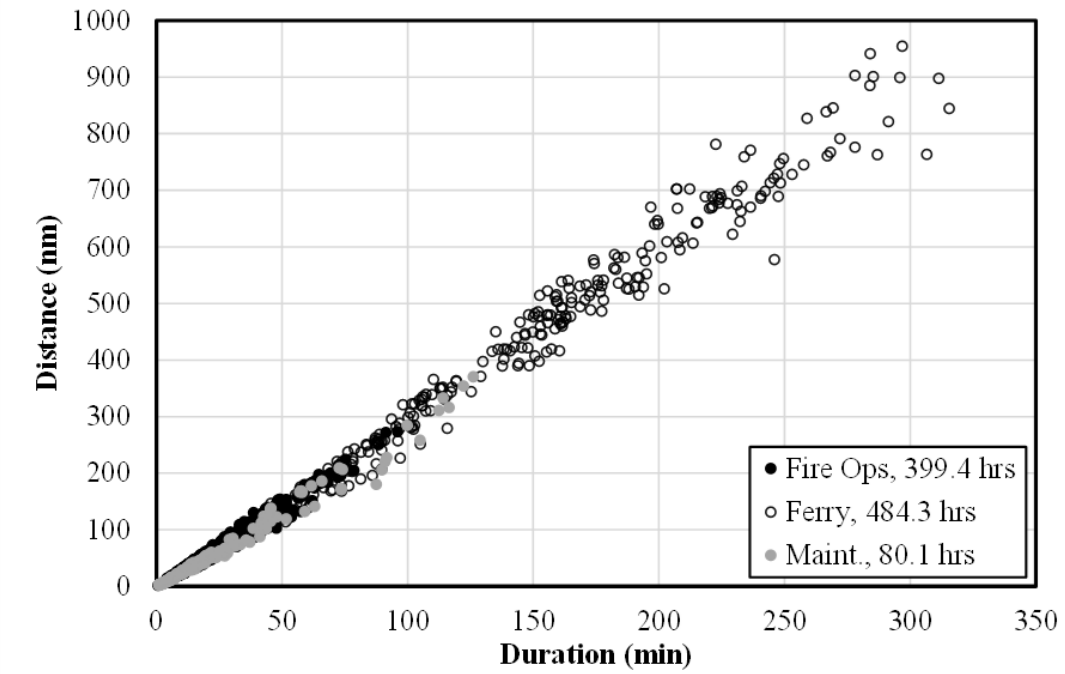

Figure A-15: Correlation of distance and duration – Cruise 2

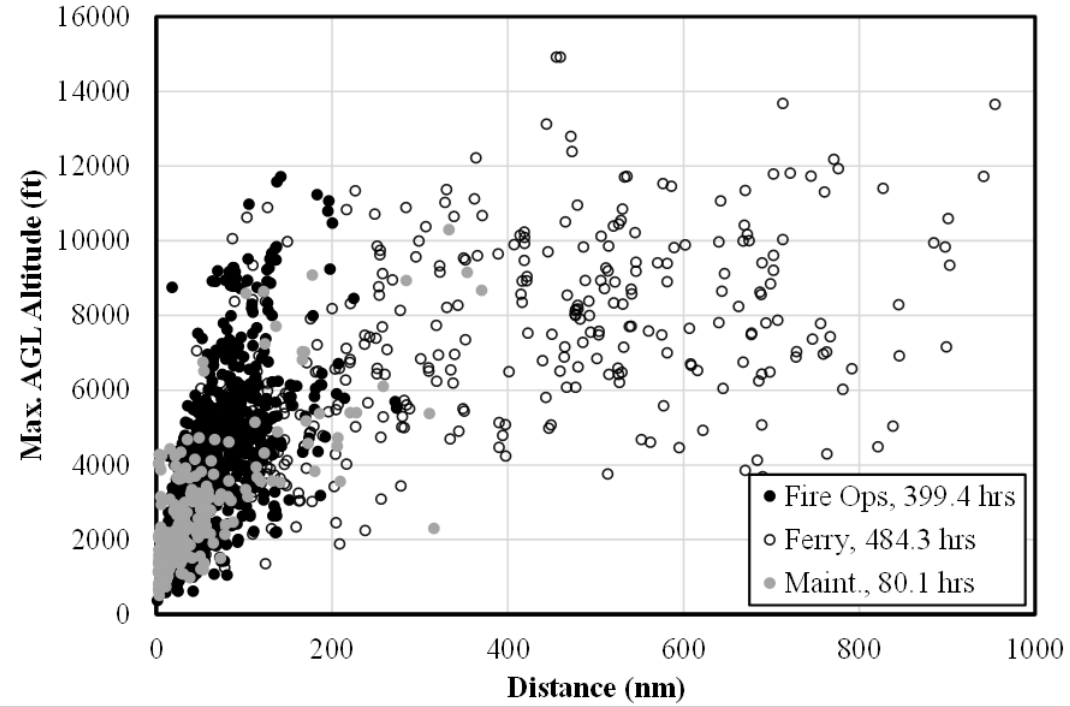

Figure A-16:Maximum AGL altitude and coincident distance – Cruise 2

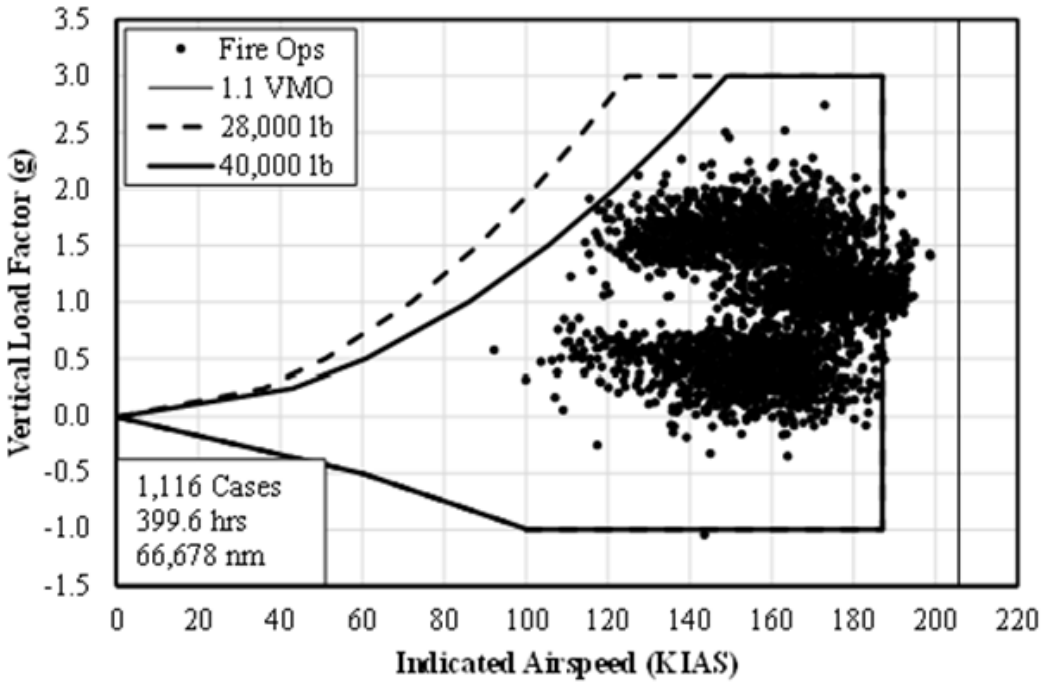

(a) Firefighting Flights

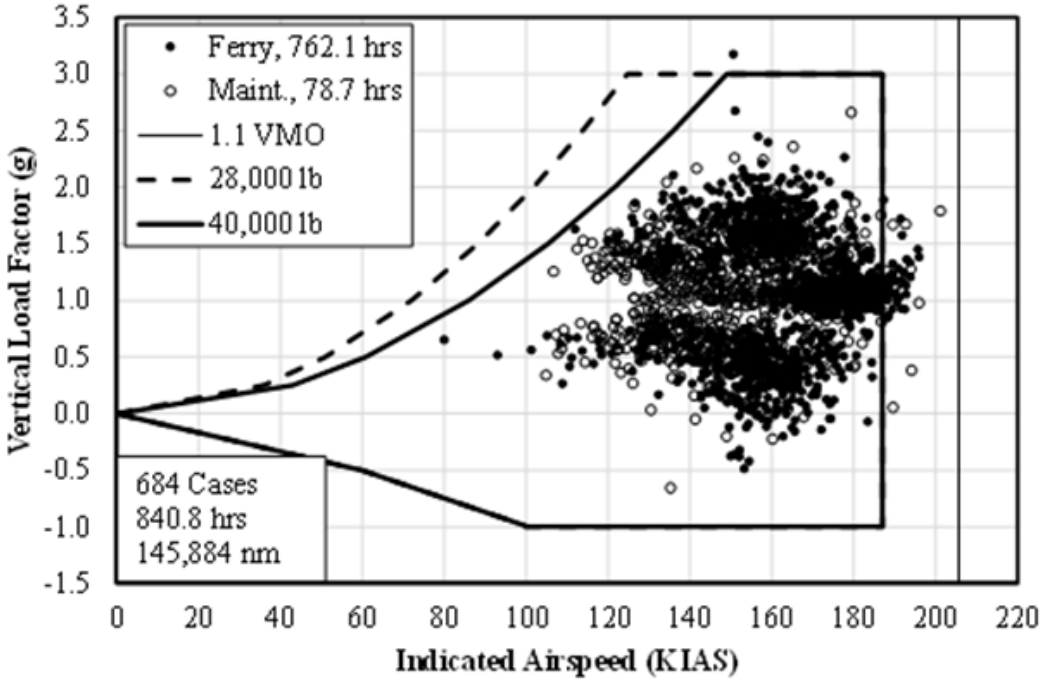

(b) Ferry and Maintenace/Traning Flights

Figure A-17: *V-n* diagram with flaps retracted – Cruise 2

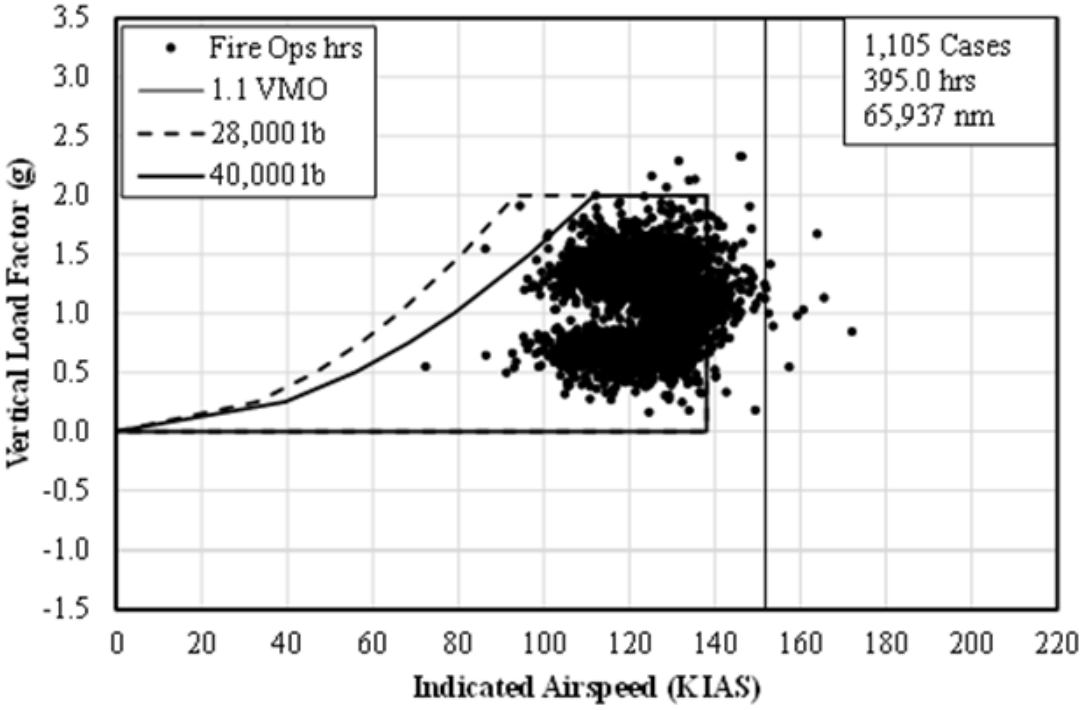

(a) Firefighting Flights

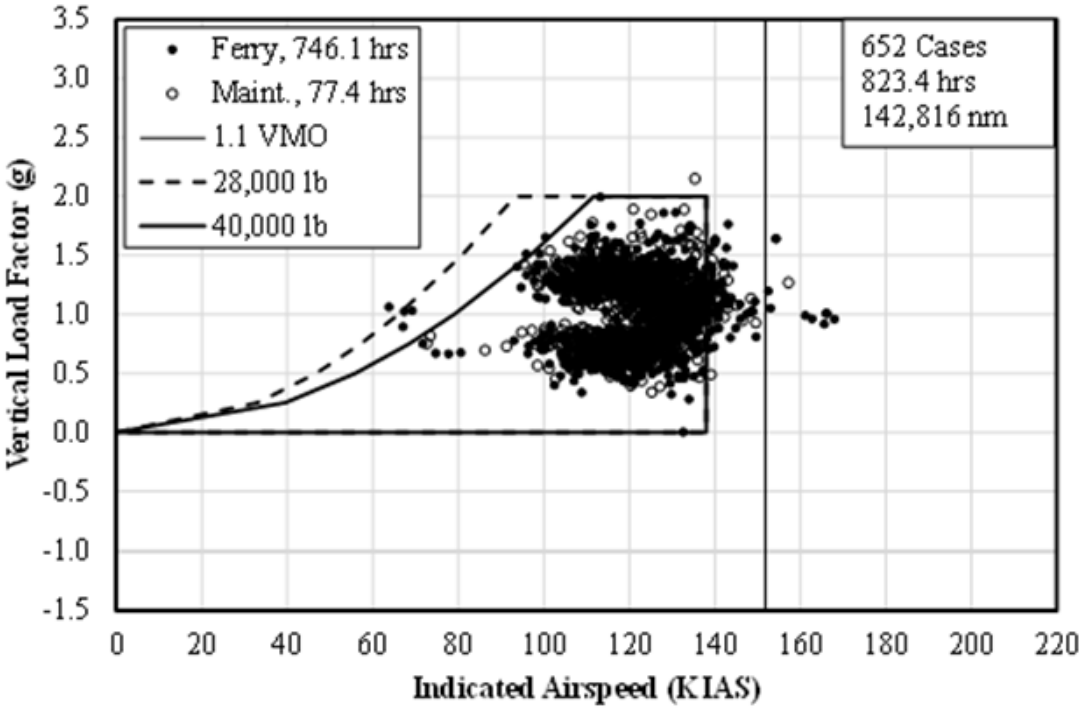

(b) Ferry and Maintenance/Training Flights

Figure A-18: *V-n* diagram with flaps in detent 1 – Cruise 2

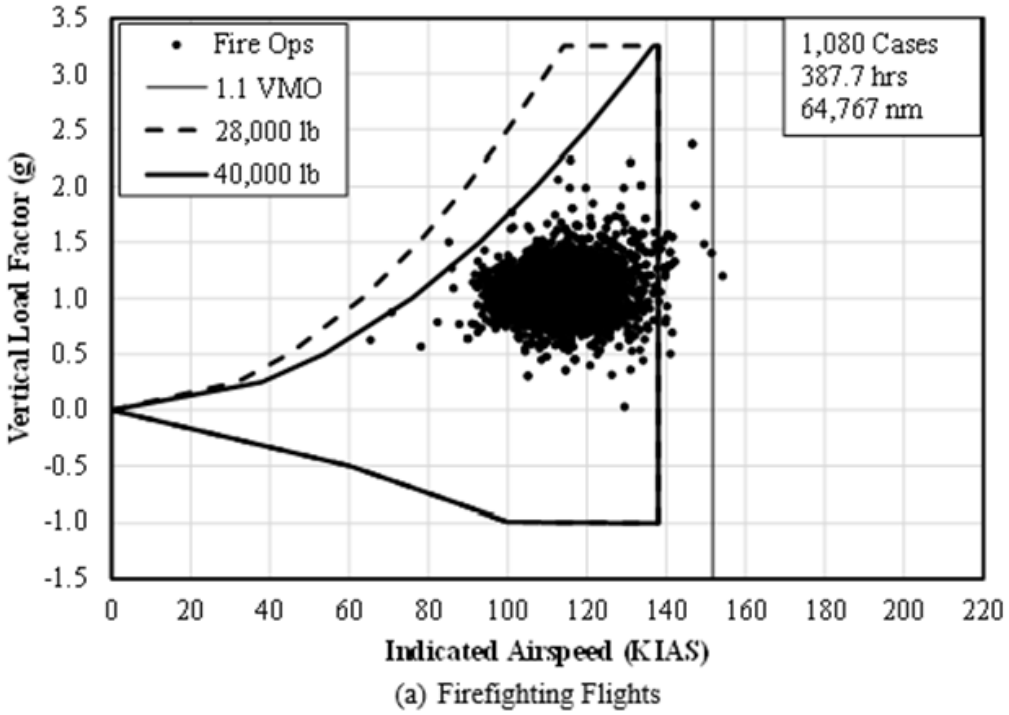

(a) Firefighting Flights

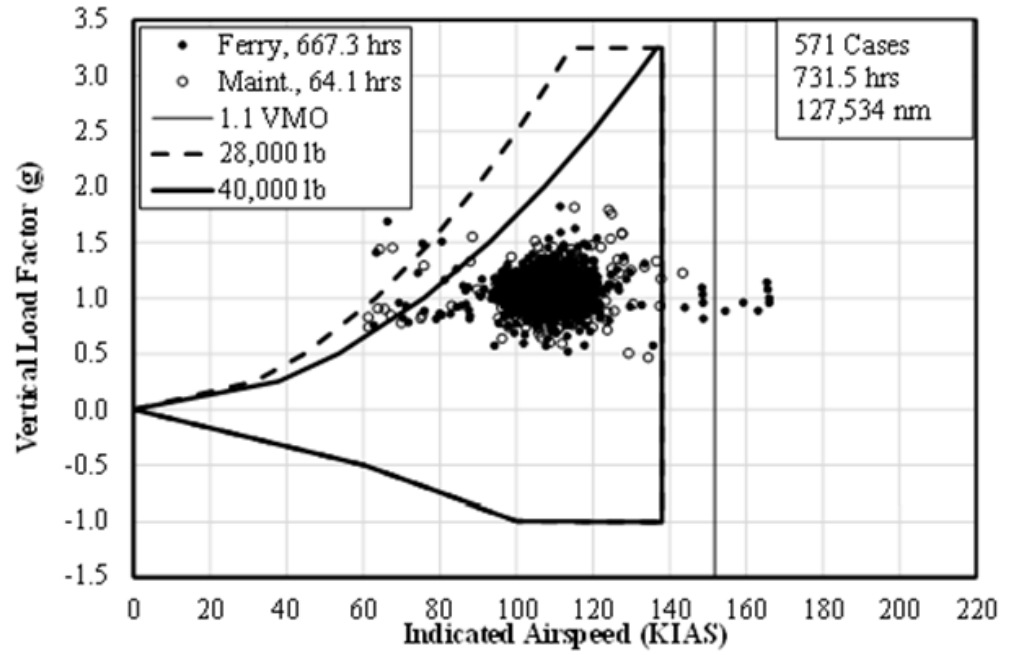

(b) Ferry and Maintenance/Training Flights

Figure A- 19: V-n diagram with flaps in detent 2 – Cruise 2

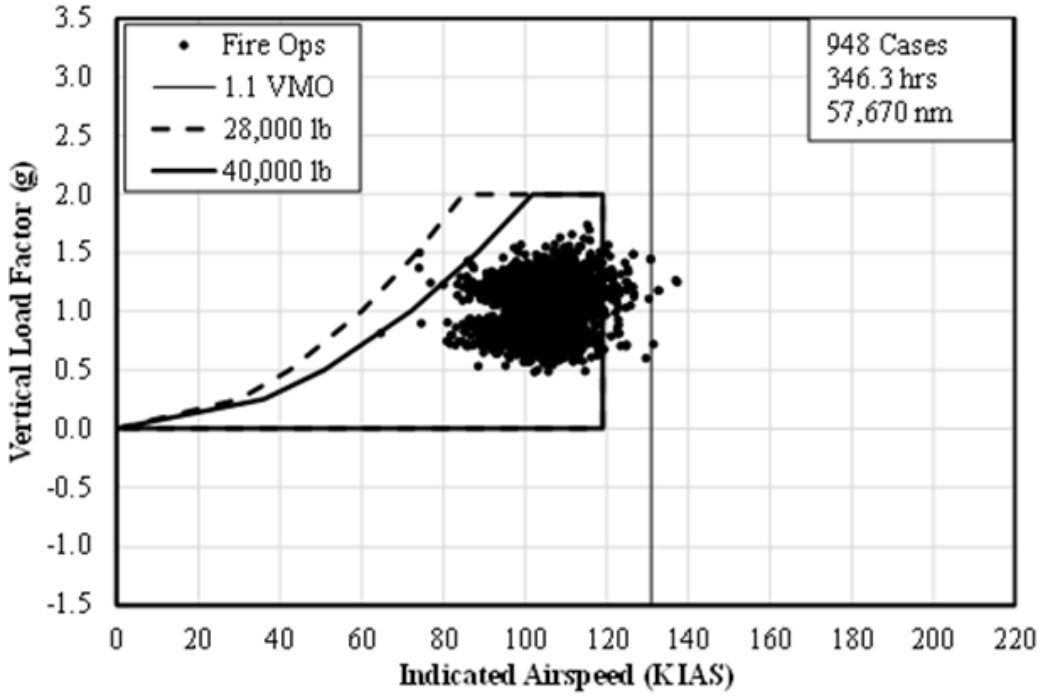

(a) Firefighting Flights

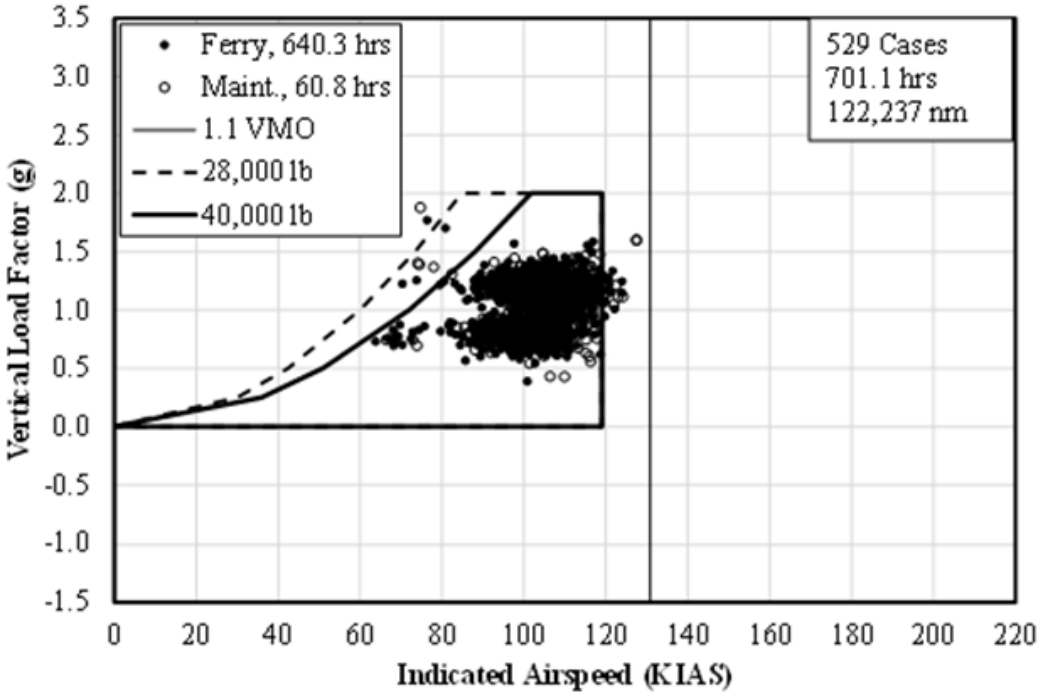

(b) Ferry and Maintenance/Training Flights

Figure A-20: *V-n* diagram with flaps in detent 3 – Cruise 2

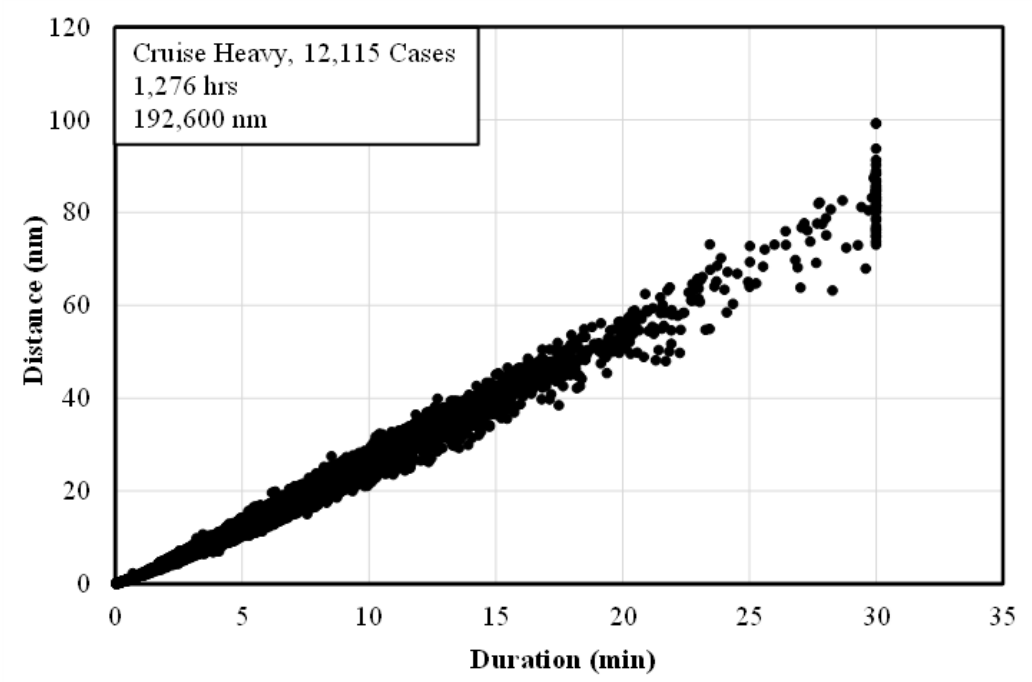

Figure A-21: Correlation of distance and duration – Cruise Heavy

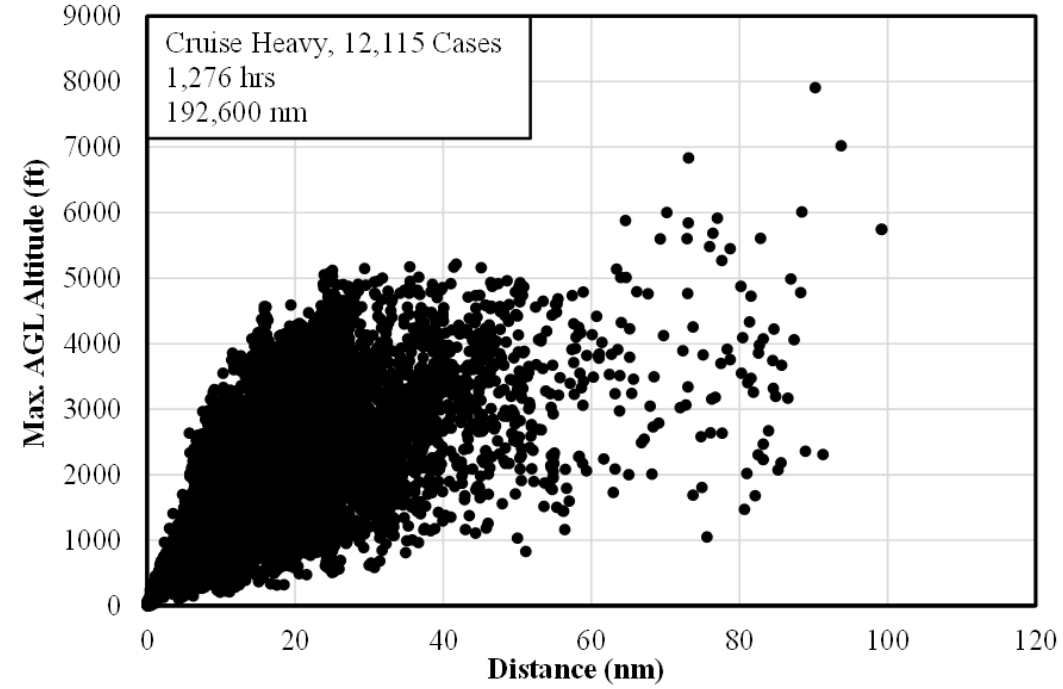

Figure A-22: Maximum AGL altitude and coincident distance – Cruise Heavy

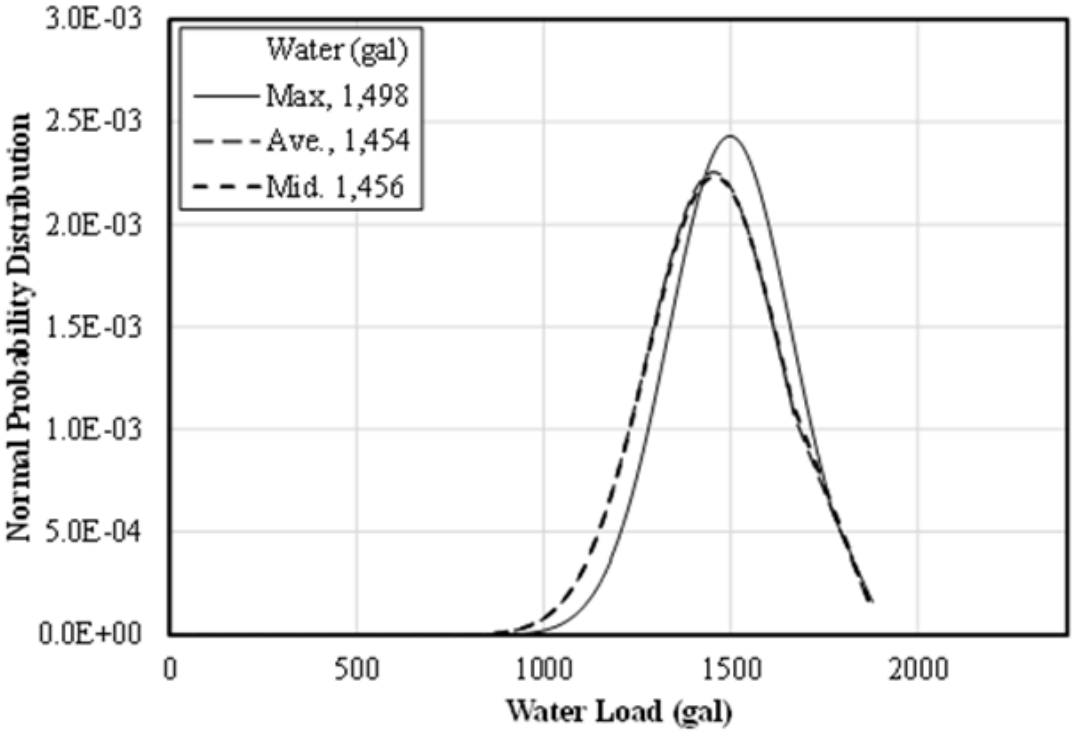

(a) Normal Probability Distribution

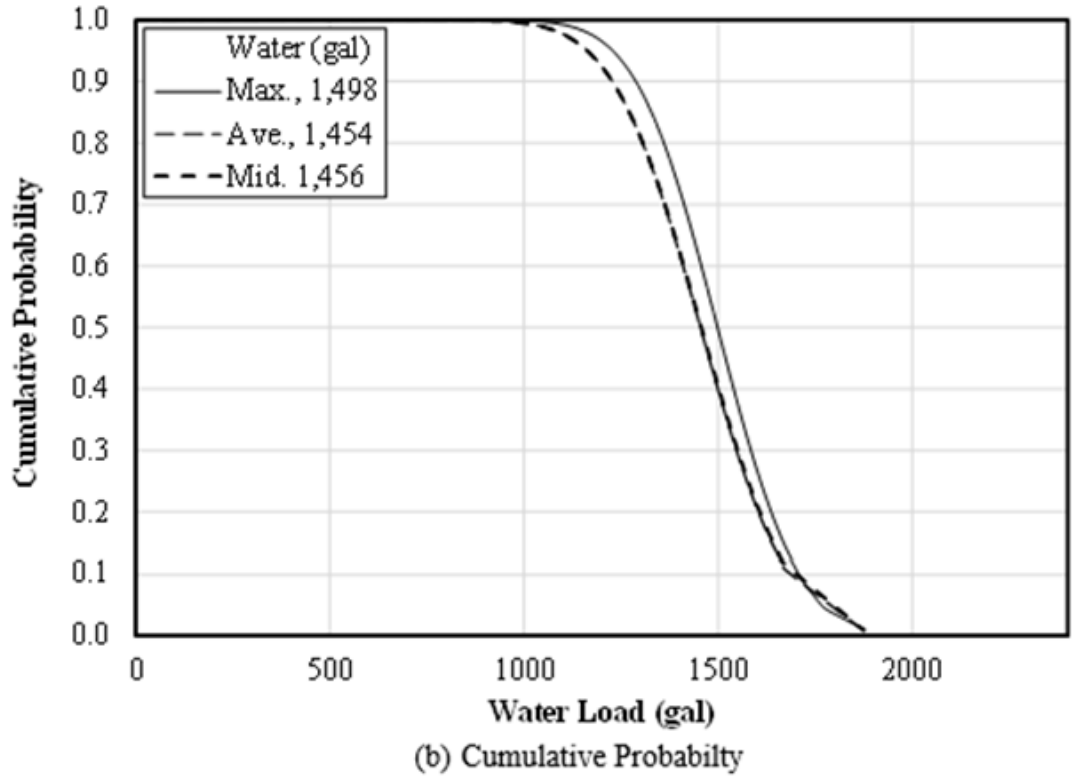

(b) Cumulative Probabilty

Figure A-23: Probability of water load carried – Cruise Heavy

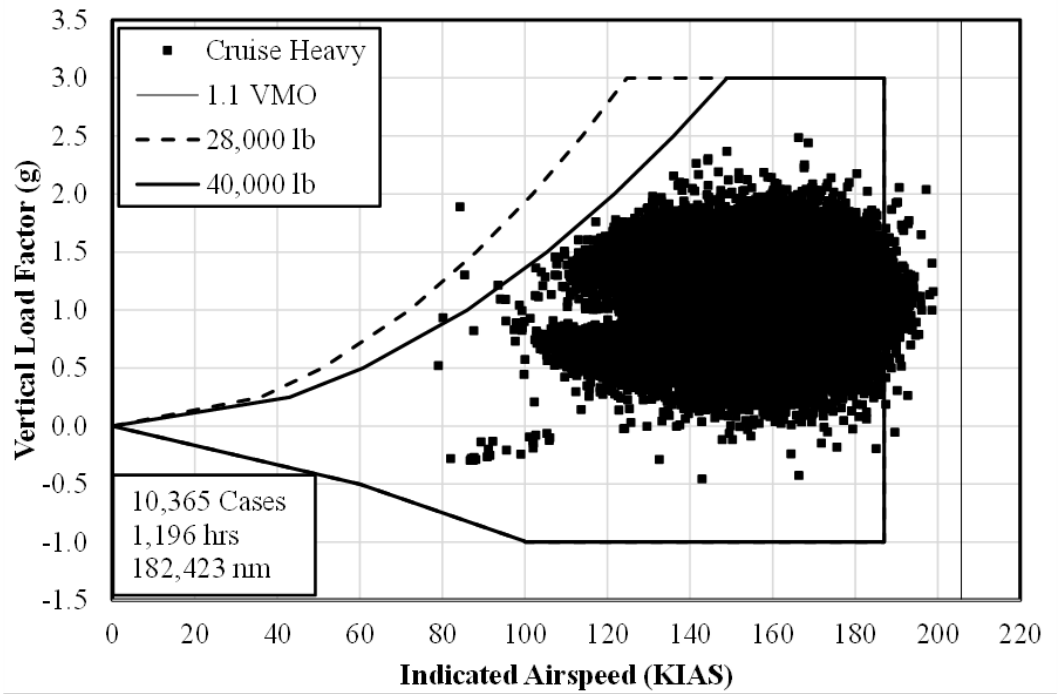

Figure A-24: *V-n* diagram with flaps retracted – Cruise Heavy

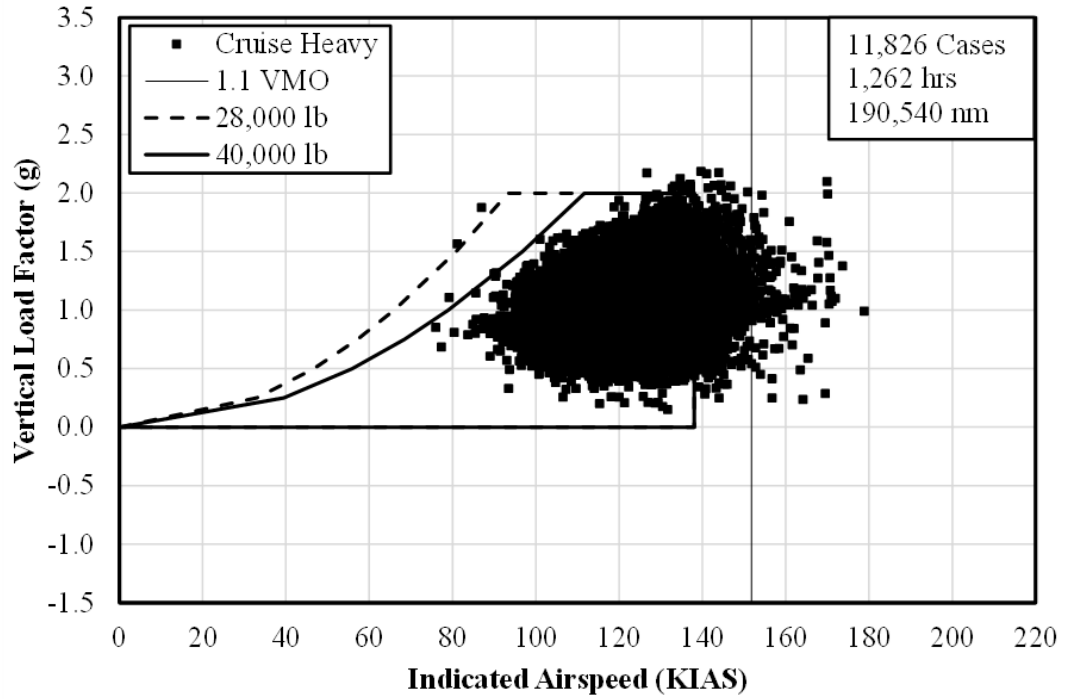

Figure A-25: *V-n* diagram with flaps in detent 1 – Cruise Heavy

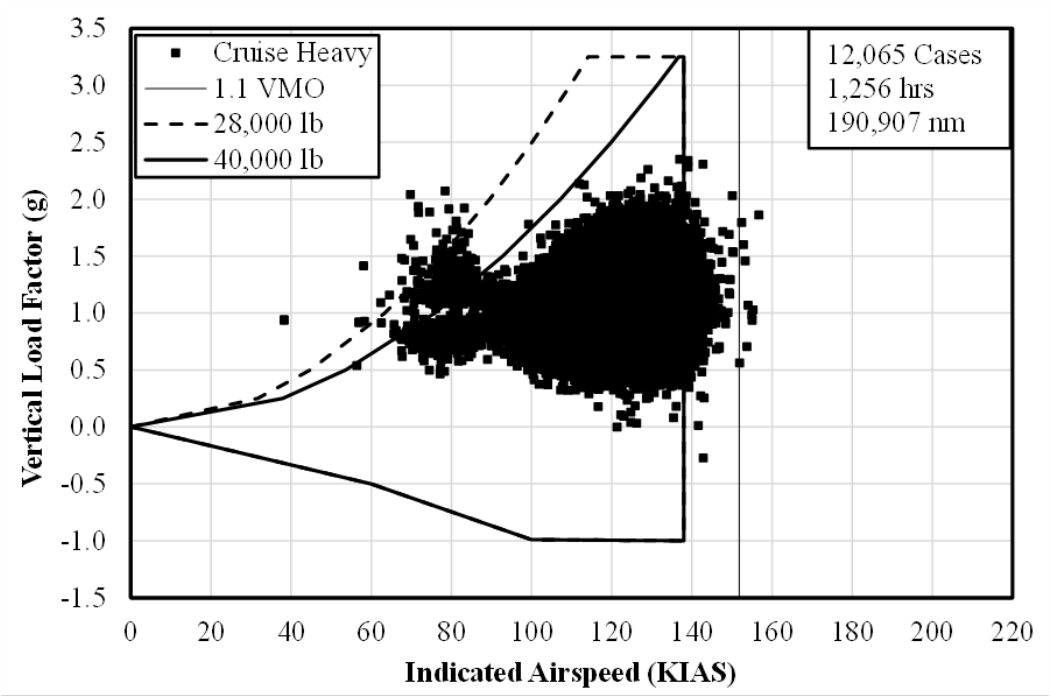

Figure A-26: *V-n* diagram with flaps in detent 2 – Cruise Heavy

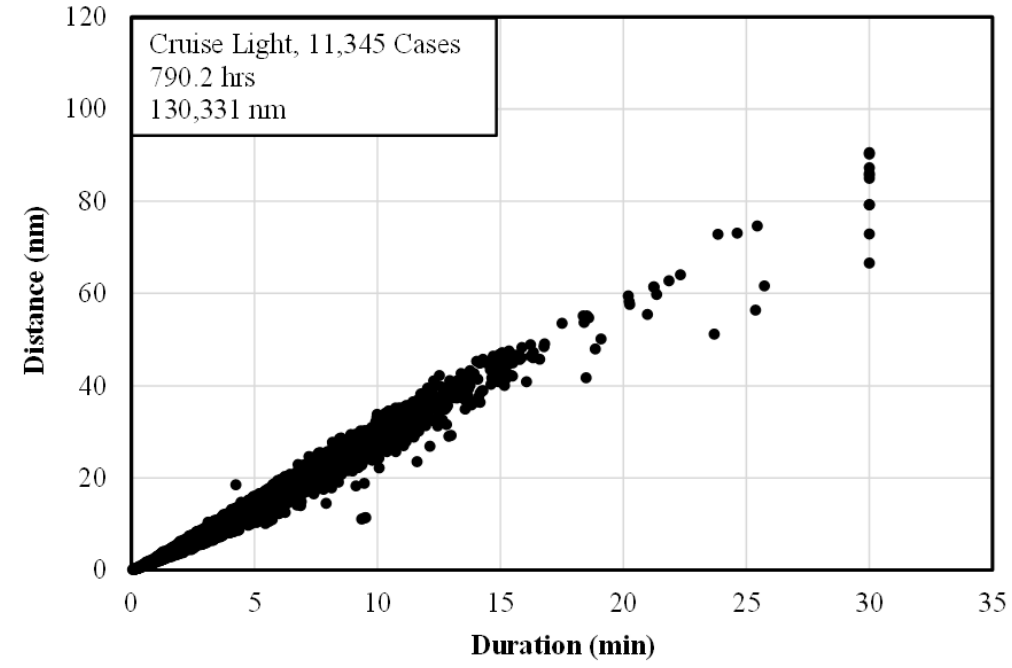

Figure A-27: Correlation of distance and duration – Cruise Light

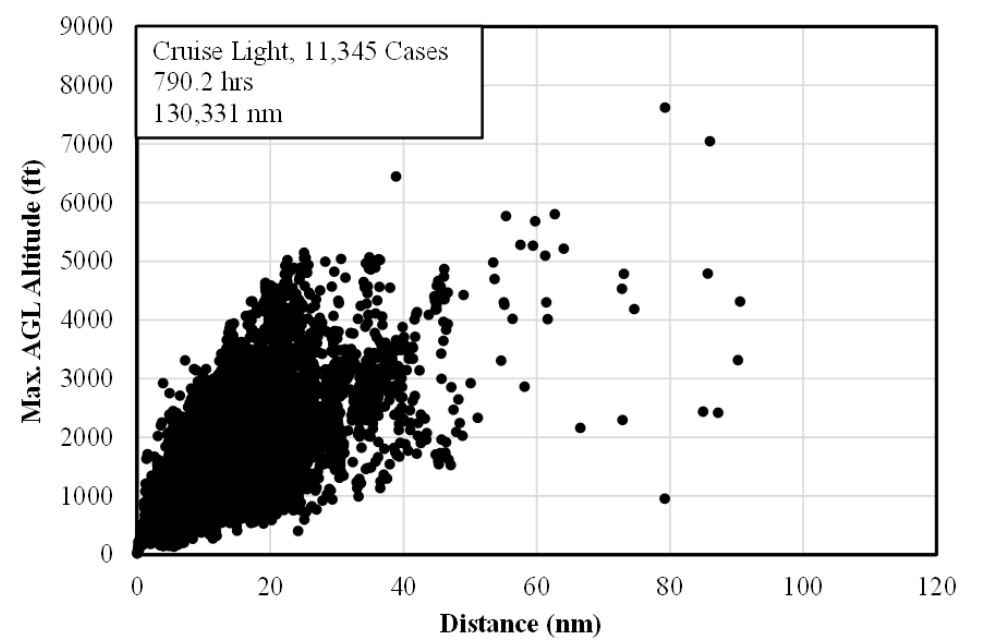

Figure A-28: Maximum AGL altitude and coincident distance – Cruise Light

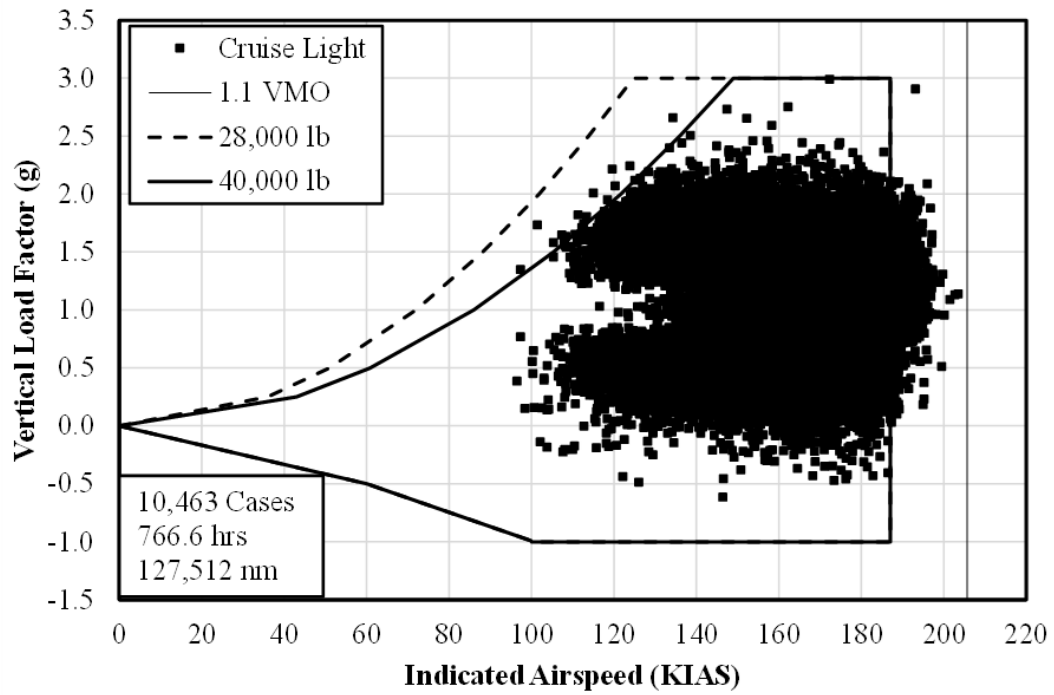

Figure A-29: *V-n* diagram with flaps retracted – Cruise Light

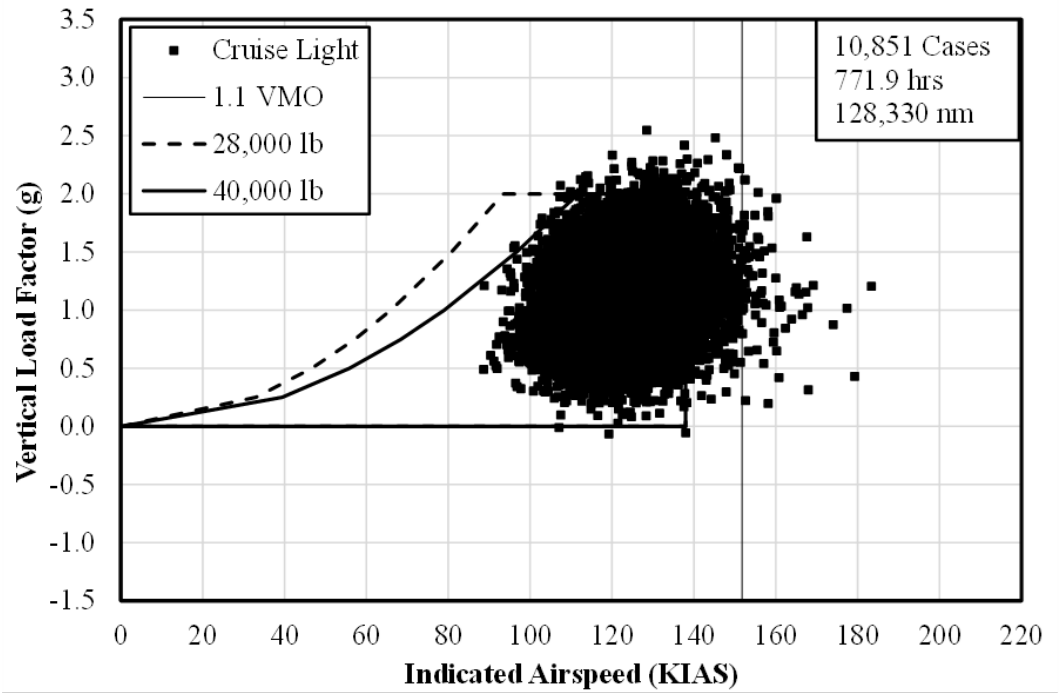

Figure A-30: *V-n* diagram with flaps in detent 1 – Cruise Light

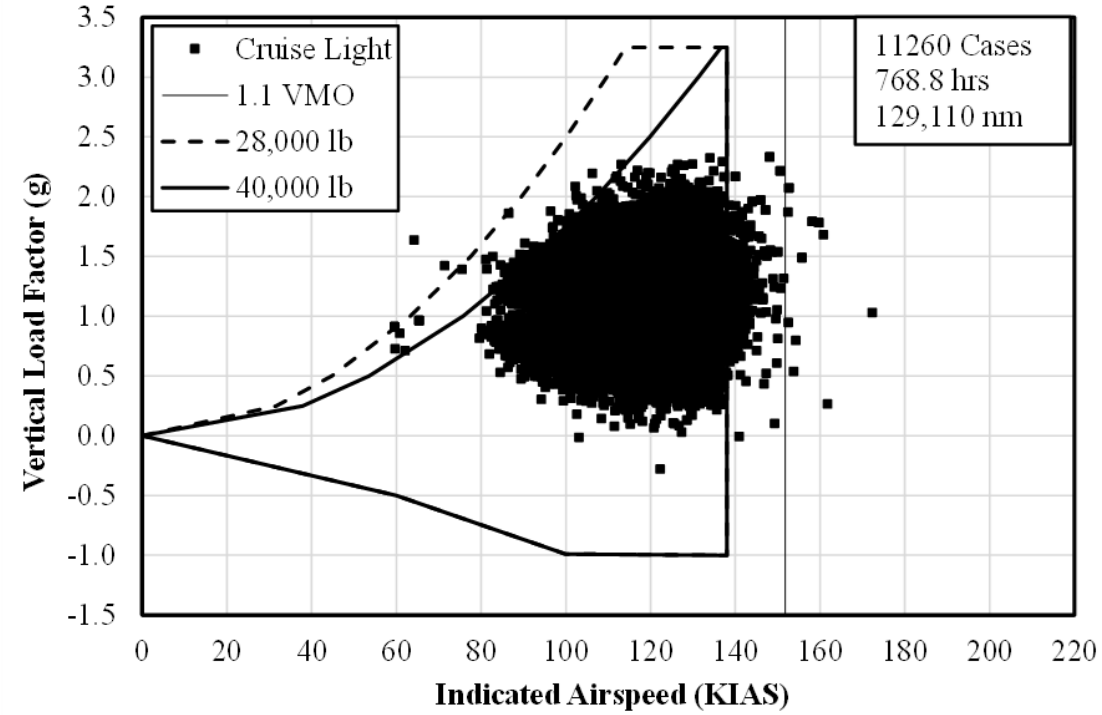

Figure A-31: *V-n* diagram with flaps in detent 2 – Cruise Light

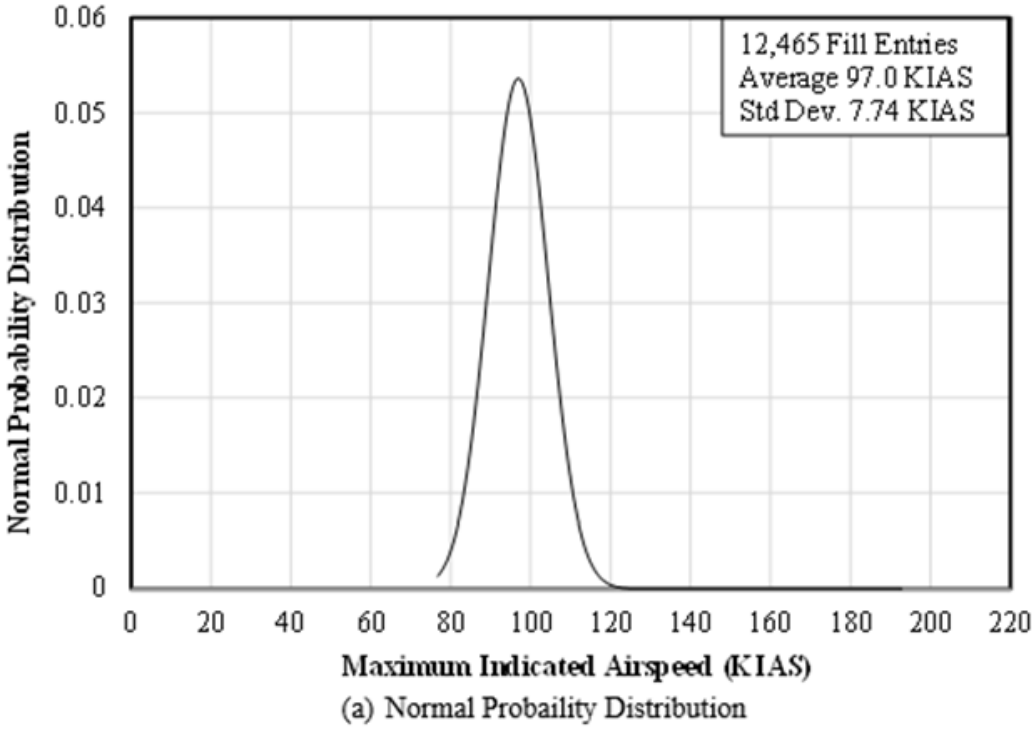

(a) Normal Probaility Distribution

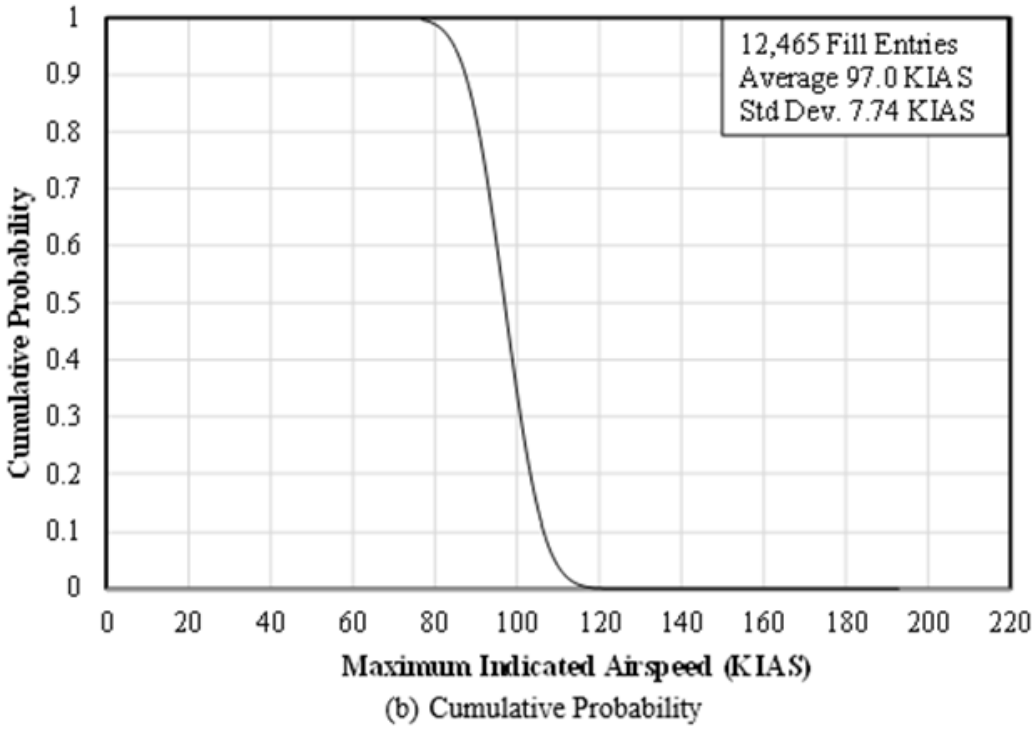

(b) Cumulative Probability

Figure A-32: Probability of maximum indicated airspeed – Fill Entry

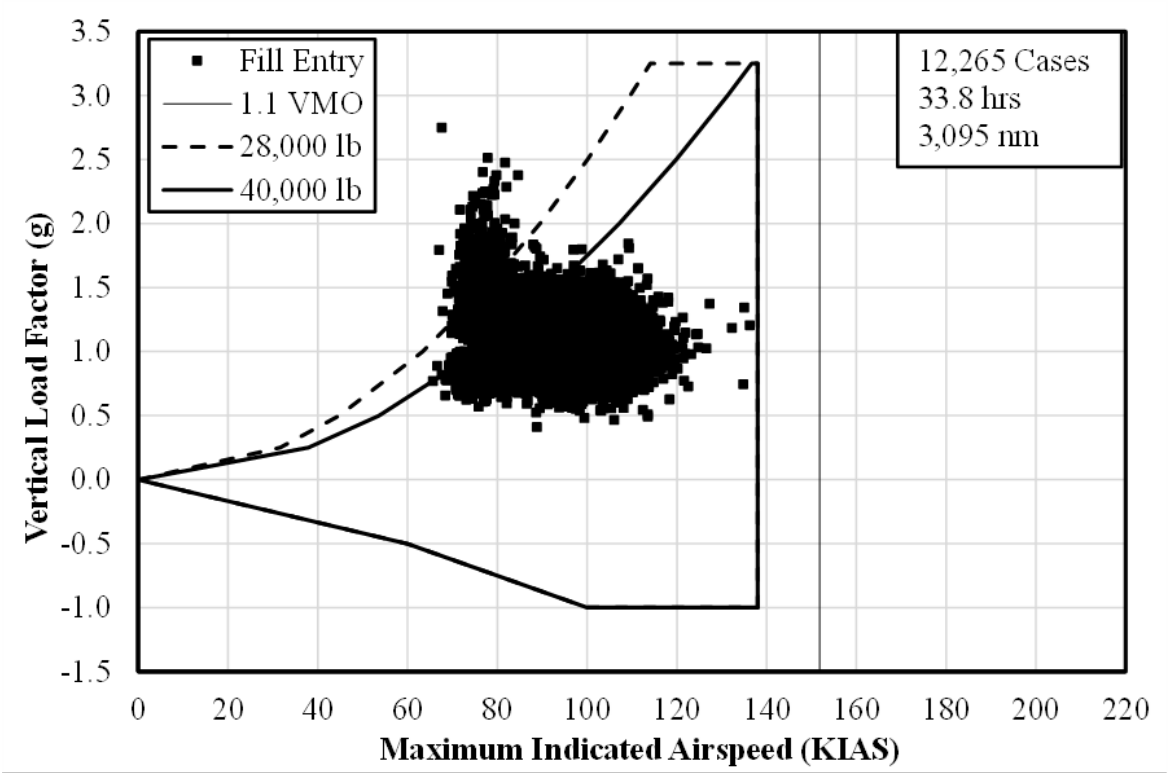

Figure A-33: *V-n* diagram with flaps in detent 2 – Fill Entry

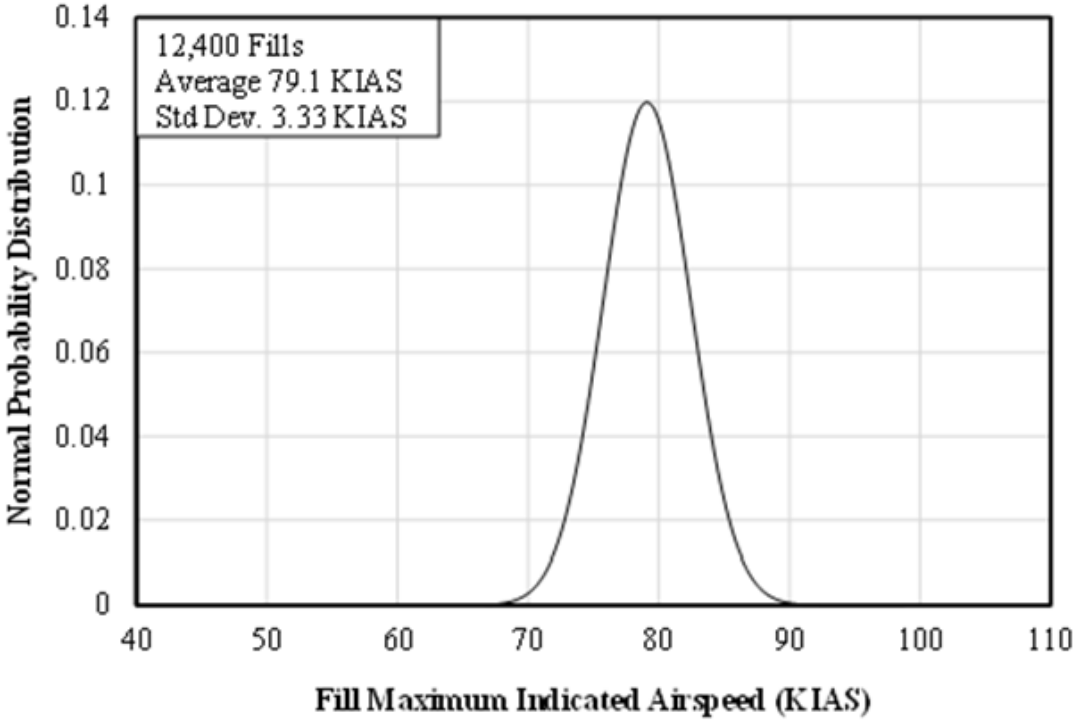

(a) Normal Probability Distribution

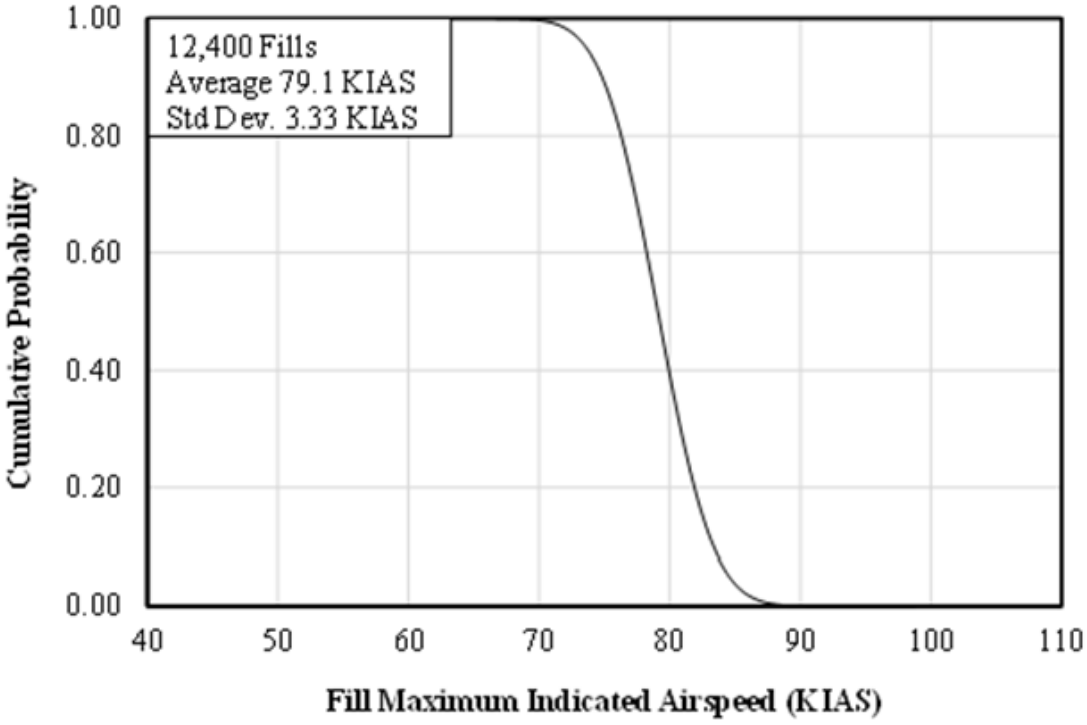

(b) Cumulative Probability

Figure A-34: Probability of maximum airspeed – Fill

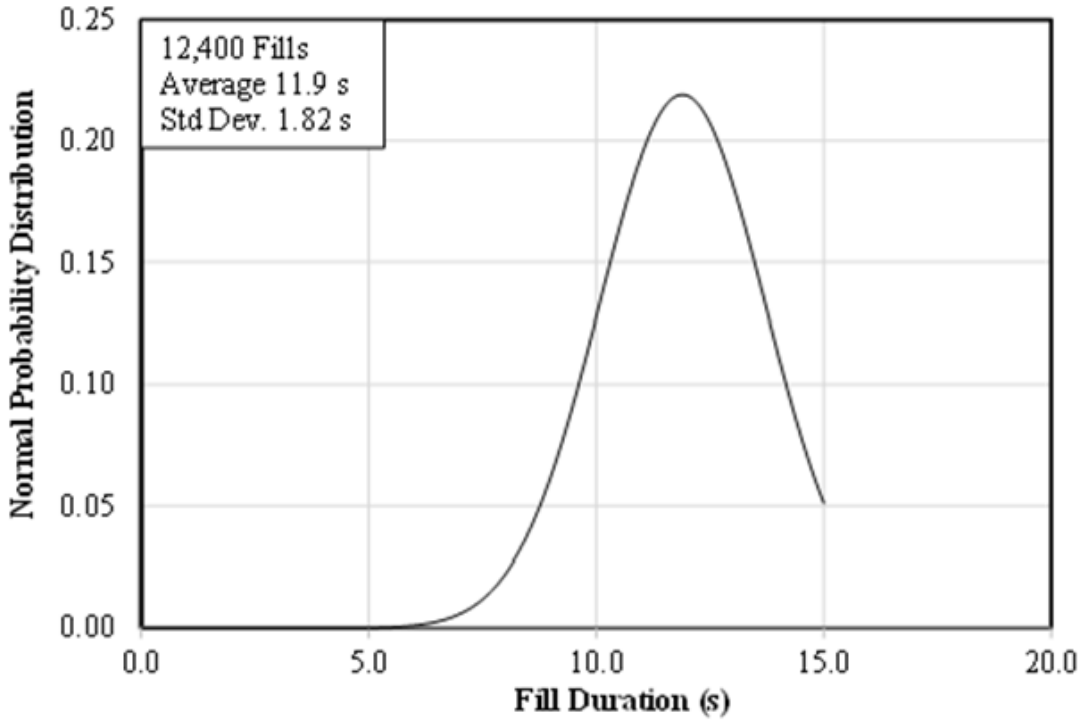

(a) Normal Probability Distribution

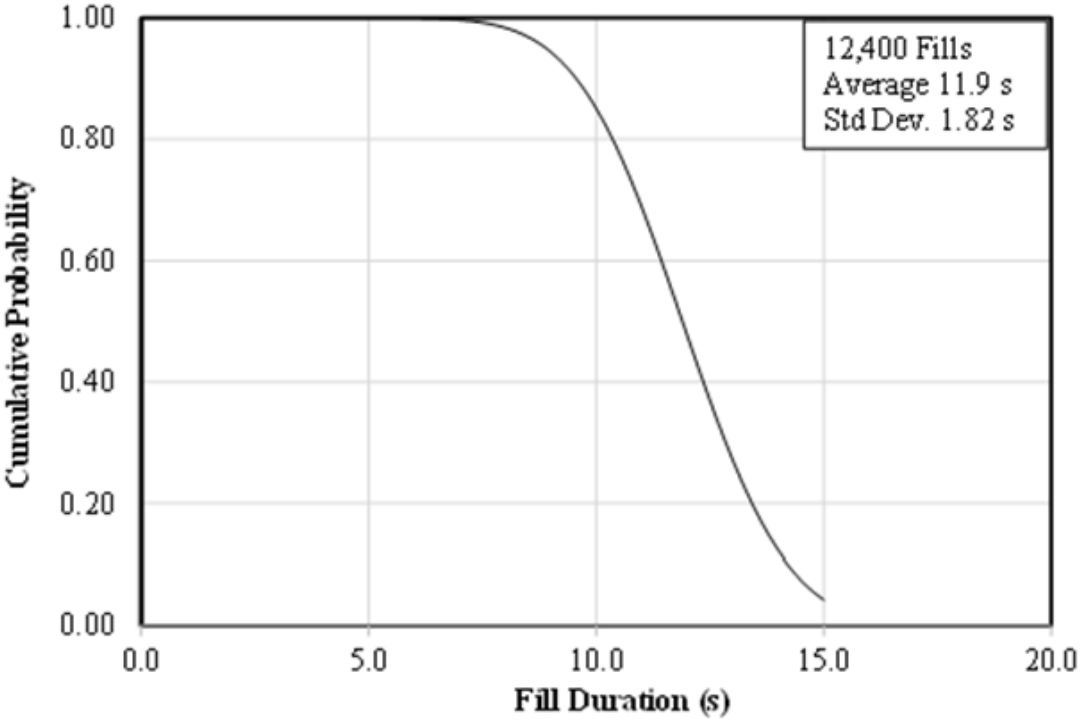

(b) Cumulative Probability

Figure A-35: Probability of duration – Fill

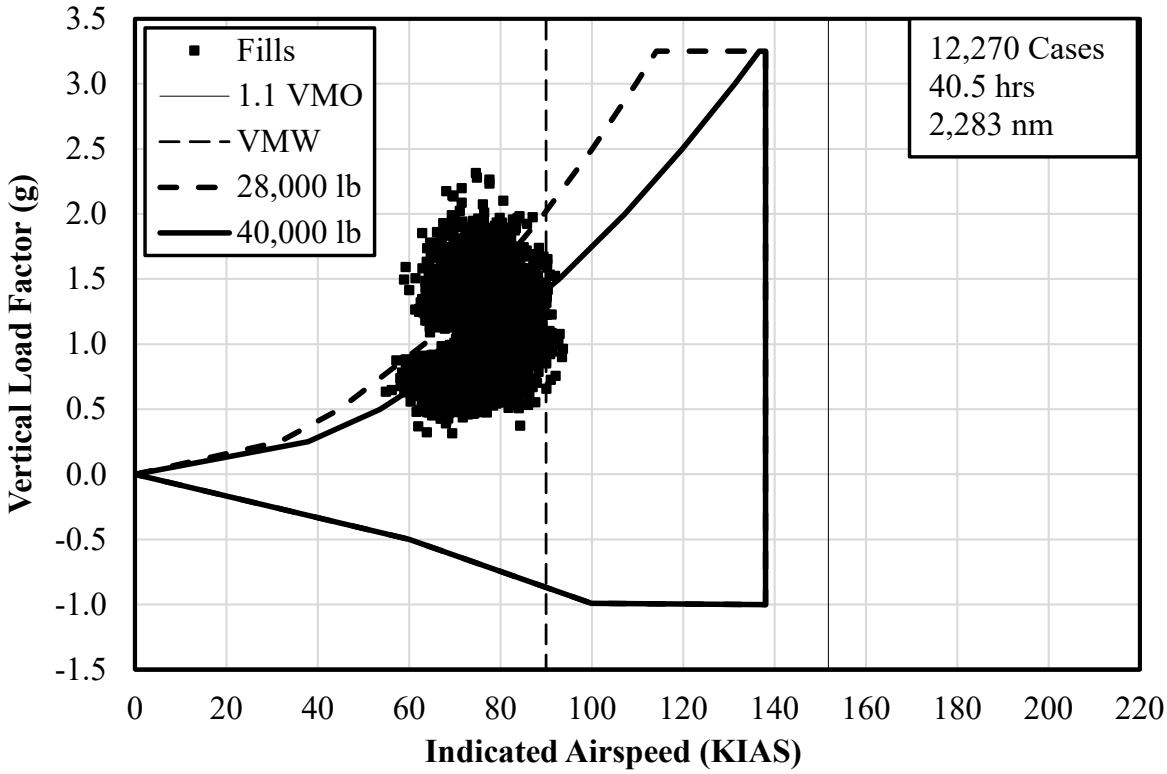

Figure A-36: *V-n* diagram with flaps in detent 2 – Fill

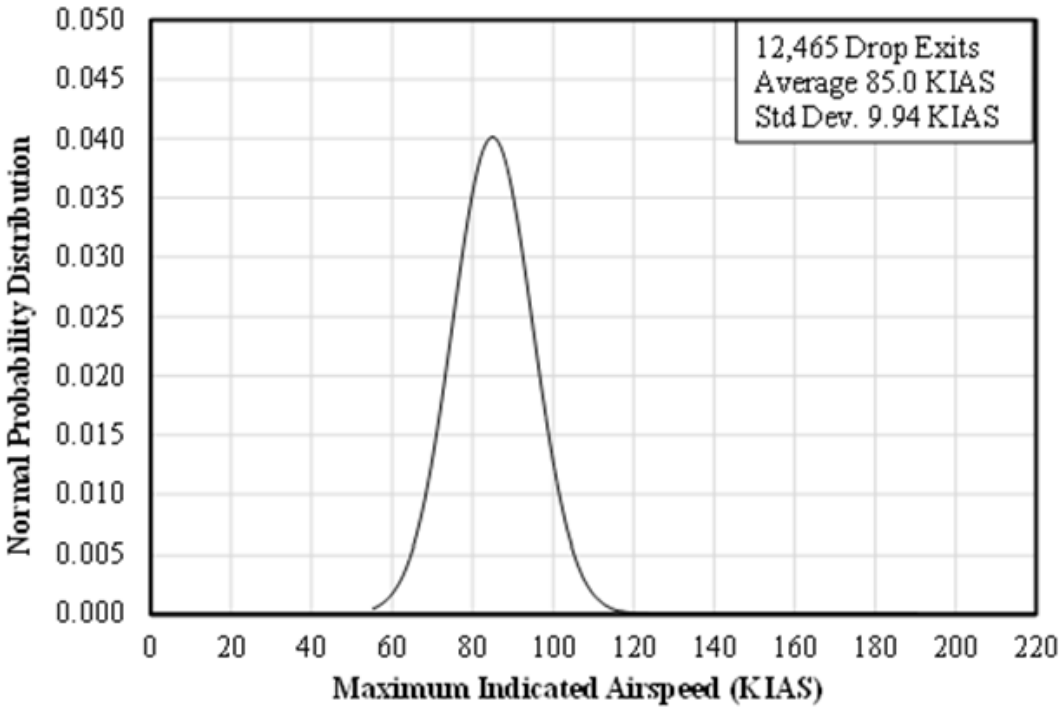

(a) Normal Probability Distribution

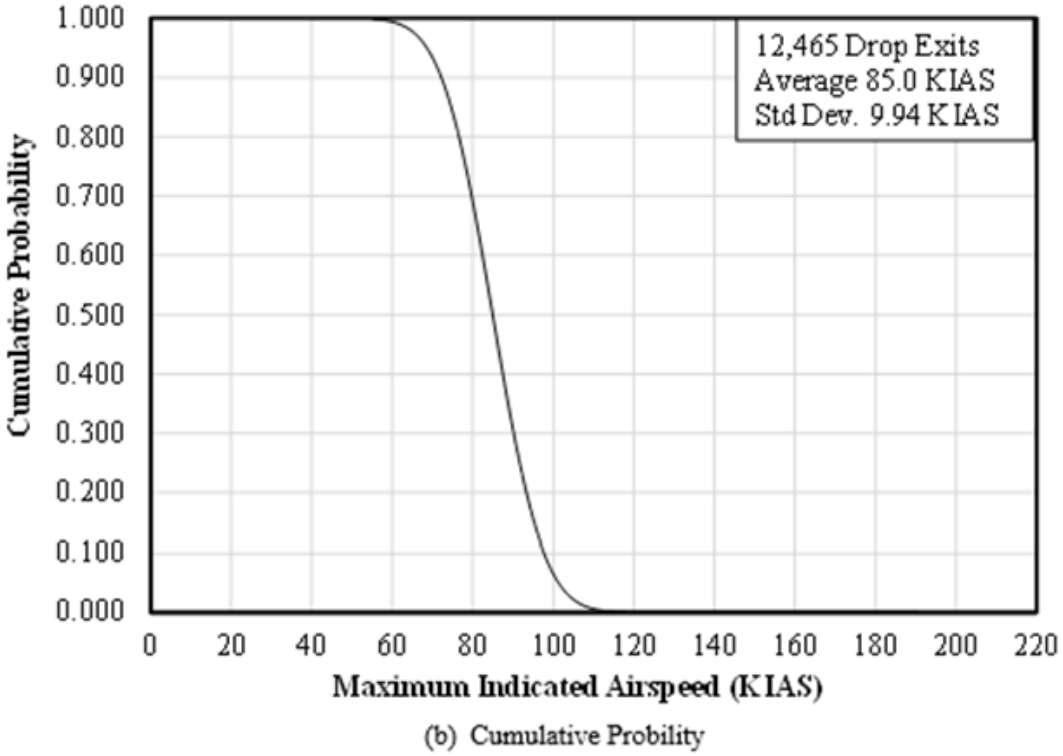

(b) Cumulative Probility

Figure A-37: Probability of maximum airspeed – Fill Exit

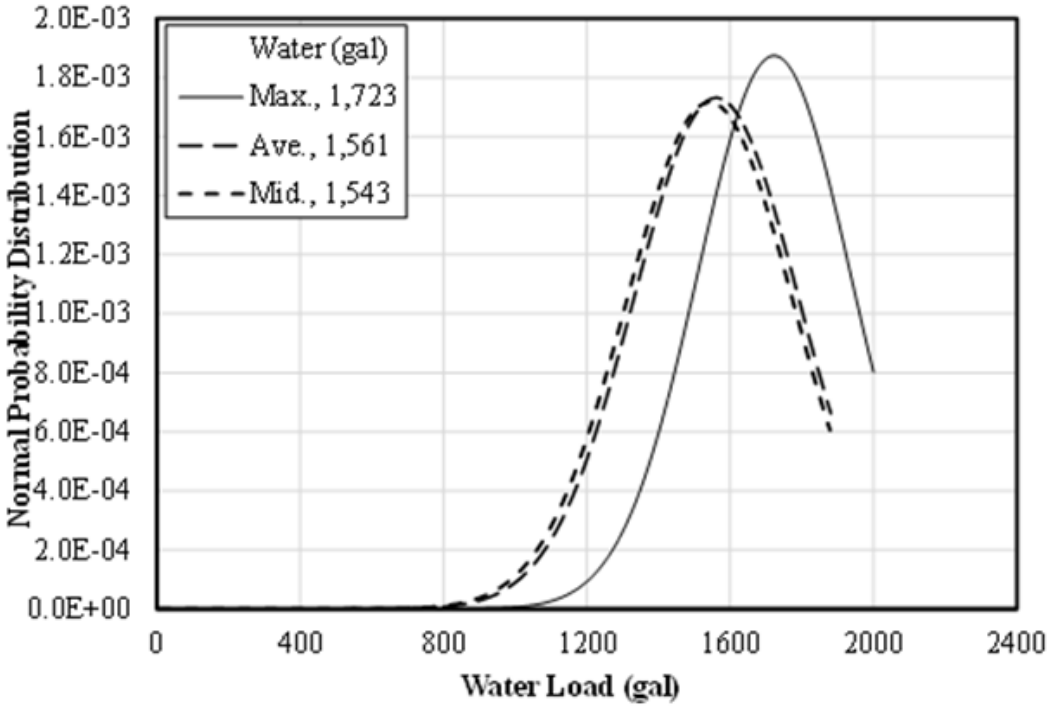

(a) Normal Probability Distribution

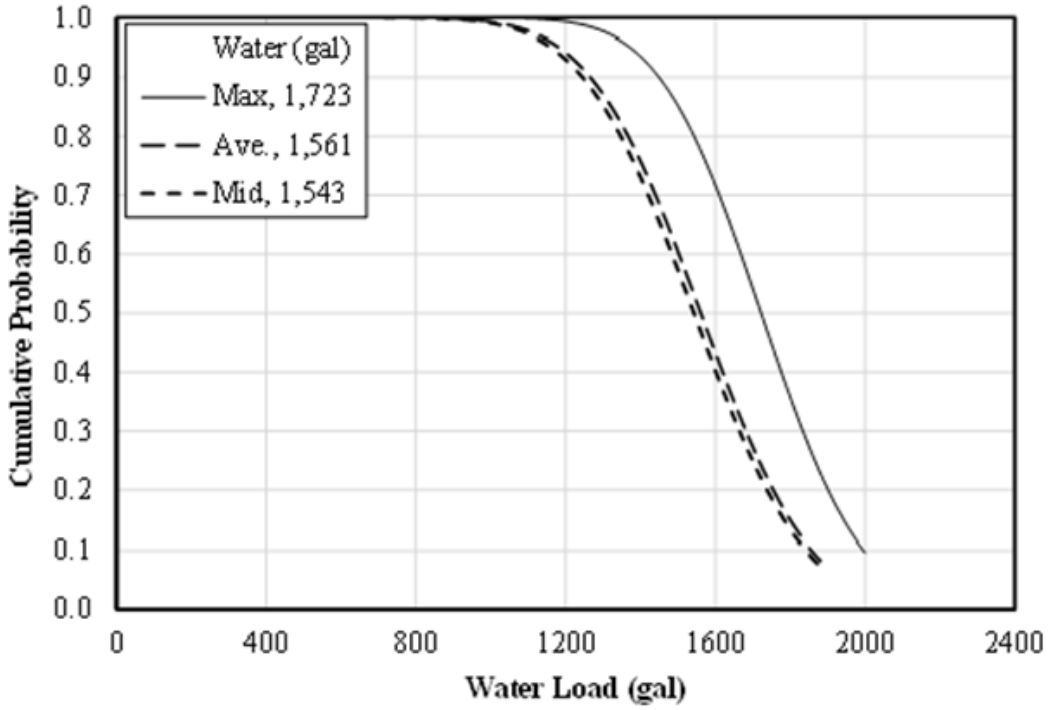

(b) Cumulative Probability

Figure A-38: Probability of water load carried – Fill Exit

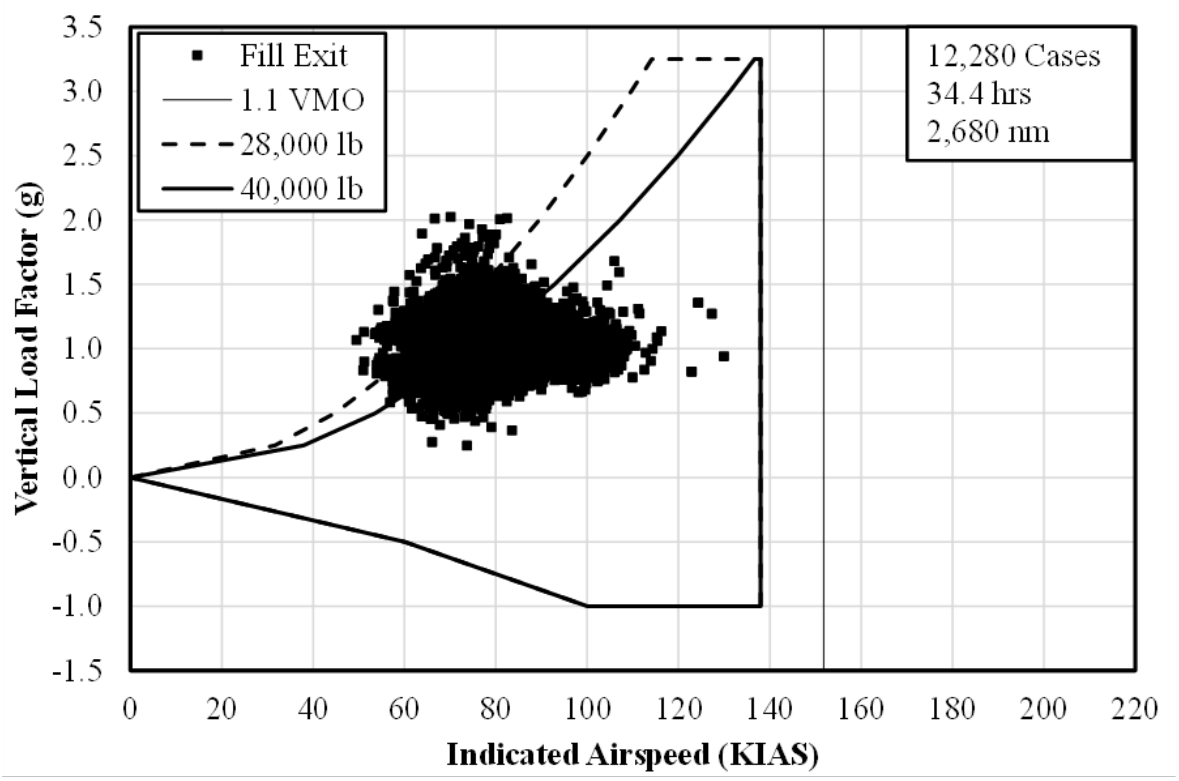

Figure A-39: *V-n* diagram with flaps in detent 2 – Fill Exit

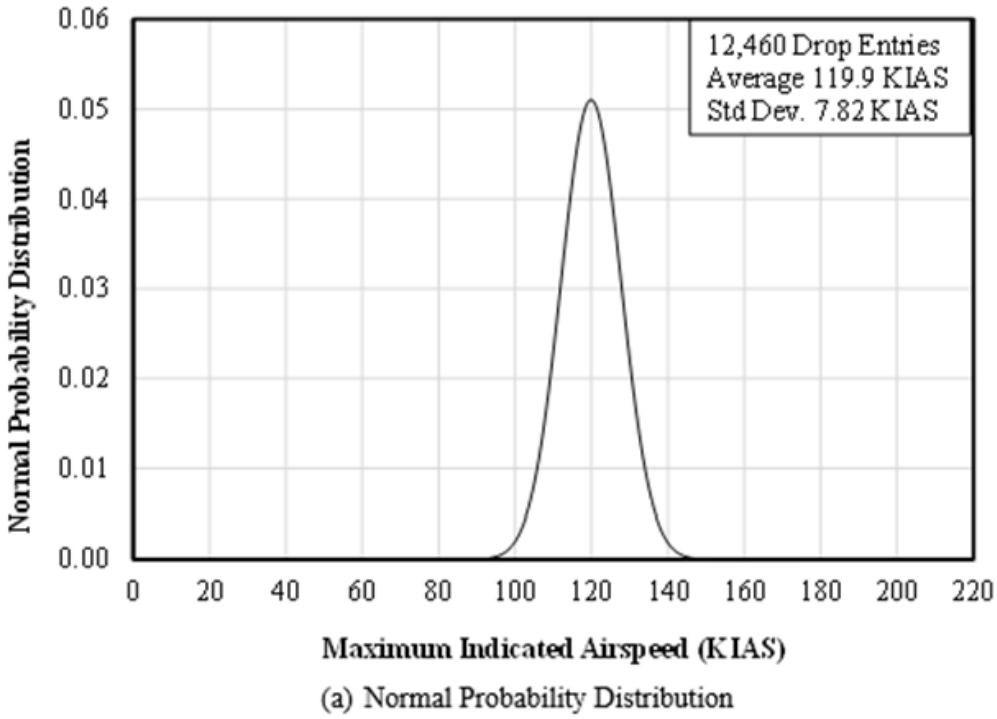

(a) Normal Probability Distribution

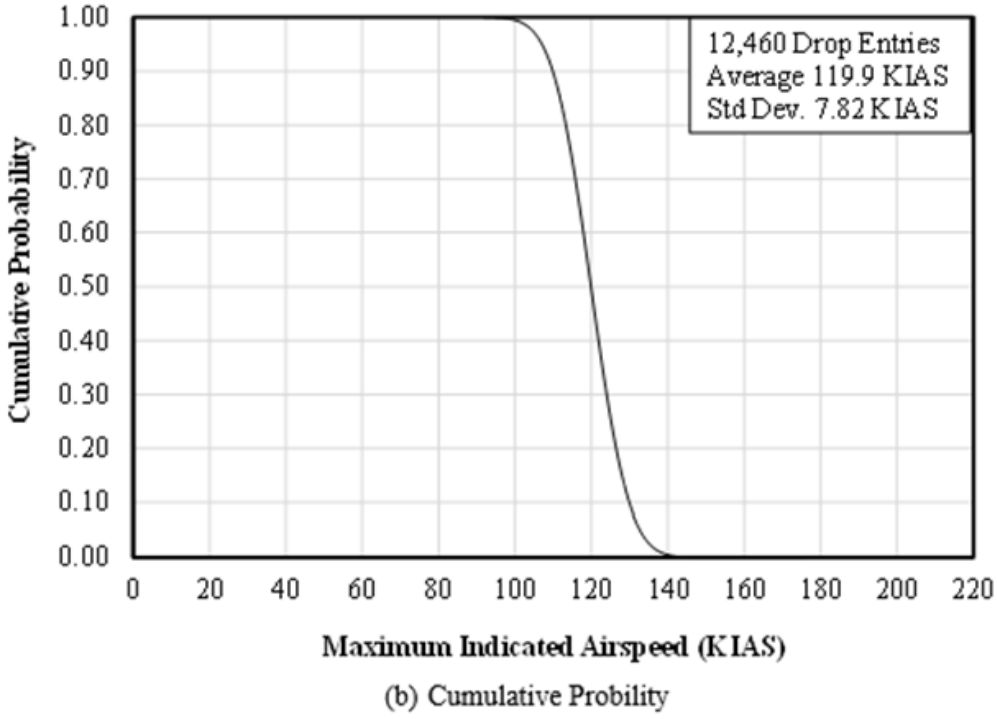

(b) Cumulative Probility

Figure A-40: Probability of maximum airspeed – Drop Entry

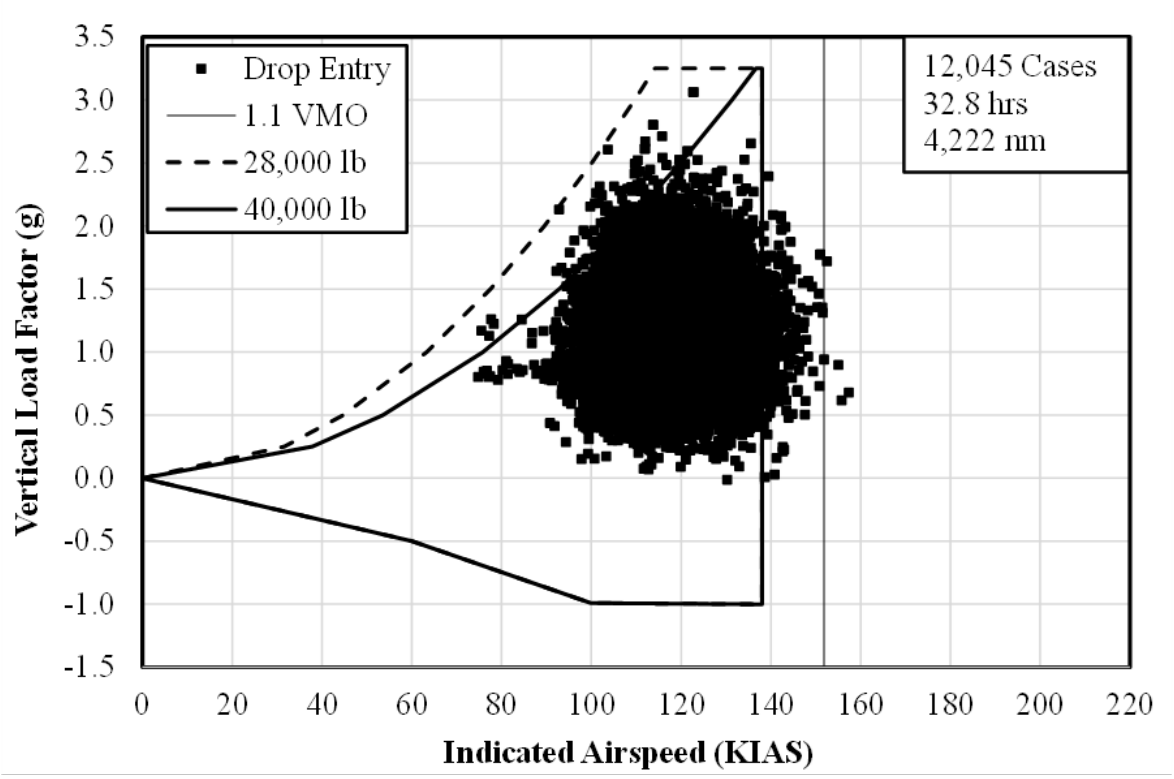

Figure A-41: *V-n* diagram with flaps in detent 2 – Drop Entry

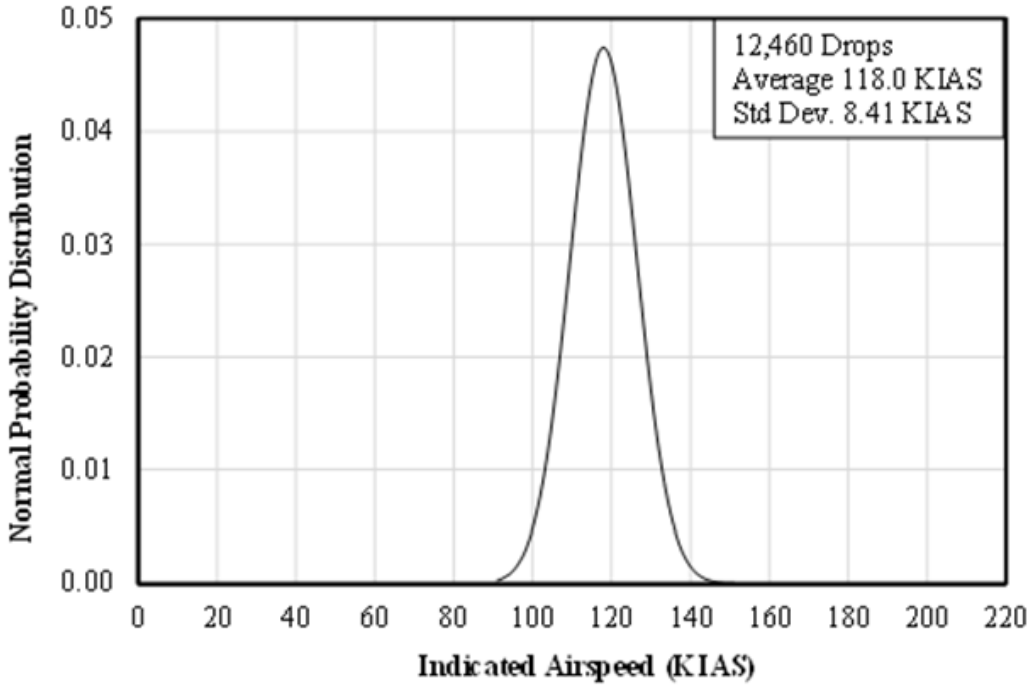

(a) Normal Probability Distribution

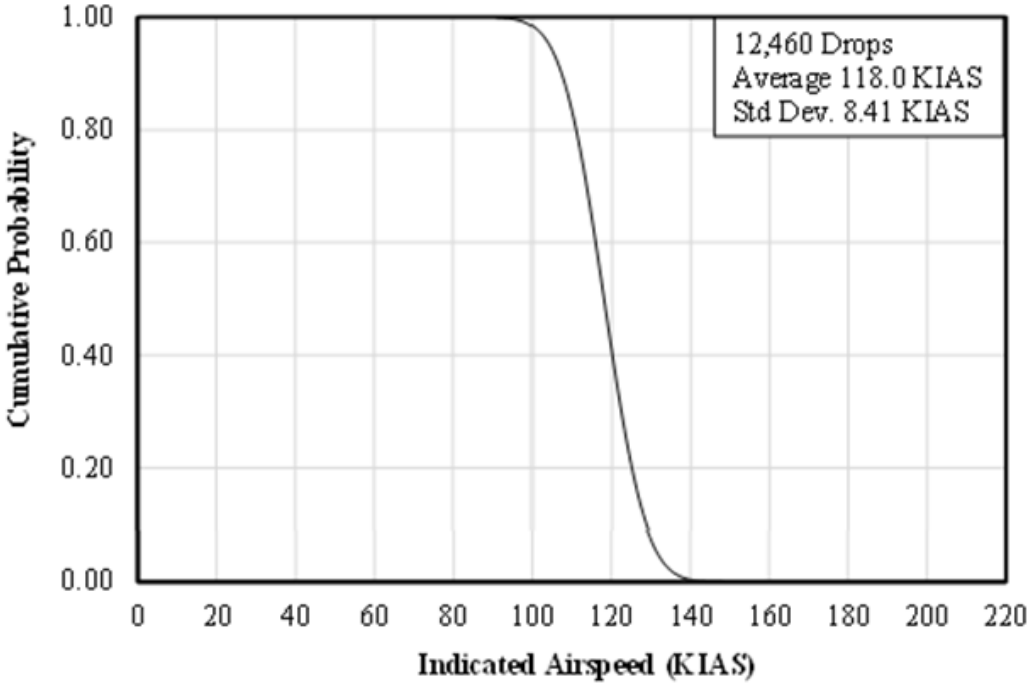

(b) Cumulative Probability

Figure A-42: Probability of maximum airspeed – Drop

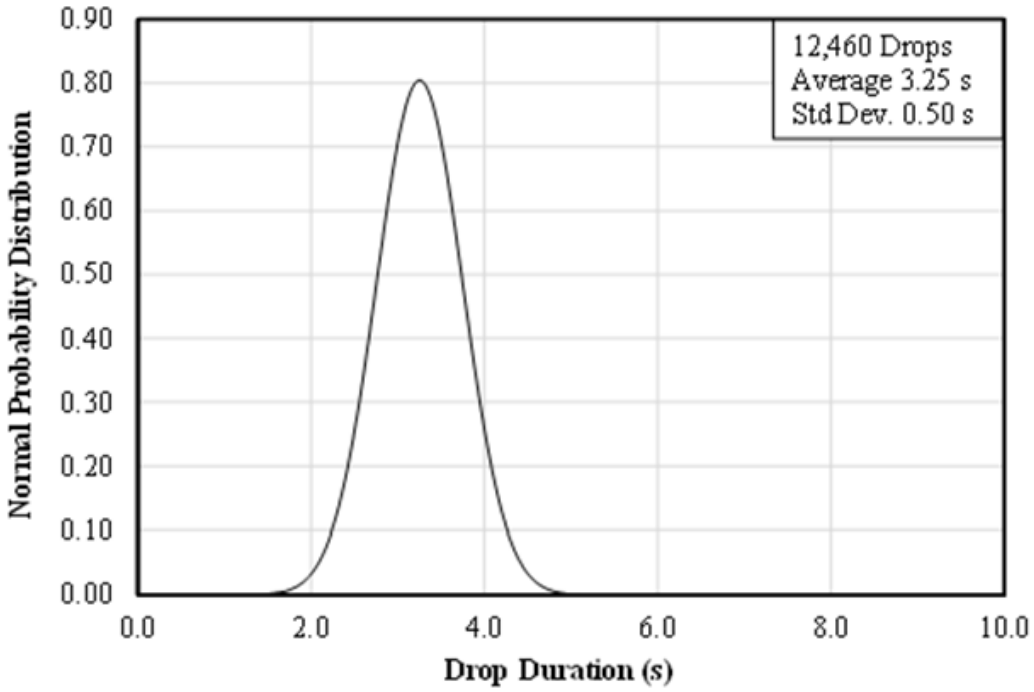

(a) Normal Probability Distribution

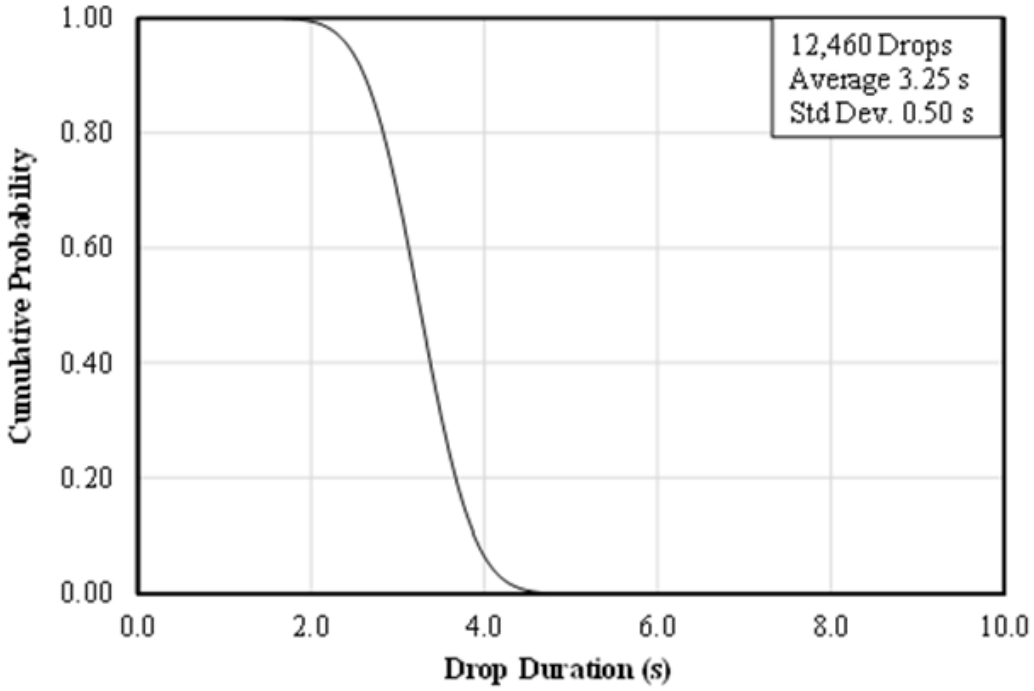

(b) Cumulative Probability

Figure A-43: Probability of duration – Drop

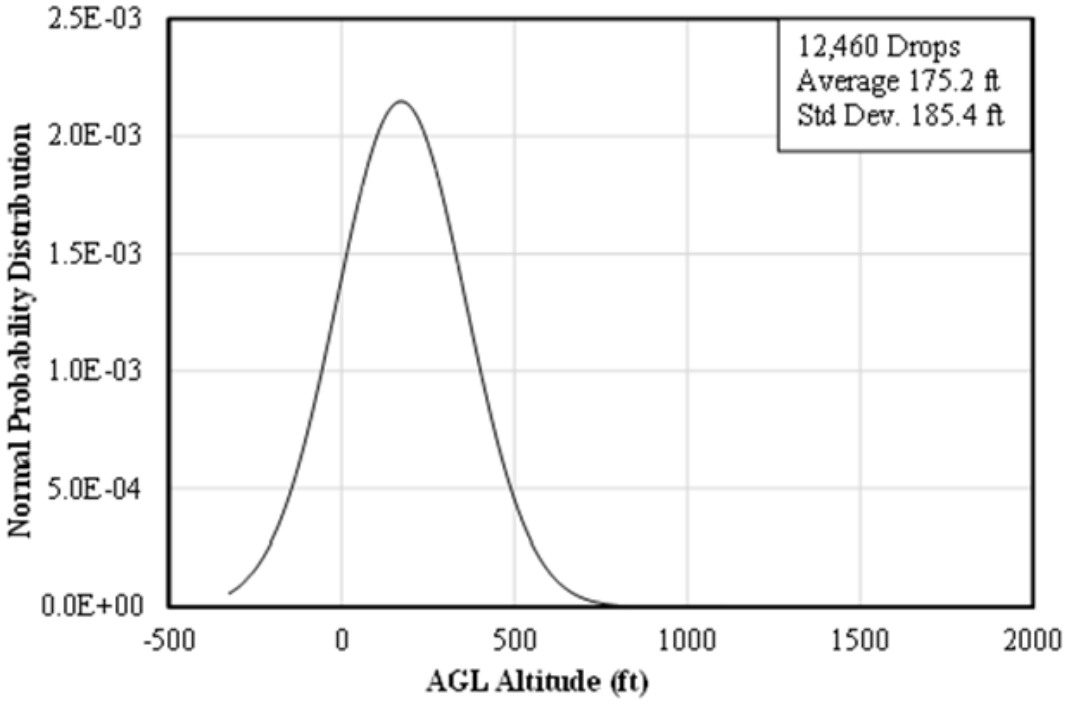

(a) Normal Probability Distribution

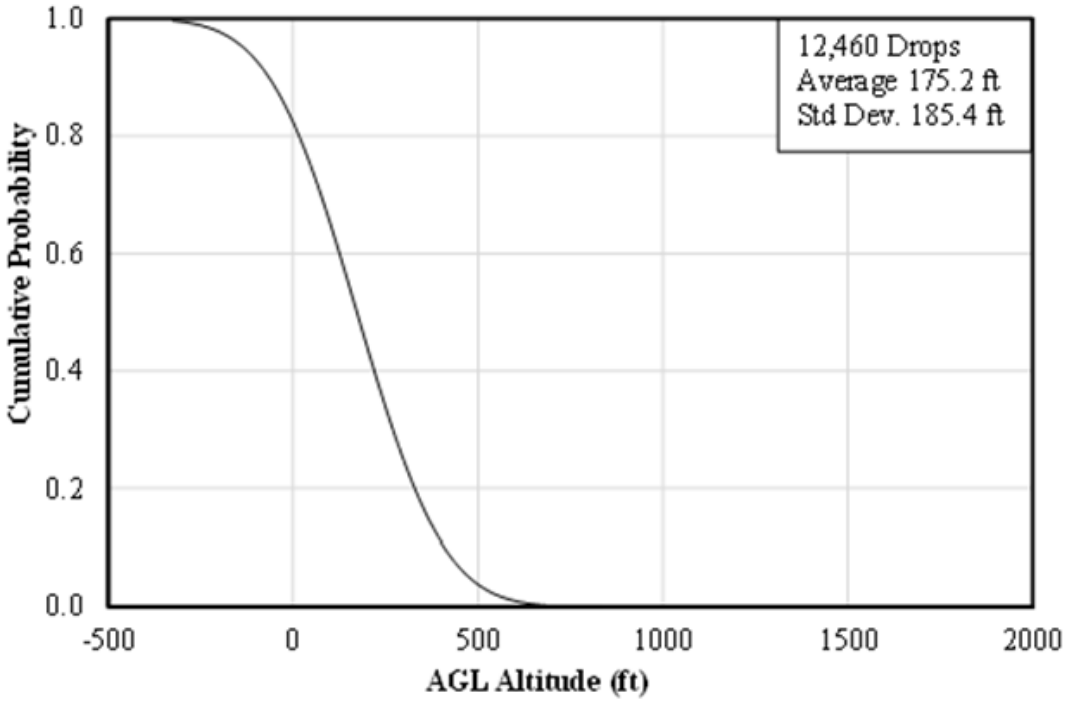

(b) Cumulative Probability

Figure A-44: Probability of altitude – Drop

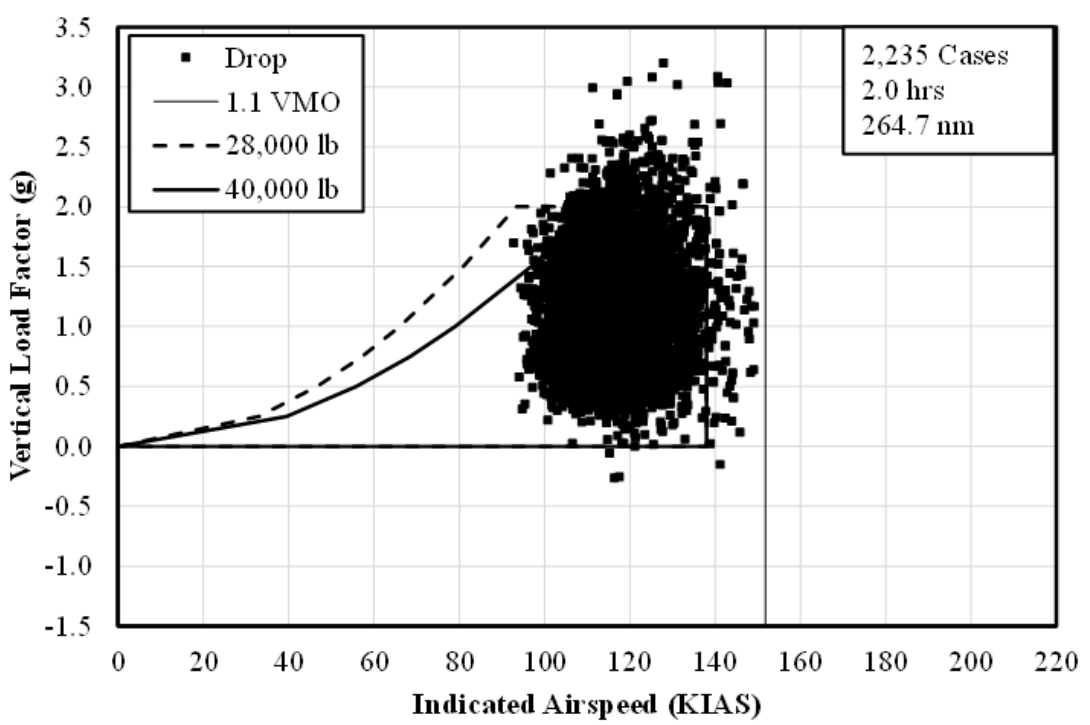

Figure A-45: *V-n* diagram with flaps in detent 1 – Drop

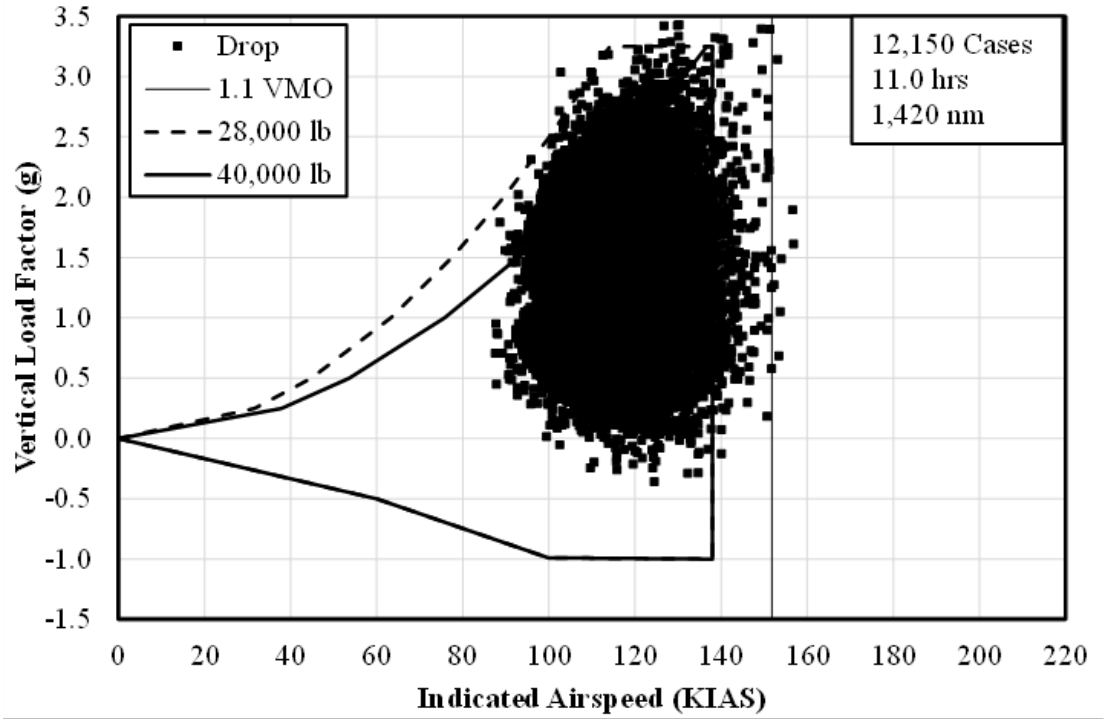

Figure A-46: *V-n* diagram with flaps in detent 2 – Drop

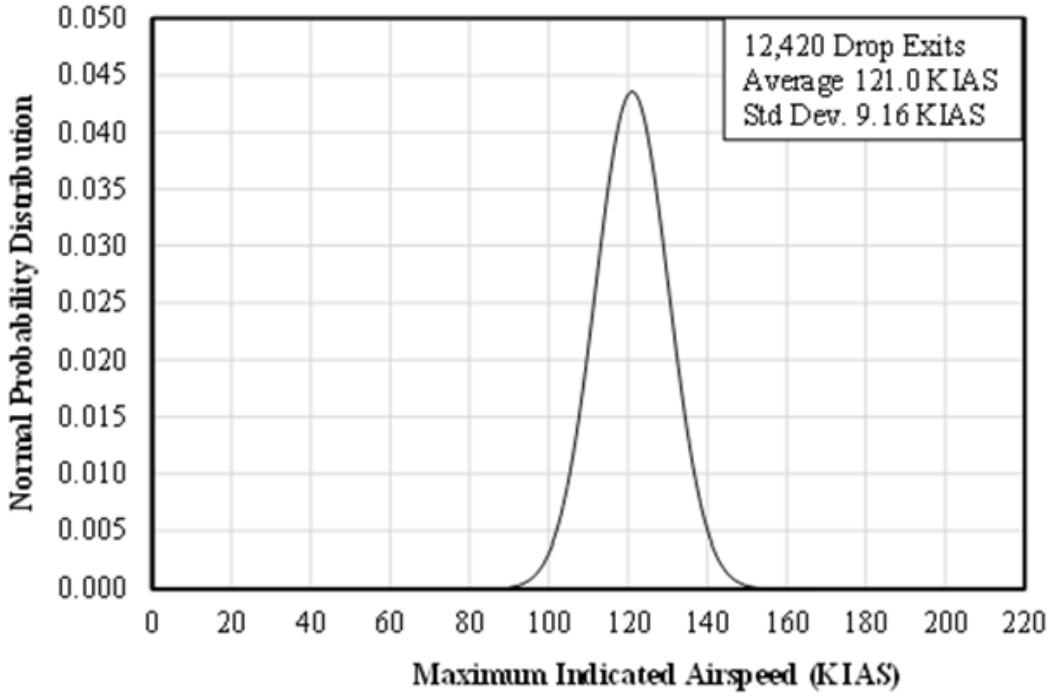

(a) Normal Probability Distribution

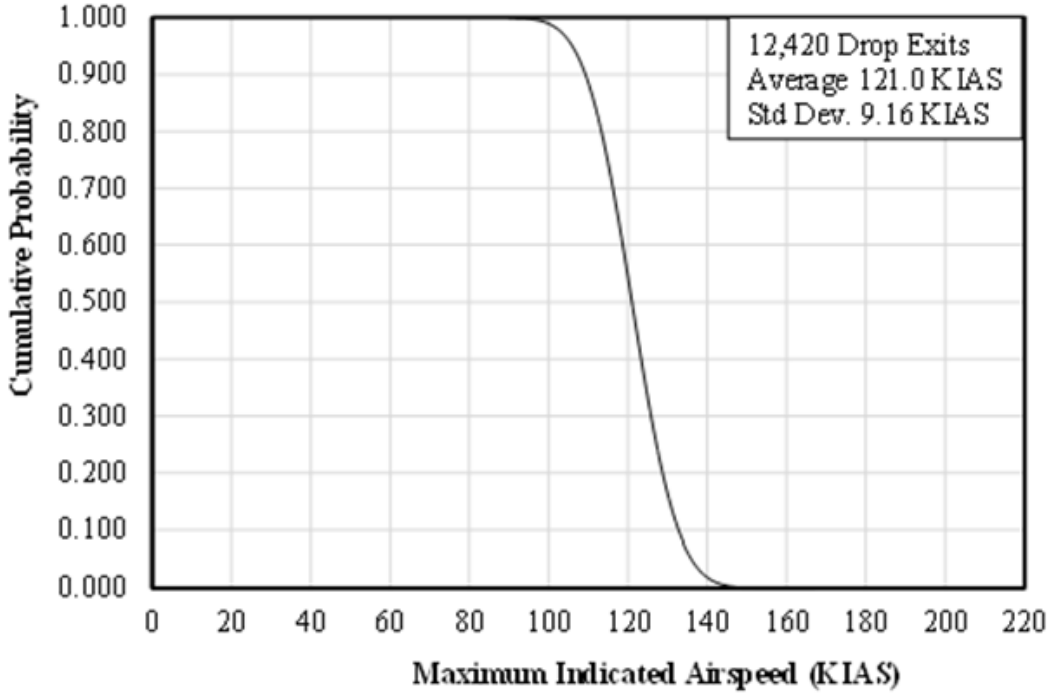

(b) Cumulative Probability

Figure A-47: Probability of maximum airspeed – Drop Exit

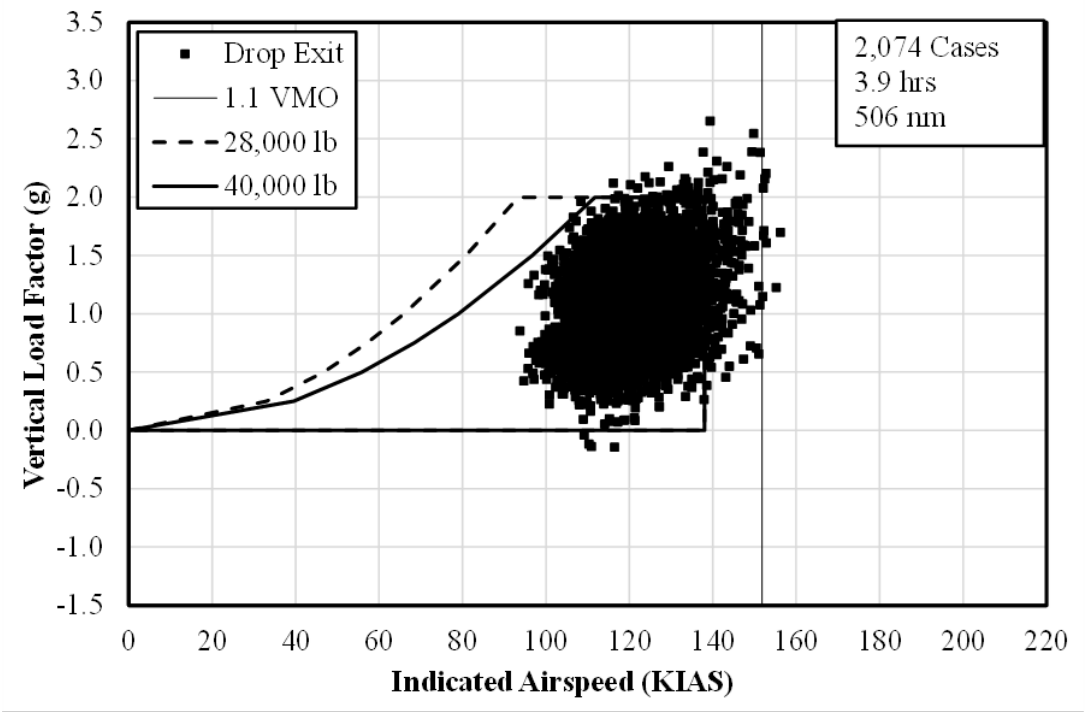

Figure A-48: *V-n* diagram with flaps in detent 1 – Drop Exit

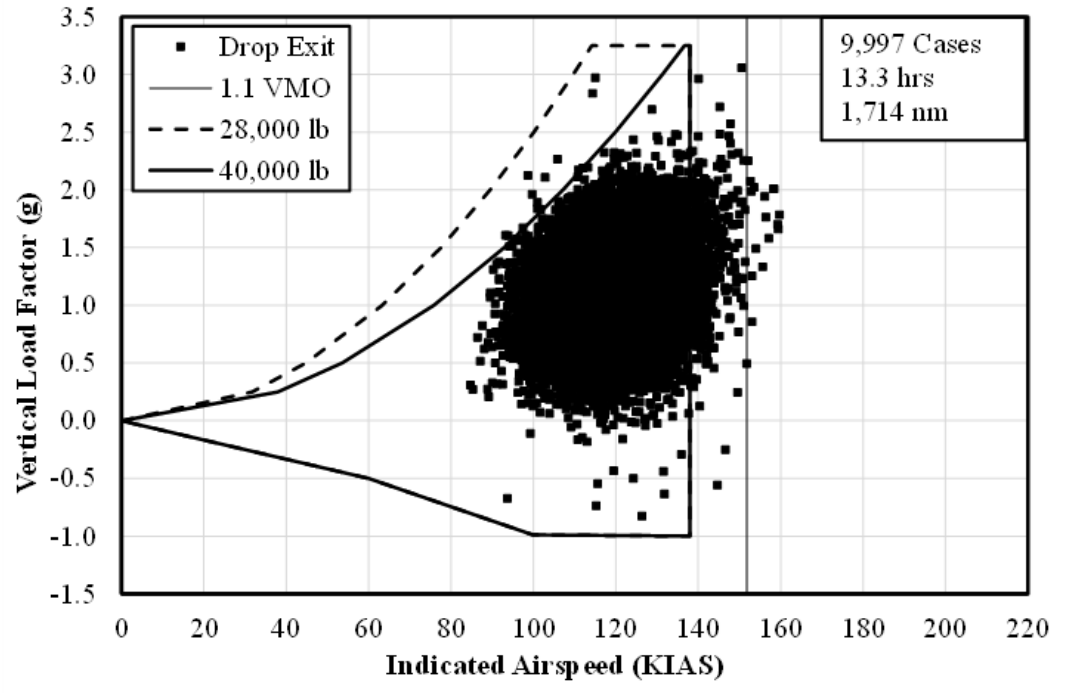

Figure A-49: *V-n* diagram with flaps in detent 2 – Drop Exit

.

B Flight loads by AGL altitude

Figures

Tables

Table B-1: Statistical formats – Flight loads data by AGL altitude

Flight Loads Data	**Table**
OVERALL SUMMARY	
Summary of Durations and Distances for all Flight Phases	B-3
CRUISE PHASES	
Summary of Durations and Distances for Cruise 1 by AGL Altitude	B-4
Summary of Durations and Distances for Cruise 2 by AGL Altitude	B-5
Summary of Durations and Distances for Cruise Heavy by AGL Altitude	B-6
Summary of Durations and Distances for Cruise Light by AGL Altitude	B-7
Summary of Durations and Distances for Ferry Flights by AGL Altitude	B-8
Summary of Durations and Distances for Maint./Training by AGL Altitude	B-9
FILL ENTRY, FILL, FILL EXIT PHASES	
Summary of Durations and Distances for Fill Entry by AGL Altitude	B-10
Summary of Durations and Distances for Fill by AGL Altitude	B-11
Summary of Durations and Distances for Fill Exit by AGL Altitude	B-12
DROP ENTRY, DROP, DROP EXIT PHASES	
Summary of Durations and Distances for Drop Entry by AGL Altitude	B-13
Summary of Durations and Distances for Drop by AGL Altitude	B-14
Summary of Durations and Distances for Drop Exit by AGL Altitude	B-15

Table B-2: Statistical Formats – Flight loads data by AGL altitude

Flight Loads Data	**Figure**
CRUISE PHASES	
Cumulative Occurrences of Incremental Vertical Gust Load Factor, Cruise 1	B-1
Cumulative Occurrences of Incremental Vertical Maneuver Load Factor, Cruise 1	B-2
Cumulative Occurrences of Incremental Vertical Gust Load Factor, Cruise 2	B-3
Cumulative Occurrences of Incremental Vertical Maneuver Load Factor, Cruise 2	B-4
Cumulative Occurrences of Incremental Vertical Gust Load Factor, Cruise Heavy	B-5
Cumulative Occurrences of Incremental Vertical Maneuver Load Factor, Cruise Heavy	B-6
Cumulative Occurrences of Incremental Vertical Gust Load Factor, Cruise Light	B-7
Cumulative Occurrences of Incremental Vertical Maneuver Load Factor, Cruise Light	B-8
Cumulative Occurrences of Incremental Vertical Gust Load Factor, Ferry	B-9
Cumulative Occurrences of Incremental Vertical Maneuver Load Factor, Ferry	B-10
Cumulative Occurrences of Incremental Vertical Gust Load Factor, Maint./Training	B-11
Cumulative Occurrences of Incremental Vertical Maneuver Load Factor, Maint./Training	B-12
FILL ENTRY, FILL, FILL EXIT PHASES	
Cumulative Occurrences of Incremental Vertical Gust Load Factor, Fill Entry	B-13
Cumulative Occurrences of Incremental Vertical Maneuver Load Factor, Fill Entry	B-14
Cumulative Occurrences of Incremental Vertical Load Factor, Fill	B-15
Cumulative Occurrences of Incremental Vertical Gust Load Factor, Fill Exit	B-16
Cumulative Occurrences of Incremental Vertical Maneuver Load Factor, Fill Exit	B-17
DROP ENTRY, DROP, DROP EXIT PHASES	
Cumulative Occurrences of Incremental Vertical Gust Load Factor, Drop Entry	B-18
Cumulative Occurrences of Incremental Vertical Maneuver Load Factor, Drop Entry	B-19
Cumulative Occurrences of Incremental Vertical Gust Load Factor, Drop	B-20
Cumulative Occurrences of Incremental Vertical Maneuver Load Factor, Drop	B-21
Cumulative Occurrences of Incremental Vertical Gust Load Factor, Drop Exit	B-22
Cumulative Occurrences of Incremental Vertical Maneuver Load Factor, Drop Exit	B-23

Table B-3: Summary of durations and distances for all flight phases

Phase	Duration (min)	Duration (hr)	Distance (nm)
Cruise 1	35,009	583.5	98,434
Fill Entry	2,471	41.2	3,944
Fill	2,960	49.3	3,817
Fill Exit	2,470	41.2	3,416
Cruise Heavy	91,825	1,530	229,730
Drop Entry	2,472	41.2	3,947
Drop	809	13.5	1,696
Drop Exit	1,307	21.8	2,814
Cruise Light	57,247	954	155,806
Cruise 2	28,810	480	80,203
Ferry	50,423	840	146,457
Maint./Training	4,893	82	12,235

Table B-4: Summary of durations and distances for Cruise 1 by AGL altitude

Altitude Band	Duration (s)	Duration (hr)	Distance (nm)
1	1,682.4	28.04	3,734
2	7,698.7	128.3	20,154
3	16,584.8	276.4	47,575
4	8,676.6	144.6	25,829
5	366.5	6.11	1,124
6	0	0	0
Total	35,009	583.5	98,416

Table B-5: Summary of durations and distances for Cruise 2 by AGL altitude

Altitude Band	Duration (s)	Duration (hr)	Distance (nm)
1	1,393.9	23.2	3,148.4
2	8,414.1	140.2	22,107.5
3	15,608.6	260.1	44,760.9
4	3,318.7	55.3	9,960.1
5	74.7	1.2	225.1
6	0	0	0
Total	28,810	480	80,203

Table B-6: Summary of durations and distances for Cruise Heavy by AGL altitude

Altitude Band	Duration (s)	Duration (hr)	Distance (nm)
1	26,335.6	438.9	58,465.0
2	42,689.4	711.5	109,229.3
3	22,552.4	375.9	61,308.5
4	248.0	4.1	727.1
5	0	0	0
6	0	0	0
Total	91,825	1,530	229,730

Table B-7: Summary of durations and distances for Cruise Light by AGL altitude

Altitude Band	Duration (s)	Duration (hr)	Distance (nm)
1	19,140.1	319.0	46,203.3
2	28,396.5	473.3	80,310.6
3	9,584.6	159.7	28,912.0
4	126.4	2.1	380.1
5	0	0	0
6	0	0	0
Total	57,247	954	155,806

Table B-8: Summary of durations and distances for ferry flights by AGL altitude

Altitude Band	Duration (s)	Duration (hr)	Distance (nm)
1	482.3	8.0	1,009.9
2	3,866.8	64.4	9,992.2
3	21,495.0	358.2	61,546.4
4	22,208.9	370.1	66,683.0
5	2,369.9	39.5	7,225.6
6	14.4	0.24	44.9
Total	50,423	840	146,457

Table B-9: Summary of durations and distances for Maintenance/Training by AGL altitude

Altitude Band	Duration (s)	Duration (hr)	Distance (nm)
1	309.4	5.2	607.1
2	1,506.9	25.1	3,515.3
3	2,483.7	41.4	6,369.0
4	574.1	9.6	1,681.8
5	18.8	0.31	61.8
6	0	0	0
Total	4,893	82	12,235

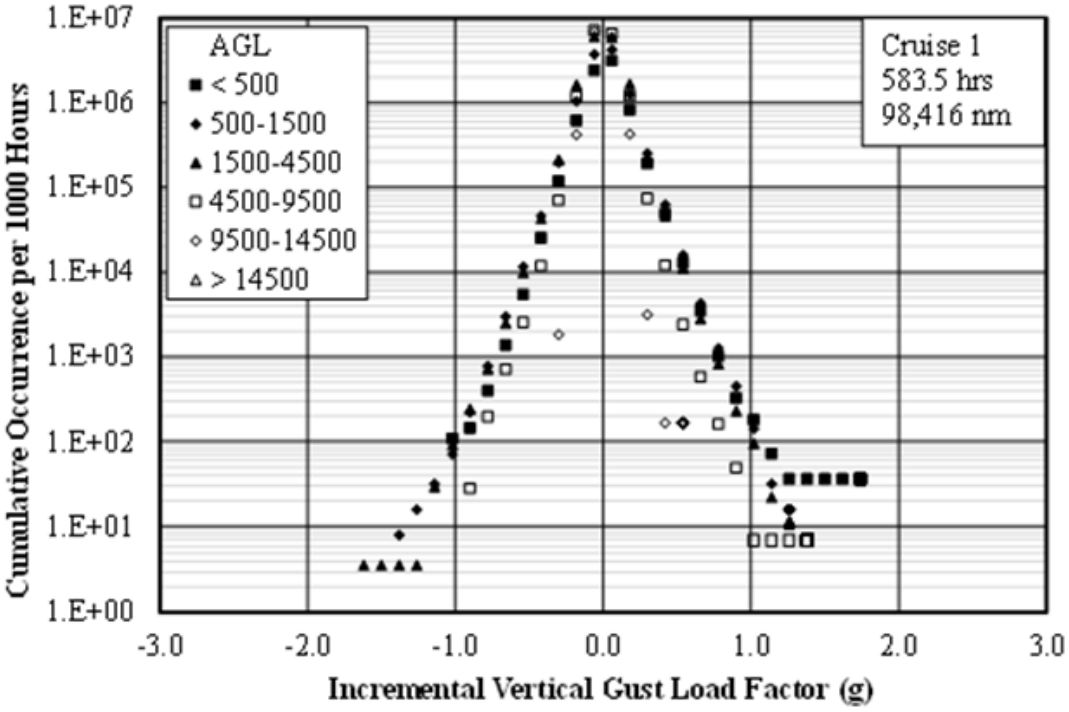

(a) Per 1000 Hours

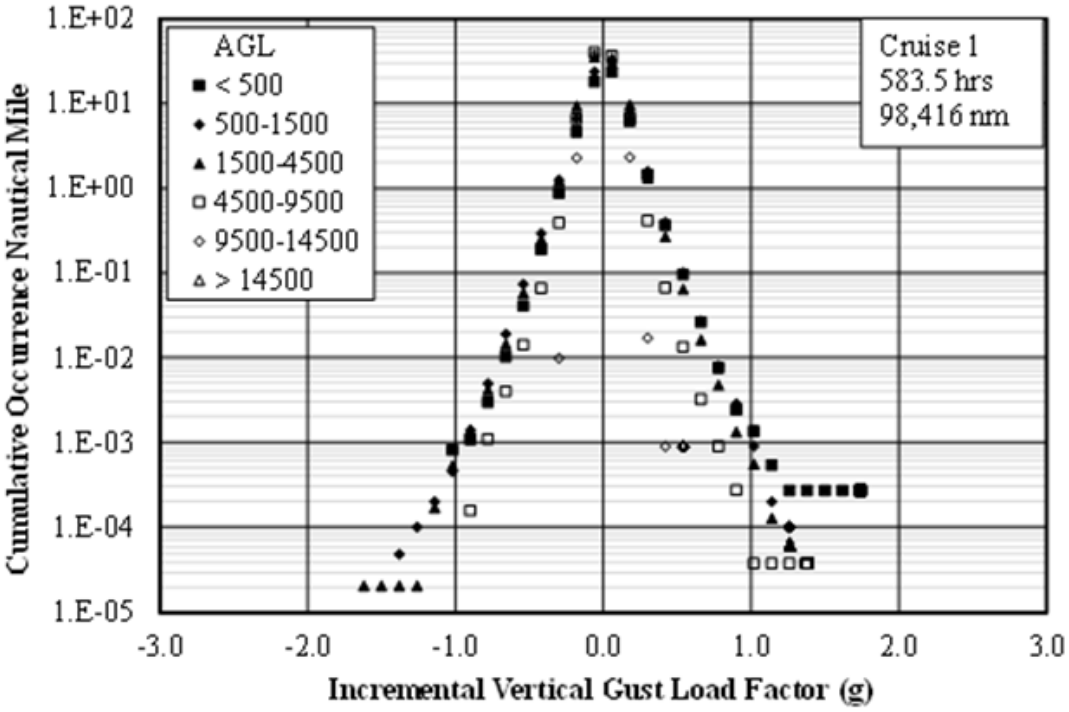

(b) Per Nautical Mile

Figure B-1: Cumulative occurrences of incremental vertical gust load factor, Cruise 1

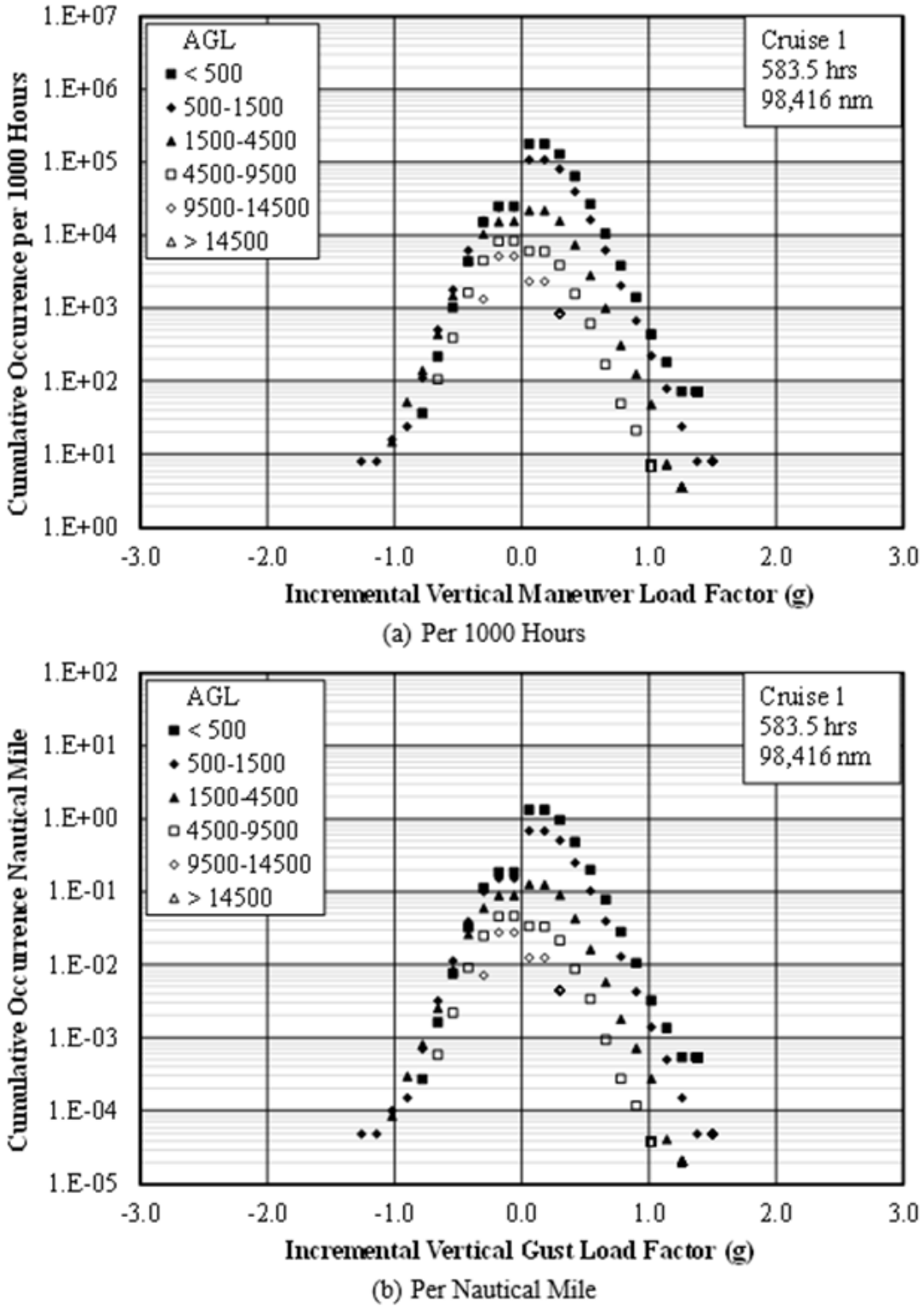

Figure B-2: Cumulative occurrences of incremental vertical maneuver load factor, Cruise 1

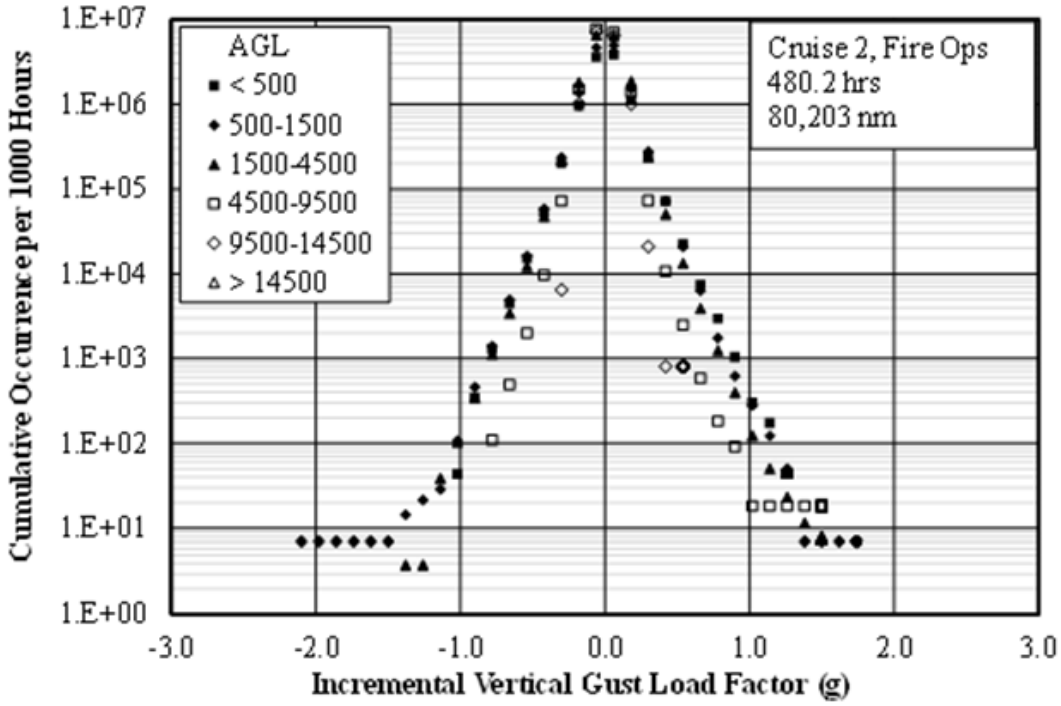

(a) Per 1000 Hours

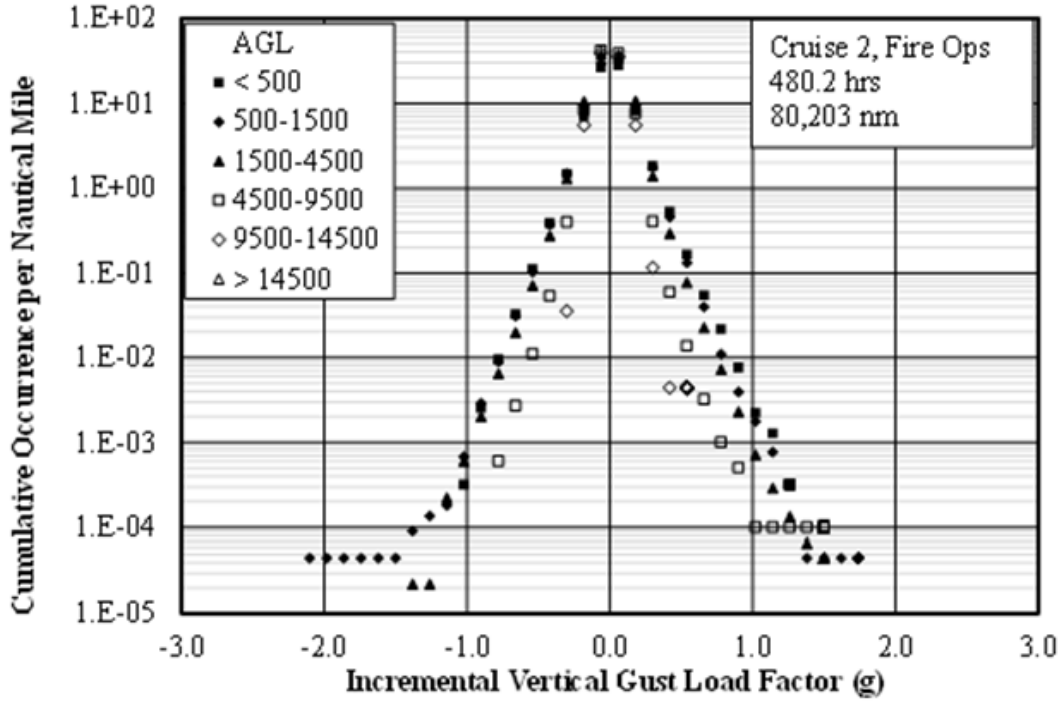

(b) Per Nautical Mile

Figure B-3: Cumulative occurrences of incremental vertical gust load factor, Cruise 2

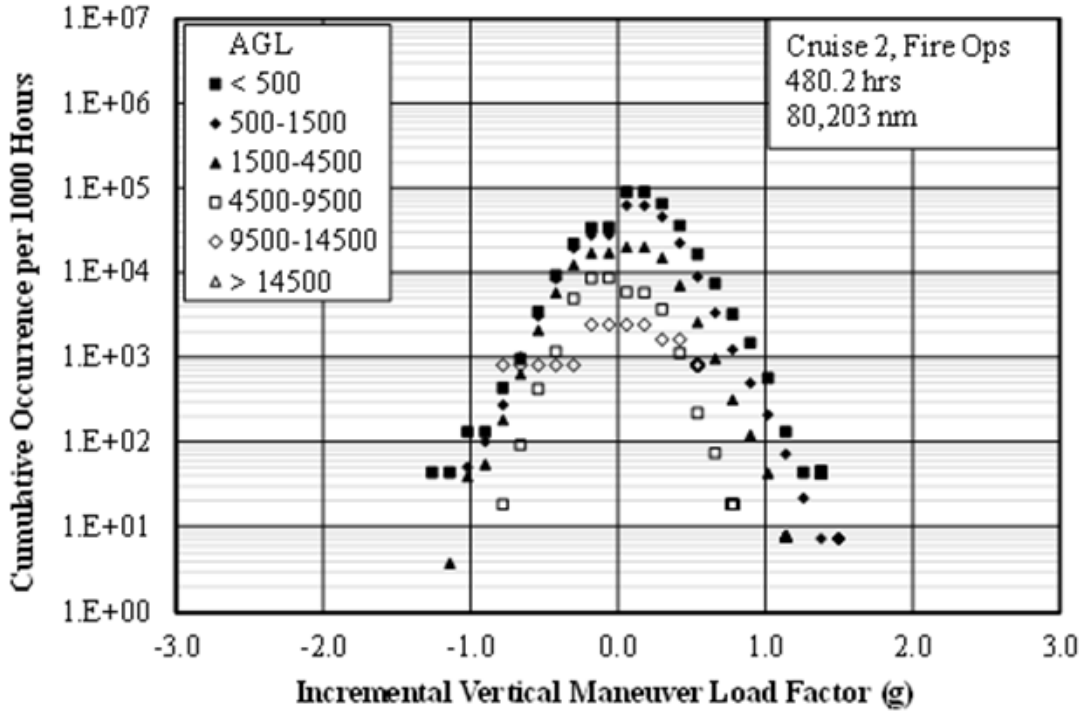

(a) Per 1000 Hours

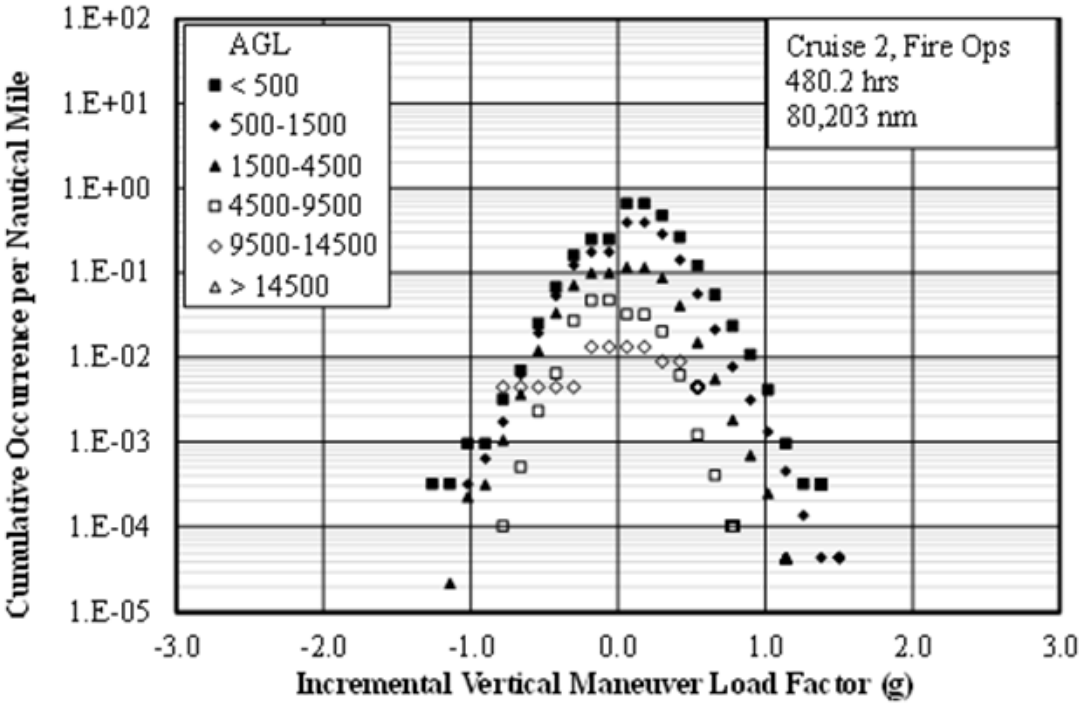

(b) Per Nautical Mile

Figure B-4: Cumulative occurrences of incremental vertical maneuver load factor, Cruise 2

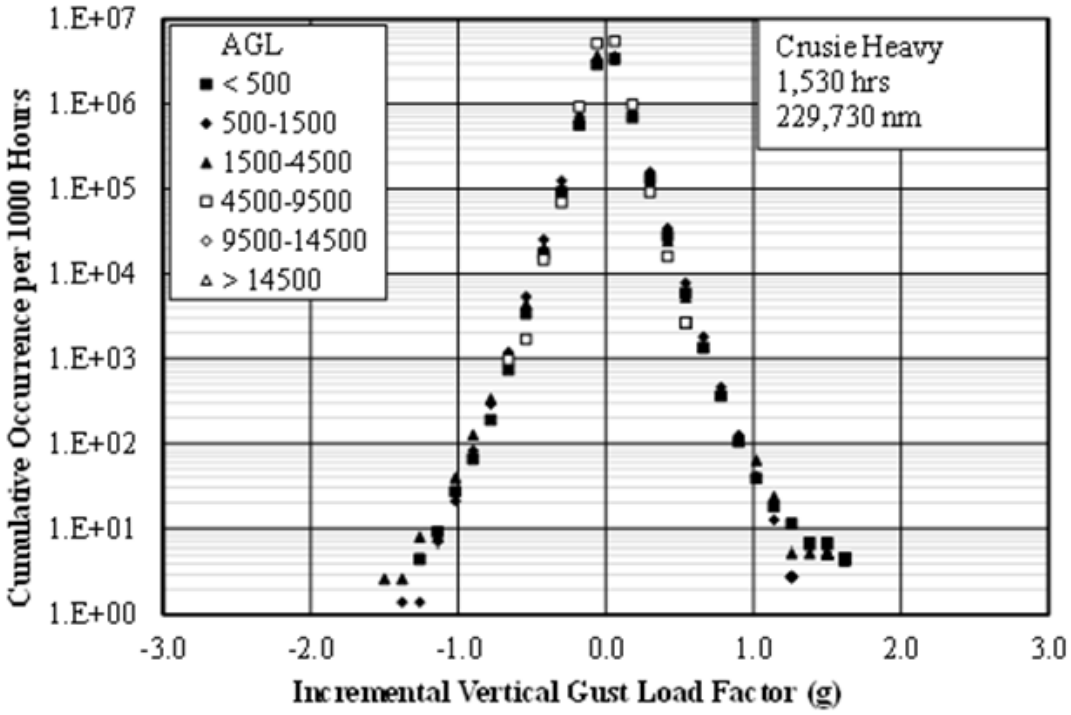

(a) Per 1000 Hours

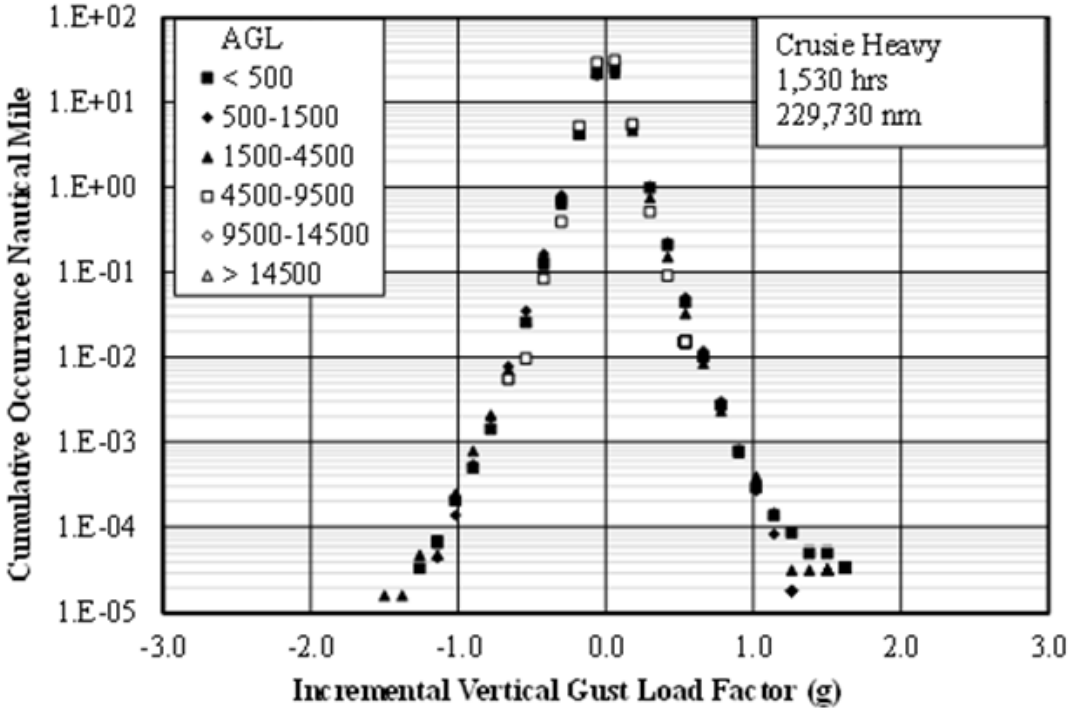

(b) Per Nautical Mile

Figure B-5: Cumulative occurrences of incremental vertical gust load factor, Cruise Heavy

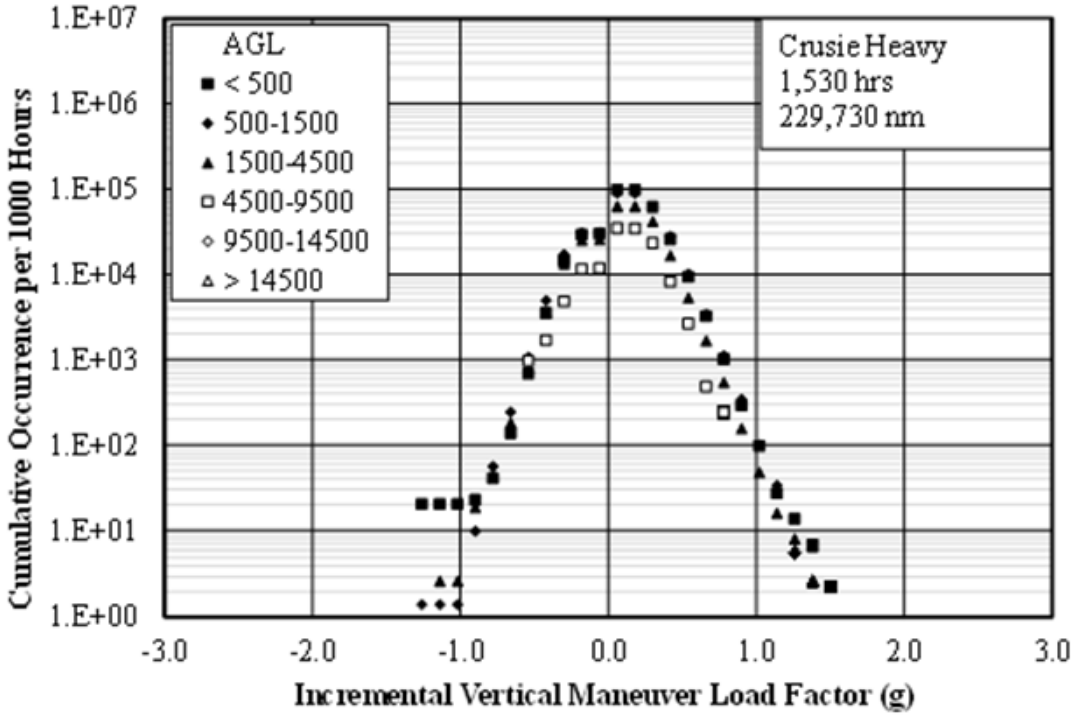

(a) Per 1000 Hours

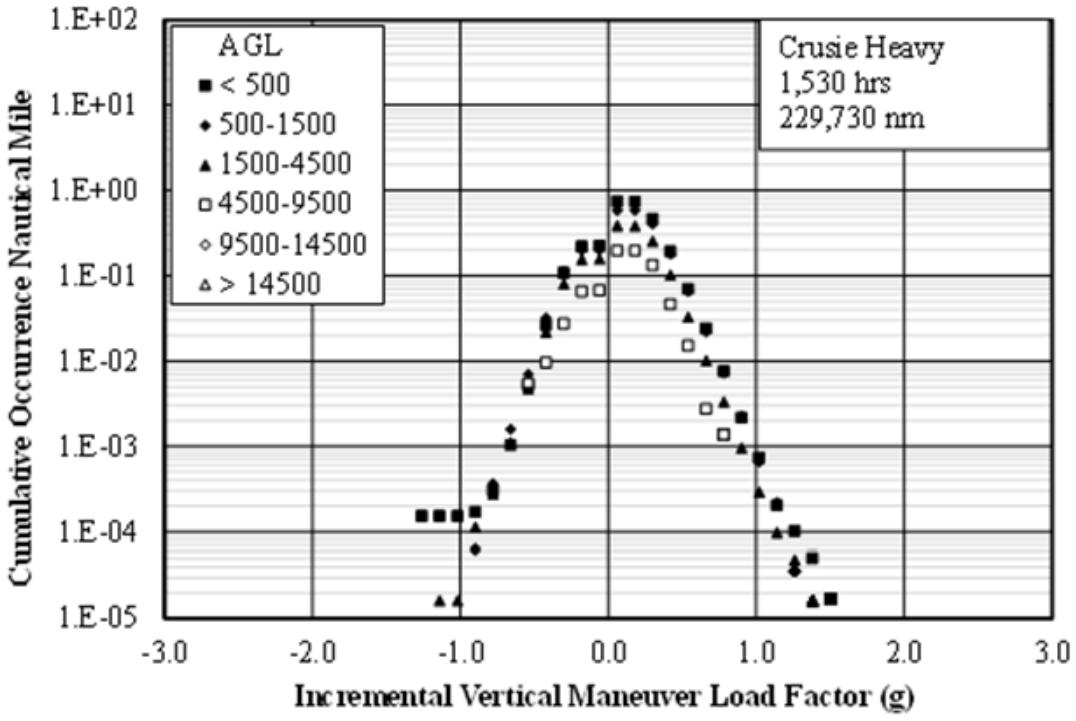

(b) Per Nautical Mile

Figure B-6: Cumulative occurrences of incremental vertical maneuver load factor, Cruise Heavy

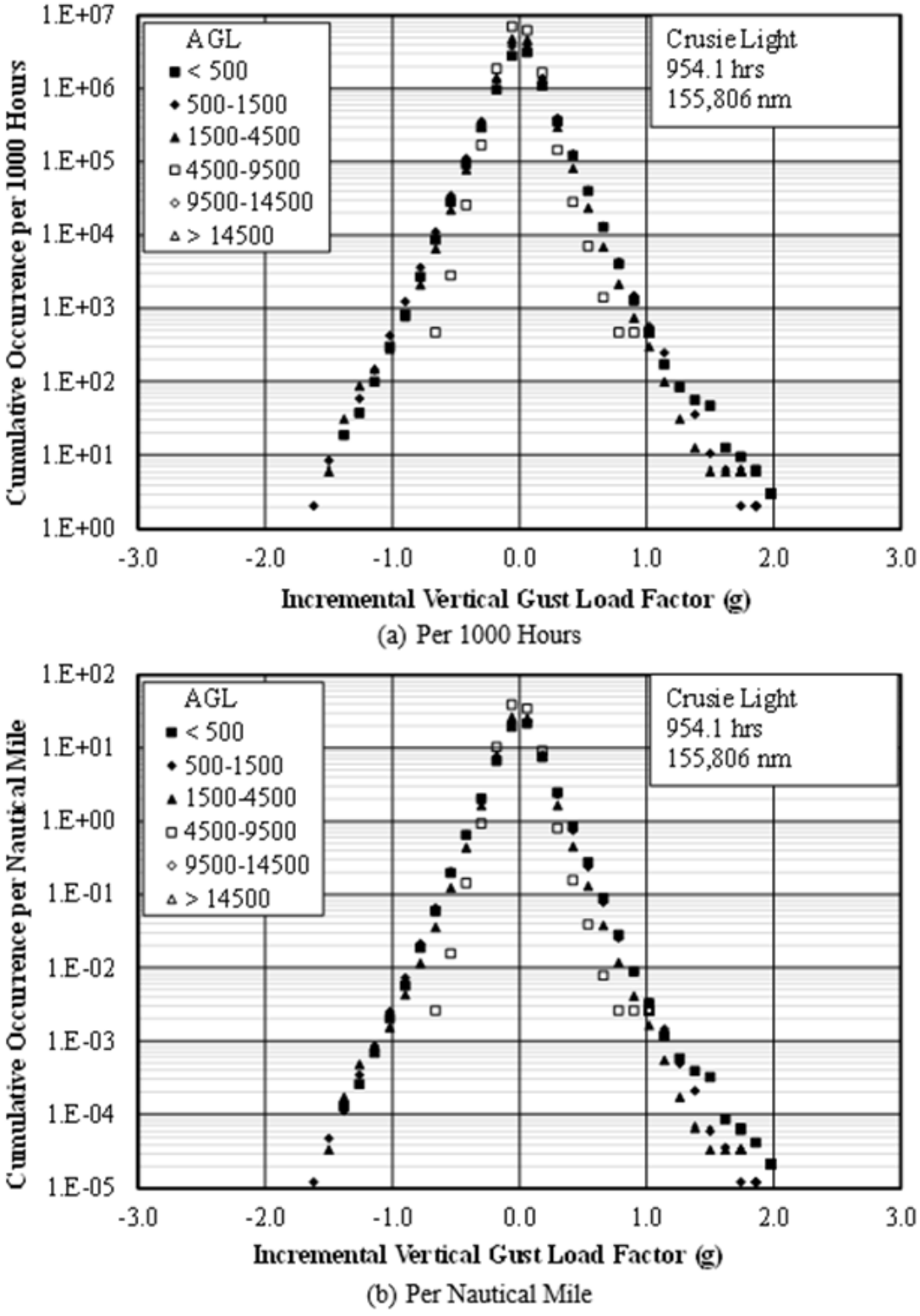

Figure B-7: Cumulative occurrences of incremental vertical gust load factor, Cruise Light

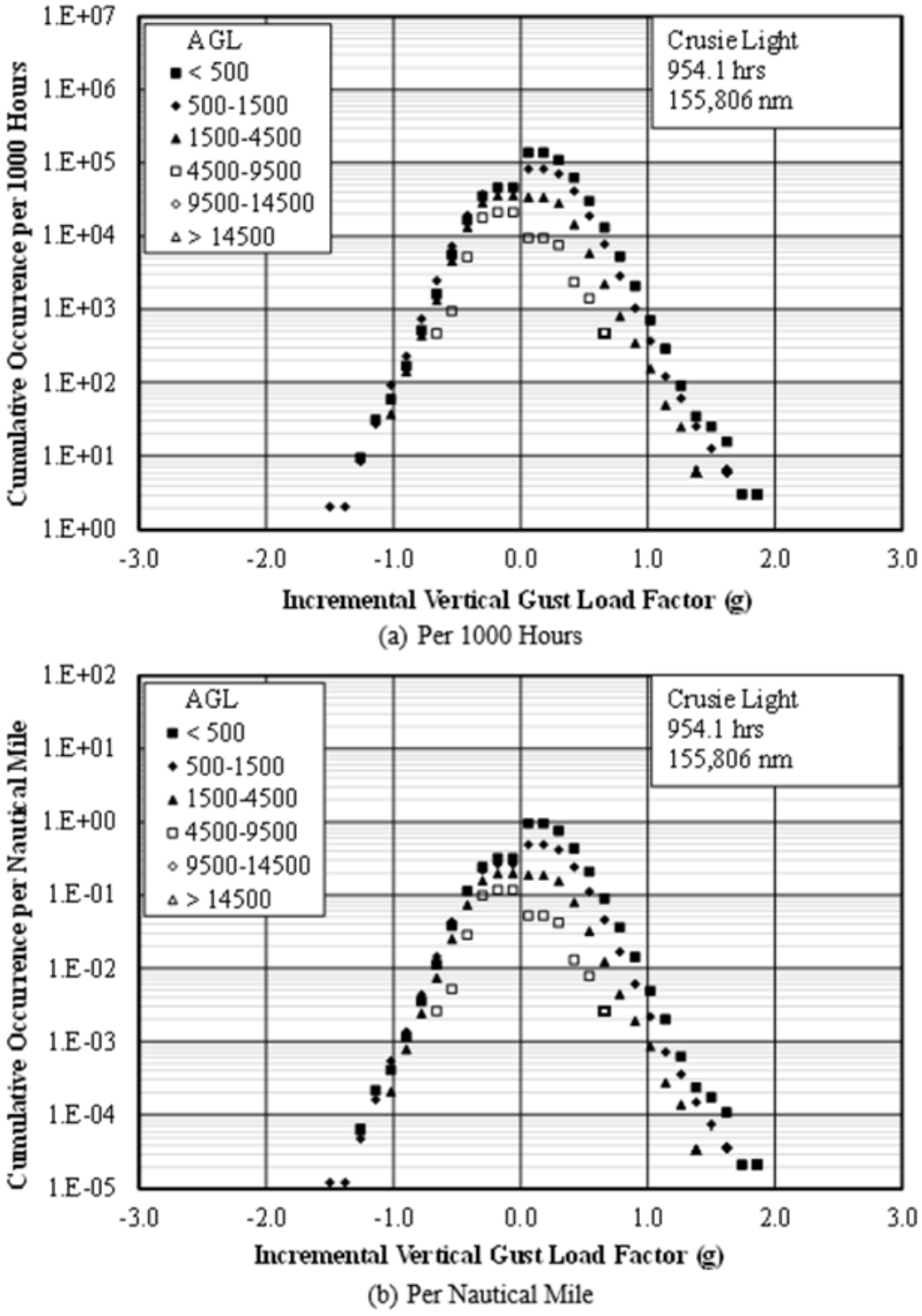

Figure B-8: Cumulative occurrences of incremental vertical maneuver load factor, Cruise Light

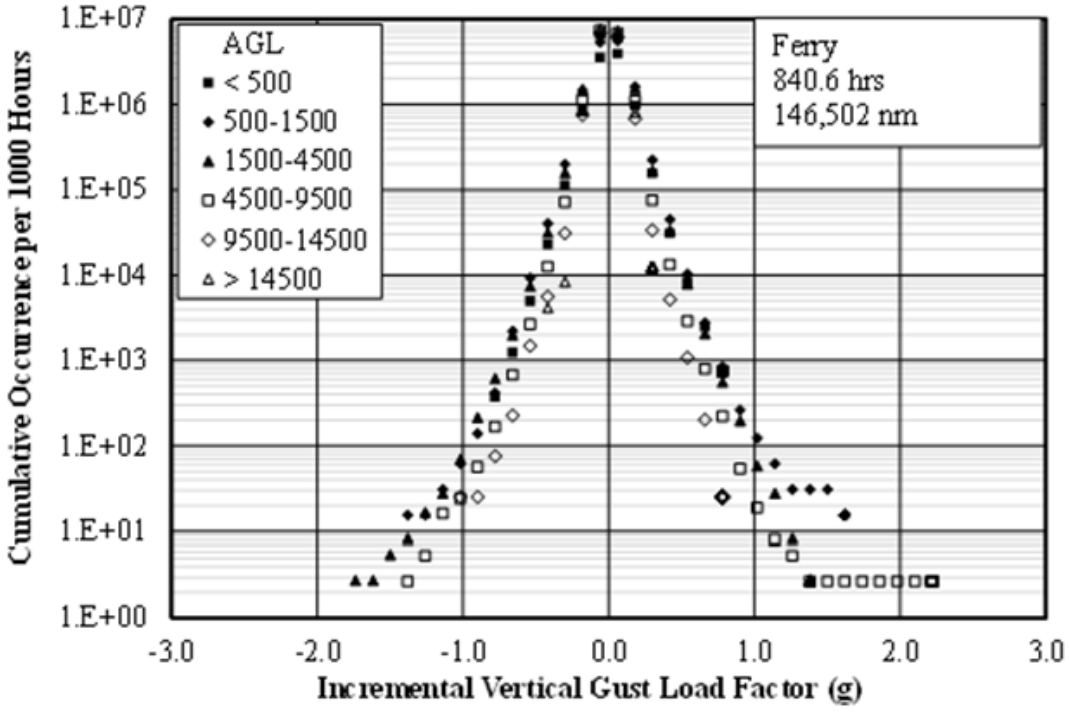

(a) Per 1000 Hours

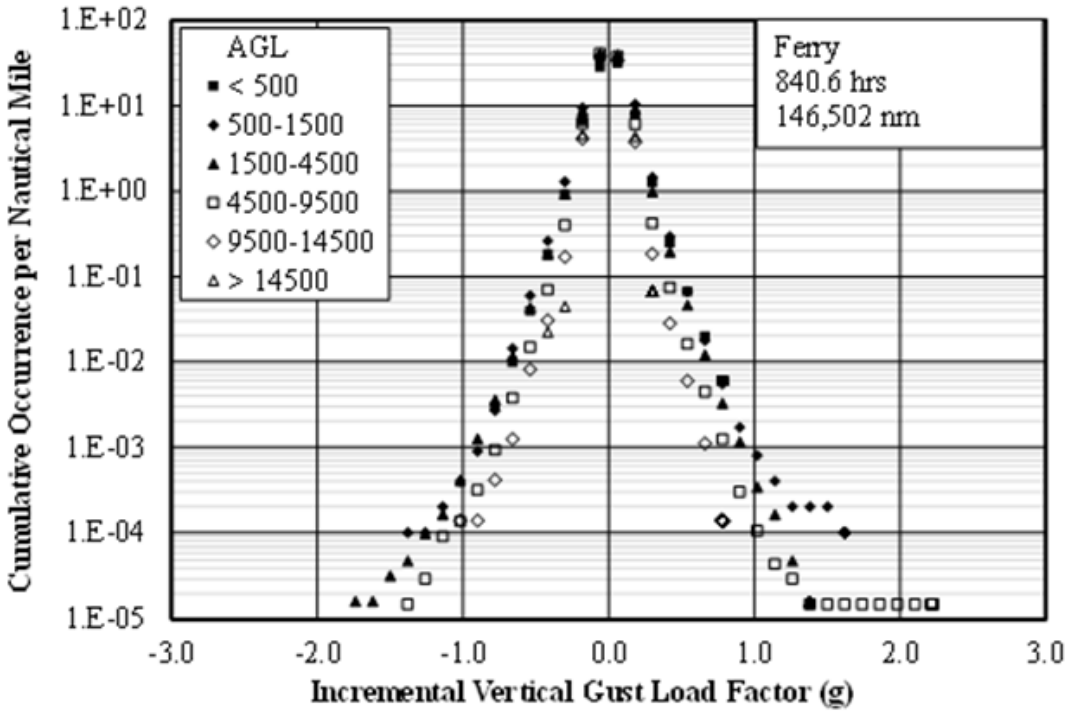

(b) Per Nautical Mile

Figure B-9: Cumulative occurrences of incremental vertical gust load factor, Ferry

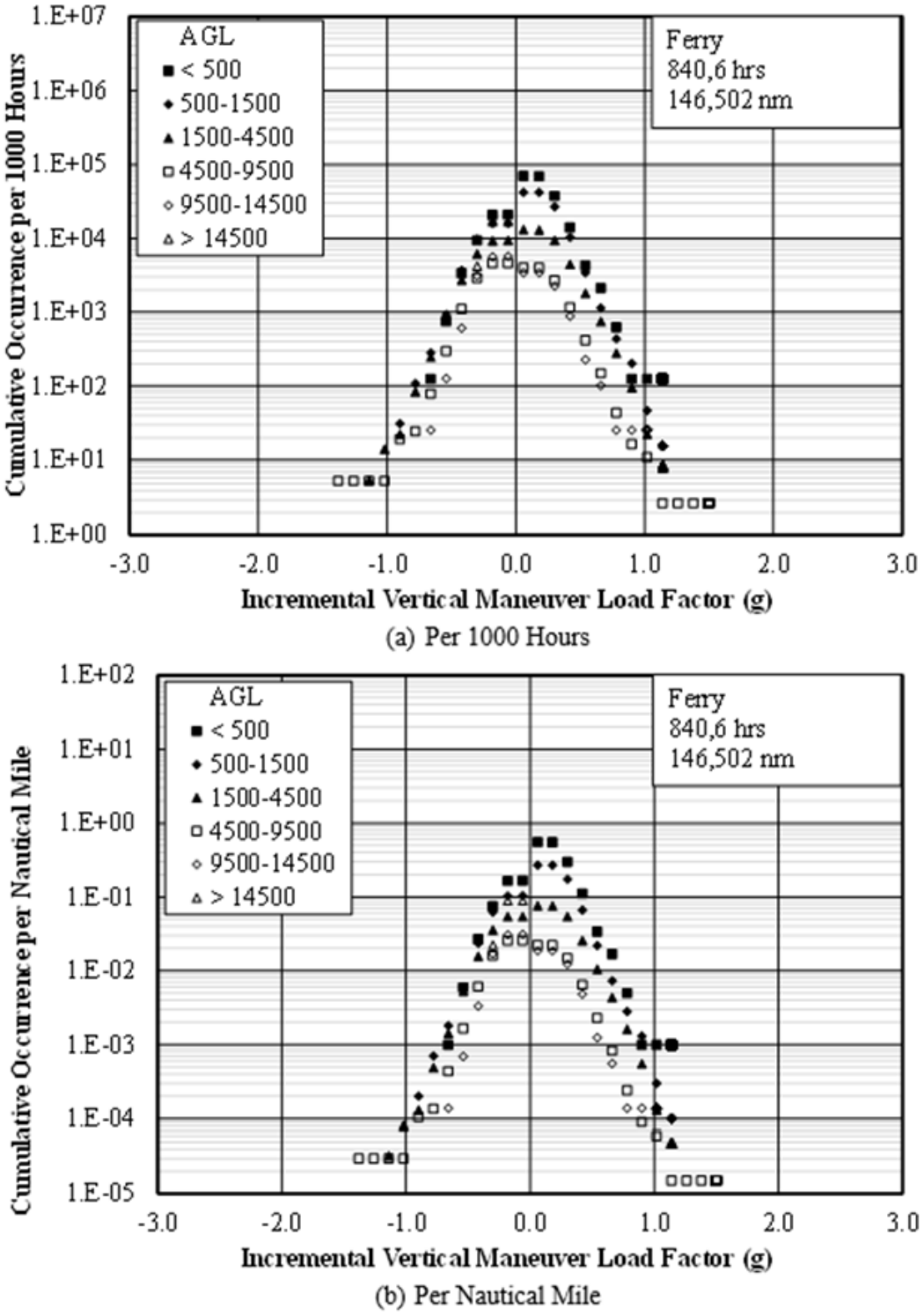

Figure B-10: Cumulative occurrences of incremental vertical maneuver load factor, Ferry

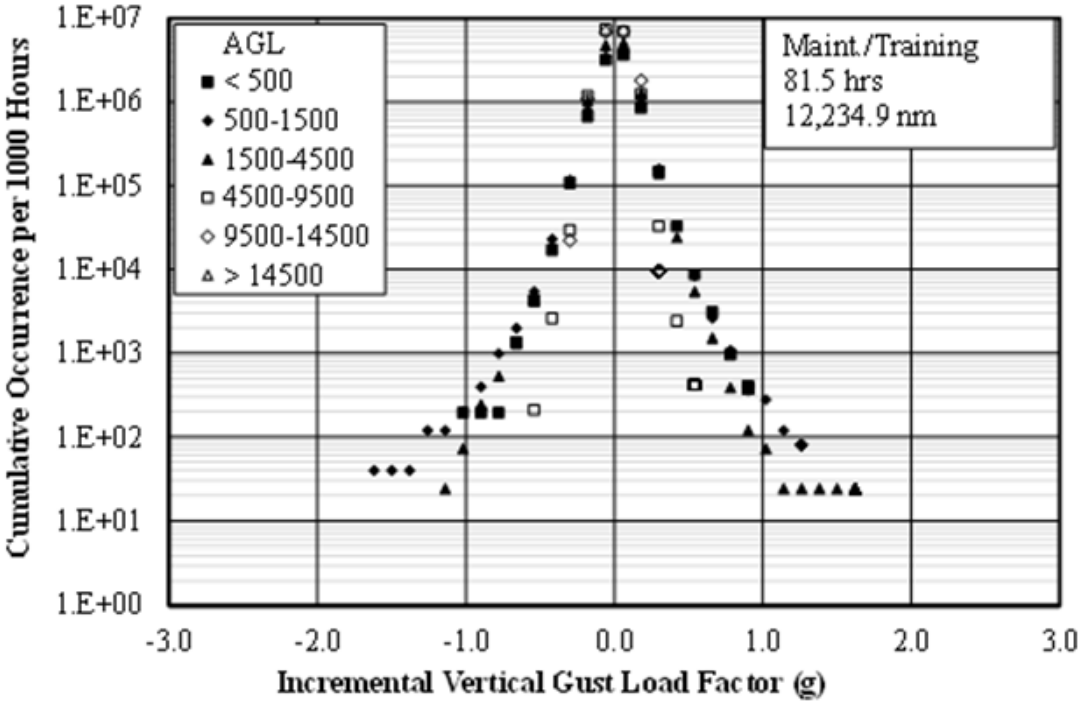

(a) Per 1000 Hours

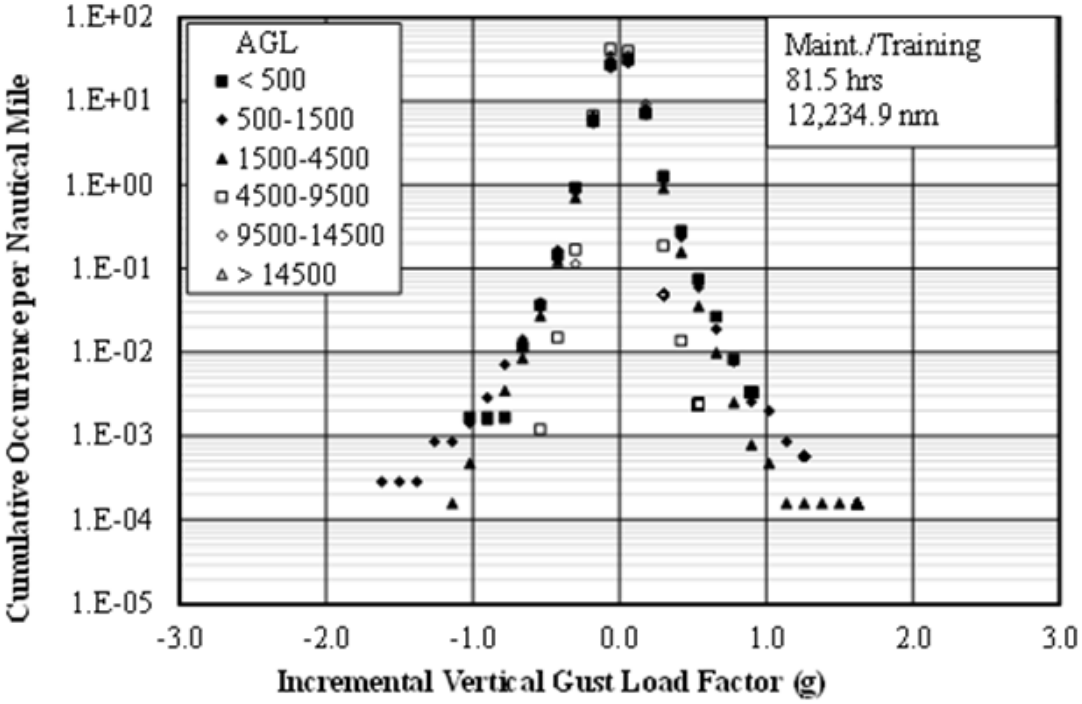

(b) Per Nautical Mile

Figure B-11: Cumulative occurrences of incremental vertical gust load factor, Maintenance/Training

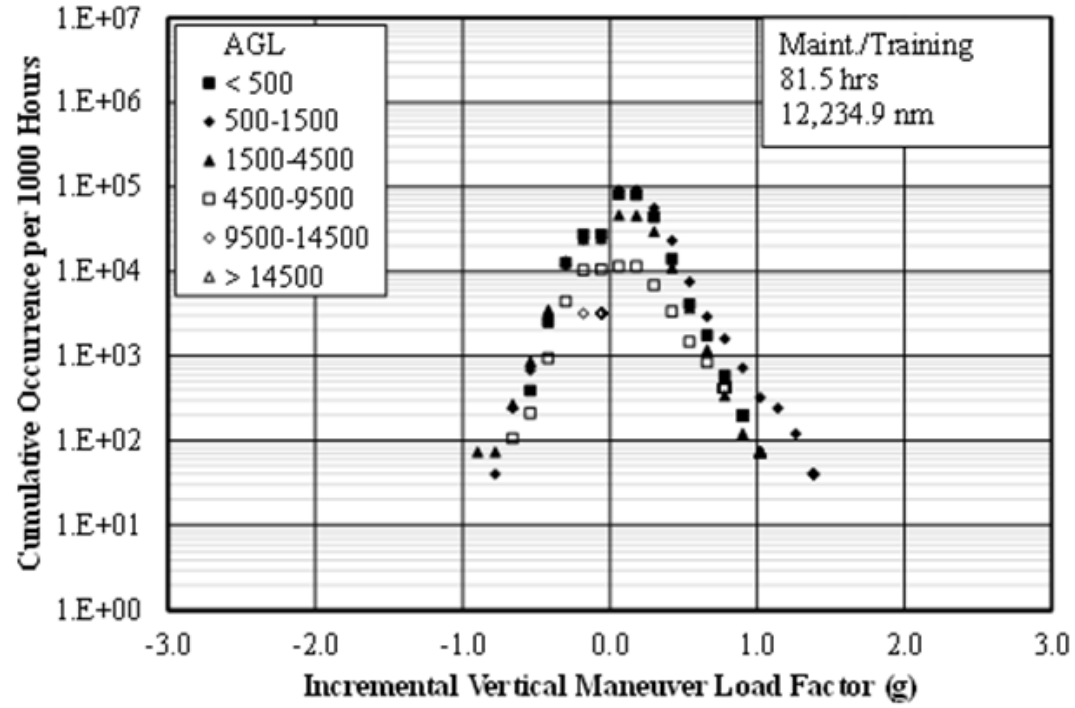

(a) Per 1000 Hours

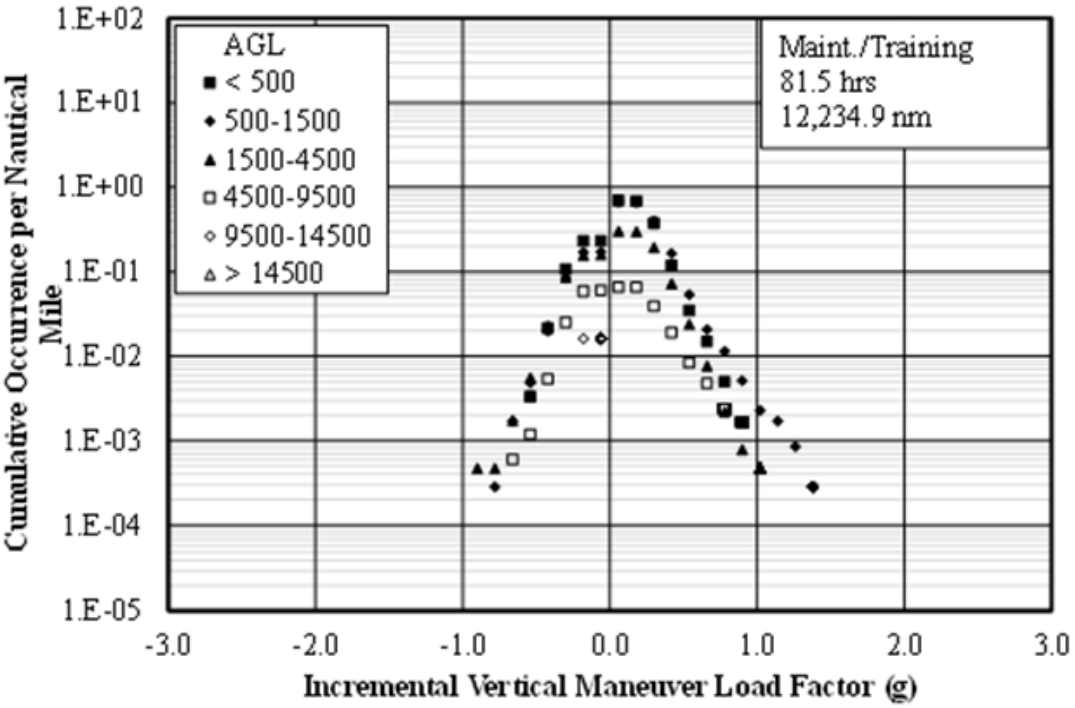

(b) Per Nautical Mile

Figure B-12: Cumulative occurrences of incremental vertical maneuver load factor, Maint./Training

Table B-10: Summary of durations and distances for fill entry by AGL altitude

Altitude Band	Duration (s)	Duration (hr)	Distance (nm)
1	2,460.2	41.0	3,912.9
2	6.2	0.10	16.3
3	4.9	0.08	14.4
4	0	0	3.2
5	0	0	0
6	0	0	0
Total	2,471	41.2	3,947

Table B-11: Summary of durations and distances for fill by AGL altitude

Altitude Band	Duration (s)	Duration (hr)	Distance (nm)
1	2,960.0	49.3	3816.8
2	0	0	0
3	0	0	0
4	0	0	0
5	0	0	0
6	0	0	0
Total	2,960	49.3	3,817

Table B-12: Summary of durations and distances for fill exit by AGL altitude

Altitude Band	Duration (s)	Duration (hr)	Distance (nm)
1	2,458.3	41.0	3,382.6
2	5.8	0.10	15.0
3	4.8	0.08	14.2
4	1.4	0.02	4.1
5	0	0	0
6	0	0	0
Total	2,470	41.2	3,416

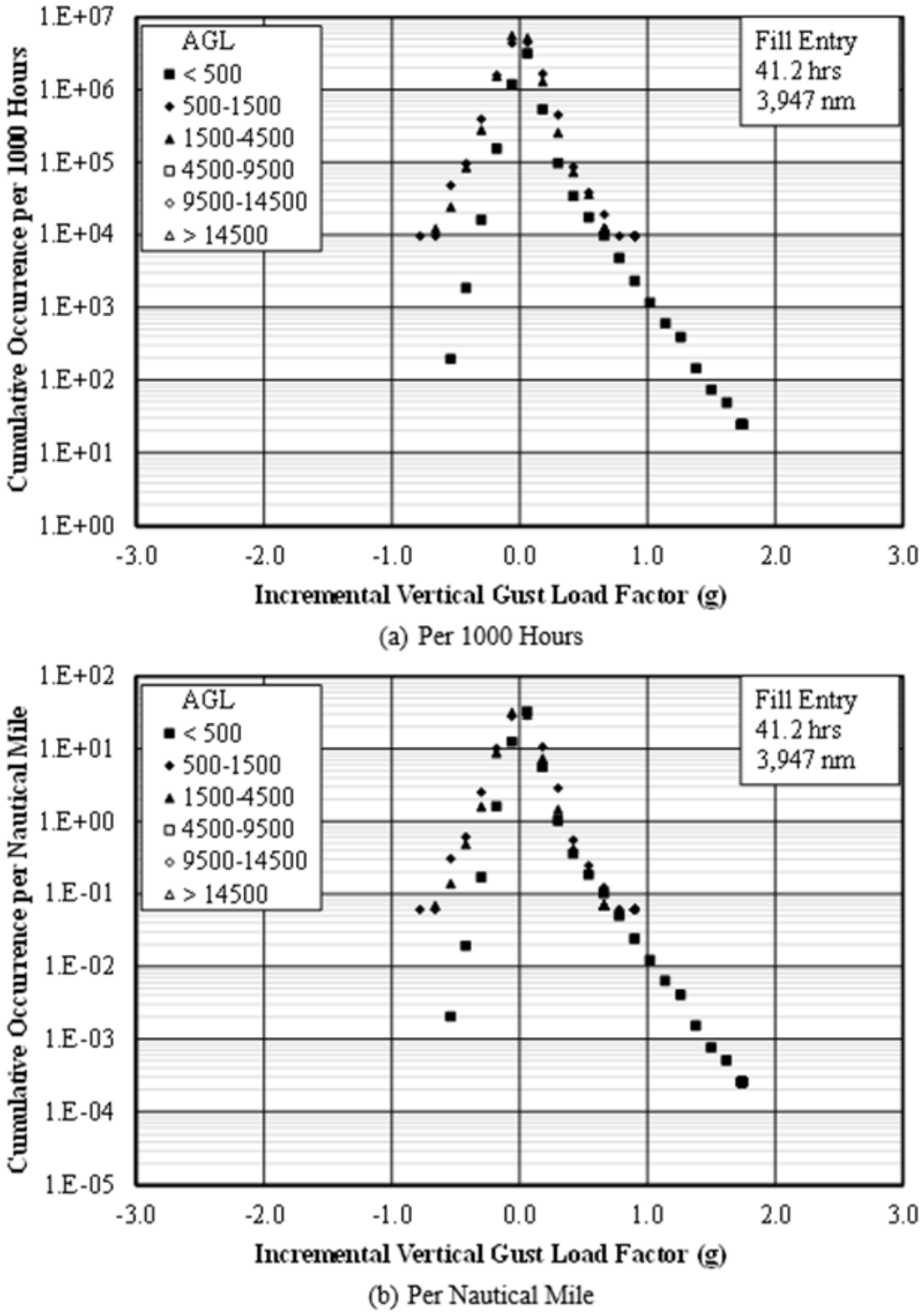

Figure B-13: Cumulative occurrences of incremental vertical gust load factor, Fill Entry

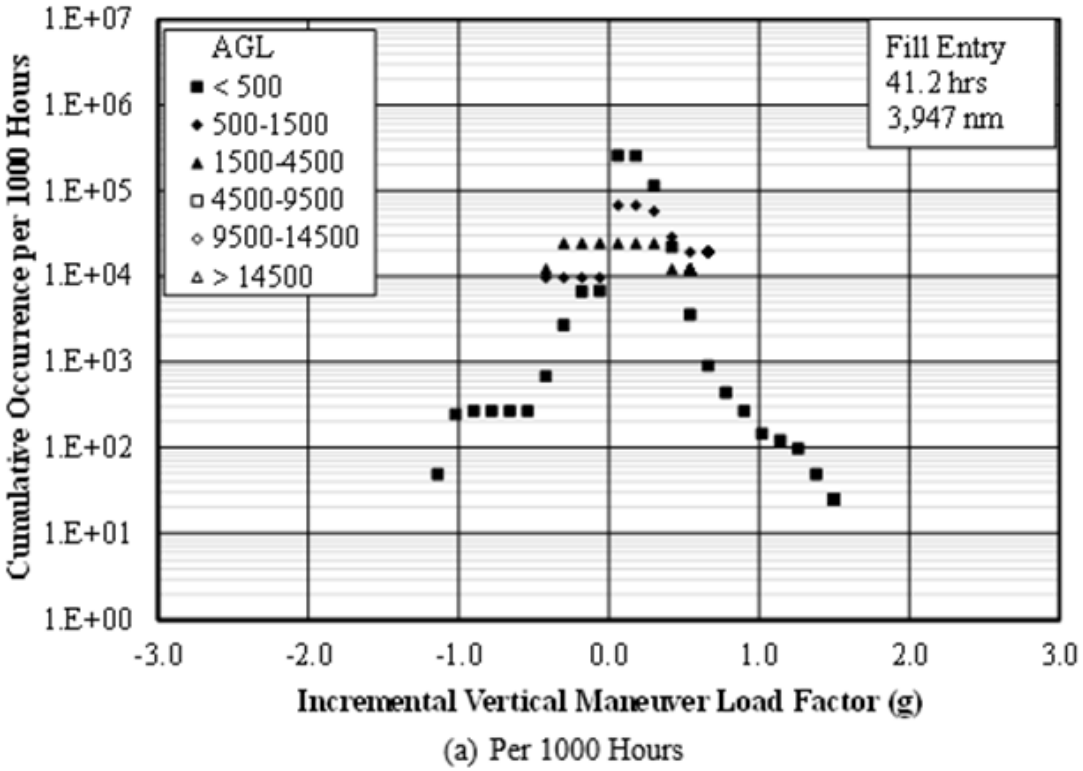

(a) Per 1000 Hours

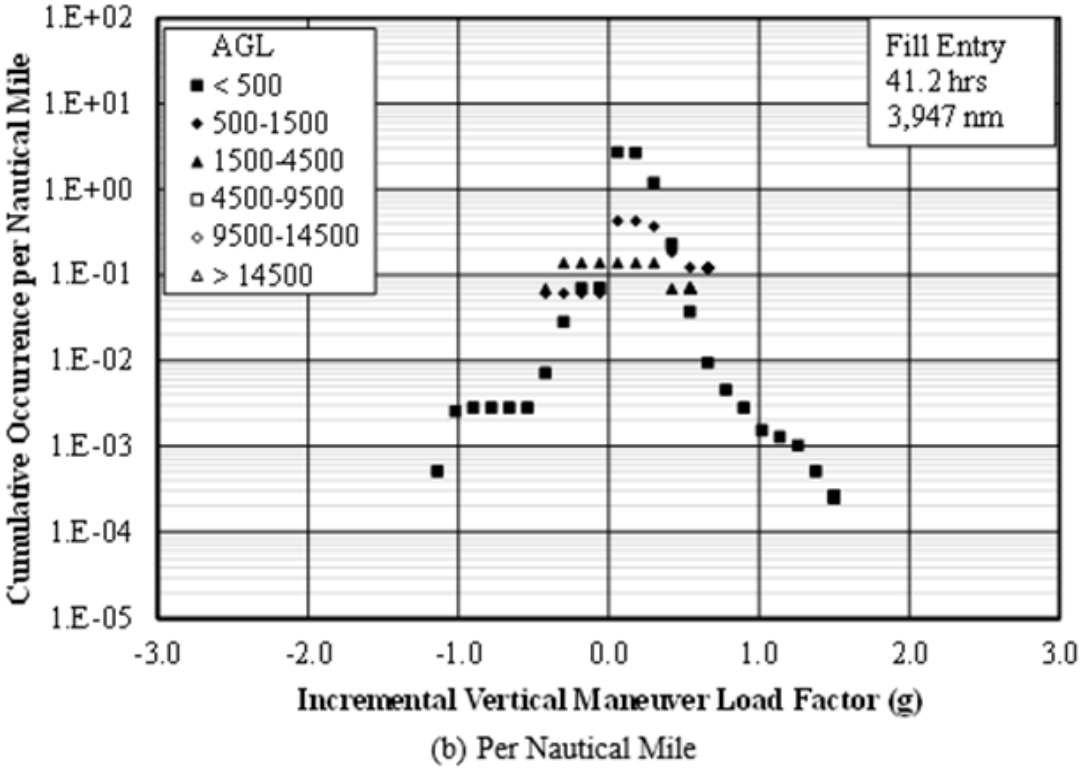

(b) Per Nautical Mile

Figure B-14: Cumulative occurrences of incremental vertical maneuver load factor, Fill Entry

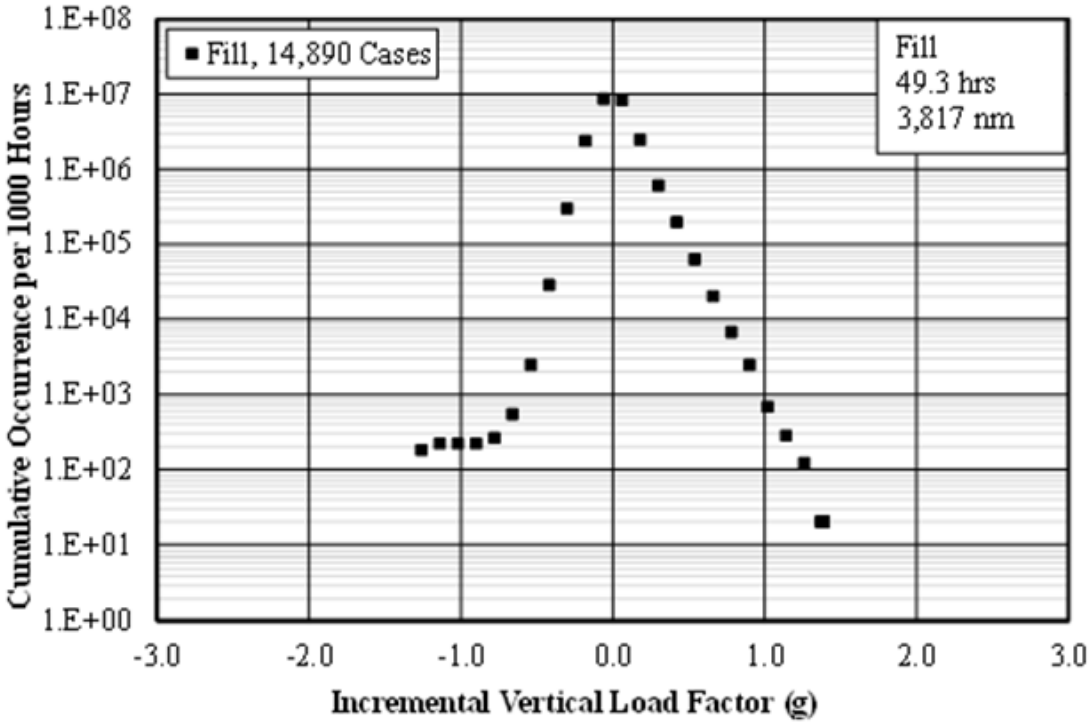

(a) Per 1000 Hours

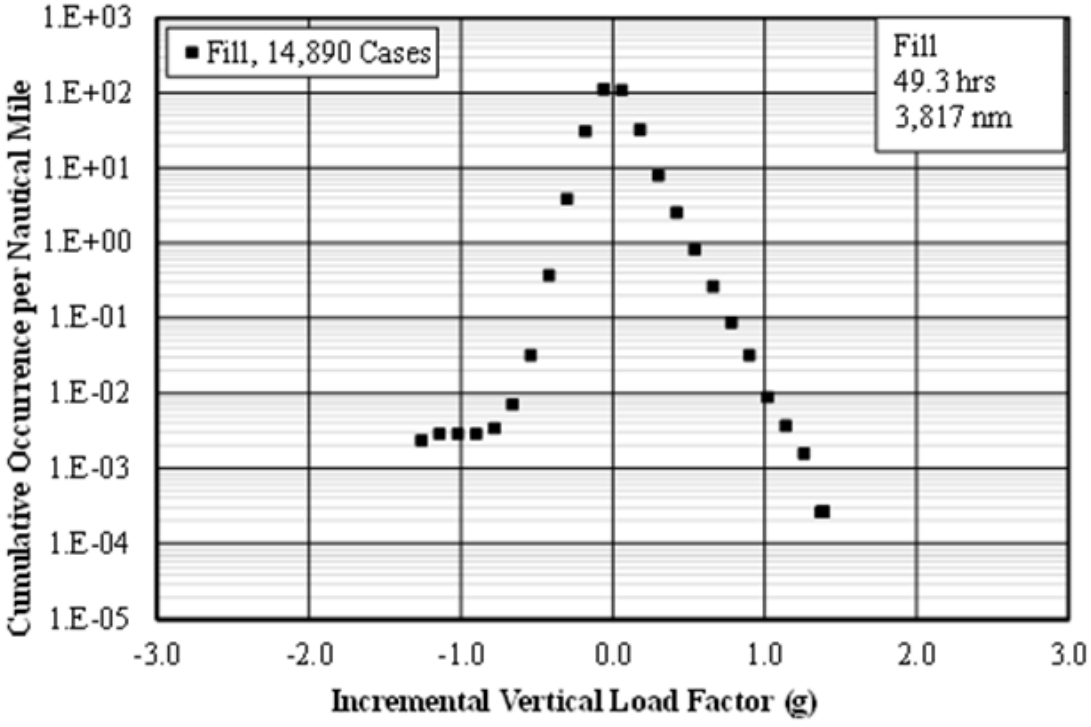

(b) Per Nautical Mile

Figure B-15: Cumulative occurrences of incremental vertical load factor, Fill

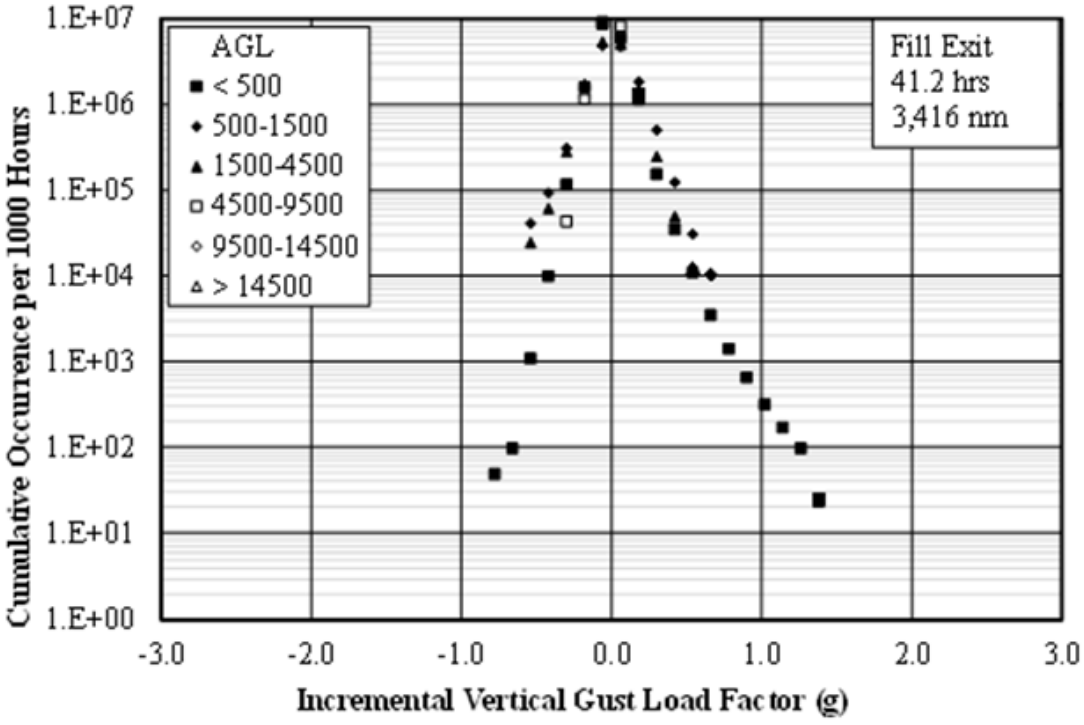

(a) Per 1000 Hours

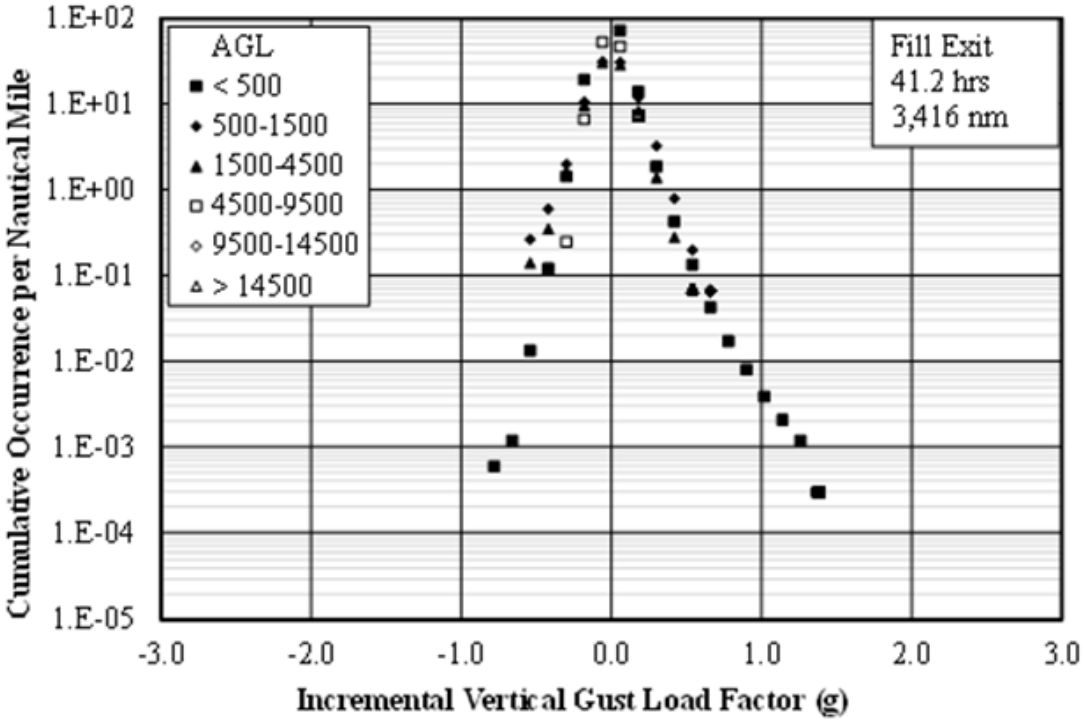

(b) Per Nautical Mile

Figure B-16: Cumulative occurrences of incremental vertical gust load factor, Fill Exit

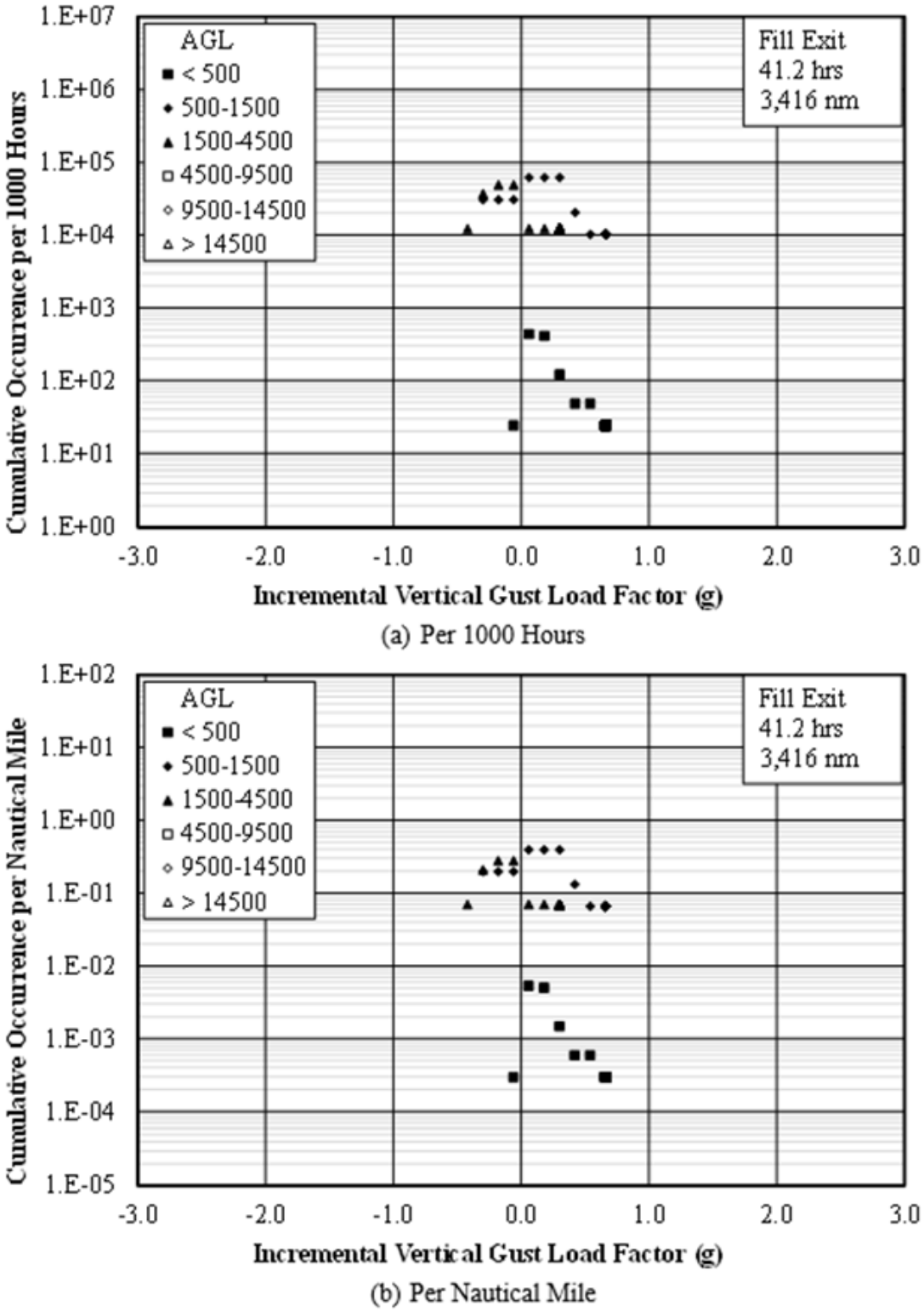

Figure B-17: Cumulative occurrences of incremental vertical maneuver load factor, Fill Exit

Table B-13: Summary of durations and distances for drop entry by AGL altitude

Altitude Band	Duration (s)	Duration (hr)	Distance (nm)
1	2,212.5	36.9	4,658.2
2	219.3	3.7	468.3
3	6.0	0.10	13.9
4	0	0	0
5	0	0	0
6	0	0	0
Total	2,438	40.6	5,140

Table B-14: Summary of durations and distances for drop by AGL altitude

Altitude Band	Duration (s)	Duration (hr)	Distance (nm)
1	800.9	13.3	1,677.6
2	7.0	0.12	14.9
3	1.6	0.03	3.4
4	0	0	0
5	0	0	0
6	0	0	0
Total	809	13.5	1,696

Table B-15: Summary of durations and distances for drop exit by AGL altitude

Altitude Band	Duration (s)	Duration (hr)	Distance (nm)
1	1,179.4	19.7	2,528.8
2	123.1	2.1	275.9
3	4.1	0.07	9.4
4	0	0	0
5	0	0	0
6	0	0	0
Total	1,307	21.8	2,814

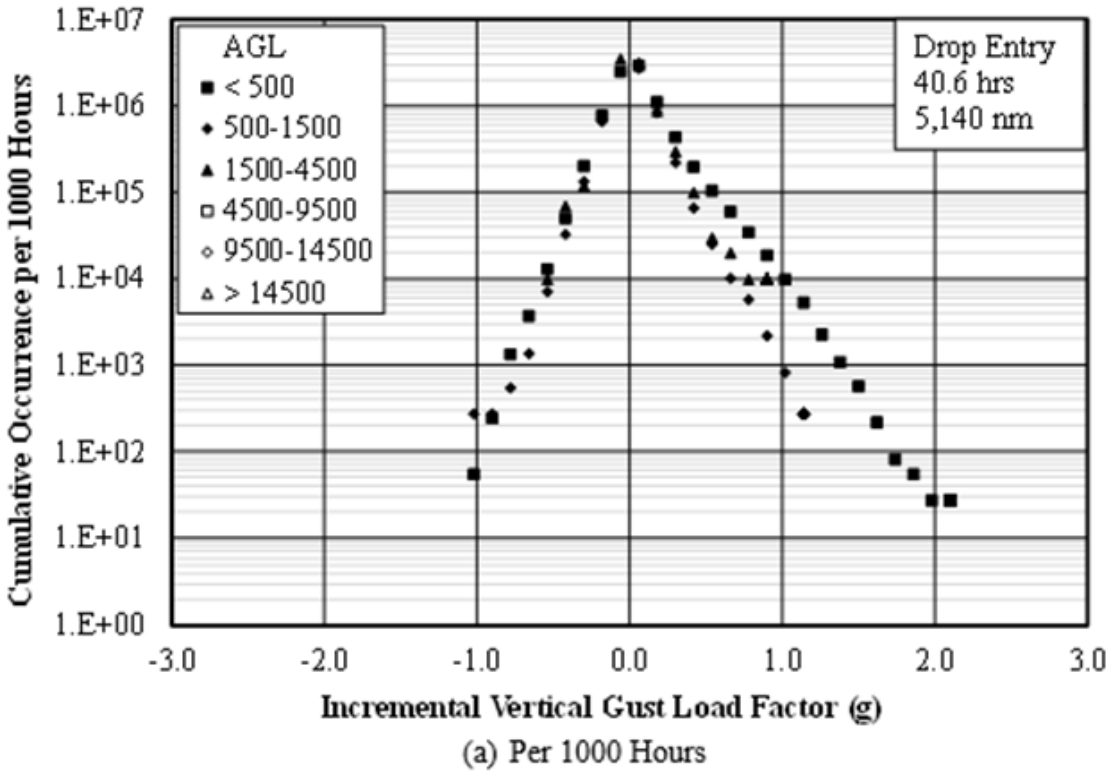

(a) Per 1000 Hours

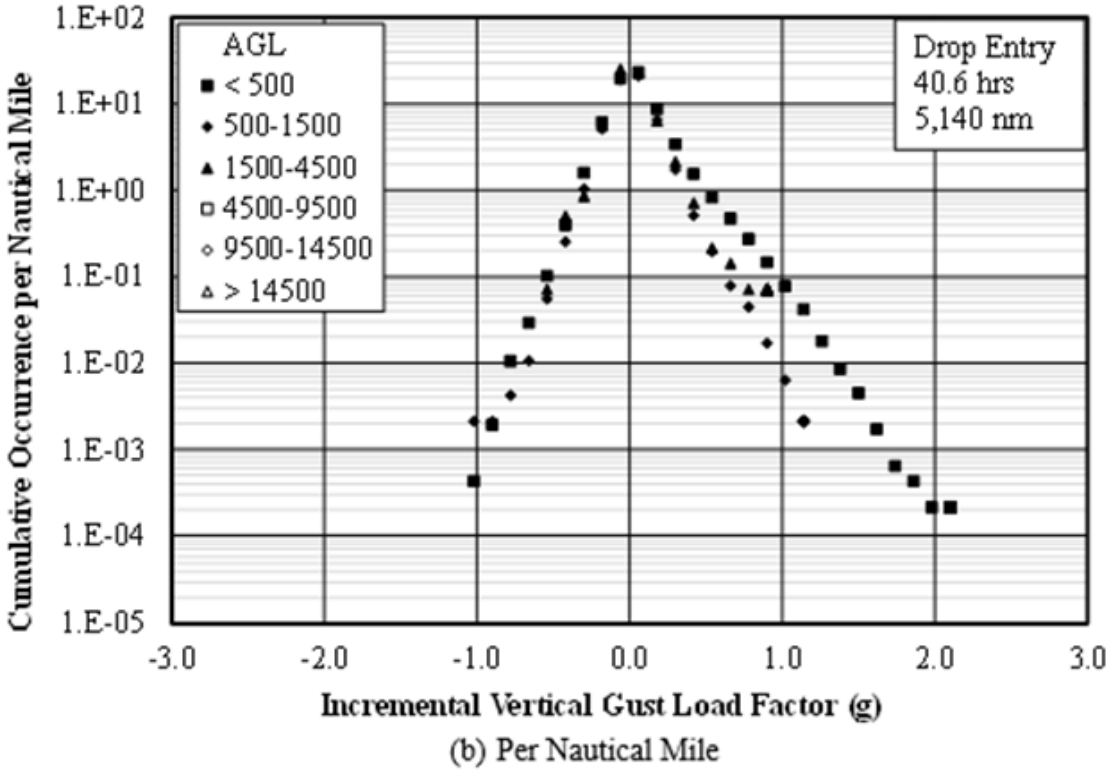

(b) Per Nautical Mile

Figure B-18: Cumulative occurrences of incremental vertical gust load factor, Drop Entry

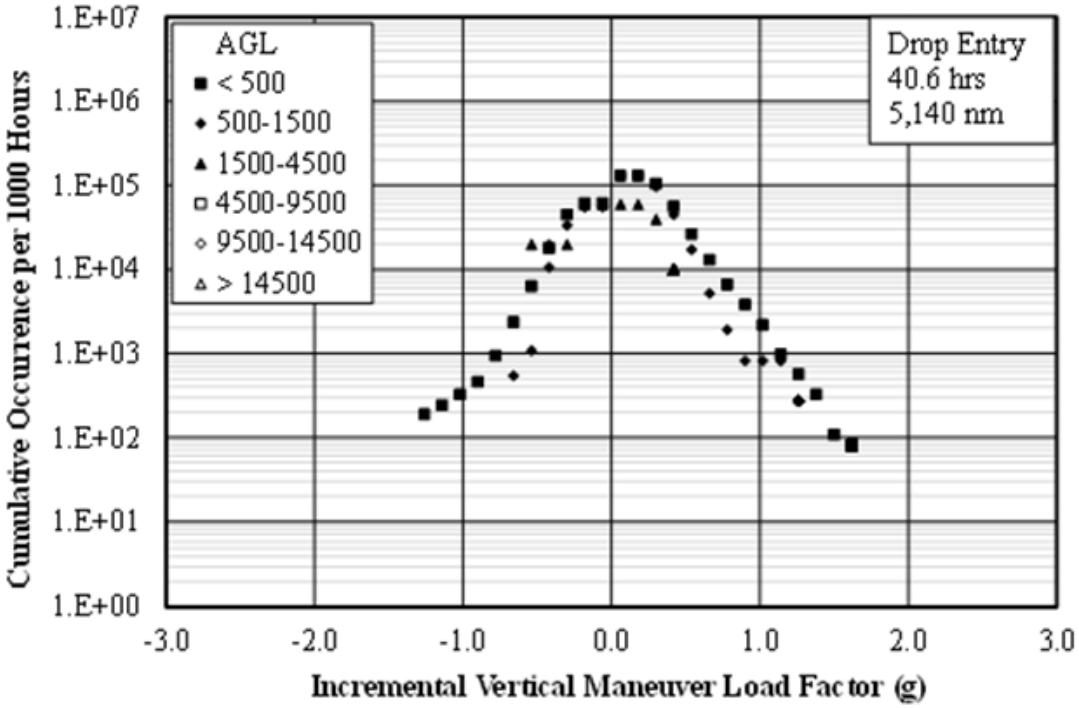

(a) Per 1000 Hours

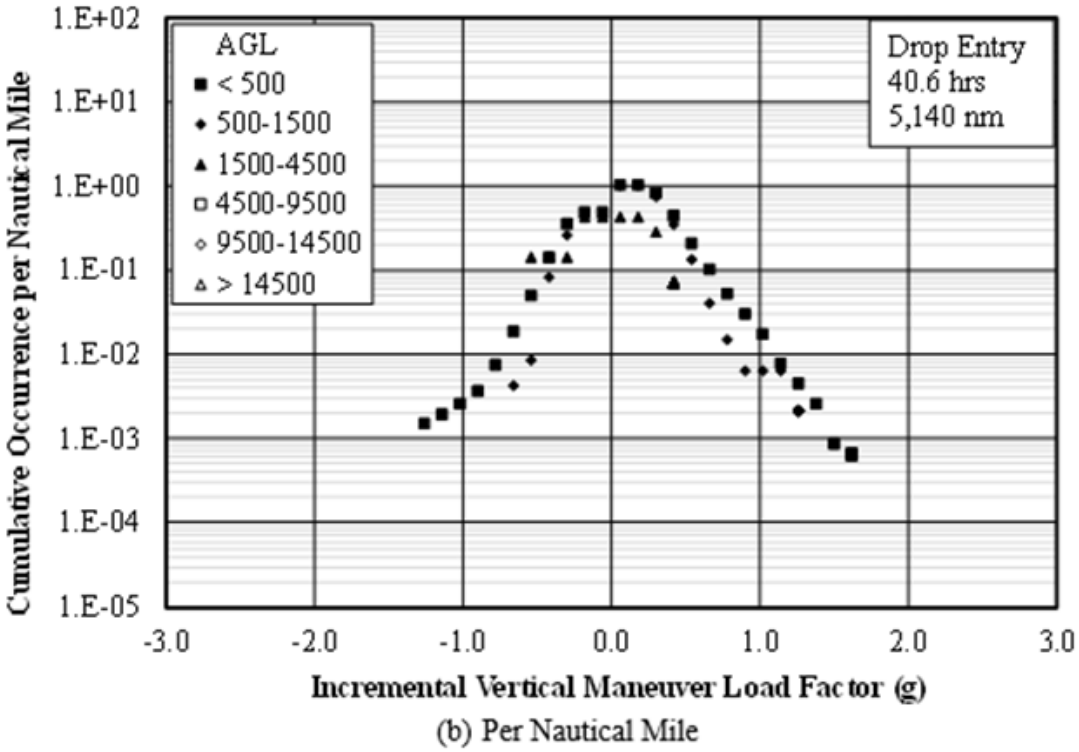

(b) Per Nautical Mile

Figure B-19: Cumulative occurrences -incremental vertical maneuver load factor, Drop Entry

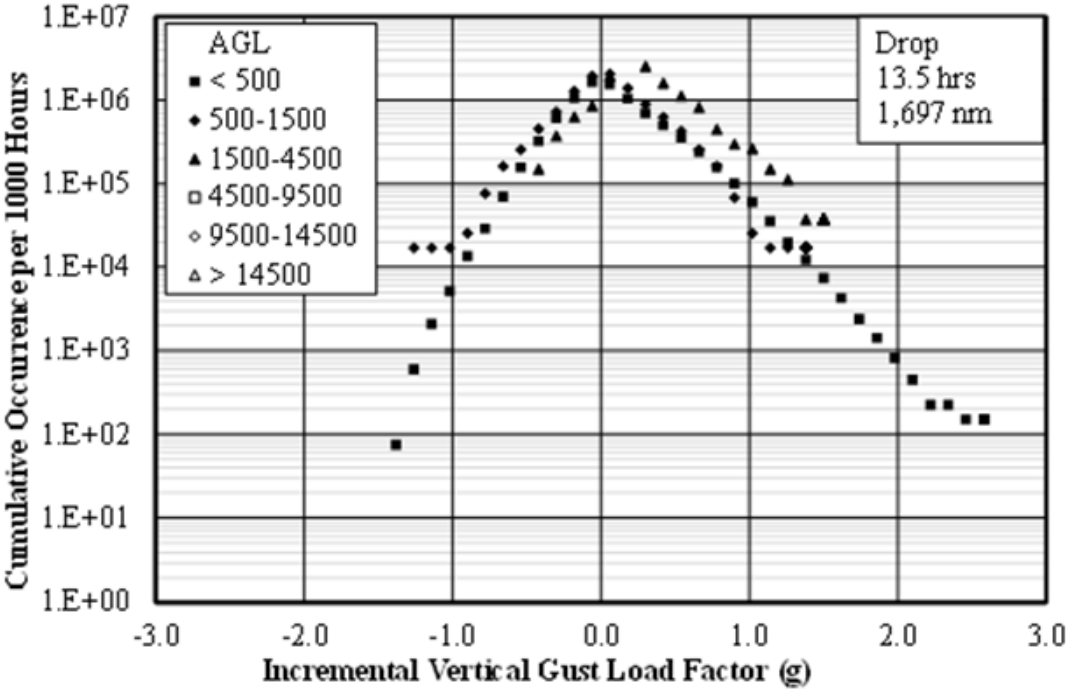

(a) Per 1000 Hours

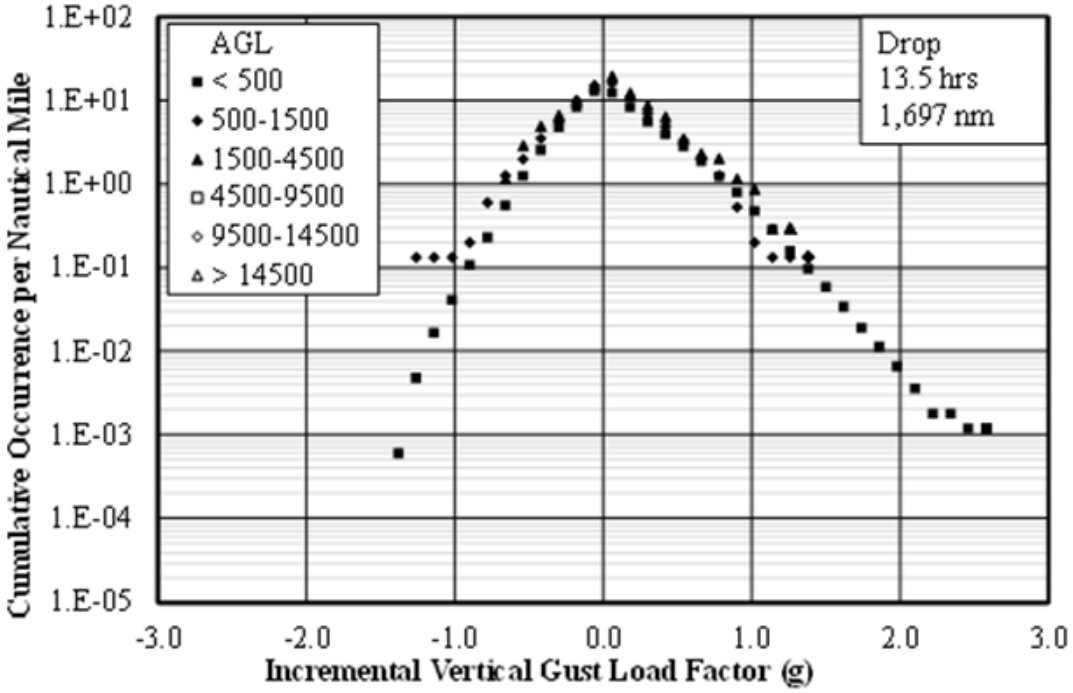

(b) Per Nautical Mile

Figure B-20: Cumulative occurrences of incremental vertical gust load factor, Drop

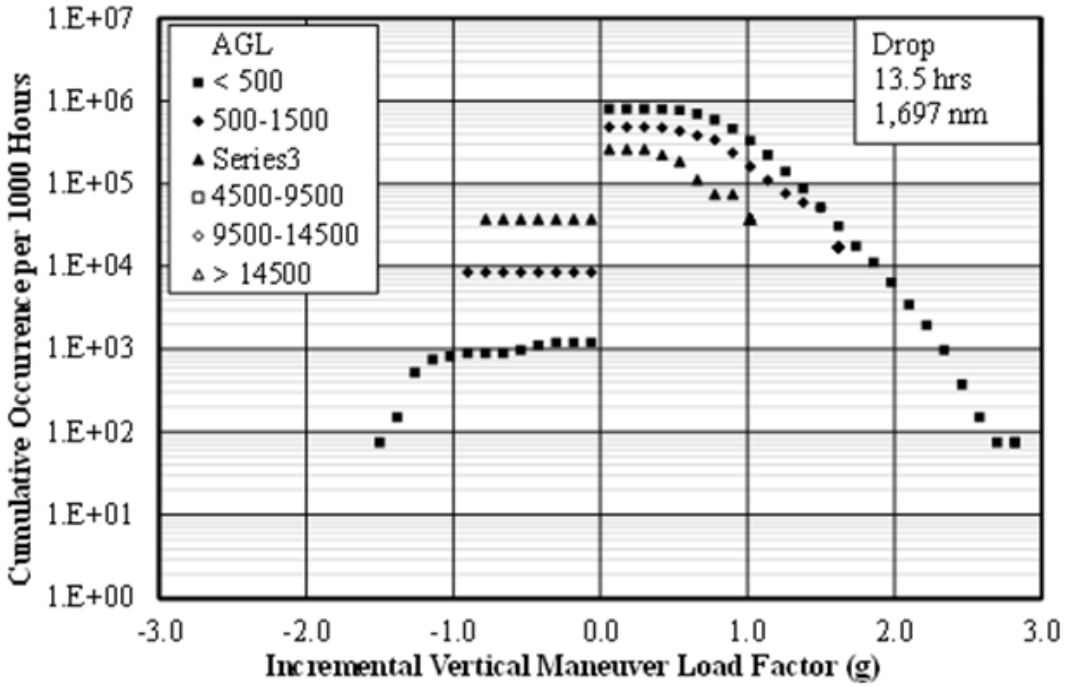

(a) Per 1000 Hours

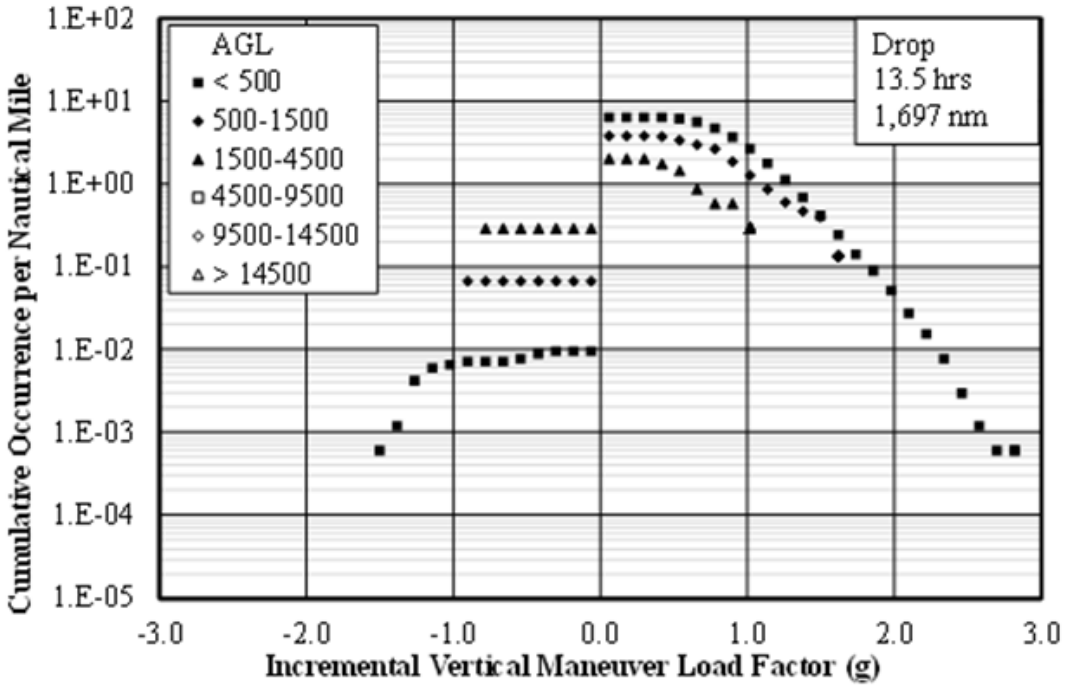

(b) Per Nautical Mile

Figure B-21: Cumulative occurrences of incremental vertical maneuver load factor, Drop

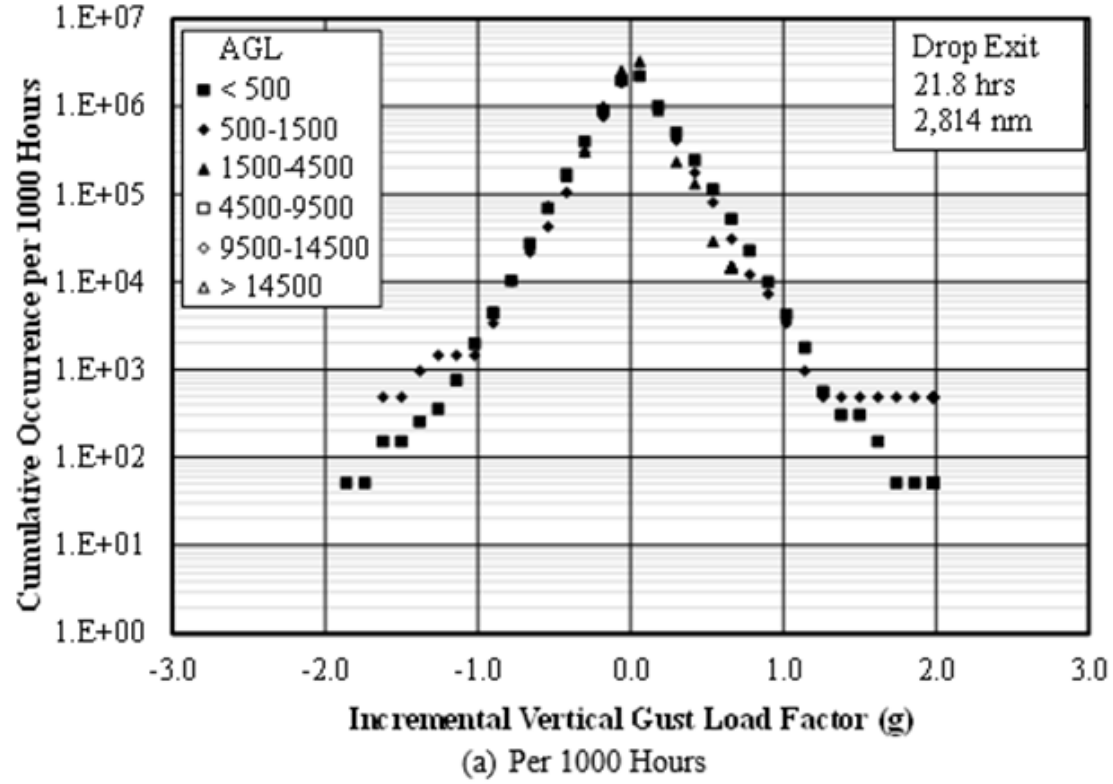

(a) Per 1000 Hours

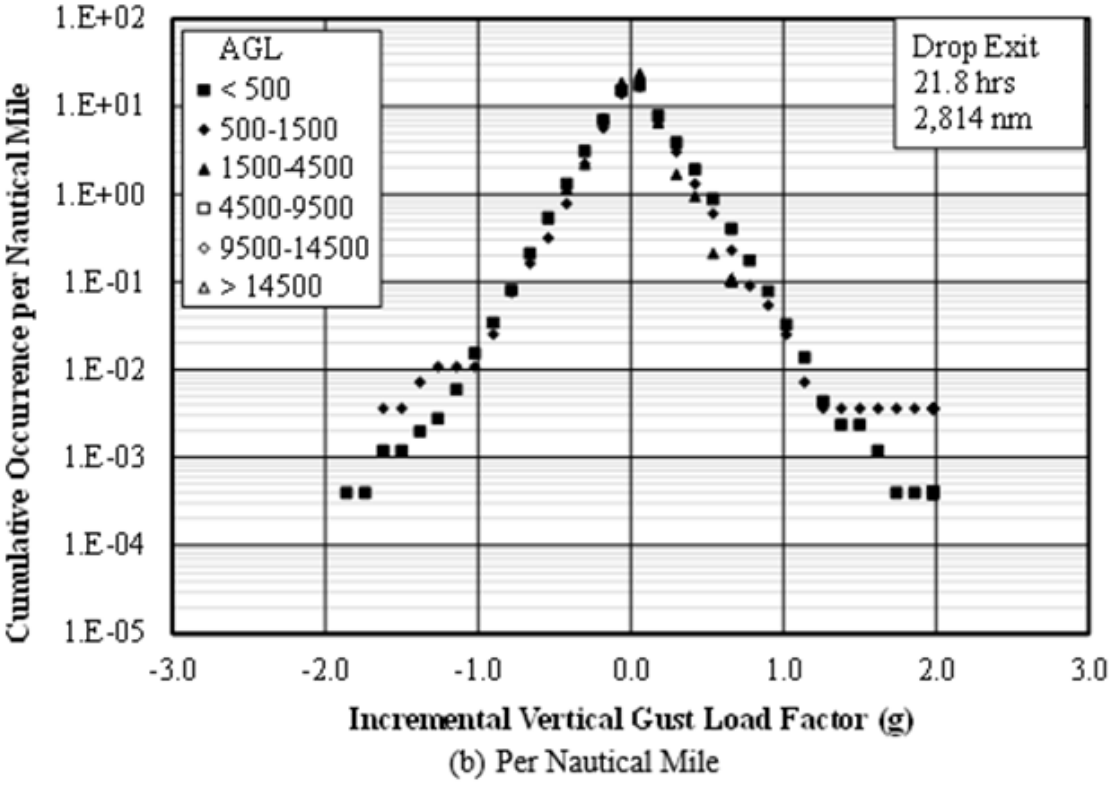

(b) Per Nautical Mile

Figure B-22: Cumulative occurrences of incremental vertical gust load factor, Drop Exit

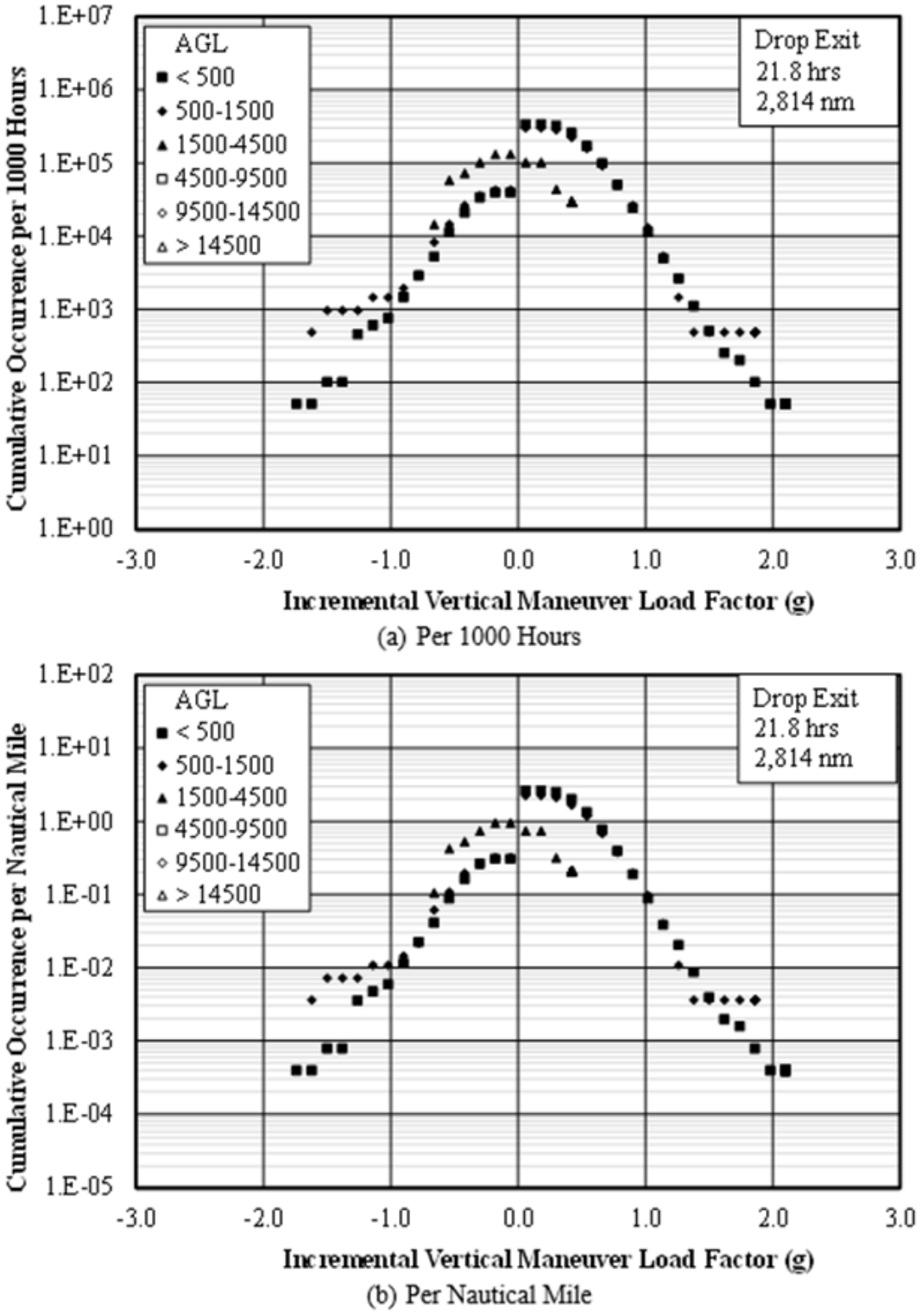

Figure B-23: Cumulative occurrences of incremental vertical maneuver load factor, Drop Exit

C Appendix placeholder

Figures

Tables

Table C-1: Statistical formats – Flight loads data by MSL altitudes

Flight Loads Data	**Table**
Summary of Durations and Distances for Cruise 1 by MSL Altitude	C-3
Summary of Durations and Distances for Cruise 2 by MSL Altitude	C-4
Summary of Durations and Distances for Cruise Heavy by MSL Altitude	C-5
Summary of Durations and Distances for Cruise Light by MSL Altitude	C-6
Summary of Durations and Distances for Ferry Flights by MSL Altitude	C-7
Summary of Durations and Distances for Maint./Training by MSL Altitude	C-8

Table C-2: Statistical formats – Flight loads data by MSL altitude

Flight Loads Data	**Figure**
CRUISE PHASES	
Cumulative Occurrences of Incremental Vertical Gust Load Factor, Cruise 1	C-1
Cumulative Occurrences of Incremental Vertical Maneuver Load Factor, Cruise 1	C-2
Cumulative Occurrences of Incremental Vertical Gust Load Factor, Cruise 2	C-3
Cumulative Occurrences of Incremental Vertical Maneuver Load Factor, Cruise 2	C-4
Cumulative Occurrences of Incremental Vertical Gust Load Factor, Cruise Heavy	C-5
Cumulative Occurrences of Incremental Vertical Maneuver Load Factor, Cruise Heavy	C-6
Cumulative Occurrences of Incremental Vertical Gust Load Factor, Cruise Light	C-7
Cumulative Occurrences of Incremental Vertical Maneuver Load Factor, Cruise Light	C-8
Cumulative Occurrences of Incremental Vertical Gust Load Factor, Ferry	C-9
Cumulative Occurrences of Incremental Vertical Maneuver Load Factor, Ferry	C-10
Cumulative Occurrences of Incremental Vertical Gust Load Factor, Maint./Training	C-11
Cumulative Occurrences of Incremental Vertical Maneuver Load Factor, Maint./Training	C-12

Table C-3:Summary of durations and distances for Cruise 1 by MSL altitude

Altitude Band	Duration (s)	Duration (hr)	Distance (nm)
1	60.6	1.0	126.2
2	1,098.6	18.3	2,579.1
3	8,108.4	135.1	21,075.3
4	19,030.9	317.2	54,358.4
5	6,715.7	111.9	20,293.9
6	0.45	0	1.4
Total	35,014	583.6	98,434

Table C-4: Summary of durations and distances for Cruise 2 by MSL altitude

Altitude Band	Duration (s)	Duration (hr)	Distance (nm)
1	78.3	1.3	162.7
2	1,445.2	24.1	3,367.6
3	8,313.8	138.6	22,106.6
4	15,456.3	257.6	44,011.0
5	3,117.9	52.0	9,402.1
6	0	0	0
Total	28,412	474	79,050

Table C-5:Summary of durations and distances for Cruise Heavy by MSL altitude

Altitude Band	Duration (s)	Duration (hr)	Distance (nm)
1	1,494.2	24.9	3,182.1
2	5,018.6	83.6	11,585.7
3	24,889.0	414.8	59,451.3
4	58,543.6	975.7	150,204.3
5	1,765.3	29.4	4,994.6
6	0	0	0
Total	91,711	1529	229,418

Table C-6: Summary of durations and distances for Cruise Light by MSL altitude

Altitude Band	Duration (s)	Duration (hr)	Distance (nm)
1	1,142.3	19.0	2,214.1
2	4,419.0	73.7	10,802.2
3	16,741.4	279.0	43,883.0
4	33,733.8	562.2	95,246.6
5	1,156.3	19.3	3,511.6
6	0	0	0
Total	57,193	953	155,657

Table C-7: Summary of durations and distances for Ferry Flight by MSL altitude

Altitude Band	Duration (s)	Duration (hr)	Distance (nm)
1	49.6	0.82	115.6
2	636.8	10.6	1,537.5
3	8,460.6	141.0	22,420.7
4	23,816.2	396.9	69,082.6
5	16,856.9	280.9	51,431.8
6	616.5	10.3	1,911.2
Total	50,437	841	146,499

Table C-8: Summary of durations and distances for Maintenance/Training by MSL altitude

Altitude Band	Duration (s)	Duration (hr)	Distance (nm)
1	19.7	0.33	39.2
2	307.7	5.1	661.3
3	2,542.2	42.4	5,991.0
4	1,806.6	30.1	4,903.9
5	205.0	3.4	604.5
6	4.9	0.08	20.8
Total	4,886	81	12,221

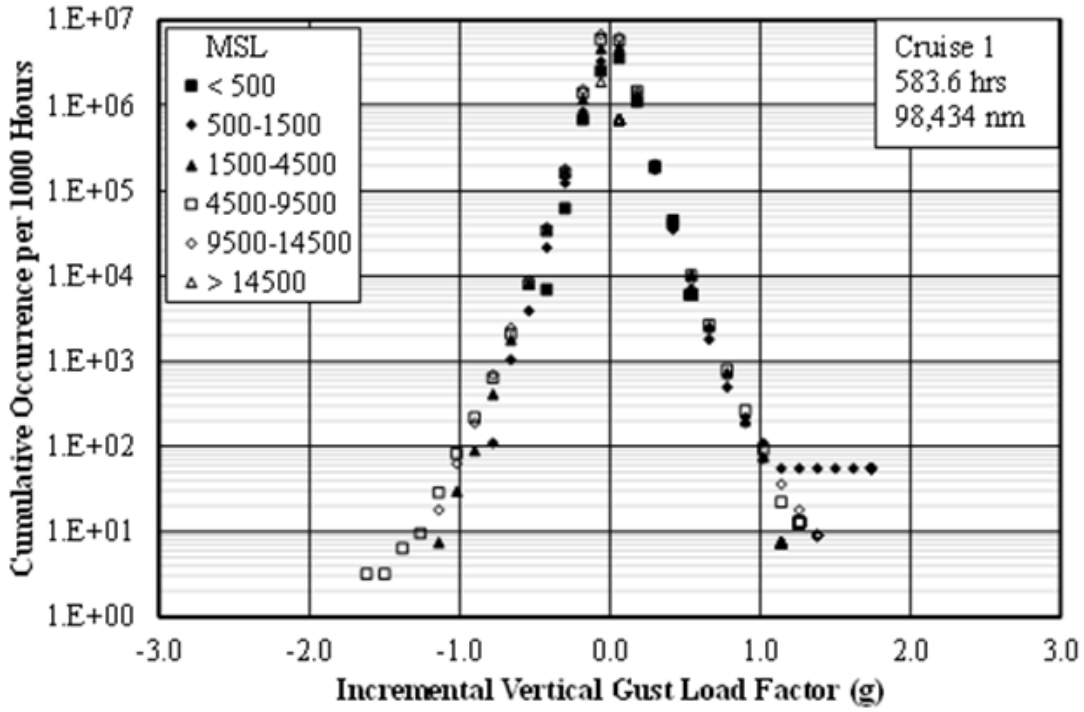

(a) Per 1000 Hours

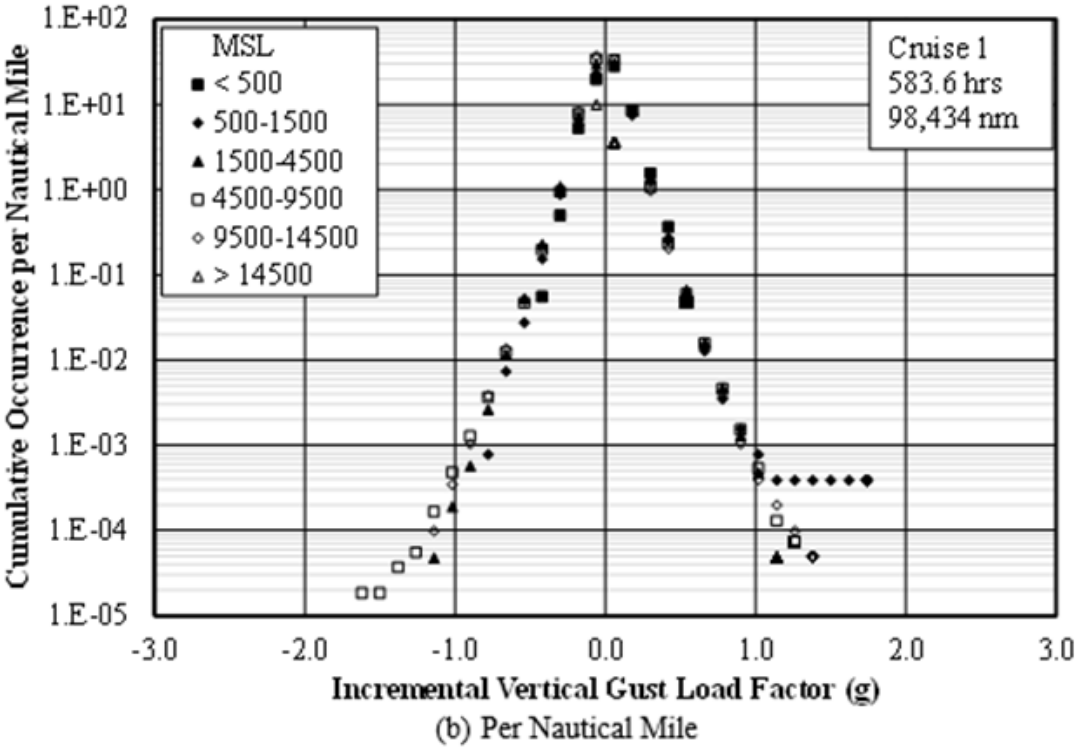

(b) Per Nautical Mile

Figure C-1: Cumulative occurrences of incremental vertical gust load factor, Cruise 1

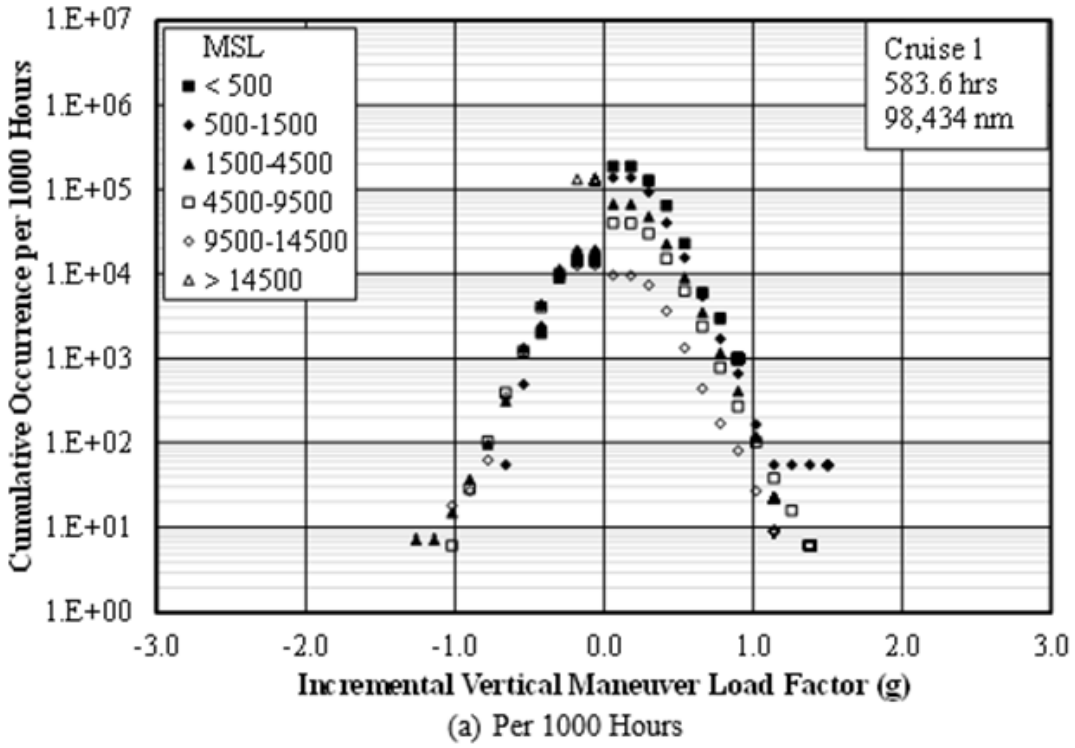

(a) Per 1000 Hours

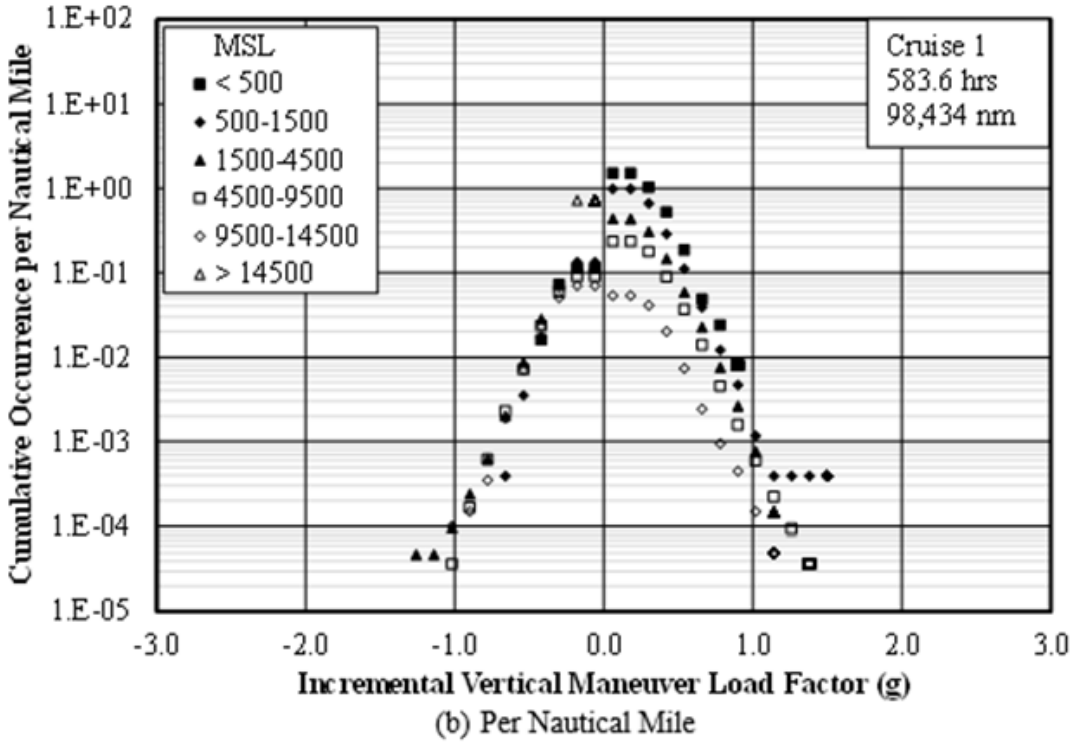

(b) Per Nautical Mile

Figure C-2: Cumulative occurrences of incremental vertical maneuver load factor, Cruise 1

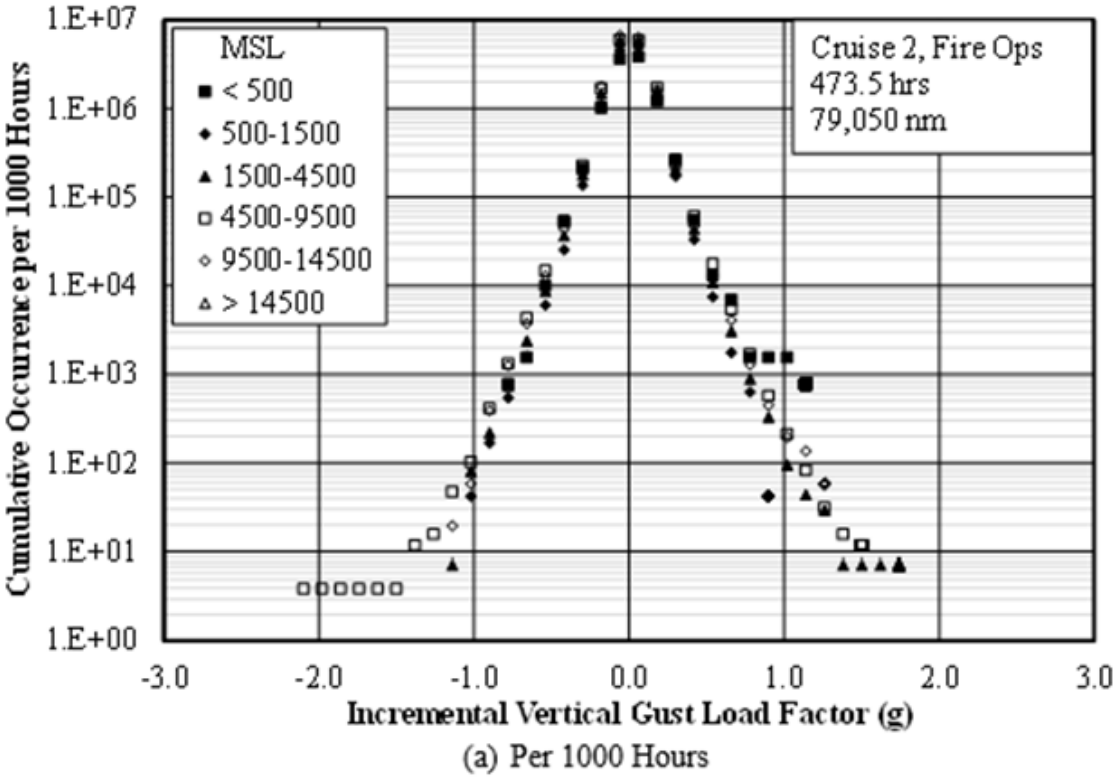

(a) Per 1000 Hours

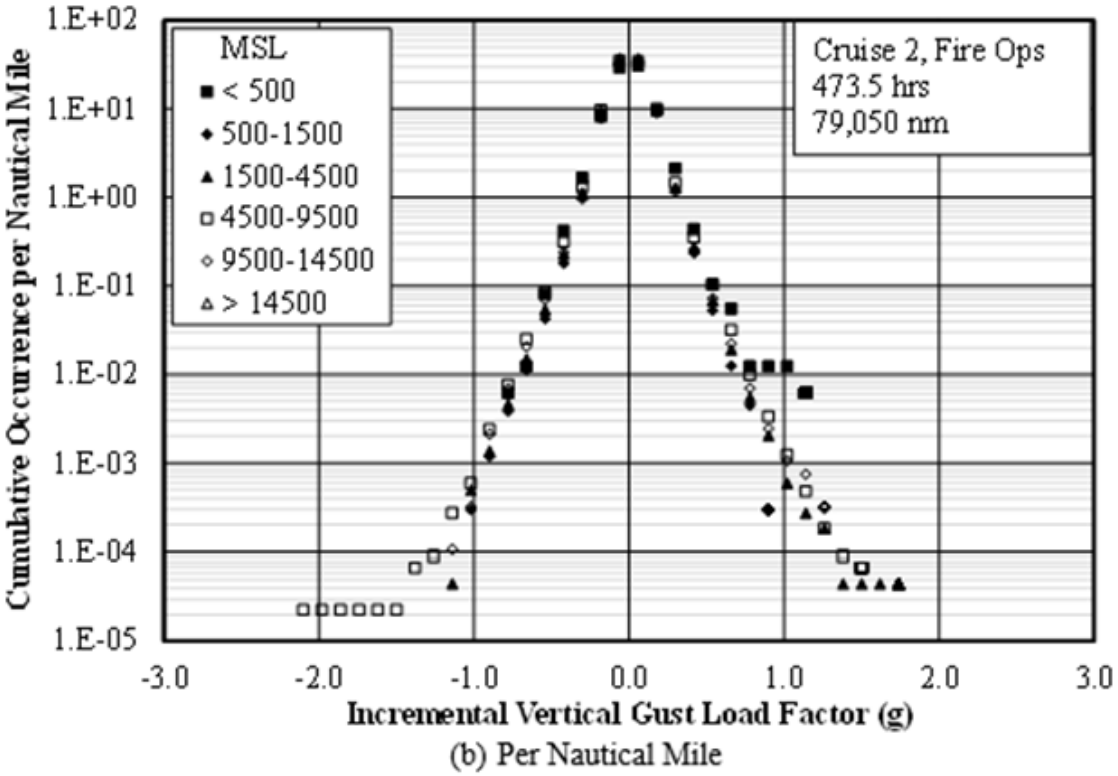

(b) Per Nautical Mile

Figure C-3: Cumulative occurrences of incremental vertical gust load factor, Cruise 2

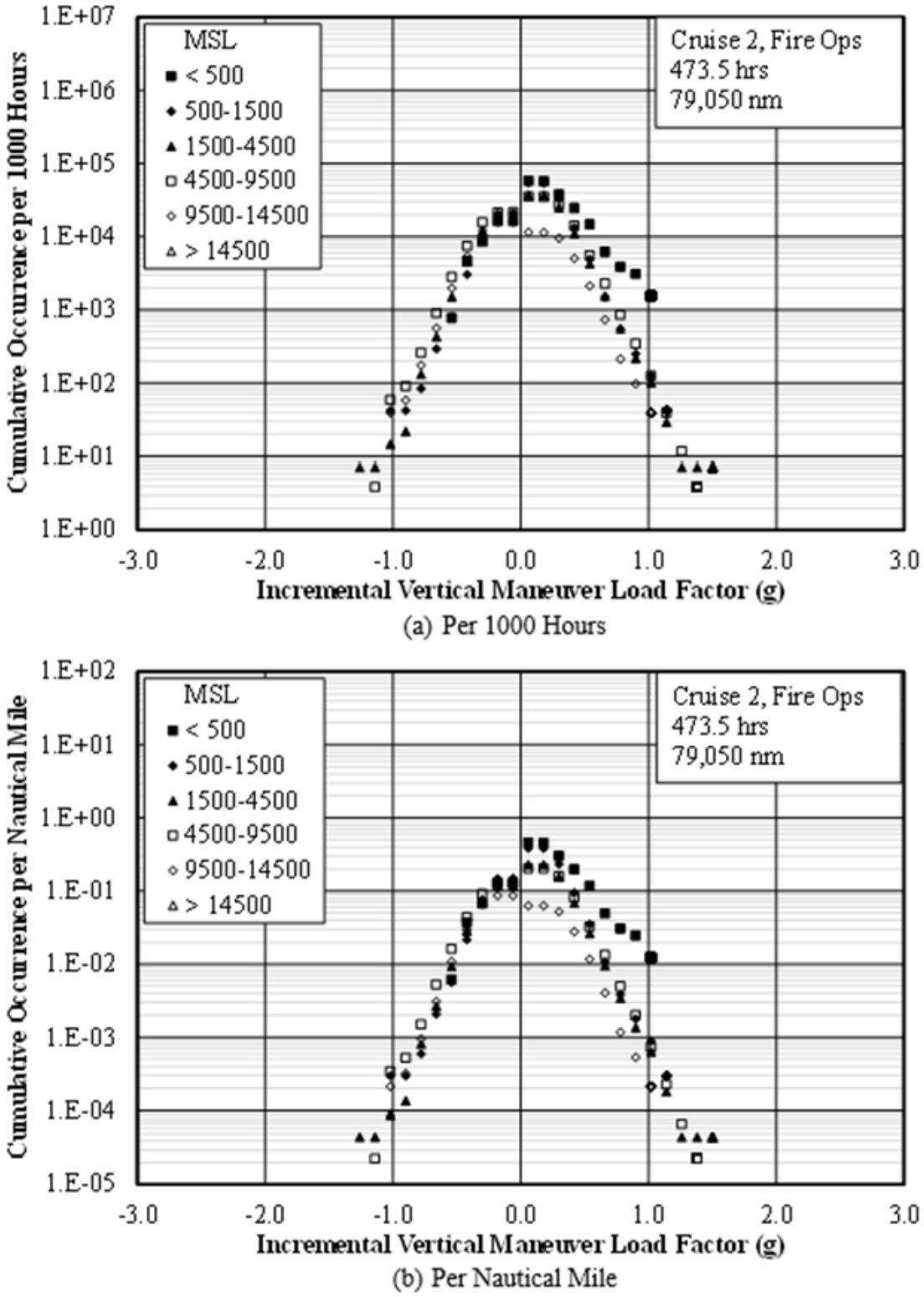

Figure C-4: Cumulative occurrences of incremental vertical maneuver load factor, Cruise 2

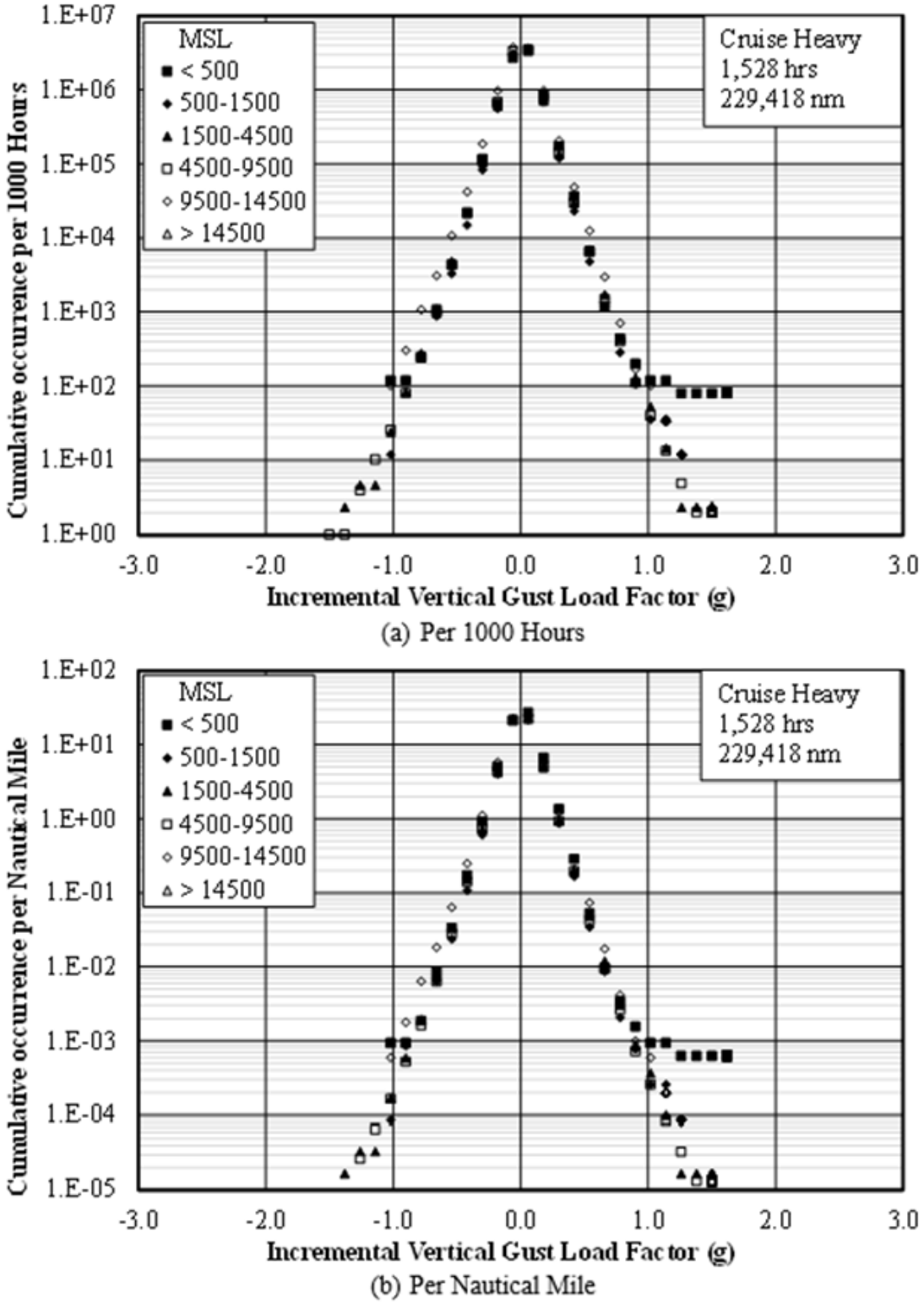

Figure C-5: Cumulative occurrences of incremental vertical gust load factor, Cruise Heavy

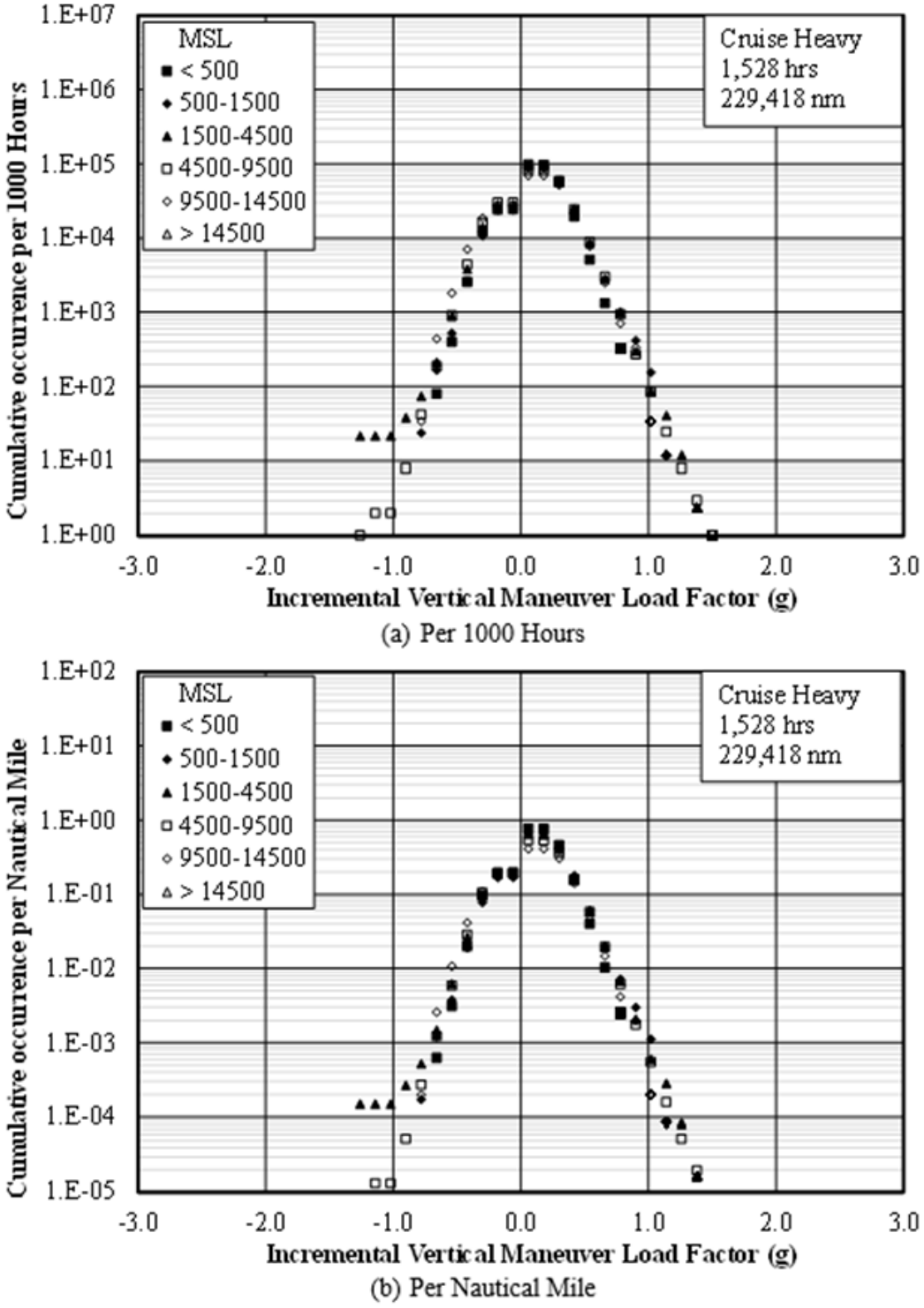

Figure C-6: Cumulative occurrences -incremental vertical maneuver load factor, Cruise Heavy

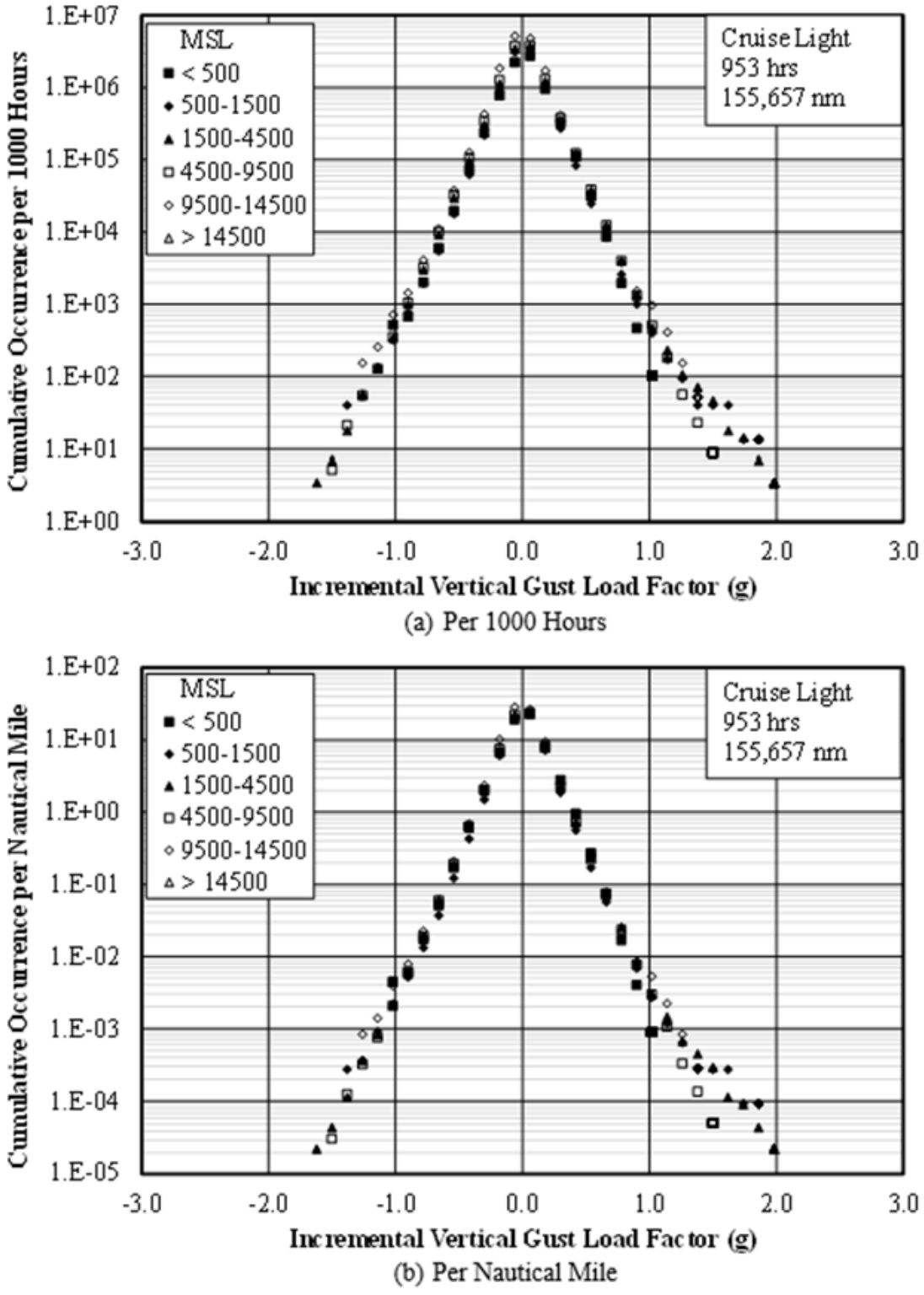

Figure C-7: Cumulative occurrences of incremental vertical gust load factor, Cruise Light

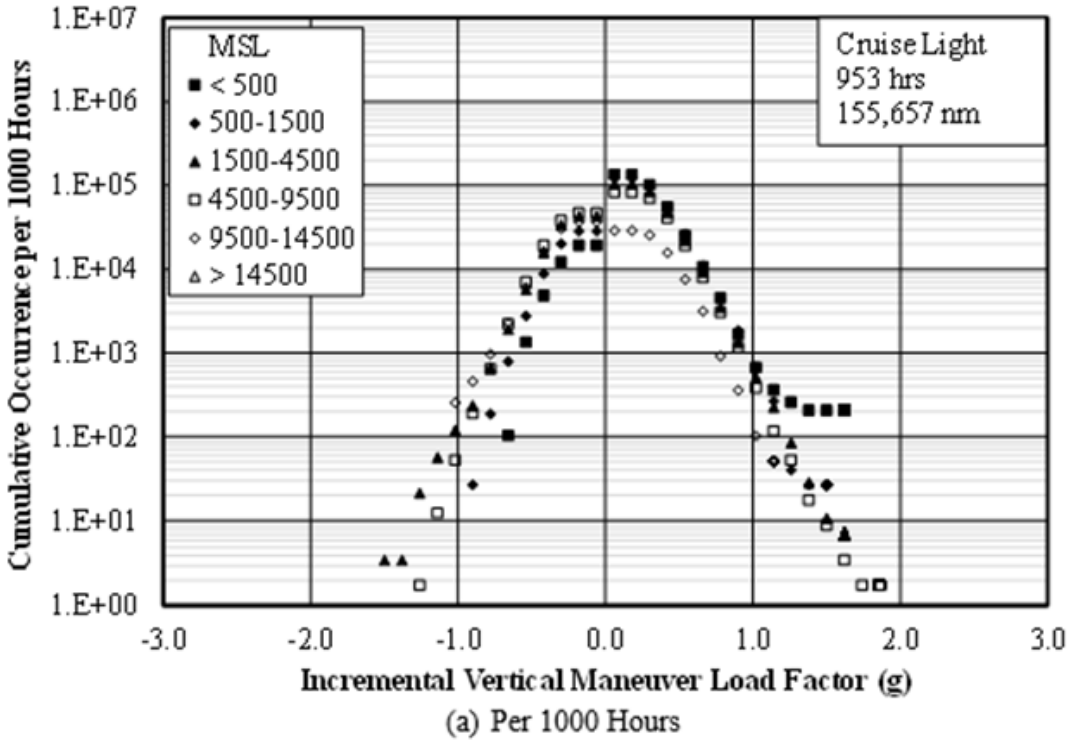

(a) Per 1000 Hours

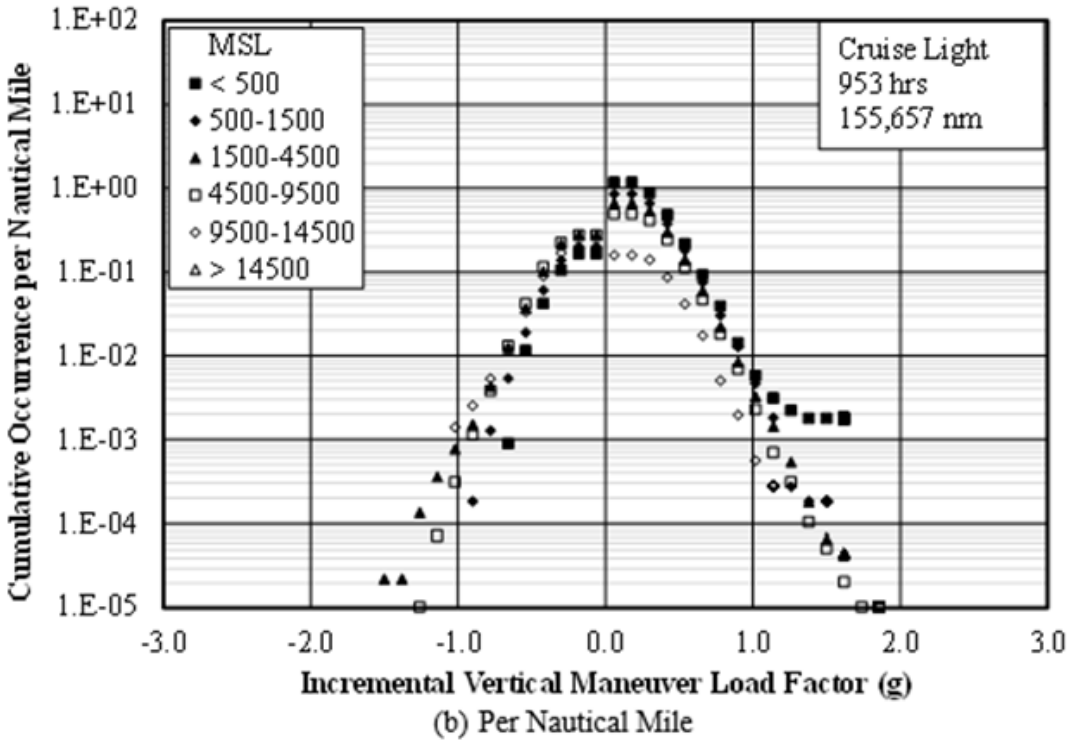

(b) Per Nautical Mile

Figure C-8: Cumulative occurrences -incremental vertical maneuver load factor, Cruise Light

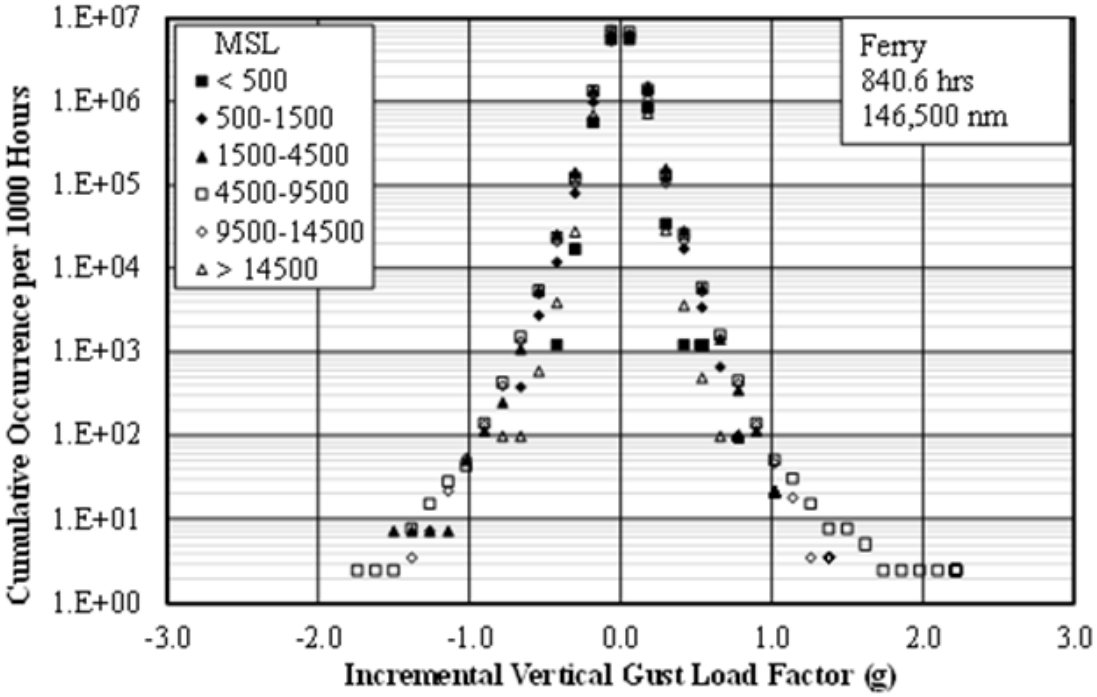

(a) Per 1000 Hours

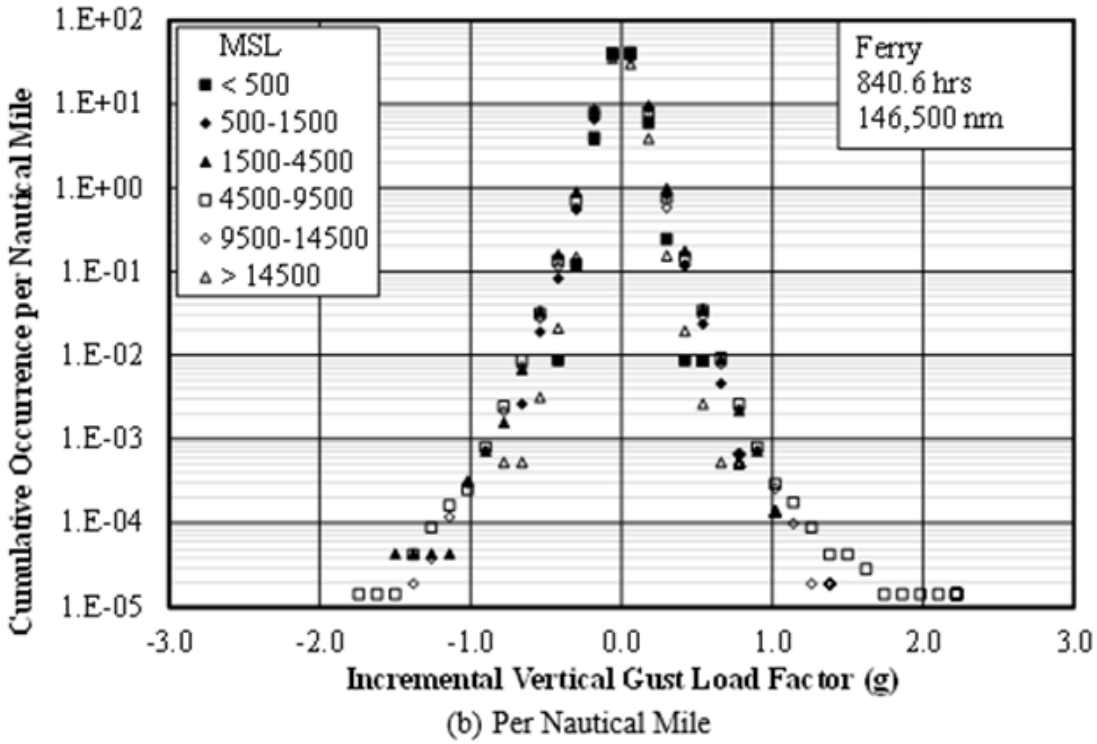

(b) Per Nautical Mile

Figure C-9: Cumulative occurrences of incremental vertical gust load Factor, Ferry

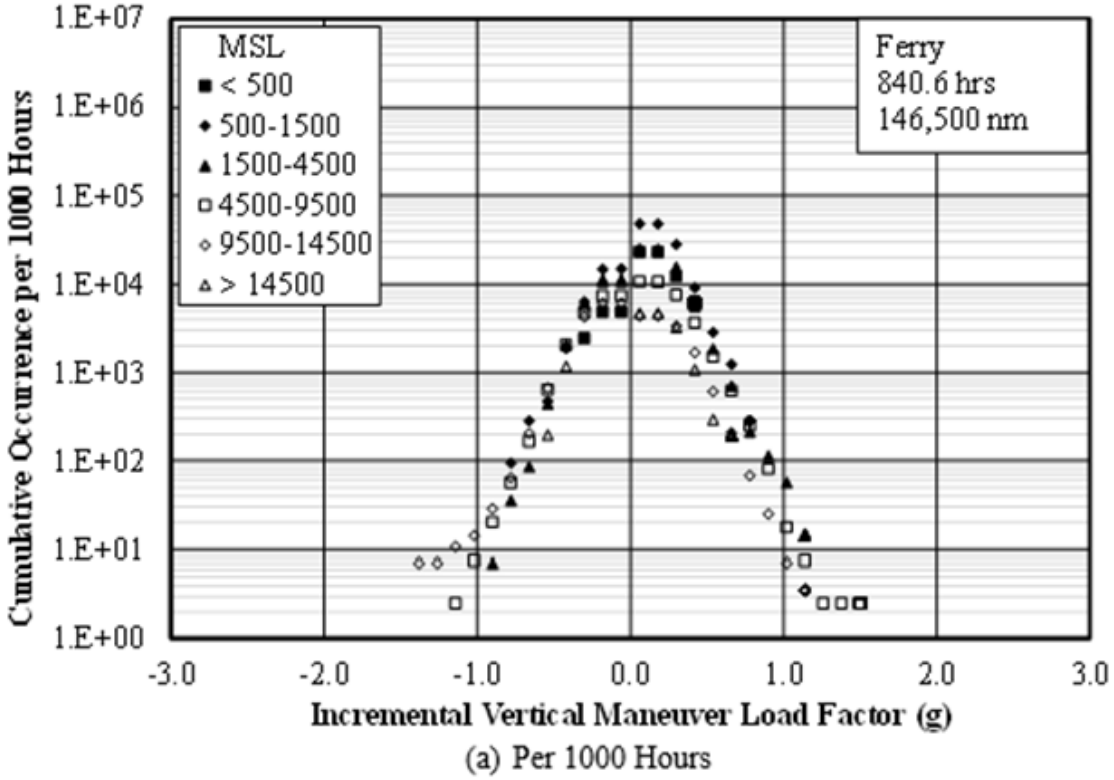

(a) Per 1000 Hours

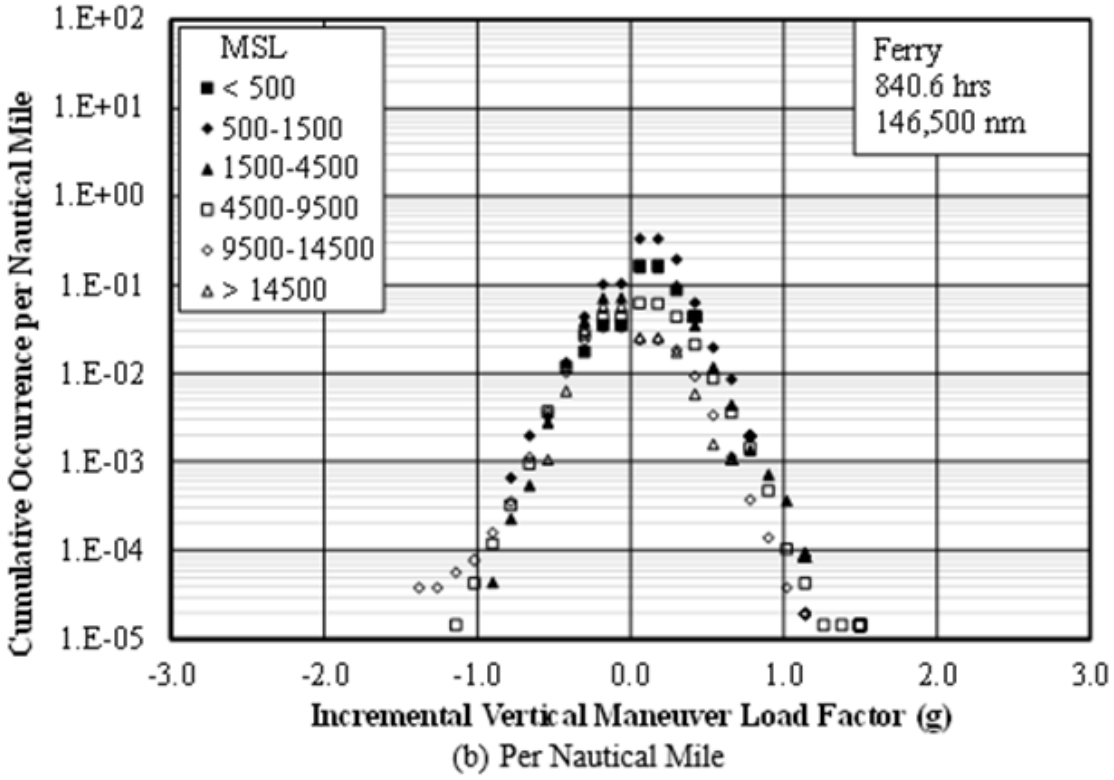

(b) Per Nautical Mile

Figure C-10: Cumulative occurrences of incremental vertical maneuver load factor, Ferry

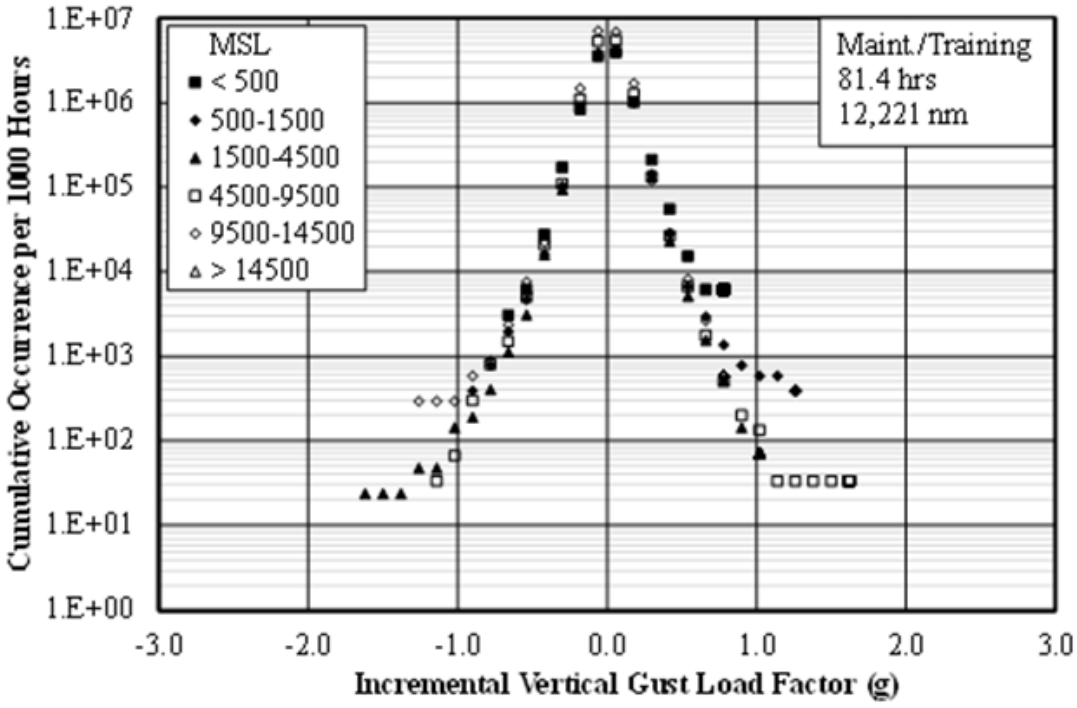

(a) Per 1000 Hours

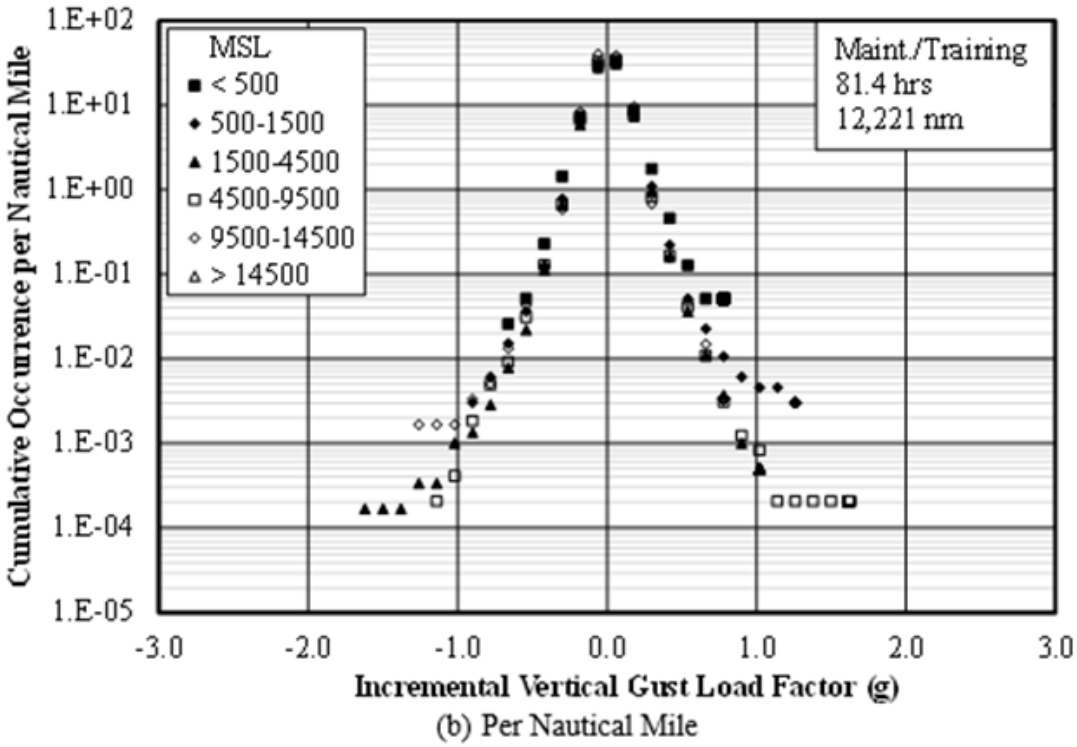

(b) Per Nautical Mile

Figure C-11: Cumulative occurrences of incremental vertical gust load factor, Maintenance/Training

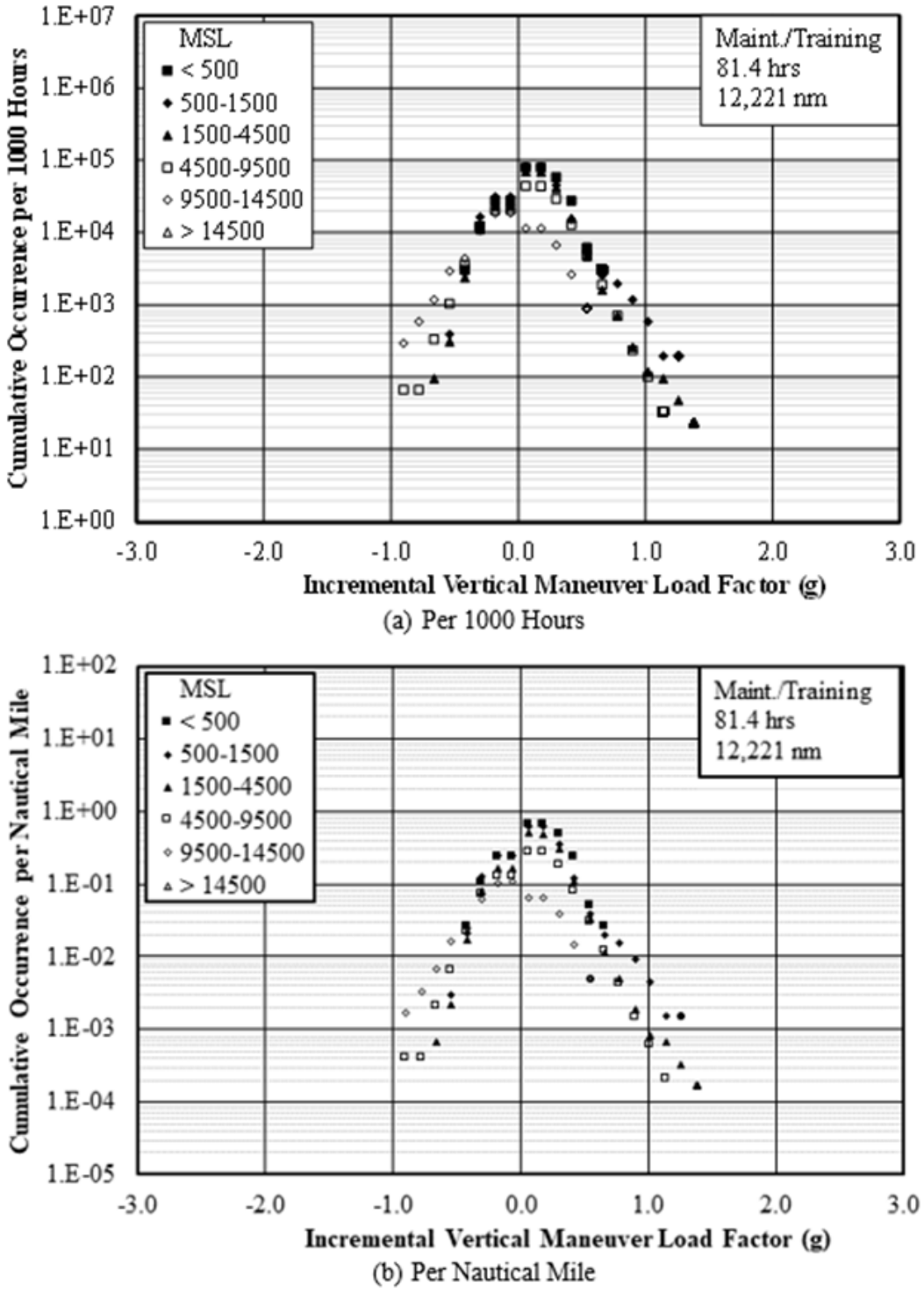

Figure C-12: Cumulative occurrences of incremental vertical maneuver load factor, Maintenance/Training

D Flight loads comparisons

Figures

Tables

Table D-1: Derived gust velocities per nautical mile

Flight Loads Data	**Figure**
Cumulative Occurrences of Incremental Vertical Gust Load Factor by Flight Phase	D-1
Cumulative Occurrences of Incremental Vertical Maneuver Load Factor by Flight Phase	D-2
Cumulative Occurrences of Incremental Vertical Gust Load Factor Compared with Other Operations	D-3
Cumulative Occurrences of Incremental Vertical Maneuver Load Factor Compared with Other Operations	D-4

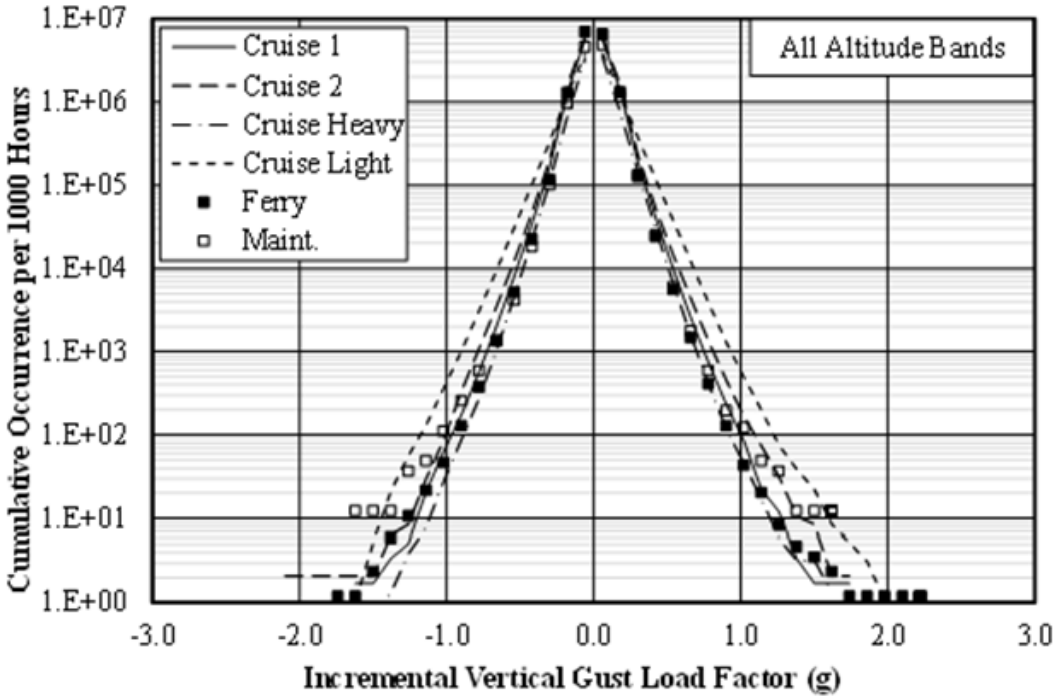

(a) Cruise Phases

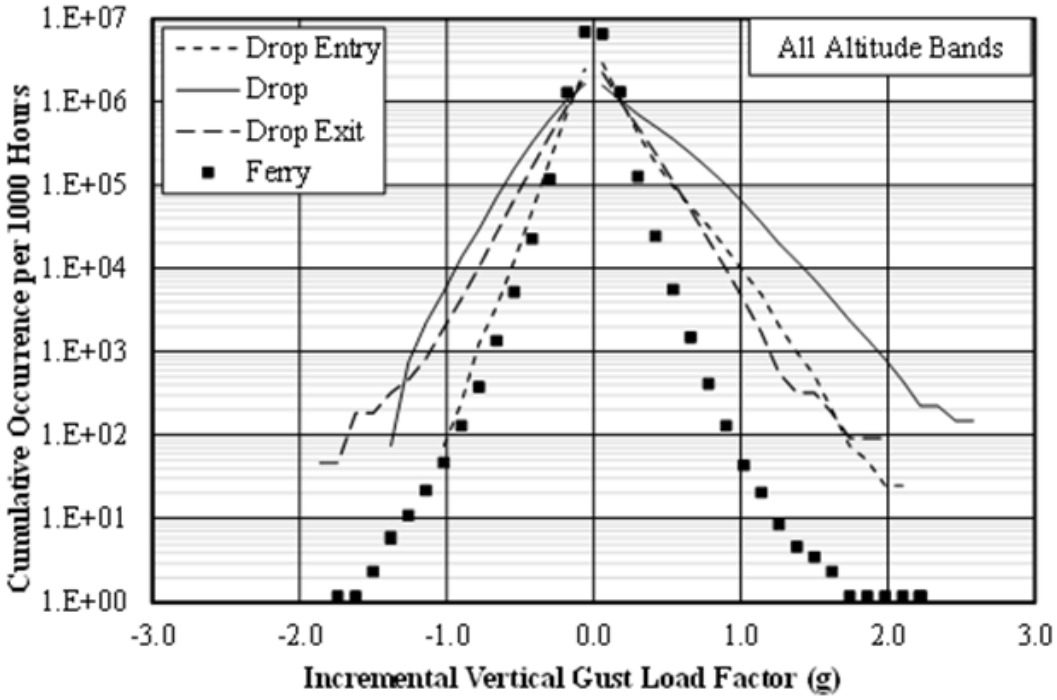

(b) Drop Phases

Figure D-1: Cumulative occurrences of incremental vertical gust load factor by flight phase

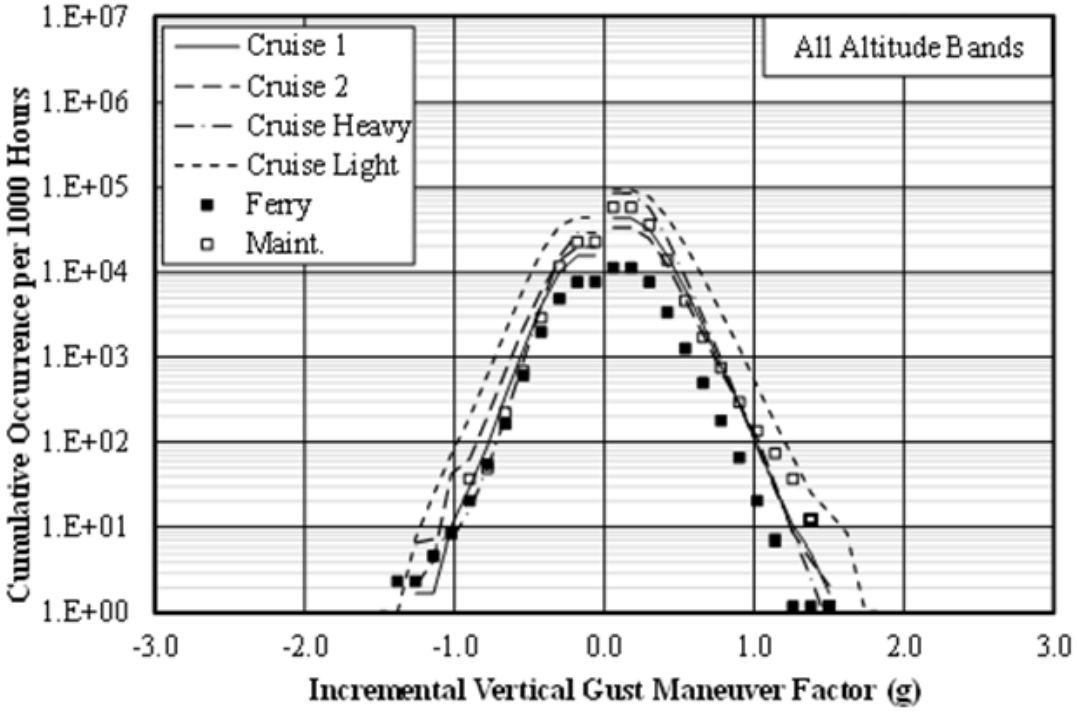

(a) Cruise Phases

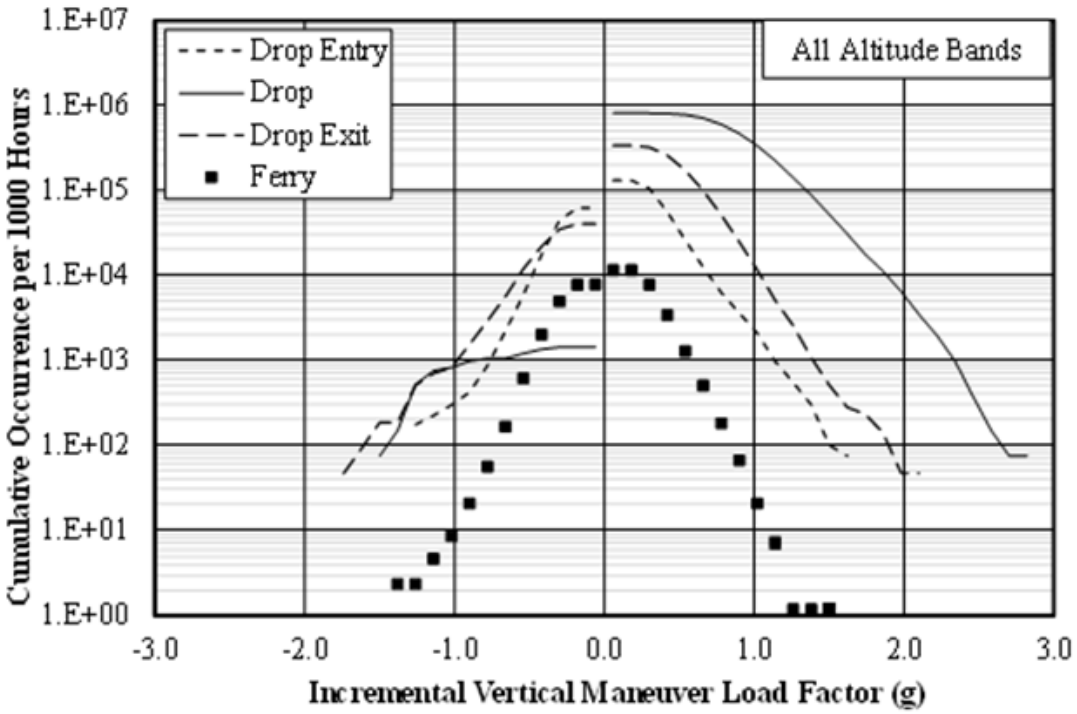

(b) Drop Phases

Figure D-2: Cumulative occurrences -incremental vertical maneuver load factor by flight phase

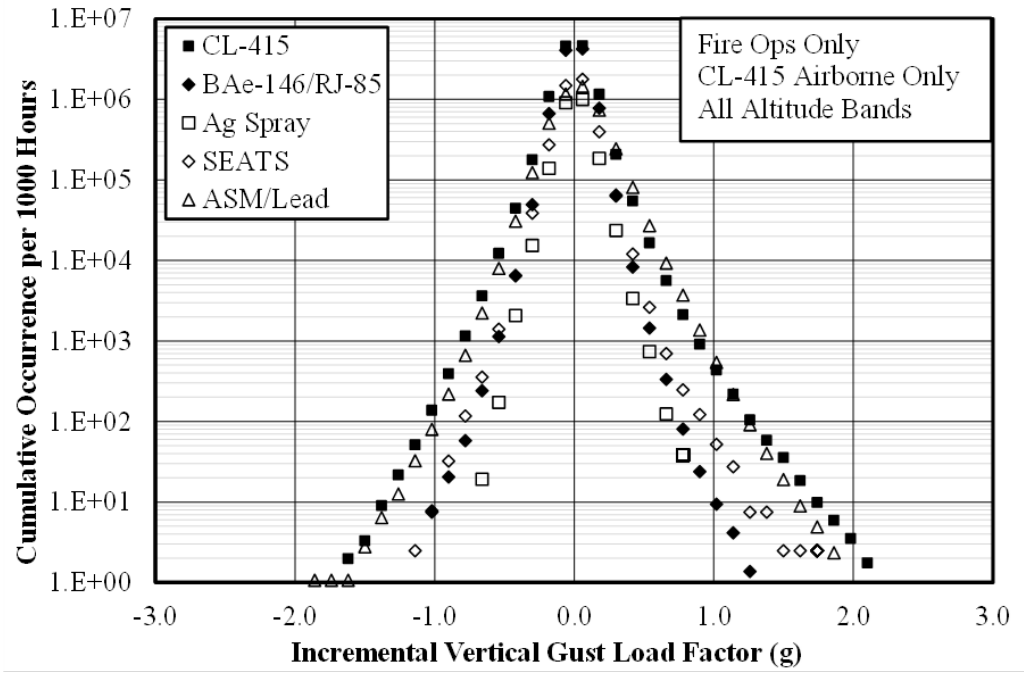

Figure D-3: Cumulative occurrences of incremental vertical gust load factor compared with other operations

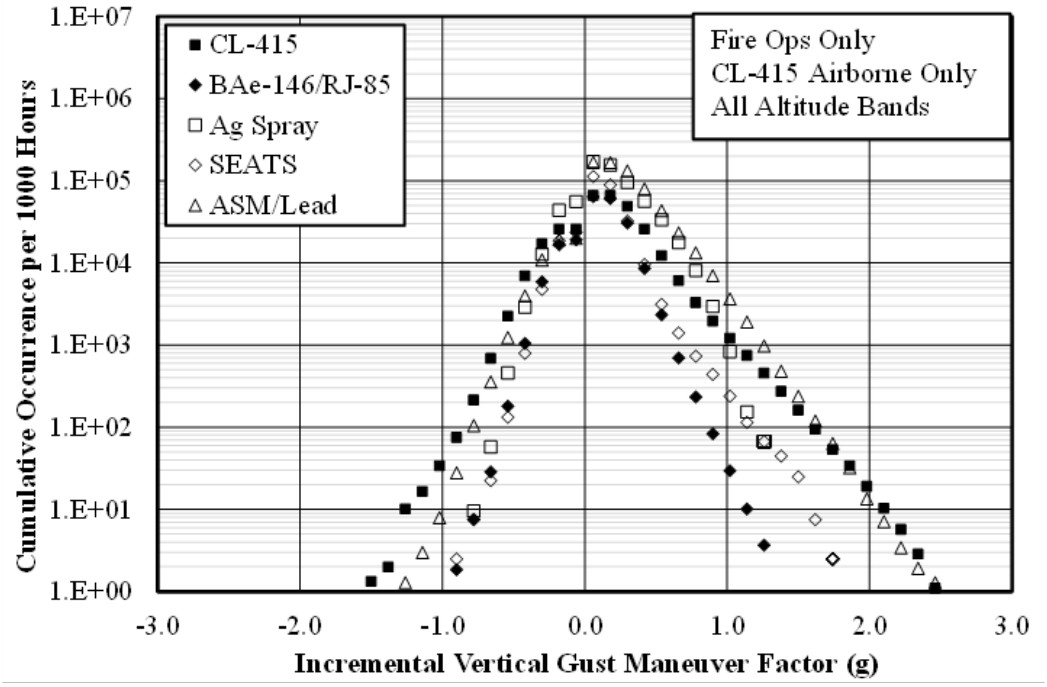

Figure D-4: Cumulative occurrences of incremental vertical maneuver load factor compared with other operations

E Derived gust velocities

Figures

Tables

Table E-1: Derived gust velocities per nautical mile

Flight Loads Data	**Figure**
CRUISE PHASES	
Cumulative Occurrences of Derived Gust Velocity by AGL Altitude, Cruise 1	E-1
Cumulative Occurrences of Derived Gust Velocity by MSL Altitude, Cruise 1	E-2
Cumulative Occurrences of Derived Gust Velocity by AGL Altitude, Cruise 2	E-3
Cumulative Occurrences of Derived Gust Velocity by MSL Altitude, Cruise 2	E-4
Cumulative Occurrences of Derived Gust Velocity by AGL Altitude, Cruise Heavy	E-5
Cumulative Occurrences of Derived Gust Velocity by MSL Altitude, Cruise Heavy	E-6
Cumulative Occurrences of Derived Gust Velocity by AGL Altitude, Cruise Light	E-7
Cumulative Occurrences of Derived Gust Velocity by MSL Altitude, Cruise Light	E-8
Cumulative Occurrences of Derived Gust Velocity by AGL Altitude, Drop Entry	E-9
Cumulative Occurrences of Derived Gust Velocity by AGL Altitude, Drop	E-10
Cumulative Occurrences of Derived Gust Velocity by AGL Altitude, Drop Exit	E-11
Cumulative Occurrences of Derived Gust Velocity by AGL Altitude, Ferry	E-12
Cumulative Occurrences of Derived Gust Velocity by MSL Altitude, Ferry	E-13
Cumulative Occurrences of Derived Gust Velocity by AGL Altitude, Maint./Training	E-14
Cumulative Occurrences of Derived Gust Velocity by MSL Altitude, Maint./Training	E-15

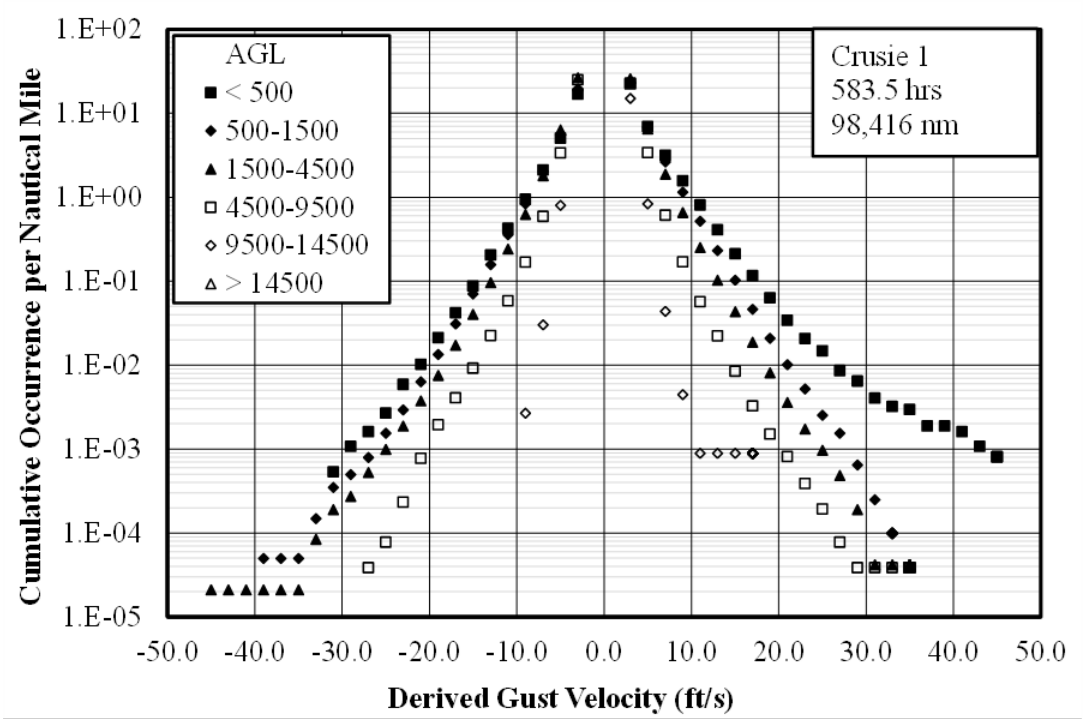

Figure E-1: Cumulative occurrences of derived gust velocity by AGL altitude, Cruise 1

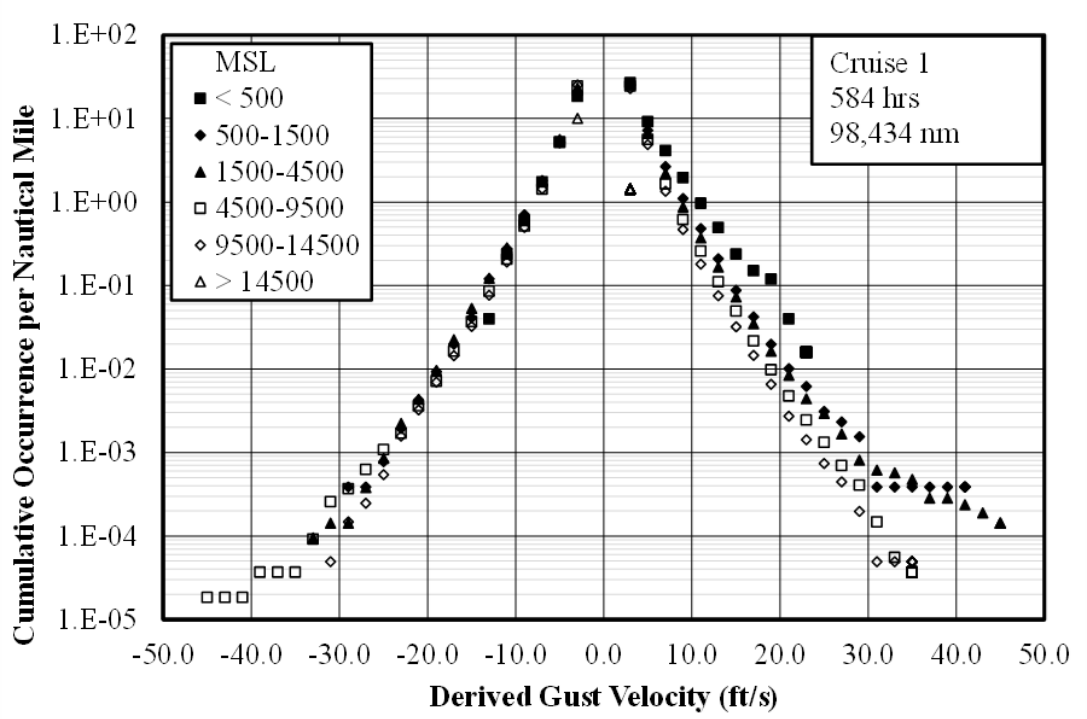

Figure E-2: Cumulative occurrences of derived gust velocity by MSL altitude, Cruise 1

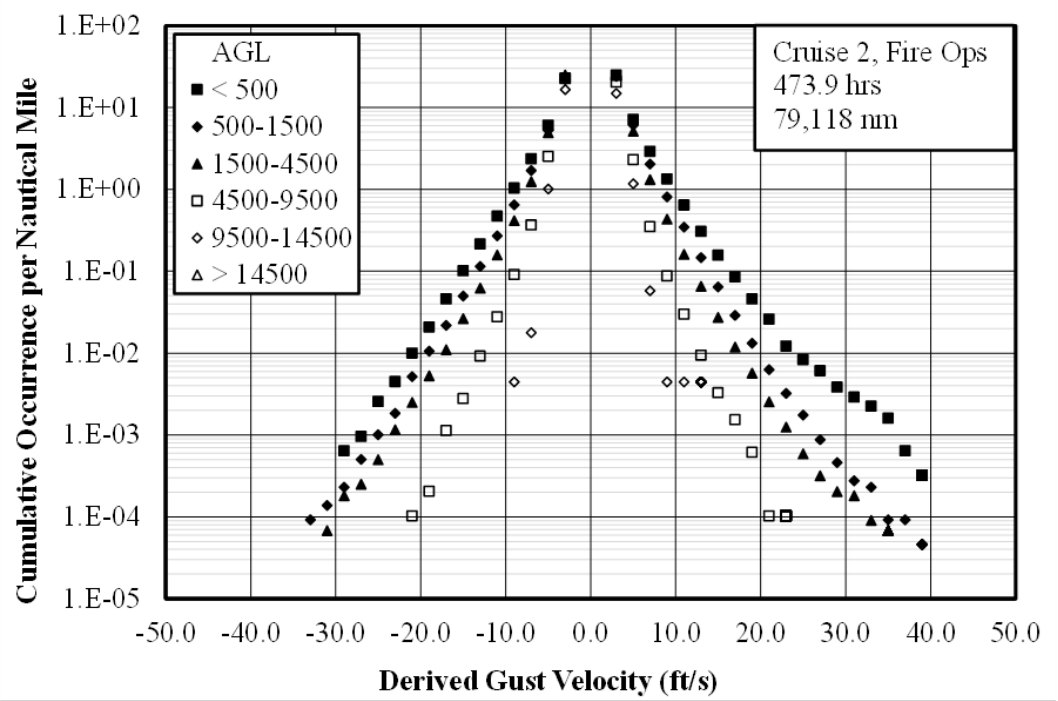

Figure E-3: Cumulative occurrences of derived gust velocity by AGL altitude, Cruise 2

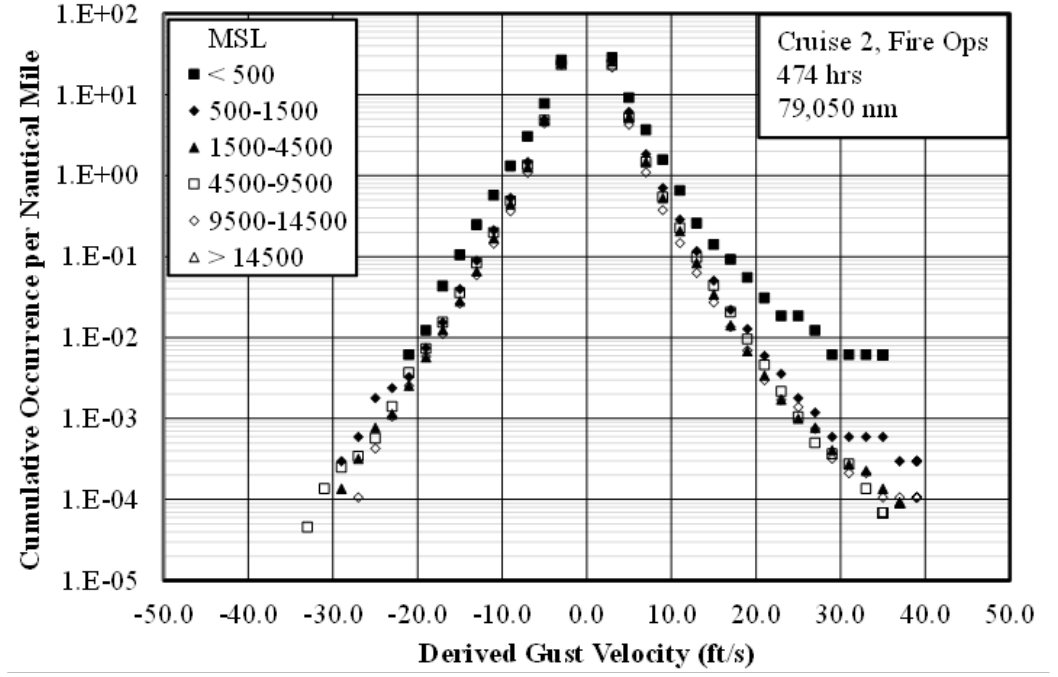

Figure E-4: Cumulative occurrences of derived gust velocity by MSL altitude, Cruise 2

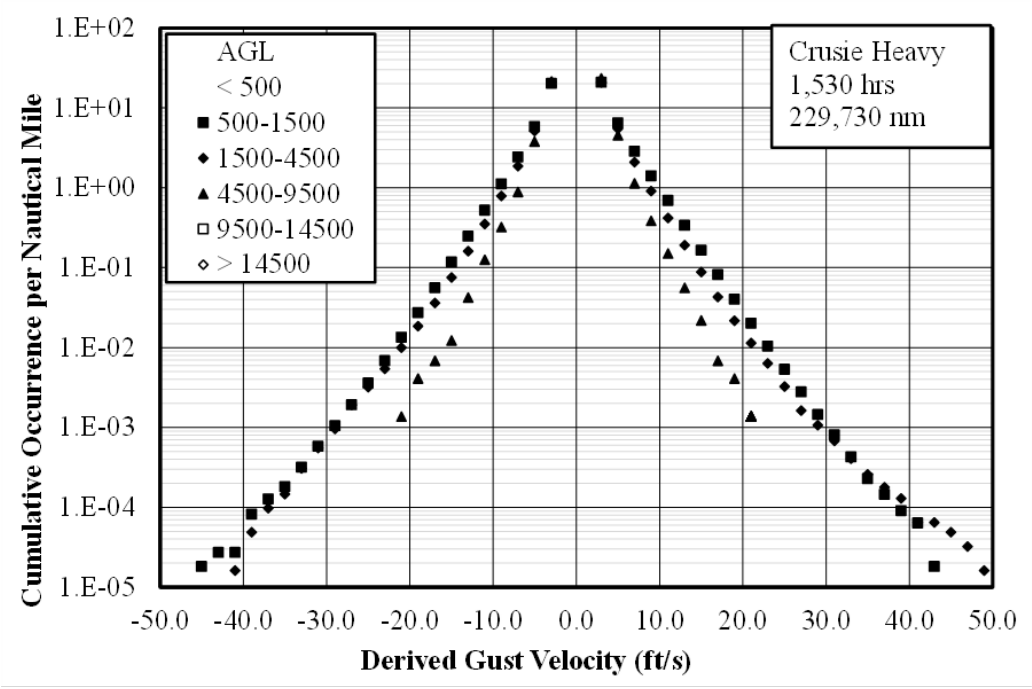

Figure E-5: Cumulative occurrences of derived gust velocity by AGL altitude, Cruise Heavy

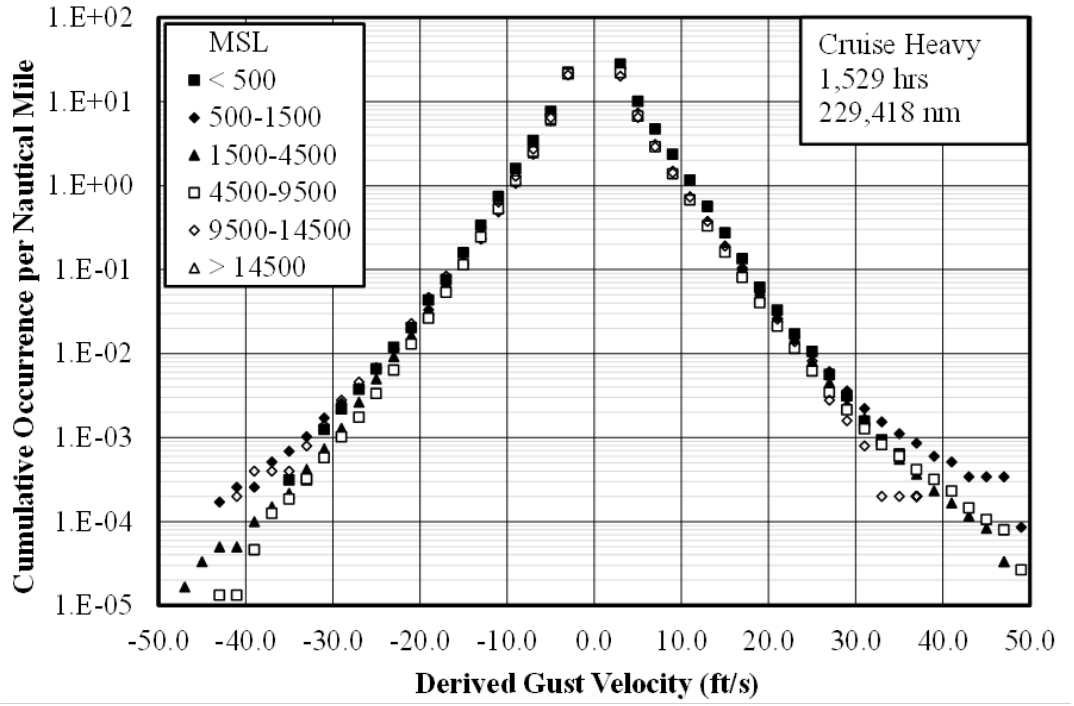

Figure E-6: Cumulative occurrences of derived gust velocity by MSL altitude, Cruise Heavy

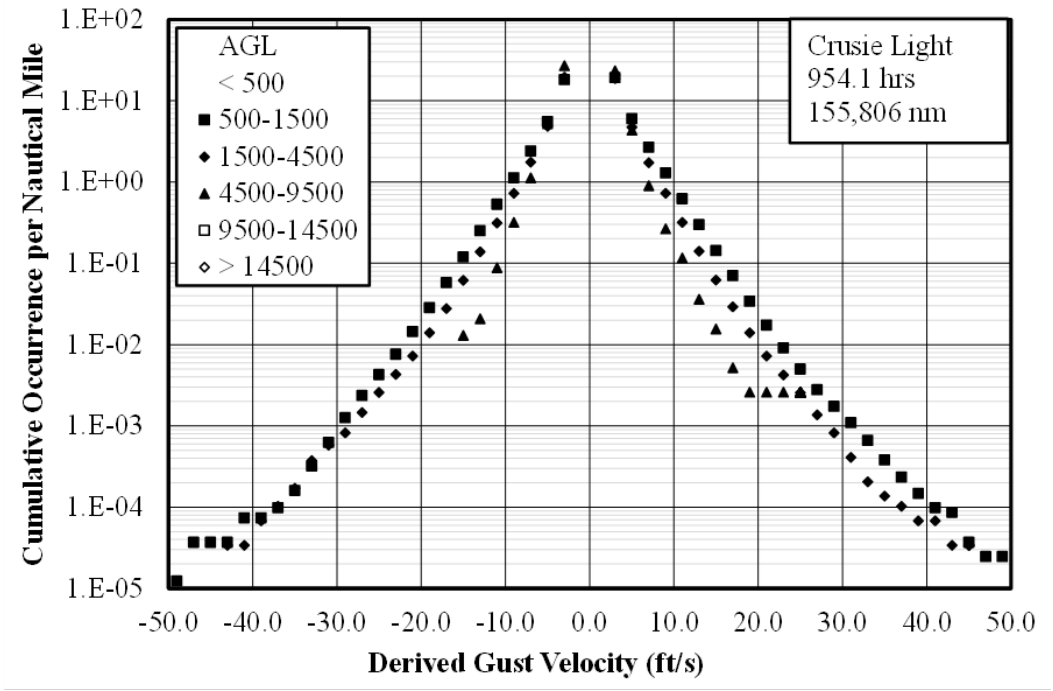

Figure E-7: Cumulative occurrences of derived gust velocity by AGL altitude, Cruise Light

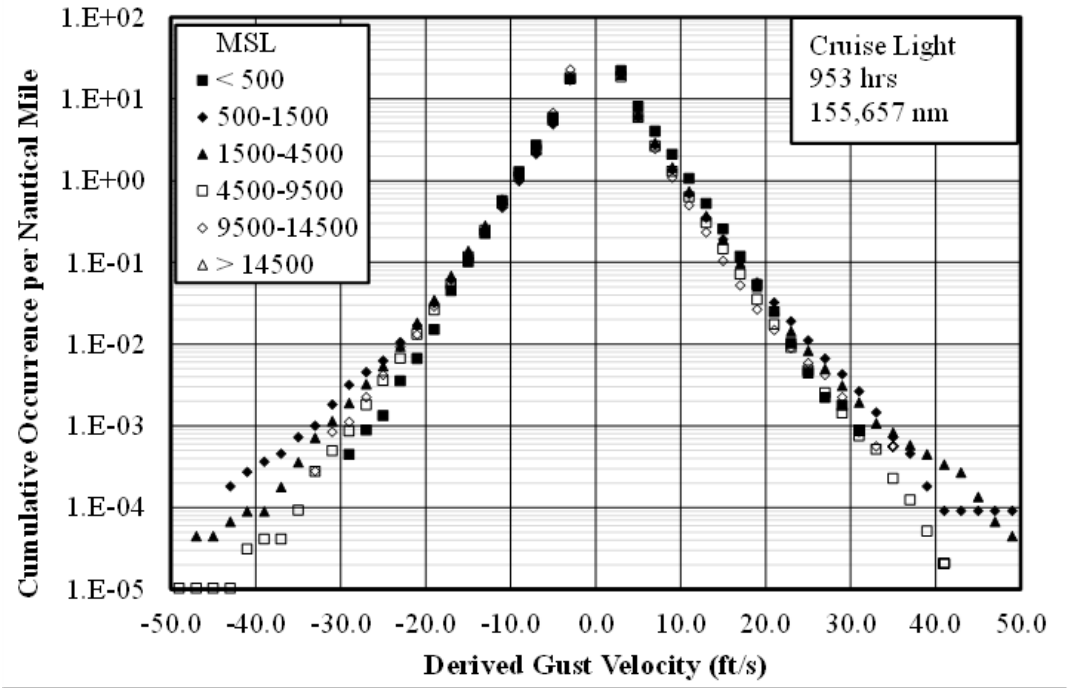

Figure E-8: Cumulative occurrences of derived gust velocity by MSL altitude, Cruise Light

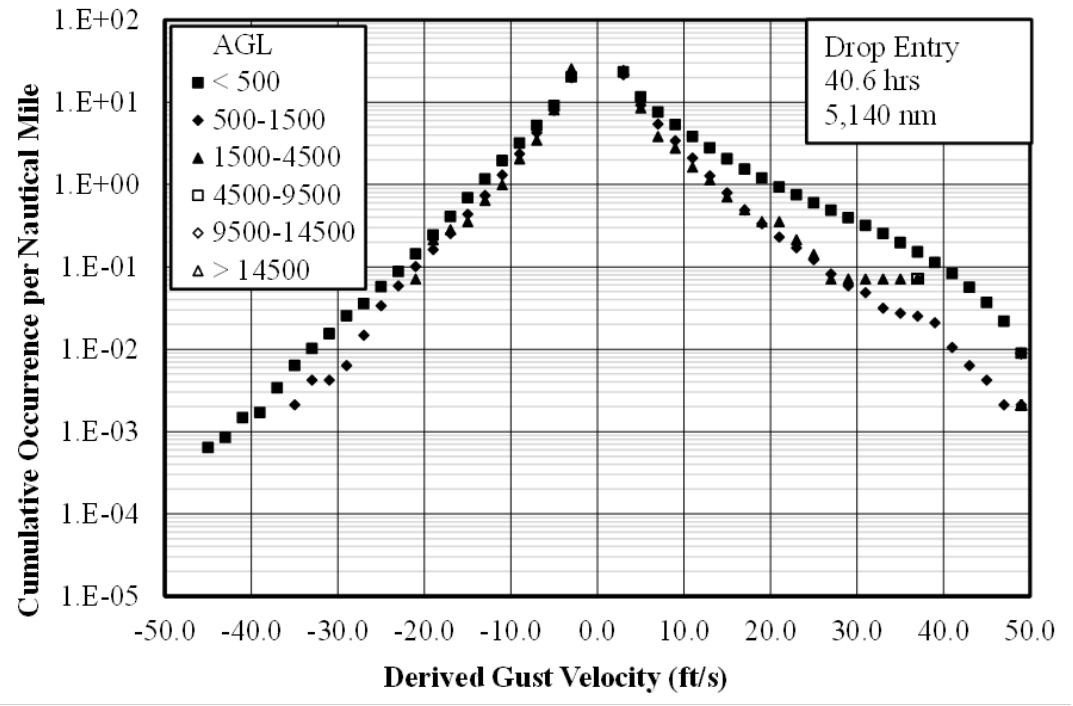

Figure E-9: Cumulative occurrences of derived gust velocity by AGL altitude, Drop Entry

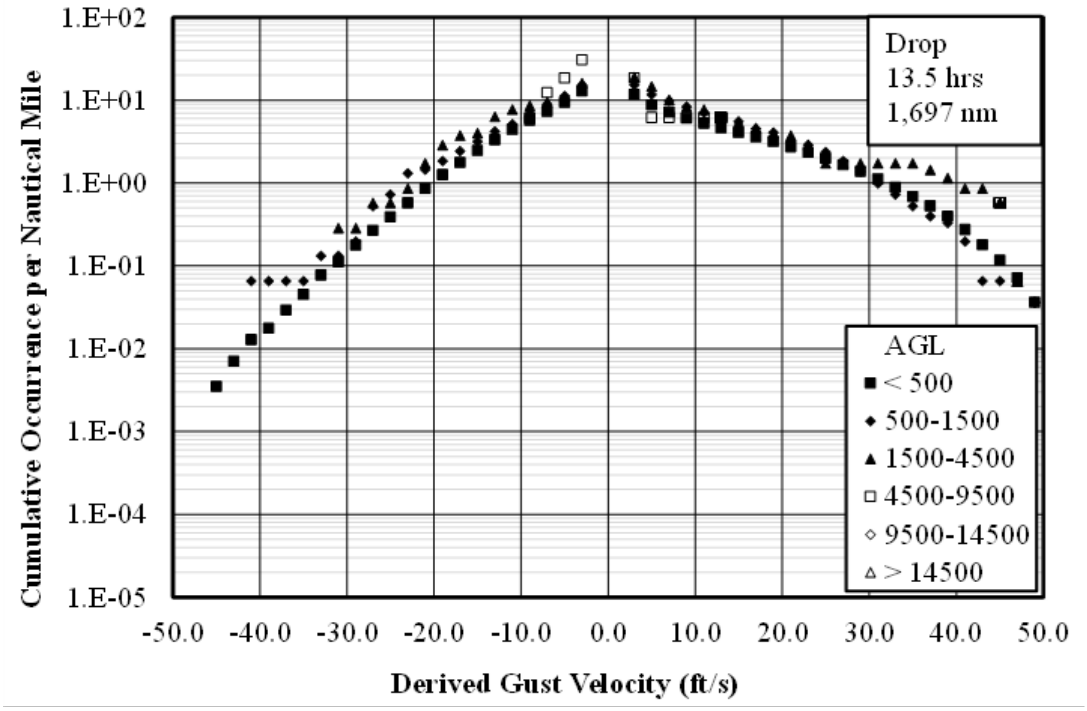

Figure E-10: Cumulative occurrences of derived gust velocity by AGL altitude, Drop

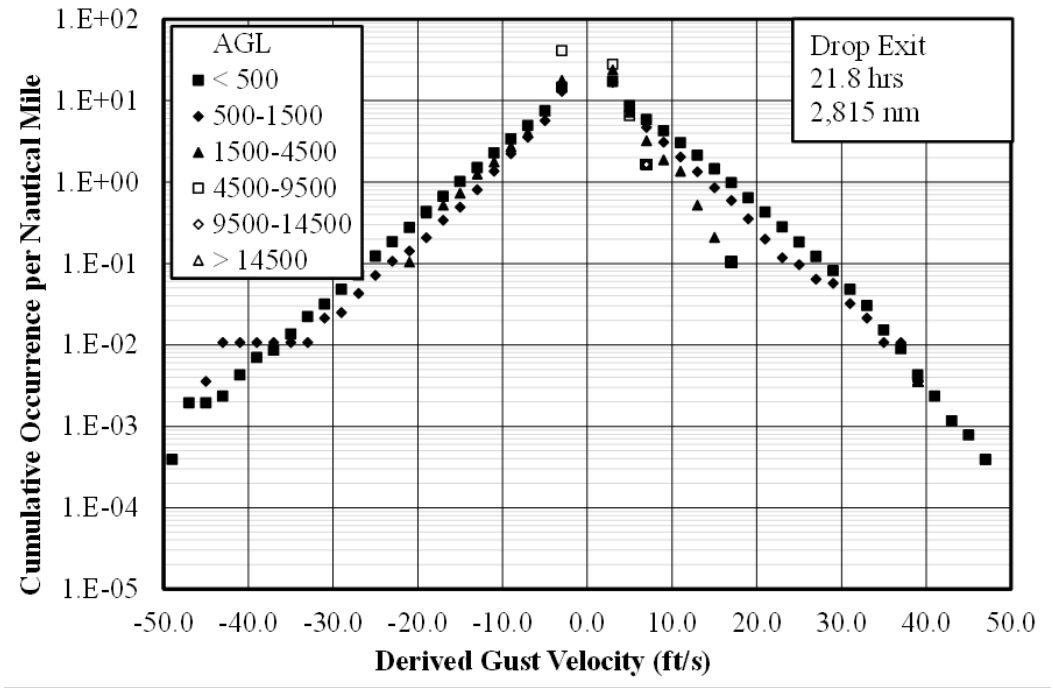

Figure E-11: Cumulative occurrences of derived gust velocity by AGL altitude, Drop Exit

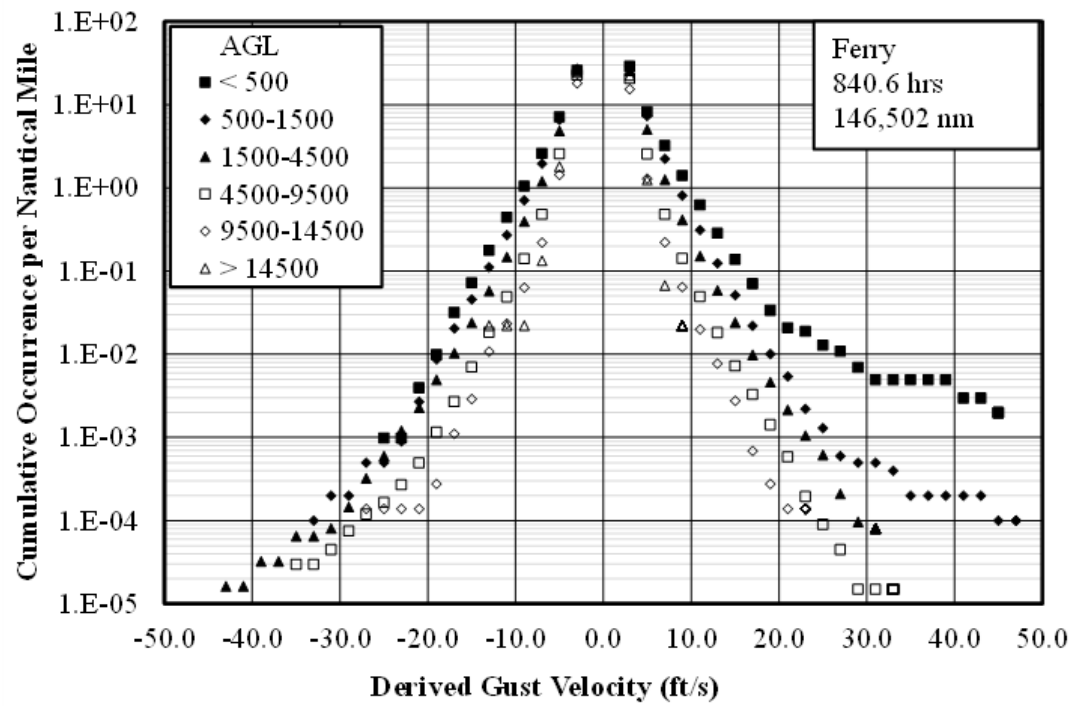

Figure E-12: Cumulative occurrences of derived gust velocity by AGL altitude, Ferry

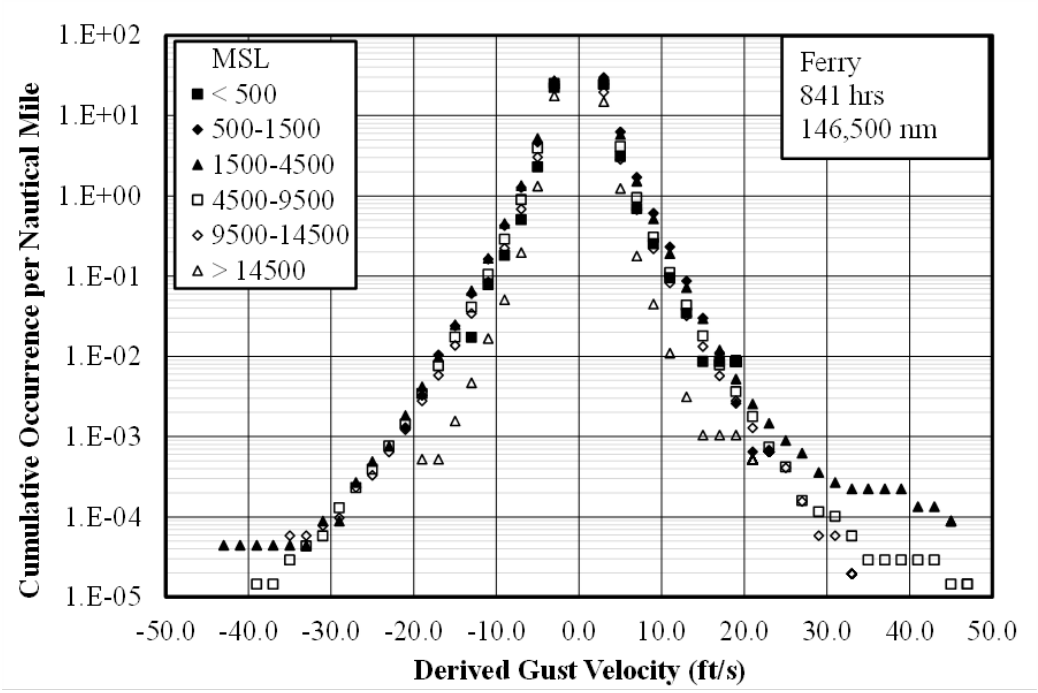

Figure E-13: Cumulative occurrences of derived gust velocity by MSL altitude, Ferry

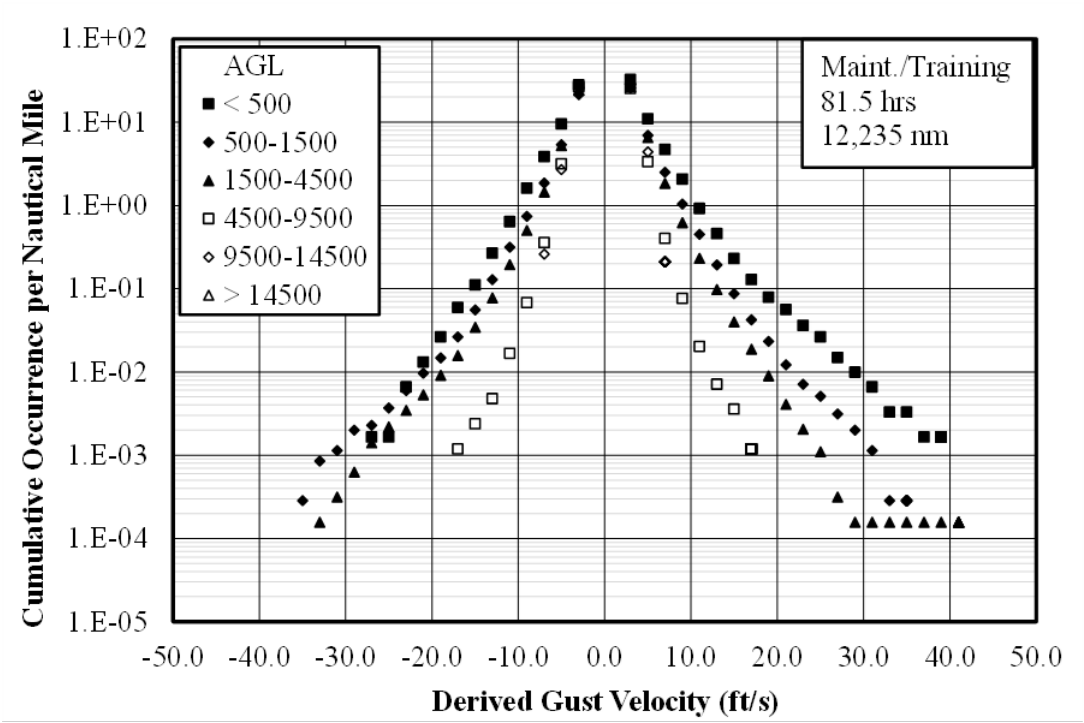

Figure E-14: Cumulative occurrences of derived gust velocity by AGL altitude, Maintenance/Training

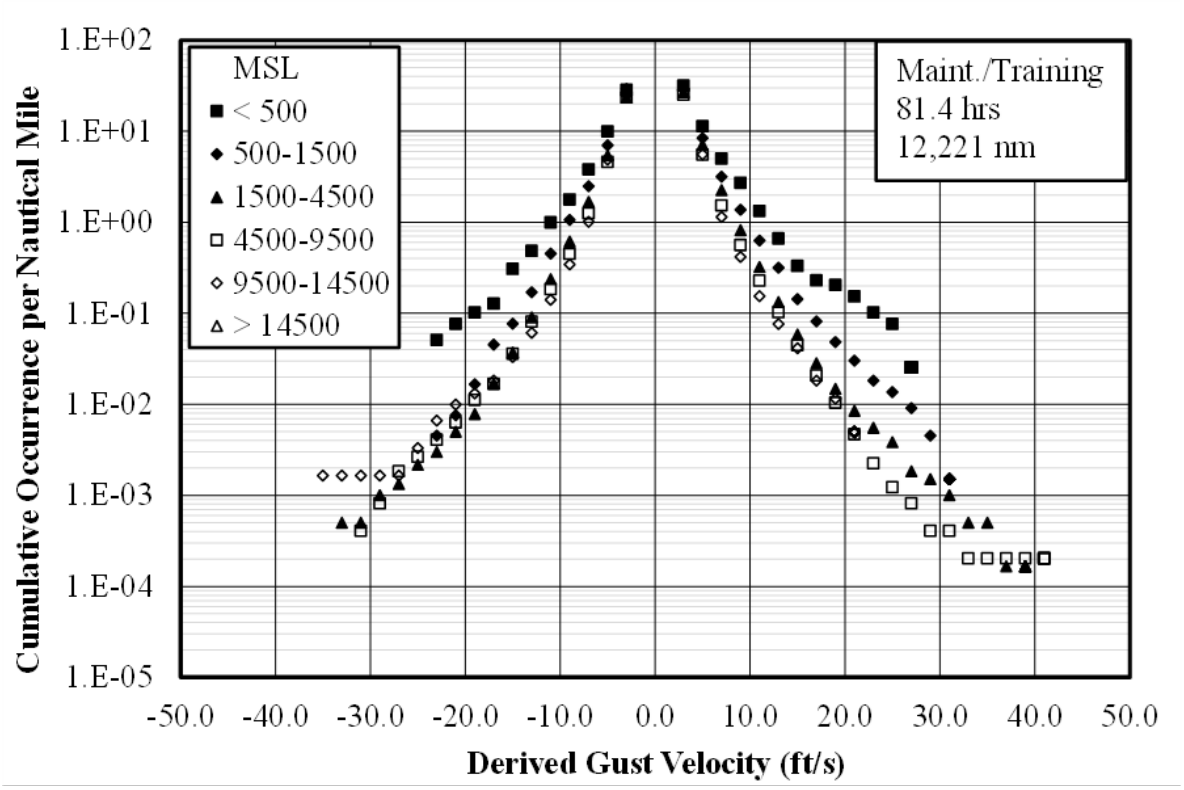

Figure E-15: Cumulative occurrences of derived gust velocity by MSL altitude, Maintenance/Training